PHARMA-ENGINEERING OF A MULTIFUNCTIONAL MICRONEEDLE ARRAY DEVICE FOR APPLICATION IN CHRONIC PAIN

SUNAINA INDERMUN

A thesis submitted to the Faculty of Health Sciences, University of the Witwatersrand, in fulfillment of the requirements for the degree of
Doctor of Philosophy

Supervisor:

Professor Viness Pillay

Department of Pharmacy and Pharmacology, Faculty of Health Sciences, University of the Witwatersrand, South Africa

Co-Supervisors:

Professor Yahya E. Choonara

Dr Lisa C. du Toit

Mr Pradeep Kumar

Department of Pharmacy and Pharmacology, Faculty of Health Sciences, University of the Witwatersrand, South Africa

Professor Girish Modi

Department of Neurology, Division of Neurosciences, Faculty of Health Sciences, University of the Witwatersrand, South Africa

Johannesburg

2014

DECLARATION

I, Sunaina Indermun, declare that this thesis is my own work. It has being submitted for the degree of Doctor of Philosophy in the Faculty of Health Sciences at the University of the Witwatersrand, Johannesburg, South Africa. It has not been submitted before for any degree or examination at this or any other University.

………………………………….

Signed this ……..day of December 2014

PUBLICATIONS

Sunaina Indermun, Yahya E. Choonara, Pradeep Kumar, Lisa C. du Toit, Girish Modi, Regina Lüttge, Viness Pillay. Patient-Controlled Analgesia: Therapeutic Interventions Using Transdermal Electro-Activated and Electro-Modulated Drug Delivery. Journal of Pharmaceutical Sciences, 2014, 103:353–366 *[Review Article]. ISI; IF: 3.13*

Sunaina Indermun, Yahya E. Choonara, Pradeep Kumar, Lisa C. du Toit, Girish Modi, Regina Lüttge, Viness Pillay. Current Advances in the Fabrication of Microneedles for Transdermal Delivery. Journal of Controlled Release, 2014, 185:130–138 *[Review Article]. ISI; IF: 7.633*

Sunaina Indermun, Yahya E. Choonara, Pradeep Kumar, Lisa C. du Toit, Girish Modi, Regina Lüttge, Viness Pillay. An Interfacially Plasticized Electro-Responsive Hydrogel for Transdermal Electro-Activated and Modulated (TEAM) Drug Delivery. International Journal of Pharmaceutics, 2014, 462: 52– 65 *[Research Article]. ISI; IF: 3.458*

APPENDIX 11.1

Sunaina Indermun, Yahya E. Choonara, Pradeep Kumar, Lisa C. Du Toit, Girish Modi, Regina Lüttge and Viness Pillay. Design, Development and Optimization of a Bipolymeric Interfacially Plasticized Electroresponsive Hydrogel (BiPErG) for Transdermal Electro-Activated and Modulated (TEAM) Drug Delivery. *(Poster Presentation). School of Therapeutic Sciences Research Day*, University of the Witwatersrand, Johannesburg, South Africa, September 10, 2013.

Sunaina Indermun, Yahya E. Choonara, Pradeep Kumar, Lisa C. Du Toit, Girish Modi, Regina Lüttge and Viness Pillay. An Electro- Modulated Transdermal Drug Delivery System for the Treatment of Chronic Pain. *(Podium Presentation). Faculty Research Day and Postgraduate Expo 2014,* University of the Witwatersrand, Johannesburg, South Africa, September 17, 2014.

APPENDIX 11.2

The Use of Microneedle Arrays for Efficient and Painless Administration of Bioactives through the Skin. Sunaina Indermun, Viness Pillay, Yahya E. Choonara, Pradeep Kumar, Lisa C. Du Toit, 2013/03983 ~ Provisional

ACKNOWLEDGEMENTS

Dimitris Georgiou and Suraksha Nowrungsah for all your help, motivation, laughs and encouragement over the years.

To my colleagues Steven Mufamadi, Nonhlanhla Masina, Felix Mashingaidze, Ahmed Seedat, Angus Hibbins, Derusha Frank, Tasneem Rajan, Karmani Murugan, Khadija Rhoda, Thiresen Govender, Teboho Kgesa, Martina Manyikana, Kealeboga Mokolobate, Khadija Rhoda, Zamanzima Mazibuko, Jonathan Pantshwa, Famida Ghulam-Hoosain, Naeema Mayet, Pierre Kondiah, Olufemi Akilo, Khuphukile Madida, Bibi Choonara, Zikhona Hayiyana, Poornima Ramburrun, Margaret Siyawamwaya and Mduduzi Sithole for their assistance and friendship.

To Mr Sello Ramarumo, Ms Pride Mothobi, Mr Kleinbooi Mohlabi, Mr Bafana Temba and Ms Phumzile Madondo for their indispensable assistance with the running of the laboratories.

To the staff of the Central Animal Services at the University of the Witwatersrand, Ms Kershnee Chetty, Ms Lorraine Setimo, Mr Nico Douths, Mr Patrick Selahle, Sr. Amelia Rammekwa and Sr. Mary-Ann Costello, for being very accommodating and always offering their assistance and expertise during my *in vivo* studies.

To the Wits Department of Pharmacy and Pharmacology staff, Mr David Bayever, Ms Shirona Naidoo, Ms Nompumelelo Damane, Mrs Neelaveni Padayachee and Professor Paul Danckwerts thank you for all the advice, assistance and much needed motivation.

I shall be telling this with a sigh

Somewhere ages and ages hence:

Two roads diverged in a wood, and I-

I took the one less travelled by,

And that has made all the difference.

-Robert Frost-

ABSTRACT

Chronic pain poses a major concern to modern medicine and is frequently undertreated, causing suffering and disability. Transdermal delivery is the pivot to which analgesic research in drug delivery has centralized especially with the confines of needle phobias and associated pain related to traditional injections, and the existing limitations associated with oral drug delivery. Highlighted within this thesis is the possibility of further developing transdermal drug delivery for chronic pain treatment using an Electro-Modulated Hydrogel- Microneedle array (EMHM) prototype device for the delivery of analgesic medication.

All available therapies designed for the treatment of chronic pain were critically reviewed. In addition, the drug delivery systems developed for this purpose and non-drug routes are elaborated on in a systematic manner. Recent developments and future goals in transdermal delivery as a means to overcome the individual limitations of the aforementioned delivery routes are also represented. Herein, this thesis highlights the application of hydrogels in electro-responsive drug delivery.

The EMHMs were synthesized by combining a microneedle array with an EMH which was synthesized from interpenetrating networks of polyacrylic acid and poly(vinyl alcohol). The networks incorporated a poly(ethyleneimine) and 1-vinylimidazole polymer blend as the novel electro-active species and ultimately resulted in the invention of a Bipolymeric Interfacially Plasticized Electro-responsive Hydrogel (BiPERG). The construction of a Box–Behnken design model was employed for the systematic optimization of the EMH composition comprising of three variables, viz. poly(ethyleneimine); 1-vinylimidazole; and applied voltage, critical to the success of the formulation. Electro-modulated drug release was determined on formulations exposed to varying environments to ascertain the optimal environment for the said desired release. A comparison method of formulation water content and swelling through gravimetric analysis was also conducted. Matrix resilience profiles were obtained as an insight to the ability of the EMH to revert to its original structure following applied stress. Response surface and contour plots were constructed for various response variables, namely electro-modulated drug release, matrix resilience and degree of swelling. The outcomes of the study demonstrated the success of electro-modulated drug release and as a result of this novelty, a new theory, Pillay's Electro-influenced Geometrical Organization-ReOrganization Theory (PEiGOR Theory) was developed and detailed herein. Volumes of poly(ethyleneimine) (>2.6 mL) and 1-vinylimidazole (>0.7 mL),resulted in ideal therapeutic electro-modulated drug release (0.8 mg) for sodium indomethacin. Lower amounts of poly(ethyleneimine) and amounts of 1-vinylimidazole ranging from 0.2 to 0.74 mL is consistent with greater than 1.6 mg release per electro-stimulation. Ex vivo results concluded that, in addition to the desired responsive nature of the EMHM device, the use of microneedles resulted in significantly less microbial permeation than their hypodermic counterpart. In vivo studies ultimately revealed a good preliminary indication of the of the EMHs electro-responsive capabilities with plasma sodium indomethacin levels differing by less than 6.76×10^{-7} μg/mL than that obtained by the conventional IV administration.

The approval of patch-like devices that contain both the microelectronic processing mechanism and the active medicament in a small portable device is still awaited by the pharmaceutical industry. This anticipated platform may prove transdermal electro-activated and modulated drug delivery systems an encouraging probability not only for the treatment of chronic pain but for other therapeutic treatments as well.

DEDICATION

This thesis is dedicated to my inspiration, to my motivation, to my parents,

Vinesh and Molly Indermun

TABLE OF CONTENTS

CHAPTER 1
INTRODUCTION AND BACKGROUND TO STUDY

CHAPTER 2

AN OVERVIEW OF SPECIALIZED TRANSDERMAL DRUG DELIVERY TECHNIQUES

CHAPTER 4
DESIGN, DEVELOPMENT AND OPTIMIZATION OF THE ELECTRO-MODULATED HYDROGEL

CHAPTER 5

PHYSICOCHEMICAL AND PHYSICOMECHANICAL CHARACTERIZATION OF THE OPTIMIZED ELECTRO-MODULATED HYDROGEL

CHAPTER 6
DEVELOPMENT AND EVALUATION OF THE MICRONEEDLE ARRAY TO BE EMPLOYED IN THE ELECTRO-MODULATED HYDROGEL-MICRONEEDLE DEVICE

CHAPTER 7
EX VIVO EVALUATION OF THE TRANSDERMAL ELECTRO-MODULATED HYDROGEL-MICRONEEDLE DEVICE

CHAPTER 8
IN VIVO EVALUATION OF THE TRANSDERMAL ELECTRO-MODULATED HYDROGEL-MICRONEEDLE DEVICE IN THE SPRAGUE DAWLEY RAT MODEL

CHAPTER 9
CONCLUSION AND RECOMMENDATIONS

LIST OF ABBREVIATIONS

AA - acrylic acid
AESC - Animal Ethics Screening Committee
AIC - Akaike's Information Criterion
AS - artificial sweat
BET - Brunauer-Emmett-Teller
BHN - Brinell Hardness Number
BiPERG- Bipolymeric Interfacially Plasticized Electro-responsive Hydrogel
BJH - Barrett, Joyner and Halenda
CFU - Colony forming units
CNCP - Chronic Non-Cancer Pain
DAA - diethyl acetamidomalonate
DEE - Drug Entrapment Efficiency
EAP - Electro-Active Polymer
ECH - Electro-Conductive Hydrogel
EMH - Electro-Modulated Hydrogel
EMHM - Electro-Modulated Hydrogel-Microneedle
FDA - Food and Drug Administration
FTIR - Fourier Transform Infrared
GA - gluteraldehyde
HCL - hydrochloride
IPN - interpenetrating polymer network
IS - internal standard
IV - intravenous
IVIVC - *in vitro-in vivo* correlation
KPS - potassium persulfate
MEMS - Microelectromechanical systems
MNA - Microneedle array
MRI - Magnetic Resonance Imaging
PA 6,10- polyamide 6,10
PAA - poly(acrylic) acid
PANi - polyaniline
PBS - phosphate buffered saline
PCA - Patient-Controlled Analgesia
PDMS - polydimethyl siloxane
PEI - poly (ethyleneimine)
PEiGOR Theory- Pillay's Electro-influenced Geometrical Organization-ReOrganization Theory
PSS - polystyrene sulfonate
PVA – poly(vinyl alcohol)
SBC - Schwarz's Bayesian Criterion
SC -stratum corneum
SE - Standard error of weighted residuals
SEM - Scanning Electron Microscopy
Si- silicon
SS - Sum of squares of residuals
TEAM - Transdermal Electro- Activated and Modulated
TEMED - N, N, N′, N′-Tetramethylethylenediamine
TSA - Tryptone Soya Agar
TSB - Tryptone Soya broth
UPLC – ultra performance liquid chromatographic
UV - Ultraviolet-visible
VI - 1-vinylimidazole
XRD - X-ray diffraction

LIST OF EQUATIONS

LIST OF FIGURES

LIST OF TABLES

CHAPTER 1

INTRODUCTION

1.1. Background to this Study

Chronic pain management has proven to be challenging to both the clinician and patient, resulting in time-consuming and sometimes unsuccessful or inadequate treatment, though this silent epidemic has not attracted the attention that it deserves (O'Brien and Breivik, 2012). More than 50 million people worldwide are affected by chronic pain, causing significant physical and emotional disability ultimately leading to substantial declines in many other areas of living (Lewandowski and Jacobson, 2011). Chronic pain poses a major societal problem with an urgent need for more advanced treatment options thereby offering a large and attractive market potential. Avoiding the emotional trauma and pain associated with injections, the risk of needle-stick injuries, increasing patient compliance, controlling plasma levels, improving bioavailability, and reducing overall doses have all made transdermal drug delivery systems an effective alternative to the available parenteral and oral routes. In addition, they offer the advantage of avoiding hepatic/gastrointestinal metabolism, hepatotoxicity, palatability issues and disease transmission (Langer *et al.*, 2004; Prausnitz *et al.*, 2004; Xie *et al.*, 2005; Escobar-Chávez *et al.*, 2011; Brogden *et al.*, 2012).

Although many methods such as the use of ultrasound, electric fields, chemical enhancers, and thermal methods have been used to successfully delivery active substances (Williams and Barry, 2004), the enhancement in the permeability of the delivered active across the skin has resulted in limited success, particularly in compounds with a high molecular weight. The past decade has seen exceptional progress in transdermal drug delivery device design and fabrication by both academic and industrial researchers alike, with some devices currently in clinical development and some awaiting US Food and Drug Administration (FDA) approval. In addition to device fabrication, integration and cost issues, many other issues are apparent from a pharmaceutical research point of view, such as optimal dose finding and minimizing adverse reactions.

Advances in the field of transdermal delivery have led to the development of Microneedle array (MNA) technology. This evolving technique combines the ease of a transdermal patch and the effectiveness of hypodermic syringes through the use of multiple microscopic projections from a backing plate to facilitate penetration of actives into the skin, ultimately providing a unique methodology of painless drug transport (Chiarello, 2004; Prausnitz *et al.*,

2009). Microneedles are developed as a solid, a dissolvable or as a microneedle device comprising of cannulae and are usually designed in arrays to improve the surface contact with the skin (Al-Qallaf and Das, 2009; Pattani *et al.*, 2012; Gratieri *et al.*, 2013). Even though great progress has been made over the years in the development of microneedles, the need for significant research and development efforts using them as delivery systems is still warranted (Arora *et al.*, 2008).

Professor Regina Lüttge at the MESA+ Institute for Nanotechnology (The Netherlands), a pioneer in MNA technology, has developed a patented concept patch comprising of 64 microneedles extending from a back plate (10.0mm diameter and 0.2mm thickness) in an arrayed fashion on an active area of 5x5mm. Each microneedle is between 200 to 500µm in length with shaft diameters ranging from 100 to 300µm with the internal volume of a single microneedle being about 1-10ηL. The placement of multiple microneedles in an array compensates for the small volume of the needles.

In order to advance this MNA technology, a novel patented Electro-Modulated Hydrogel (EMH) was developed in this study and was combined with the MNA technology in order to produce a pharma-engineered Electro-Modulated Hydrogel-Microneedle array device, subsequently referred to as the *EMHM device*. Similar to an Electro-Conductive Hydrogel (ECH), the EMH consists of co-networks or polymeric blends that inherently combine Electro-Active Polymers (EAPs) with highly hydrated hydrogels, with the difference being that the drug release from the EMH is in a responsive manner as opposed to the ECH's conductive manner (Guiseppi-Elie, 2010). In addition to developing the prototype device, this study has resulted in the identification and optimization of a novel EAP blend.

Shen and co-workers (2009) confirm that poly(acrylic) acid (PAA) gels exhibit pH-responsive behavior and that PAA behaves as an electrolyte due to the protons originating from the many carboxylic acid groups present along the polymer molecules. It was found in the study that at higher pH concentrations, the PAA gels expand. Upon contact with the skin, the PAA-EMH shall be exposed to a higher pH, resulting in the required pH-responsive and electrolytic behavior. To maintain its structural integrity after repeated exposure to electro-stimuli, the EMH will be formulated as a semi-interpenetrating polymer network (semi-IPN). Poly (vinyl alcohol) (PVA) was instituted as the second component to the semi-IPN, primarily for containing a spatially extended π bonding system, which is the reason for its intrinsic semiconducting nature (Chen *et al.*, 2012; Bajpai *et al.*, 2008).

1.2. Rationale and Motivation for this Study

A single assembled device responsive to a patient's individual therapeutic requirements and biological state may potentially advance the field of drug delivery. Such smart therapeutics possess one or more properties such as precise controlled release, local targeting, self-regulated therapeutic action, proper drug protection, enzyme inhibiting, permeation enhancing, imaging, and reporting. The difficulty with such a device lies in the ability to incorporate all or the majority of these functions into a single device, this study aims to try to fulfill this highly challenging design predicament.

MNA technology is currently at the forefront of 'pain free' delivery of drugs, as it merely pierces the epidermis. The unique ability of MNAs to release drug in a minimally invasive manner allows renders them an attractive candidate as a physical enhancer to administer drugs throughout the skin. In many studies, microneedle piercing has been shown to significantly increase skin permeability of a variety of drugs.

Due to the electro-responsive release of the active agent, adverse effects will be avoided with the use of the EMHM device. Drug dosages may be modified electronically preventing over-doses and analgesic tolerance, and will have the ability to act rapidly. The device will be designed to allow for easy application and therefore will significantly desensitize the patient to chronic pain by providing immediate pain relief.

1.3. The Implications of the Integumentary System in the Development of the Electro-Responsive Delivery Device

The skin consists of three layers, i.e. epidermis, dermis and subcutaneous fat layer (subcutis), collectively serving as an external physical barrier (Figure 1.1), with the real barrier to transdermal diffusion being specifically the stratum corneum (SC) (Escobar-Chávez *et al.*, 2011). Delivery from hypodermal administration results in the compound being deposited either intramuscularly, subcutaneously or intradermally. The microscopic projections on the microneedle arrays allow for compounds to be delivered either precisely into or just beyond the epidermis without stimulating pain receptors (Hedge *et al.*, 2011).
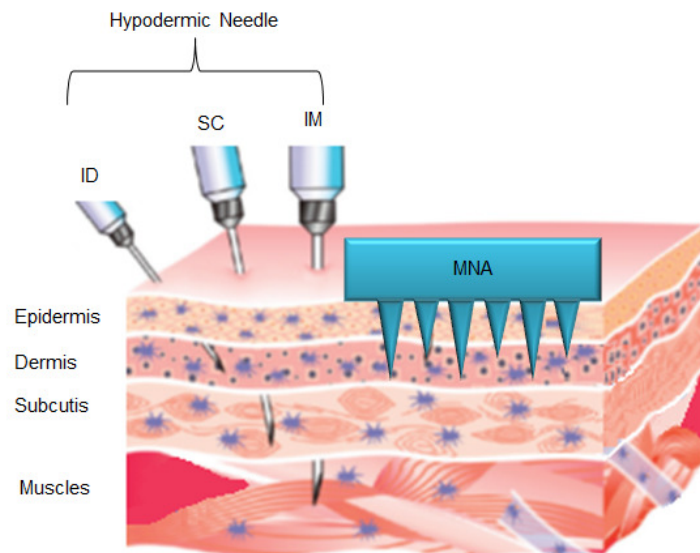
Figure 1.1: Classical and transdermal needle-driven delivery in relation to the anatomy of the skin (Hedge *et al.*, 2011).

1.4. The Mechanism by which Electro-Responsive Drug Delivery will be Achieved

This invention encompasses the design of a drug delivery device that is capable of drug release via electro-stimulus activation. The electrical stimulation of the hydrogel will allow for the formation of water channels in the hydrogel network facilitating the immediate release of the entrapped drug into the tissues. Under normal conditions the drug compound will stay entrapped in the hydrogel, but upon the actuation using the electro-stimulus, the drug will be released into the skin. When the external stimulus is removed, the change is reversed and thus drug release is ceased. The concept addressing this unique drug delivery phenomenon is shown below in Figure 1.2 and is detailed later in Chapter 5, Section 5.3.13 as a new theory, Pillay's Electro-influenced Geometrical Organization-ReOrganization Theory (PEiGOR Theory). A patient with chronic pain can easily apply this device anywhere on the body at the site of the pain. The main advantage is that due to the controlled release, patients can wear the device for at least an entire day.

The EMHM being applied to the skin.

The microneedles do not penetrate below the epidermis, evading the sensation of pain.

Electro-stimulation will allow for the controlled release of drug. Following cessation of the stimulus, drug release will cease.
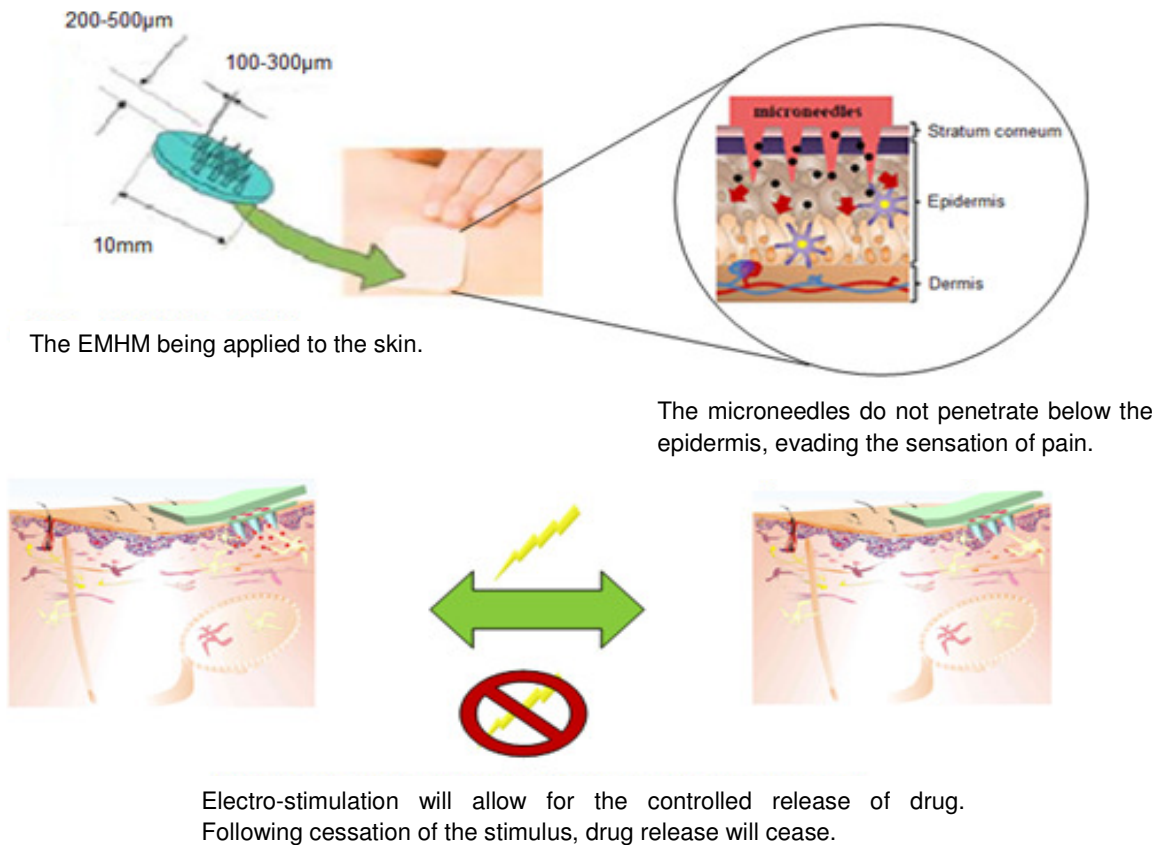
Figure 1.2: Schematic concept of the integration of the microneedle platform combined with Electro-Modulated Hydrogel technology.

Indomethacin will be the first active candidate drug considered for the novel hydrogel. Although a potent anti-rheumatic used to relieve pain and inflammation, indomethacin is more inclined to cause gastrointestinal disturbances as well as Central Nervous System (CNS) effects. In addition to pain relief, the EMHM device will prohibit any unwanted adverse effects in chronic use patients.

Following the successful electro-responsive delivery of indomethacin from the EMH, scheduled drugs with greater potency will be used to prove formulation versatility: morphine hydrochloride (HCL); fentanyl citrate; and celecoxib. Regular oral administration of morphine HCL is recommended for the management of severe chronic pain as well as cancer- related pain, requiring repeated doses of opioid analgesics when less effective drugs are no longer adequate (Morales *et al.*, 2004).

Fentanyl citrate is commonly indicated for post-operative surgical procedures and chronic pain management primarily for cancer patients (Almousa *et al.*, 2011). The synthetic μ-opioid agonist is commonly subjected to misuse due to its high potency being illicitly used in

combination with other drugs such as opioids, antidepressants, amphetamines and benzodiazepines, or alone (Woodall *et al.*, 2008).

Celecoxib, like indomethacin, is a Non-Steroidal Anti-Inflammatory (NSAID) and is indicated for the treatment of rheumatoid arthritis, sever pain and acute post-operative pain treatment. Celecoxib has been chosen as an additional drug candidate to prove versatility of the optimized EMH with drugs that belong in the same NSAID class but have different chemical structures.

1.5. Novelty of this Study

The consortium of MNA technology is a promising technique that has the ability to facilitate drug transport by combining the advantages of both transdermal patches and hypodermic syringes. The approval of patch-like devices that contains both the microelectronic processing mechanism and the active medicament, formulated as a Bipolymeric Interfacially Plasticized Electro-responsive Hydrogel (BiPERG) developed herein, in a small portable device is still awaited by the pharmaceutical industry. This anticipated platform will provide Transdermal Electro- Activated and Modulated (TEAM) drug delivery and is a feasible attempt in the search for ideal chronic pain treatment.

1.6. Possible Therapeutic Applications of this Delivery System

Approximately 3.0-4.5% of the 1.5 billion people suffering from chronic pain worldwide also suffer from neuropathic pain, with the incidence rate increasing complementary to age. Major adjustments that chronic pain patients usually make include changing of jobs or taking disability leave from work, moving to a more manageable home and getting assistance with daily living activities. Because numerous patients in routine practice settings feel they have some or no control over their pain or fail to achieve adequate pain relief, chronic pain is now considered to be a public health problem of major proportions.

Although not a relatively new concept, drug delivery research has focused on the transdermal delivery route due to the limitations of oral drug delivery and the needle phobias, accidental needle-sticks and pain associated with conventional injections. In the past, the therapeutic application of transdermal delivery was restricted to the application of: creams; poultices; ointments; pastes; and gels; all of which are prone to messing and difficult to apply uniformly to ensure reproducible dosing. By pharma-engineering and prototyping such a device, chronic pain sufferers will receive controlled delivery of analgesics resulting in relief and a better quality of life.

1.7. Aim and Objectives of this Study

This project's principle aim is the pharma-engineering and prototyping of a versatile multifunctional EMHM device for the treatment of chronic pain. This aim will be achieved through the development of the novel EMH technology that will be combined with an MNA to produce an intelligent device for advanced pain-free administration of drugs through the skin. The aforementioned EMH will be formulated to meet the following design criteria:

1. For the purposes of stability, the EMH will be designed to have adequate structural and mechanical stability.
2. The EMH will allow for the efficient controlled release of the drugs once the MNA has been applied.
3. The EMH technology consists of a hydrogel mixed with an EAP.
4. The candidate drugs must remain entrapped in the EMH under normal conditions, and be released into the skin upon the actuation of an electrical stimulus. Drug release must cease when the external stimulus is removed, therefore facilitating electrically controlled release.

For pragmatic fulfillment of the design strategy, the following objectives are apparent:

i.   To design and formulate a novel mechanically stable EMH semi-IPN through the process of solution polymerization which culminates in the controlled release of entrapped drugs via electrical stimulation of the array, and possesses appreciable adhesive characteristics.
ii.   To determine the swelling behavior of the EMH.
iii.   To characterize the EMH, the following tests will be conducted: Fourier Transform Infrared (FTIR) spectroscopy; Scanning Electron Microscopy (SEM) imaging; Differential Scanning Calorimetry (DSC) and cyclic voltammetry tests.
iv.   To conduct *in vitro* release studies from the EMH in the presence and absence of an electric current.
v.   To fabricate a MNA patch device through which drug release will be facilitated.
vi.   The clinical potential of the prototype EMHM, based on its ability to meet the design criteria *in vitro*, will be ascertained in the Sprague Dawley rat model terms of penetration, *in vivo* release kinetics, distribution, and biocompatibility. Subsequently the feasibility of the device in human patients will be corroborated.

1.8. Overview of this Thesis

Chapter One provides an introduction and background to this study and highlights the rationale, aim, objectives and potential benefits of this study.

Chapter Two critically reviews the available therapies designed for the treatment of chronic pain. The drug delivery systems developed for this purpose and non-drug routes are elaborated on, in a systematic manner. Recent developments and future goals in transdermal delivery as a means to overcome the individual limitations of the aforementioned delivery routes are represented as well. This chapter also reviews the use of hypodermic needles and their delivery limitations in comparison to that of microneedles, in addition to the various advances in fabrication techniques of microneedles, providing an update of pharmaceutical research in the field of microneedle-assisted transdermal drug delivery systems.

Chapter Three describes the preliminary experimental laboratory formulation and development of a suitable EMH formulation, outlining the formulation parameters, physicochemical and physicomechanical characterization, and *in vitro* drug release analyses. This chapter also outlines the various therapeutic aspects considered for optimal formulation.

Chapter Four highlights the investigation of the various attributes of the EMH, through institution of a statistical experimental Box-Behnken design model. Herein, the design, development and optimization of the EMH are detailed. *In vitro* release studies as well as extensive physicochemical and physicomechanical properties of the formulations of the experimental design was studied.

Chapter Five exhibits physicochemical and physicomechanical testing conducted on the optimized EMH. In addition, simultaneous qualitative and quantitative analyses were conducted on the optimized EMH.

Chapter Six evaluates the physicochemical properties of the MNA component of the drug delivery device. In addition, this chapter evaluates the device's capability of electro-activated and modulated drug delivery. A microbiological assessment quantifying the permeation allowance of microneedles through the stratum corneum was also evaluated.

Chapter Seven introduces *ex vivo* permeation studies on the EMHM device. Studies were conducted to ensure viability of the prototype device prior to *in vivo* studies. The permeation

experiments were performed on porcine skin tissue to ascertain the electro-responsive capabilities of the device in addition to determining the microbial penetration ability of the microneedles across the viable epidermis in microneedle-punctured skin as well as hypodermic needle-punctured skin.

Chapter Eight details the *in vivo* evaluation of the electro-modulated delivery system in the Sprague Dawley rat model. Histopathological studies were conducted on skin samples to ensure proper device application. Pharmacokinetic modeling was conducted to determine *in vitro-in vivo correlation* (IVIVC) establishment

Chapter Nine concludes this thesis, discussing the limitations and recommendations for future use of the device.

CHAPTER 2

AN OVERVIEW OF SPECIALIZED TRANSDERMAL DRUG DELIVERY TECHNIQUES

2.1. Introduction

Although hailed as a medical breakthrough for pain treatment, the risks and limitations of Patient-Controlled Analgesia (PCA) outweigh the benefits associated with its use; the main risk being overdose and subsequent death and the main limitation being high costs. Many clinicians believe that analgesic doses need to be increased to provide adequate pain relief yet they fail to see the underlying problem related to drug delivery. Although numerous pain treatment therapies are available on the market, a point regarding drug delivery made by Stapleton and co-workers (1978) still holds true:

"The plethora of new parenteral agents which the pharmaceutical companies have introduced over the past 20 years is not a reminder that we have not found the right drug but a reminder that we have not found the optimal mode of administration of perfectly adequate analgesic drugs."

Pain according to the International Association for the Study of Pain can be defined as "an unpleasant sensory and emotional experience associated with actual or potential tissue damage, or described in terms of such damage" (Merskey and Bogduk, 1994). Three classifications of Chronic Non-Cancer Pain (CNCP) are identified: nociceptive, neuropathic, and functional (Merskey and Bogduk, 1994). CNCP may result from numerous medical conditions and although there are corresponding large numbers of specific injections, rehabilitation programs, and pharmacological treatments available, many patients are still left with continued pain even after repeated treatment attempts, necessitating controlled delivery of analgesic drugs.

Since CNCP causes sleeplessness and depression, and interferes with normal physical and social functioning (Becker *et al.*, 1997), the impact and prevalence of chronic pain warrants serious attention as the condition may influence the overall quality of life (Lewandowski and Jacobson, 2011; O'Brien and Breivik, 2012). In America alone, chronic pain affects more than 50 million people (Lewandowski and Jacobson, 2011) causing significant physical and emotional disability, ultimately leading to substantial declines in many other areas of living. The economic consequences of long-term pain are thought to be vast, with the annual cost of chronic pain in the United States, including lost income, lost productivity and healthcare expenses, being estimated to be $100 billion (Institute of Medicine Report from the

Committee on Advancing Pain Research, Care, and Education, 2012) and the cost to the patient in terms of lost earnings, lost ambitions, lost potential, lost life-quality and lost relationships being immeasurable. CNCP thus poses a major societal problem with an urgent need for more advanced treatment options.

The search for pain relief has taken on many variations through the ages resulting in some atypical methods and some worthy of further investigation. The last 40 years has seen numerous developments that have improved available medications, clinical understanding, and pain management related patient outcomes (Painter, 2005) with inherent advantages and disadvantages as highlighted in Table 2.1.

Table 2.1: Comparison of pain treatment interventions (Pain Research Center, 2012).

Treatment	Advantages	Disadvantages
Opioids (oral)	• Treats both localized and generalized pain. • Multiple drugs are available. • Some inexpensive drugs are available. • Can be administered by a proxy. • Long acting, controlled-release forms available. • Sedative and anxiolytic properties useful.	• Adverse effects may limit use. • Prescriptions of opioids are regulated. • Fear/stigma associated with use.
Analgesics (oral)	• Some inexpensive drugs are available. • Can be administered by a proxy. • Widely available, some over-the-counter. • Can treat moderate to severe pain. • Additive analgesia possible when combined with opioids and other modalities.	• Some expensive drugs are available. • Serious adverse effects possible. • Anti-coagulant risk. • Ceiling effect to analgesia.
Epidural, intrathecal, and intracerebral ventricular routes	• Local anesthetics may be added to spinal opioids and may produce additive analgesia. • Useful for pain that has not responded to less invasive measures.	• May require expensive drug infusion pump, intervention fees, and recurring charges for disposables. • Contraindicated in presence of acute spinal cord compression. • Pruritus and urinary retention are more common than with oral or parenteral opioid administration. • Infection at catheter site can produce meningitis and/or epidural abscess.

Treatment	Advantages	Disadvantages
		• Requires careful monitoring, especially when therapy begins and when doses are increased.
		• Requires special expertise.
		• Tolerance may occur sooner than with oral or rectal administration.
Intravenous (IV) infusion	• Rapid pain relief provided. • Many opioids given this route. • In PCA mode, allows for rapid individual dose titration and provides sense of control for patient.	• Requires a healthcare profession to be administered. • Infection and infiltration of IV lines are potential complications. • Often requires expensive drug infusion pump and recurring charges for disposables.
Patient education	• Promotes self-care in pain treatment and management of side effects. • Effective in improving ability to follow medical regimen and in decreasing pain. • Multiple teaching aids available.	• Requires professional time to teach pain management regimens.
Relaxation, imagery, biofeedback, distraction, and reframing	• Most are inexpensive, require no special equipment, and are easily administered. • May increase patient's sense of control. • May be used as adjuvant therapy. • May decrease pain and anxiety without drug-related side effects	• Requires professional time to teach interventions.

Treatment	Advantages	Disadvantages
Psychotherapy, structured support, and hypnosis	• May increase patient's coping skills. • May decrease pain and anxiety for patients who have pain that is difficult to manage.	• Requires skilled therapist.
Pastoral counseling	• May provide spiritual and emotional comfort. • May increase patient's coping skills.	• None identified.
Acupuncture	• Can be used as adjuvant with most other therapies.	• Requires skilled therapist.
Peer support groups	• Provides support for families and patients. • May increase patient's coping skills. • Increases sense of control.	• None identified.

2.2. Recent Approaches to Patient-Controlled Analgesia

Traditional oral or parenteral drugs do not always provide adequate therapeutic effects to treat chronic pain and as a result, PCA has rapidly become a popular and effective means of providing analgesia to patients with various etiologies of pain. PCA is a welcomed advancement in the treatment of pain, for the first time, the actual patient is empowered to control their own pain relief treatment. Patients are no longer required to receive analgesics by intramuscular injection, often long after the healthcare professional had been beckoned for assistance. Nor are the patients subjected to the lengthy process of procuring and preparing the medication, which ultimately delays patient access to pain relief.

2.2.1. Benefits and limitations associated with Patient-Controlled Analgesia infusion pumps

Currently, PCA is mostly limited to infusion pumps as a mode of drug delivery (Grass, 2005). The concept of PCA presented further is not restricted to a single administration route or analgesic class but rather an overview on the concept of the PCA infusion pump device and its relevant aspects.

PCA has been shown to improve pain management with less opioid consumption, potentially fewer adverse effects, such as respiratory complications and less sedation, in non-critically ill patients (Santell, 2005) being hailed as a major advancement both in the medical and pharmaceutical field alike with many different types of infusion pump devices being available today (Figure 2.1). The concept of PCA offers numerous benefits to patients which include: patient autonomy with safe individualized dosing, improved analgesia with less sedation and enhanced satisfaction; earlier mobilization and better respiratory function resulting in less risk of pneumonia and pulmonary emboli and, a reduced length of stay; which results in patients not being subjected to nosocomial infections. In addition, the pumps offer several safety features to prevent the administration of excessive amounts of analgesic medication.
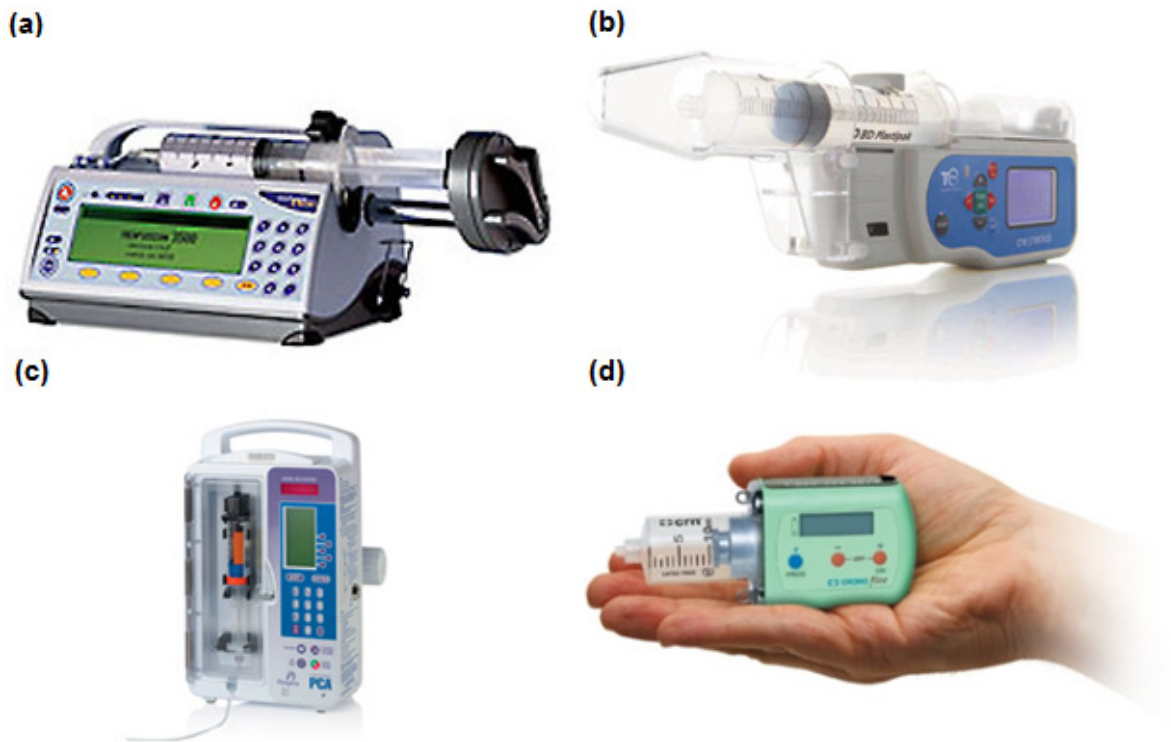
Figure 2.1: Types of PCA devices available. (a) Medfusion 3500 Syringe Infusion Pump; (b) Syringe Pump with motor driven linear actuator; (c) Hospira PCA 3 Syringe Infusion Pump; and (d) Cane Crono Micropump.

Although PCA has resulted in relief to many patients, it is not without shortcomings, which could be listed as: i) incorrect drug or drug concentration, ii) triggering in error by the proxy (i.e., family member, nurse), iii) false triggering (various reasons), iv) hardware or software/malfunction, v) drug accumulation, siphoning, or retrograde flow due to dead space or catheter blockage, vi) duplicate analgesic orders or poorly-written orders, vii) accidental mis-programming at the caregiver-pump interface, viii) anaphylaxis/countless drug interactions, ix) extraordinary drug sensitivity, x) reprogramming with criminal or "mercy" intent, xi) high cost implications, xii) overuse due to misunderstanding that PCA is a magic black box for pain relief.

In addition to using many drugs for pain relief, it has become evident that continuous, demand-independent background infusions usually did not improve the quality of analgesia but increased overall opioid consumption with the risk of higher incidences of respiratory depression (Lehmann, 2005). Thus, newer, advanced systems need to be developed to prevent any unwanted adversities and provide rapid, effective pain relief.

2.2.2. Utilizing Patient-Controlled Analgesia as an effective pain treatment

Since its introduction years ago, PCA has become the gold standard for severe pain management, the pioneering PCA technology has led to its routine use for post-surgical pain management today (Lehmann, 2005; Beresford, 2007). The concept of pain management using the notion of so-called "patient-controlled analgesia" or "on-demand analgesia" by IV administration of opioids was published in the late 1960s (Hamilton and Baskett, 2000) yet evidence suggests that PCA was first used experimentally by Philip H. Sechzer in 1965 (Sechzer, 1971). Sechzer evaluated the analgesic response to small IV opioid doses given on patient demand first by a nurse and then by a machine, in 1968 and 1971 respectively (Sechzer, 1971). Further advances in PCA led to the development of electronic programmable pumps making the patient-controlled analgesia safe and efficient in clinical practice (O´Neil *et al.*, 1997).

The concept of obtaining analgesic from the infusion device is easily understood from the patient's perspective. When the patient is in pain, or foresees pain due to an activity like getting out of bed, the PCA infusion pump push-button is switched on. Without waiting for the nurses to answer a call button, analgesics can be conveniently delivered intravenously via a computerized pump. The computerized pump is capable of confirming, preparing, and administering the analgesic treatment depending on the patient's eligibility to receive the requested drug. The computer accepts the request provided enough elapsed time from the time of the last dose, e.g., the lockout period (Beresford, 2007). PCA does cause alarm for patient overdose (Lehmann, 2005; Beresford, 2007) whether it is accidental or intended. A basic safety measure of the PCA in overdose prevention is that when the opioid analgesic takes effect, it will start to make the patient drowsy; decreasing the possibility of the patient to continue pressing the button for another dose. If the button is pushed on the patient's behalf out of a well-intentioned desire to prevent or minimize pain, the risk of overdose increases therefore the PCA must be patient-controlled (Beresford, 2007).

Increasingly, PCA is also used for patients with cancer-related moderate to severe chronic pain or who are being followed by palliative care or hospice services (Beresford, 2007). Although first reports of a then new concept of pain management surfaced in the 1960s, it can be argued that people have always taken medications based on their needs using either sublingual or oral doses (Painter, 2005).

Unfortunately, with the use of the devices comes the use of multiple drugs (Lehmann, 2005). The combination of IV morphine and dextromethorphan (Weinbroum *et al.*, 2002); morphine and clonidine (Jeffs *et al.*, 2002); morphine and ketamine (Murdoc *et al.*, 1992); morphine

and diclofenac (Nagasaki *et al.*, 2002); morphine, tramadol, and propacetamol (Dejonckheere *et al.*, 2001); morphine and ketorolac (Reuben *et al.*, 1998); magnesium, tramadol, and ketamine (Ünlügenc *et al.*, 2002); tramadol and metamizol (Stamer *et al.*, 2003); or oxycodone and diclofenac or oxycodone and ketoprofen (Silvanto *et al.*, 2002) have all been used for postoperative pain management and often result in unnecessary adverse effects such as respiratory depression and reduced peristalsis. In addition, PCA medications may have anaphylactic implications (Beresford, 2007). Currently there are no transdermal systems available for the drugs in PCA research, as a future direction, looking into a single system that delivers the drug concurrently and/or concomitantly is warranted.

2.2.3. Economic implications arising from Patient-Controlled Analgesia

Only a few publications exist reflecting the economic aspects of PCA. Thus far, no agreement has been reached if total costs match the outcome of using PCA (Brodner, *et al.*, 2000). Although patients' acceptance of PCA is overwhelming, it cannot be considered an entity by itself as there are too many application modes combined with too many drug interactions and numerous modifications in use, all of which in an individual setting, influence efficacy and efficiency (Lehmann, 2005). With this being said, the treatment of CNCP is still so valued that patients are willing to find any financial means necessary for pain relief (Savage *et al.*, 2008).

2.3. Drug Delivery Using the Transdermal Route

Human civilizations have applied substances to the skin as cosmetic and medicinal agents for thousands of years paving the way to the discovery and utilization of medicaments used today (Arora *et al.*, 2008). Since 1979, when the first transdermal drug delivery system, Transderm Scop® Patch, was approved by the FDA for the treatment of motion sickness, to the current transdermal delivery systems, a successful alternative to systemic drug delivery has evolved (Chiranjib *et al.*, 2010). Transdermal delivery systems have also proven to be efficacious in managing both chronic non-malignant and malignant pain in the long term (Milligan *et al.*, 2001) with various function-appropriate types available today (Figure 2.2a). Currently marketed and widely used patches available include Duragesic® for relief from moderate to severe pain, Ortho-Evra® for continuous delivery of estrogen and progestogen, Androderm® for continuous delivery of testosterone and Nicoderm CQ® used by smokers to reduce cigarette cravings. The patches facilitate other medicinal substances with dosing schedules that foster greater satisfaction and patient compliance to be administered (Kim and Simon, 2011). The principle delivery mechanism is dependent on the slow process of diffusion driven by the concentration gradient that exists between the zero concentration prevailing in the skin and the delivery system's high drug concentration (Scheindlin, 2004;

Brown *et al*., 2006). The speed of drug release is determined by the complex relationships between the membrane permeability, the polymer matrix used, the layer thickness, and the content and concentration of drug. In certain cases, diffusion alone is an inadequate mechanism to penetrate the SC preventing optimal drug delivery. Numerous procedures have been developed to aid drug delivery in such instances, with most being in the electro-chemical field. The chief pathways for the molecules to penetrate the SC is by intercellular, intracellular (transcellular) and follicular (appendage) pathways (Figure 2.2b; Alexander *et al*., 2012).
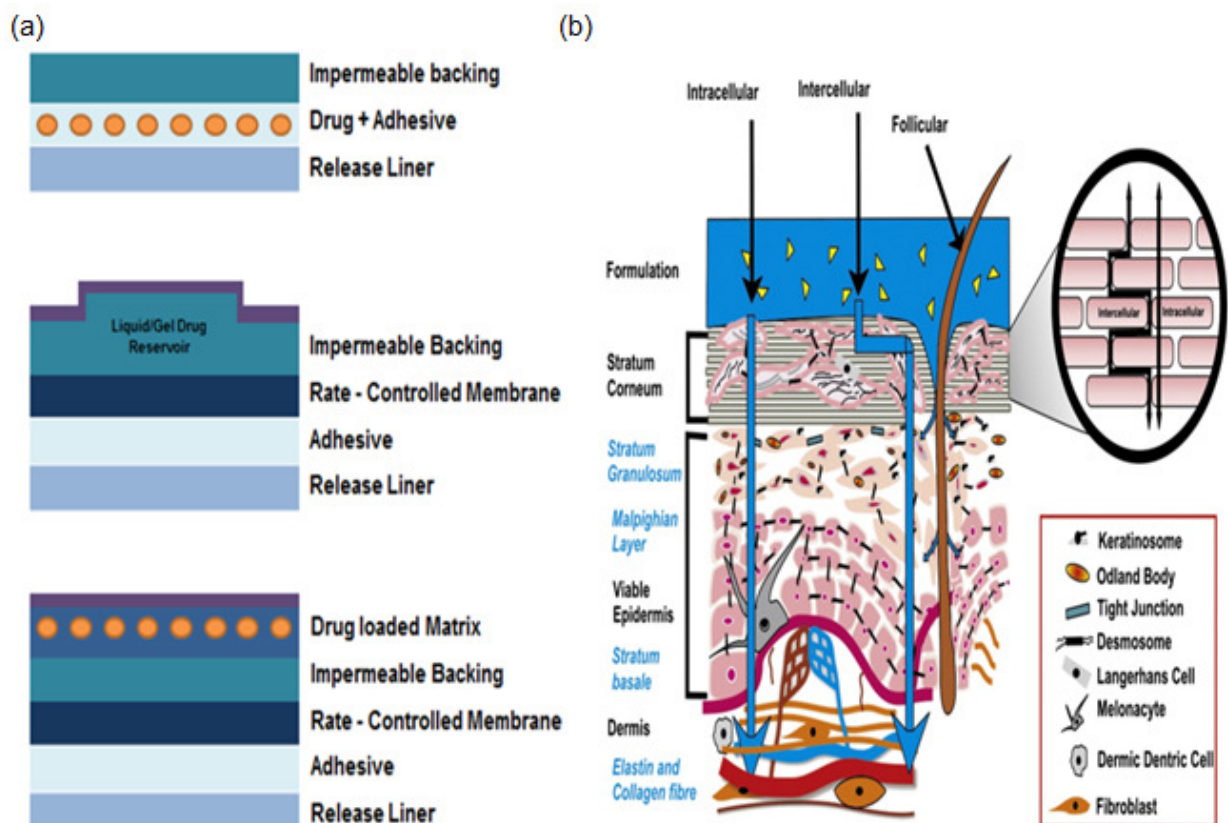
Figure 2.2: (a) Components of various types of transdermal patches. (b) Anatomy of the skin showing the path of action for drugs and topical formulations (Brown *et al*., 2006).

2.3.1. Types of transdermal delivery systems

Transdermal drug delivery systems may be classified into two types, namely passive and active, each of the types depending on the principle of diffusion based on the concentration gradients (Joshi, 2008). In addition to being driven by diffusion, active transdermal drug delivery systems comprise of different penetration enhancing technologies ranging from electro-poration, microporation, electrical current, iontophoresis, mechanical arrays, radio frequency thermal/heat, ultrasound, and laser ablation. In the past, the therapeutic application of transdermal delivery was restricted to the application of: creams, poultices,

ointments, pastes, and gels, all of which are prone to be messy and difficult to apply uniformly to ensure reproducible dosing (Sivamani *et al.*, 2008). In drug delivery, offering the possibility of controlled drug release over time across the skin using a patch is an approach that is presumably more attractive to patients (Bronaugh and Maibach, 1999; Touitou, 2002). When compared with oral drug delivery and more conventional methods the skin has both limitations and benefits, like many other alternative routes of delivery which are detailed in Table 2.2 (Brown *et al.*, 2006).

Table 2.2: Benefits and limitations of transdermal delivery.

Benefits	Limitations
• The simplified non-invasive medication regimen leads to convenient and painless administration resulting in leads to improved patient compliance and reduced inter & intra-patient variability (Rasheed *et al.*, 2011).	• A molecular weight less than 500 Da is essential to ensure ease of diffusion across the SC (Bos and Meinardi, 2000), since solute diffusivity is inversely related to its size.
• It is an alternative in circumstances where oral dosing is not possible e.g.in unconscious or nauseated patients.	• Sufficient aqueous and lipid solubility, a Log P (octanol/water) between 1-3 is required for the permeant to successfully traverse the SC and its underlying aqueous layers for systemic delivery to occur (Bos and Meinardi, 2000).
• Ease of use may reduce overall health care treatment costs as well as medical waste (Wilson, 2011).	• Pre systemic metabolism; the presence of enzymes in the skin such as peptidases and esterases might metabolize the drug into a form that is therapeutically inactive, thereby reducing the efficacy of the drug (Bos and Meinardi, 2000).
• Rapid notification of medication in the event of emergency as well as ease of dose termination by flexibility of terminating the drug administration patch removal in the event of any adverse reactions either systemic or local (Alexander *et al.*, Rasheed *et al.*, 2011).	• Skin irritation and sensitization; referred to as the "Achilles heel" of dermal and transdermal delivery. The skin as an immunological barrier may be provoked by exposure to certain stimuli, this may include drugs, excipients, or components of delivery devices resulting in erythema, edema, etc (Toole *et al.*, 2002).

Benefits	Limitations
Improved patient acceptance as self-administration is possible with these systems as well as improved patient compliance and comfort via non-invasive, painless and simple application (Rasheed *et al.*, 2011; Archer *et al.*, 2004).	The drug must have some desirable physicochemical properties for penetration through SC and if the drug dose required for therapeutic value is more than 10mg/day, the transdermal delivery will be very difficult (Rasheed *et al.*, 2011).
The avoidance of first pass metabolism and other variables associated with the GI tract such as pH, gastric emptying time (Rasheed *et al.*, 2011; Kumar and Philip, 2007).	Only relatively potent drugs are suitable candidates for transdermal drug delivery systems because of the natural limits of drug entry imposed by the skin's impermeability (Rasheed *et al.*, 2011).
Due to the sustained and controlled delivery over a prolonged period of time, transdermal delivery is associated with a reduction in side effects associated with systemic toxicity i.e., minimization of peaks and troughs in blood-drug concentration. Adverse effects or therapeutic failures frequently associated with intermittent dosing can also be avoided (Rasheed *et al.*, 2011).	Some patients develop contact dermatitis and local irritation at the site of application for one or more of the system components, necessitating discontinuation. Erythema, itching, and local edema can be caused by the drug, the adhesive, or other excipients in the patch formulation (Rasheed *et al.*, 2011).
Utilization of drug candidates with short half-life and low therapeutic index (Barry, 2002).	Clinical need is another area that has to be examined carefully before a decision is made to develop a transdermal product (Yadav, 2012).
Transdermal delivery can increase the therapeutic value and bioavailability of many drugs by avoiding specific problems associated with the drug e.g., gastro-intestinal irritation, low absorption, decomposition due to hepatic "first-pass" effect, formation of metabolites that cause side effects, short half-life necessitating frequent dosing etc (Rasheed *et al.*, 2011).	High cost of the product is also a major drawback for the wide acceptance of this product (Yadav, 2012).

2.3.2. Barriers to transdermal delivery

Even though transdermal drug delivery systems have been found to be effective, success is controlled by the SC, the rate-limiting step in the penetration process, (Tadicherla and Berman, 2006) prohibiting the entry of most drugs into the skin at therapeutically useful rates (Prausnitz, 2004; Rasheed *et al.*, 2011). Owing to the dead nature of the SC, solute transport across the SC is maintained principally by passive diffusion in accordance with Fick's Law (Flynn *et al.*, 1974). In addition, the SC has many unpopular properties, namely i) it is hygroscopic, yet impermeable to water, ii) layer thickness varies for different areas of the body, iii) it is a tough but flexible membrane, and iv) it is an intercellular space rich in lipids (Brown *et al.*, 2006). Although it has these undesirable properties, the SC does however allow penetration of some chemicals to reach into the blood vessels and tissue underneath the skin, provided that these chemicals and drug candidates fulfill several requirements in terms of aqueous solubility, lipophilicity, molecular weight, melting point, pH of saturated aqueous solution and the dose deliverable (Naik *et al.*, 2000; Joshi, 2008). Since transdermal drug delivery has been limited to low amounts of drug due to the extremely low rate of drug release from the matrix and the low permeability of drug through the skin, one of the primary challenges for transdermal drug delivery is to increase the permeation of drug through skin tissue by overcoming the barrier function from the SC (Zhang and Michniak-Kohn, 2011).

2.4. Transdermal Delivery Optimization Technologies

The search for methods of improving delivery of drugs through the SC has been emphasized. The optimization of the drug therapy can be achieved if the drug carrier responds and activates in a predictable and reproducible fashion under an external or internal stimulus such as temperature (Xu *et al.*, 2006), pH (Gudeman and Peppas, 1995) and electric field (Murdan, 2003). Many methods being either physical or chemical have been researched and investigated. Table 2.3 summarizes some ways in which the SC barrier may be eluded. While these methods of optimization were well accepted into the world of pharmaceutical research and development, they are not without their shortcomings. From the above mentioned techniques of enhancing transdermal delivery, microneedles and iontophoresis have the most favorable properties. In combination, the summative advantages are worth more than any single technique alone.

Table 2.3: Comparison of methods of enhancing transdermal delivery (Kumar and Philip, 2007).

Delivery method	Low cost/ Complexity	Increased transport	Sustained delivery	No pain/ irritation
Thermal Poration	+	++	+++	+++
Iontophoresis	+++	+	+++	+++
Ultrasound	+	++	+++	+++
Electroporation	+	++	+++	++
Microneedles	+	++	+++	+++
Jet injection	+	+++	+	+
Chemical enhancers	+	+++	++	+

*+ limited, ++ moderate, +++ good

2.4.1. Iontophoresis: Mechanism and formulation considerations

The experimental study of electro-transport or iontophoresis has a long history, and the technique has been applied in numerous clinical situations (Banga and Chien, 1993). Three types of iontophoresis units are commercially available (a) rechargeable power sources (b) line-operated units, and (c) simple battery-operated units. Iontophoresis being a non-invasive technique uses a low current ($0.5mA/cm^2$) to administer polar and charged species through the skin (Mudry *et al.*, 2007; Sieg and Wascotte, 2009).This ultimately broadens the range of transdermal administration drug candidates. Iontophoresis acts on the molecule itself, unlike other techniques of transdermal delivery enhancement and thus allows for better control of the dose applied (Sieg and Wascotte, 2009). By the process of electro-osmosis and electromigration, the permeation of neutral and charged compounds is increased by iontophoresis, offering a programmed drug delivery option. Although it has been most predominantly applied to the delivery of anti-inflammatory agents for local effects, iontophoretic methods are gaining attention in the area of pain relief for the systemic administration of minute amount of drugs in a non-invasive manner. This technique is one of the most evolved of these delivery optimization technologies and uses a small electrical current (<500 microamperes cm^{-2}) to facilitate the transfer of drugs across the skin (Singh and Maibach, 1996; Naik *et al.*, 2000). In order to facilitate drug transport through the advancement of iontophoretic systems, microneedle devices that use an array of micro needle-like structure to penetrate and thereby open pores in the SC may be used. These systems have been reported to greatly enhance the permeation of macromolecules through skin up to 100,000 fold (Chiranjib *et al.*, 2010). A large volume of literature already exists on electrophoresis in the field of transdermal and dermal drug delivery with the safe range of electric field strengths for topical application already determined (Delgado-Charro and Guy,

2001). Electro-responsive drug delivery thus seems feasible option for drug delivery, albeit a difficult option. By controlling the electric current iontophoresis may lead to the development of a new era of PCA.

Based on the principle that like charges repel and opposing charges attract drug is applied under an electrode having the same charge, and a return electrode opposite in charge to the drug is placed at a neutral site on the body surface (Banga and Chien, 1993; Sieg and Wascotte, 2009). In anodal iontophoresis, the positive active ion drug containing solution is placed under anode at the desired site while the receiving electrode, the cathode, is placed at another site. In cathodal iontophoresis, the electrodes are reversed (Sieg and Wascotte, 2009). Anodal delivery is the preferred method of drug delivery as at physiological pH, the skin carries a net negative charge, rendering it, under the imposition of an electrical field, permselective to positively charged species (Naik *et al.*, 2000). Through changes in formulation pH, alteration of the skin's charge prospectively changes the balance of electro-repulsive and electro-osmotic contributions to iontophoretic transport, which has been convincingly proven in *in vitro* systems (Merino *et al.*, 1999). Transport is not limited to molecules having a charge as the transport of uncharged or neutral molecules can also be facilitated by iontophoresis. The iontophoretic theory (Figure 2.3a) is based on the general principle of electricity which involves passing a direct electrical current through a medicated solution to facilitate the delivery of selected ions into tissues (Sieg and Wascotte, 2009). The efficiency of this iontophoretic process is dependent on: the delivery formulation composition; the permeant's valency, polarity, and ionic mobility; and the current profile (Naik *et al.*, 2000). The principal transport mechanism during iontophoresis is electromigration: where the intensity of current applied (I) is linked to the transdermal flux of ion "i" (J_i) via Faraday's law (Bajpai *et al.*, 2009):

$$J_i = \frac{t_i . I}{z_i . F}$$

Equation 2.1

Where z_i and t_i are the valence and transport number, respectively, and F is Faraday's constant. The transport number is defined as the fraction of the total charge transported by a specific ion during iontophoresis and is related to its effectiveness as a charge carrier, as well as the presence of competitor counter- and co-ions and their respective abilities to carry charge (Delgado-Charro and Guy, 2001; Kalia *et al.*, 2004).

Iontophoretic devices are generally designed to deliver therapeutically active materials in small amounts for a given time with the magnitude of current determining the number of ions

transported across the skin and thus the amount of charge generated in the circuit (Singh and Maibach, 1996; Naik *et al.*, 2000). Controlling the current ensures an efficient and controlled drug delivery method with the amount of drug compound delivered being directly proportional to the applied charge. The pH of the formulation plays a critical role in iontophoretic delivery efficiency as it impacts both the permeant's ionization state and the permselectivity of the skin which in turn determines its electrical mobility.

Other properties that influence iontophoresis include: i) the degree of skin hydration, ii) presence of chemical additives (Allenby *et al.*, 1969; Clar *et al.*, 1982) iii) pH (Allenby *et al.*, 1969), iv) electrolyte concentration (Allenby *et al.*, 1969; Clar *et al.*, 1982), v) temperature, (Allenby *et al.*, 1969; Oh *et al.*, 1993) vi) thyroid activity (Edelberg, 1972), vii) perspiration (Oh *et al.*, 1993), viii) skin disease (Clar *et al.*, 1982) , and ix) emotional state (Oh *et al.*, 1993). Decreased skin resistance often correlates with increased skin permeability (Lawler *et al.*, 1960; Allenby *et al.*, 1969; Burnette and Ongpipattanakul, 1988).

To account for the resistance of the skin being treated, iontophoretic devices operate at a constant voltage in order to vary the current. The likelihood of electric shocks is thus reduced thereby increasing patient acceptability and compliance. The significant considerations for an iontophoretic device include convenience, cost, safety, portability and reliability. In order to succeed and compete with those novel delivery methods already available on the market, the prime issues that require consideration include device safety and design, cost-effectiveness, efficacy, and ease of handling (Brown *et al.*, 2006). Iontophoretic delivery seems a promising system for future developments as the systemic adverse effects of drugs are significantly reduced since only small amounts of drug are delivered; while locally, a relatively high concentration is administered, possibly achieving the maximum benefit. Patient acceptance is generally remarkable, and the phobia associated with injections is eliminated. The possibilities for the systemic control of transdermal drug delivery are greater with iontophoresis than with passive diffusion. Iontophoretic delivery does however have some disadvantages: only hydrophilic drugs (<10 000Mw) are amenable to deliver with some problems of burning, along with itching and redness at the administration site (Wang *et al.*, 2003).

The first iontophoretic system to be approved by the FDA as a physical medicine was the Phoresor™ device (Iomed Inc.) in the late 1970s (Fischer, 2005). As an external stimulus, the use of an electric field has been employed successfully to enhance the amount of drug released. To name a few drugs and analgesics: atenolol hydrochloride (Jacobsen, 2001), buprenorphine (Fang *et al.*, 2002) and diclofenac (Hui *et al.*, 2001) have been investigated

for iontophoretic delivery. E-trans® (Alza Corporation) is another electro-transport system that utilizes a low-power electric current to control drug administration of fentanyl through intact skin. These systems are currently being developed to provide patient-controlled pulsatile delivery and continuous drug delivery (Verma and Garg, 2001). Other iontophoretic technologies that have been marketed include Lectro Patch® (General Medical Company), Accuresis™ (Acient Inc.), Phoresor® (Iomed Inc.), Lidosite ® (Vyteris Inc.), Acyclovir Direct® (BioPhoretic Systems), Iontopatch ® (Birch Point Medical Inc.), Glucowatch® (Cygnus Inc.), Iontocaine® (Iomed Inc.). Some of the current iontophoretic and sonophoretic devices under development are depicted in Figure 2.3 (b) in addition to a microneedle device.
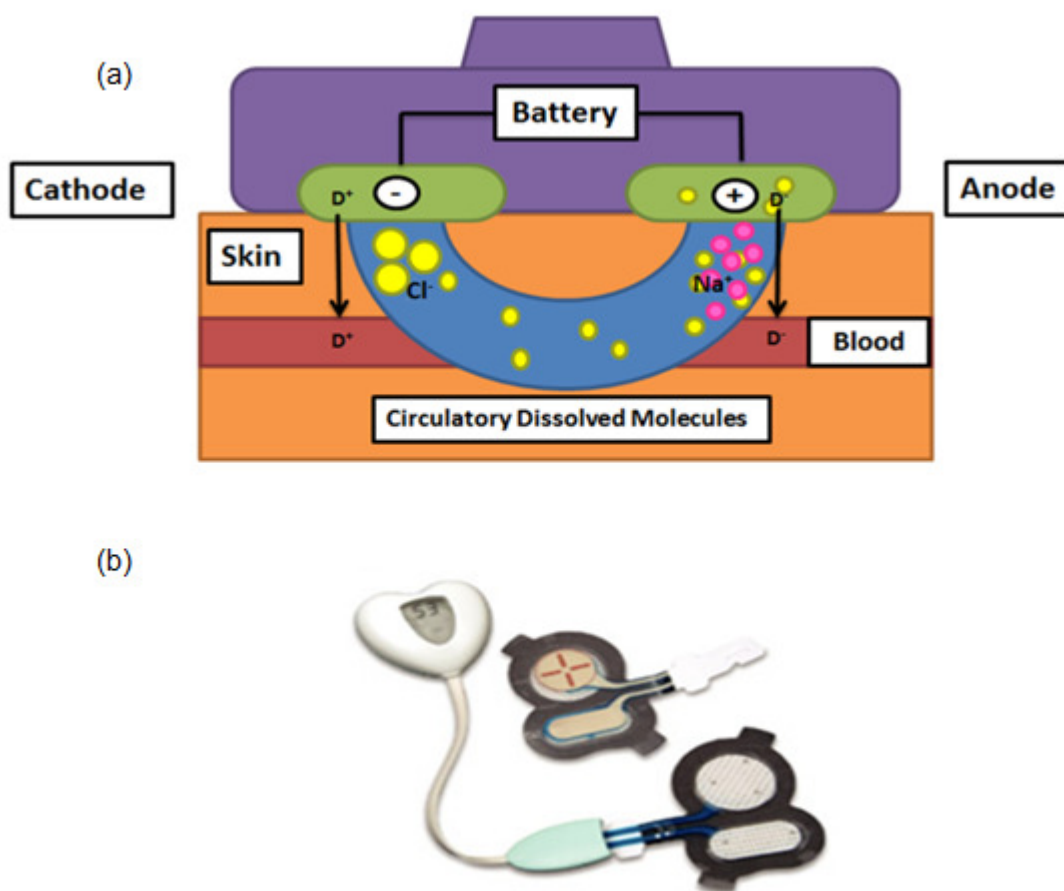
Figure 2.3: (a) Schematic of an iontophoretic device. (b) An iontophoresis device under development at Vyteris (Pty) Ltd. (New Jersey).

2.4.2. Microneedle arrays: Methods of drug delivery and current challenges

In order to provide optimal delivery of analgesic medication, the existing iontophoretic patches alone are insufficient. The use of MNAs in combination with such a patch will provide optimal delivery (Henry *et al.*, 1998; Barry and Williams, 2003; Tao and Desai, 2003; Doukas, 2004). To date, no such device has been developed.

One of the earliest patents filed for a percutaneous drug delivery device was based on this method of microneedle arrays (Gerstel and Place, 1976). Since microneedles enable painless insertion, they allow for increased control over drug dosage, cause minimal tissue damage, and are independent of drug concentration and composition, they can be deemed as properties of significance when compared with commercially available hypodermic needles (Bronaugh and Maibach, 1999; Barry and Williams, 2003). It is thus not surprising that there is an extensive interest in microneedles, as indicated by the extensive patent activity and the literature available the in the field (Doukas, 2004; Langer, 2004; Verbaan *et al.*, 2007; Vandervoort and Ludwig, 2008).

Microneedles are an attractive candidate as a physical enhancer to administer drugs throughout the skin as a function of their inherently promising and unique release of drugs in a minimally invasive manner (Santell, 2005). Microfabrication techniques for the production of silicon, metal, glass and polymer MNAs with micrometer dimensions have been described in a plethora of geometries (Figure 2.4; McAllister *et al.*, 2003; Teo *et al.*, 2005) and in terms of processing, there are many advantages: thousands of needles can be fabricated on a single silicon substrate wafer due to their small size, leading to worthy reproducibility and high accuracy, and a modest production cost, which ultimately reduces costs to the patient.
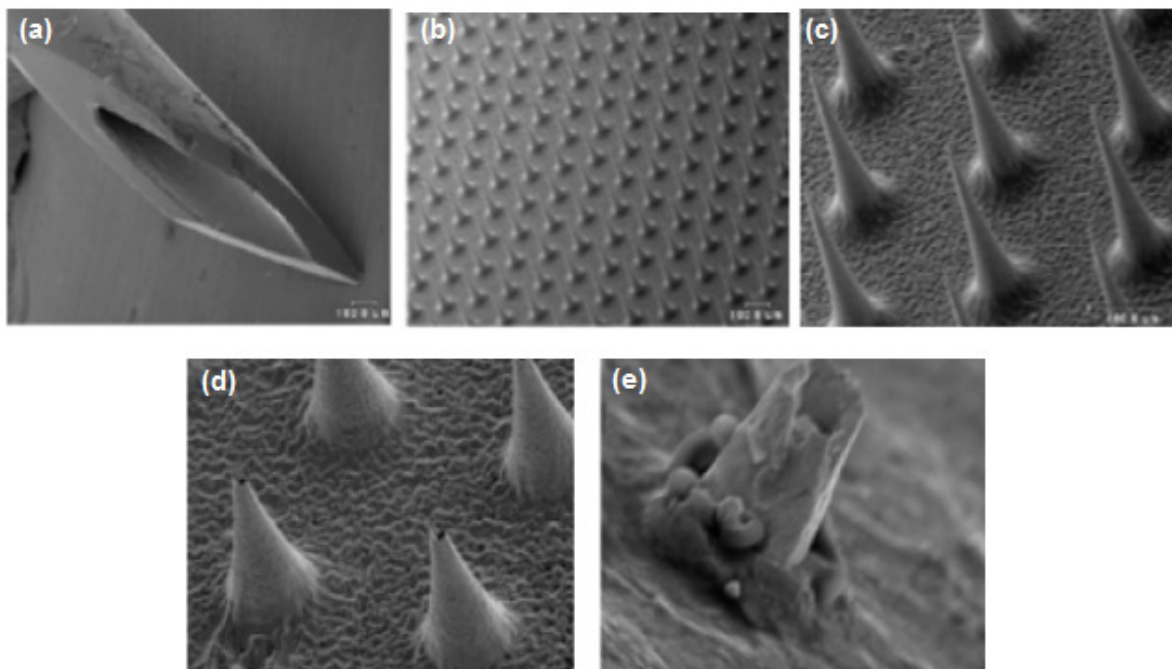
Figure 2.4: Scanning electron micrographs of various needle types (a) A 26-guage hypodermic needle (b) A silicon microneedle array at the same magnification as the 26-guage hypodermic needle (c) A silicon microneedle array at a higher magnification (d) A hollow metal microneedle (e) A tip of a hollow metal microneedle penetrating through the human epidermis (Hui *et al.*, 2001).

2.4.2.1. Comparison between microneedles and hypodermic needles as methods of delivery

Even though hypodermic needles are the norm for parental delivery, there are several disadvantages relating to their use (Birchall, 2006; Giudice and Campbell, 2006; Prausnitz and Langer, 2008):

- pain and needle phobia, leading to poor patient compliance
- if re-used, possibility of disease transmission
- administration requires trained personnel
- erratic delivery
- rapid degradation or poor absorption, leading to poor bioavailability and thus requiring a higher drug amount to achieve the therapeutic dose
- the possibility of needle-stick injuries
- potentially dangerous biological waste and sharps disposal hazard
- possibility of hematoma formation or bleeding

Besides the aspect of painless delivery, numerous other advantages of microneedles are presented in reference to the existing hypodermic injection in existing literature, including: minimal skin trauma following microneedle insertion (Bal *et al.*, 2008); no bleeding or introduction of pathogens associated with microneedle use (Matriano *et al.*, 2002; Martanto *et al.*, 2006; Gill and Prausnitz, 2007; Prausnitz *et al.*, 2009); appropriateness and a comparatively effortless application or ease of use for non-skilled and/or self-administration (Haq *et al.*, 2009; Kim *et al.*, 2009, Davidson *et al.*, 2008); reduced risk of needle-stick injury and cross-contamination (Haq *et al.*, 2009) as well as the increased ease in disposal (Prausnitz *et al.*, 2009).

Transdermal delivery facilitated by microneedles may be summarized into four methods. (Prausnitz, 2004; Gill and Prausnitz, 2007; Arora *et al.*, 2008; Davidson *et al.*, 2008; Sachdeva and Banga, 2011; Bariya *et al.*, 2012; Kuila *et al.*, 2012; van der Maaden *et al.*, 2012). Hailed as a breakthrough in transdermal delivery, these four methods: the (i) poke and flow, (ii) poke and patch, (iii) poke and release, and (iv) coat and poke, have key features that may influence selection and suitable use (Table 2.4).

Table 2.4: Features of microneedle facilitated transdermal delivery methods (Kuila *et al.*, 2012).

Transdermal Delivery Method	Type of Microneedle Used	Rate- Limiting Step	Advantages	Disadvantages
Poke and flow	Hollow	• Pressure resistance at high volumes • Solvent flow through bore	• Allows for accurate dosing • Greater volumes may be delivered • Drug delivery may regulated • Drug reformulation limited/not needed	• Bore may become blocked by tissue/drug resulting in leakage • Device design more complex
Poke and patch	Solid	• Diffusion	• Extended release • Simple process • No pump required	• Administration requires 2 steps • Low amount of drug delivered • Drug reformulation may be required • Dosing is not precise
Poke and release	Solid	• Rate of dissolution (dissolving microneedle) • Rate of diffusion (porous microneedle)	• Allows for precise dosing • No pump/patch required • No waste produced • Small amount of drug may be lost during production	• Drug reformulation may be required • Questionable strength • Reduced penetration ability • Low doses • Drug reformulation required
Coat and poke	Solid	• Surface coating detachment possible • Dissolution rate for thicker coatings	• No pump/patch required • Allows for precise dosing • Retained strength after coating	• Low doses • Drug reformulation required • Reduced penetration ability • Efficient coating procedure required

2.4.2.2. Microneedles: Advancing the hypodermic needle

In certain cases, diffusion alone is an inadequate mechanism to penetrate the SC preventing optimal drug delivery and numerous procedures have been developed to aid drug delivery in such instances. It must be stated that diffusion is not the only factor controlling delivery through the SC: permeability; aqueous/lipid solubility ratio; and molecular size are critical as well in facilitating permeation (Raphael *et al.*, 2013). Martanto and co-workers (2006) have tested the hypothesis of compressed dermal tissue trapped within a hollow microneedle after insertion offering resistance to flow through the microneedle and into the skin. Results have concluded that skin infusion can be increased by retracting the microneedle.

Although for many years, hypodermic needles have been synonymous with the gold standard for drug delivery; recent biotechnological advances are making their limitations increasingly apparent (McAllister *et al.*, 2003). As devices capable of transporting nano-sized molecules are available, the larger length scales of these needles are often unnecessary, causing pain and limit targeted delivery.

The SC prevents the passage of micro-organisms through the skin, and although microneedle puncture breaches this epidermal layer, this technology causing skin or systemic infection has not been reported on (Prausnitz, 2004). Donnelly and co-workers (2009) have investigated the ability of Gram positive (*S. epidermidis*), Gram negative (*P. aeruginosa*) and fungi (*C. albicans*) to transverse the SC as mimicked by Silescol®. Results from the study have concluded that microneedles allow for significantly less microbial penetration as compared to the hypodermic syringe, resulting in an added advantage to the use of microneedles.

Studies by Baek and co-workers (2011) and Donnelly and co-workers (2013) utilizing various micro-organisms to assess microneedle safety were conducted. The studies have concluded that skin treated with microneedles is not susceptible to micro-organisms penetration. A primary skin irritation test using the Draize dermal scoring criteria after microneedle penetration was conducted by Liu and co-workers (2014), the slight redness observed was attributed to physical compression of the microneedles and it was concluded that irritation and skin damage caused by microneedle were insignificant.

Since transcutaneous immunization is limited by poor macromolecular skin permeation, as a vaccination tool, microneedle arrays could offer easier and painless administration, in addition to reducing vaccination costs (Bal *et al.*, 2008; Ding *et al.*, 2009; Matsuo *et al.*, 2012; Vrdoljak *et al.*, 2012). In addition, vaccine delivery via the skin or via other mucosal

membranes may improve effectiveness and result in better cellular immunity by eliciting immune responses at the virus entry site. Research has suggested that the transport mechanism appears non-dependent on cellular uptake functions, allowing for physical methods to be applied to all cell types at all stages of the cell cycle, resulting in a biologically nontoxic and minimally invasive process (Chen *et al.*, 2009).

The perceived disadvantages that may occur with the use of microneedles include the possibility of inflammation in the surrounding tissues, and the fact that there is a certain likelihood of the microneedles to break off and be left under the skin. Due to the small size of microneedles the latter may occur unnoticed causing unforeseeable adverse reaction.

2.4.2.3. Types of microneedles and their methods of use

Microneedles differ in design and composition, currently, four distinct types of microneedles exist (Figure 2.5): solid microneedles often used to pretreat the skin prior to the administration of bioactives; drug-coated solid microneedles for drug dissolution in the skin; hollow microneedles for injections; and dissolving microneedles prepared from a polymer in which the drug or vaccine is embedded in the polymer matrix for the controlled or rapid release in the skin (Sivamani *et al.*, 2007; Gratieri *et al.*, 2013).
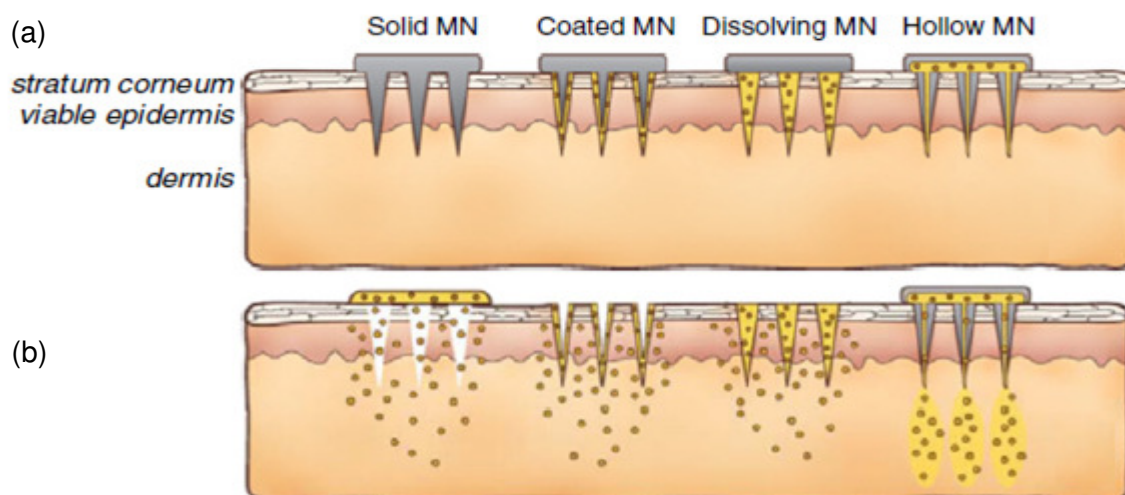
Figure 2.5: (a) Types and (b) methods of drug delivery to the skin using microneedles (Kim *et al.*, 2012).

Since microneedles are specifically designed and developed according to their use and needs, these approaches have key features that may influence selection and suitable use. Although not exhaustive, Table 2.5 summarizes some of the research on microneedles comparing the results of the above delivery approaches to an appropriate control experiment utilizing the gold standard hypodermic needle.

Table 2.5: Recent research on microneedle-assisted vs. hypodermic needle delivery claiming improved delivery performance.

Paper	Research Area	Drug/Compound	Reference
Drawing lithography for microneedles: A review of fundamentals and biomedical Applications	A negative control of p2CMVmIL-12 V (20mg) was released into the skin using the dissolving microneedle without electric pulses. The same electric pulses were applied by electrode tweezers after intra-tumoral injection of p2CMVmIL-12 using a hypodermic needle (20mg/30mL in D.I.) and served as a positive control. Subcutaneous tumoral expression of IL-12 was significantly greater in mice transferred with p2CMVmIL-12 by the HEM and the positive control compared to the 2 negative controls (cutaneous control pCI plasmid transfer by the HEM, and p2CMVmIL-12 release using a dissolving microneedle without electric pulses).	• p2CMVmIL-12	• Lee and Jung, 2012
Separable arrowhead microneedles	The sharp-tipped polymer arrowheads encapsulating drug separate from their metal shafts and remain embedded in the skin for subsequent dissolution and drug release. Arrowheads were shown to separate in skin within 1s and administer over 80% of encapsulated compounds. Thus, the time required to administer drug using arrowhead microneedles can be comparable to hypodermic needles.	• sulforhodamine B • inactivated influenza virus	• Chu and Prausnitz,2011
Effect of delivery parameters on immunization to ovalbumin following intracutaneous administration by a coated microneedle array patch system	Different routes of administration were compared. As per the results, it was found that at low dose of antigen delivered (1µg), the immune response, as measured by specific antibody titers, was most efficient following microneedle and ID administration as compared to SC or IM administration. The immune response was more than one order of magnitude higher following microneedle-based administration versus SC delivery, and about two orders of magnitude greater as compared to IM delivery.	• antigen OVA	• Widera *et al.*, 2006 • Matriano *et al.*, 2002

Paper	Research Area	Drug/Compound	Reference
Transdermal delivery of insulin using microneedles *in vivo*	This pharmacodynamic response of the microneedles was similar to that seen following subcutaneous hypodermic injection of 50mU of insulin and less than that seen for injection of 500mU of insulin, which were used as positive controls. The study concluded that the solid metal microneedles are capable of increasing transdermal insulin delivery and lowering blood glucose levels by as much as 80% in diabetic hairless rats *in vivo*.	• Insulin	• Martanto *et al.*, 2004
Transdermal delivery of desmopressin using a coated microneedle array system	Pharmacologically relevant amounts of desmopressin were delivered after 5min. bioavailibility (85%) showed acceptable variability (30%). Immunoreactive serum desmopressin reached peak levels after T_{max} of 60 minutes. Elimination kinetics were similar to IV delivery, suggesting the absence of a skin depot. Additionally, the patches were well tolerated and are a safe and efficient alternative to current available administration routes.	• Desmopressin	• Cormier *et al.*, 2004

2.4.2.4. Advancing methods of delivery using microneedles

The earlier produced microneedles used for drug delivery were made from silicon wafers through deep reactive ion etching and photolithography (Henry *et al.*, 1998; Smart and Subramanian, 2000, Gardeniers *et al.*, 2003). Microfabrication techniques for the production of silicon, metal, glass and polymer MNAs with micrometer dimensions have been described in a plethora of geometries as it provided unique new design opportunities to lithographically produced polymeric microneedles (McAllister *et al.*, 2003; Teo *et al.*, 2005; Davis *et al.*, 2005; Park *et al.*, 2006, Lüttge *et al.*, 2007). By fabricating these needles on an industrial-scale silicon substrate, it allows for thousands of needles to occupy on a single wafer, leading to good reproducibility, high accuracy, and a moderate fabrication cost, which in turn reduce costs to the patient.

While the first microneedles were fabricated solely out of silicon by lithography followed by wet and dry etching (based on the utilization of an alkaline solution and reactive ion etching with some sort of mask, respectively), divergent technologies today employ various other materials including polymer, metal, ceramic and glass, providing microneedles of many shapes and sizes, according to various applications (Kim *et al.*, 2012). Interestingly, Bal and co-workers (2010) have proved that microneedle shape and speed application both effect the depth and shape of formed conduits using fluorescein in human subjects. Materials used in the development of solid microneedles include next to silicon, titanium, stainless steel and nickel-iron, glass and ceramics (Martanto *et al.*, 2004; Doddaballapur, 2009; Li *et al.*, 2010, Bystrova and Lüttge, 2011). Water soluble polymers and engineering plastics such as carboxymethyl-cellulose, polylactic-coglycolic acid and polycarbonate respectively are used in the fabrication of polymeric needles (Arora *et al.*, 2008).

Lithography as well as wet and dry etching techniques are adapted from Microelectromechanical systems (MEMS) technology. In addition to the on-going developments in microfabrication using silicon, glass and metal; also more advanced microscale polymeric drug delivery devices have become available (Ochoa *et al.*, 2012). These techniques comprise of three categories divided by the manner in which the polymeric material is processed *(*Becker and Gärtner, 2008):

- Photolithography: the polymerization of a substance constructs and defines the desired structures (Figure 2.6)
- Replica moulding: a polymer is injected into or cast onto a hard or soft master mould which is fabricated using MEMS microfabrication techniques

- Polymer micromachining: micromilling or ablation is used to modify a slab of the material to achieve the anticipated structure
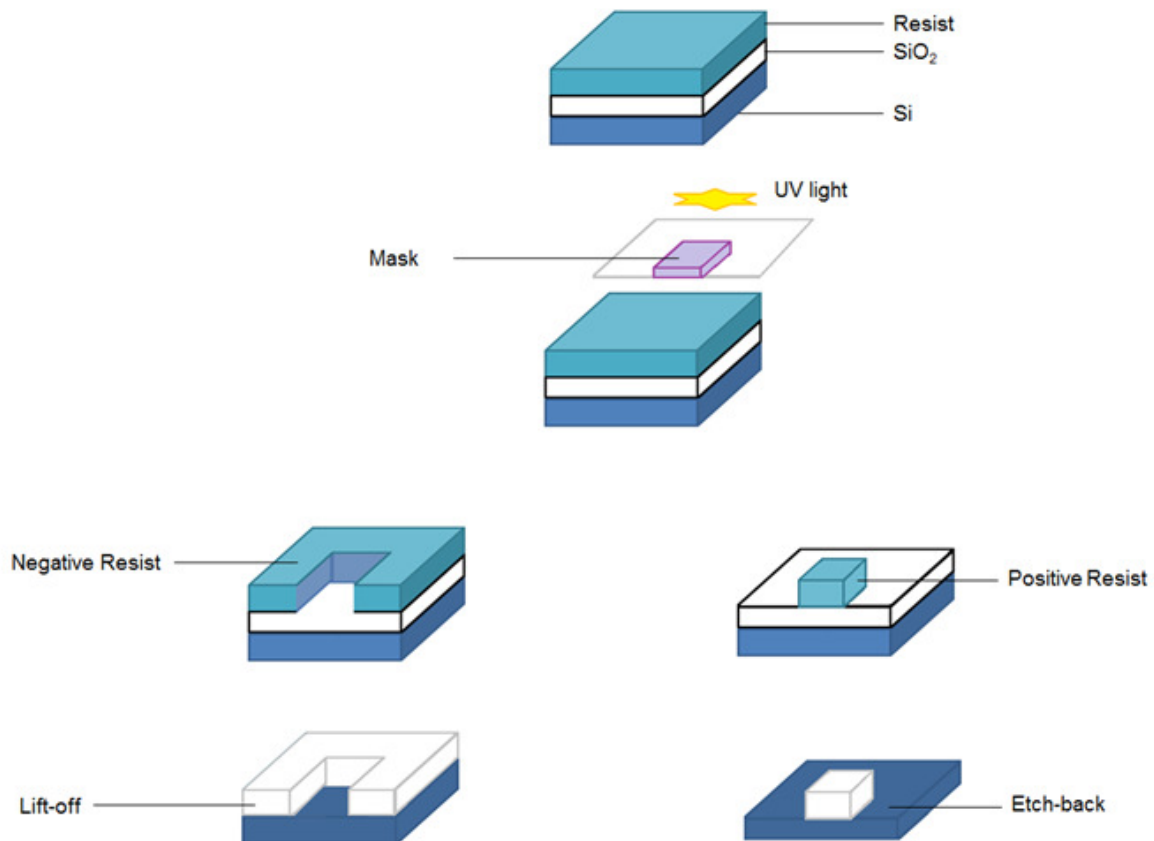
Figure 2.6: Schematic highlighting silicon wafer photolithographic processing. A 'mask' is a square glass plate with a patterned emulsion of metal film on one side. The mask is aligned with the wafer, so that the pattern can be transferred onto the wafer surface. Each mask must be aligned to the previous one. The photoresist is exposed through the pattern on the mask with a high intensity ultraviolet light.

The most commonly used techniques in microneedle manufacture are: wet and dry etching (Jung *et al.*, 2008), laser cutting (Aoyagi *et al.*, 2007), micromoulding (Park *et al.*, 2007) and lithography (Perennes *et al.*, 2006).

2.4.2.4.1. Separable arrowhead microneedles

Chu and Prausnitz (2011) developed microneedles with a separable arrowhead (Figure 2.7). The associated disadvantages with biodegradable microneedle are overcome by the increased mechanical strength associated with metal microneedles. In addition, the issue of biohazardous sharp waste disposal is overcome by the microneedles' dissolving component. Photolithography and moulding techniques was used to prepare a polydimethyl siloxane (PDMS) mould to generate a 10×10 array of pyramid-shaped microneedle cavities, which

were eventually utilized in the formation of the microneedle arrowheads (Choi *et al.*, 2006). Dissolution and drug release was successful as the sharp-tipped polymer arrowheads remained embedded in the skin. *Ex vivo* testing employing human cadaver skin used to evaluate the effectiveness of the microneedles shows that cavities formed in shape similar to that of the arrowheads. Furthermore, local release of the desired therapeutic agent from the arrowheads was achieved.
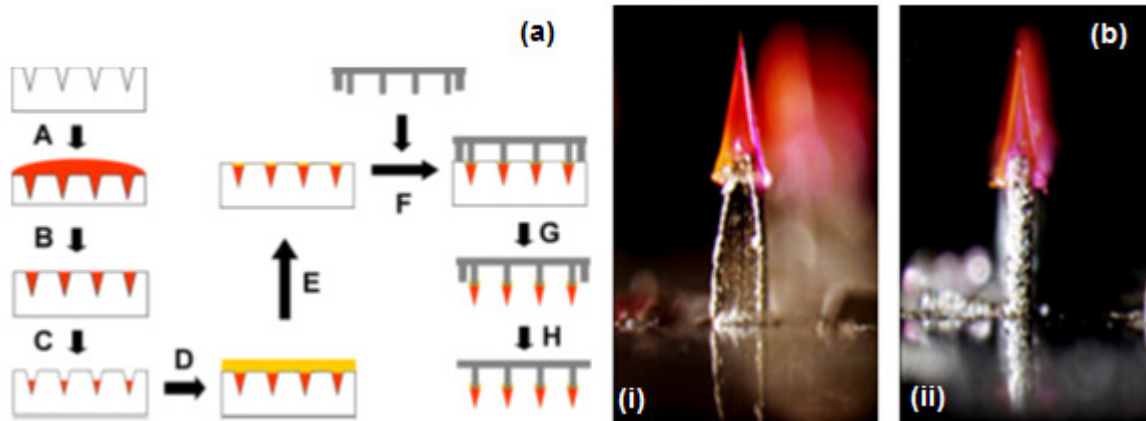
Figure 2.7: (a) Schematic diagram of separable arrowhead microneedle fabrication process. (A) A drug solution was applied to a polydimethyl siloxane micromould under vacuum. (B) Excess drug solution on the mould surface was removed and saved for re-use. (C) The drug solution loaded in the mould cavities was dried under centrifugation. (D) A polymer solution was cast into the mould under vacuum. (E) Excess polymer solution on the mould surface was spun off by centrifugation. (F) Blunt metal shafts prepared by laser-cutting were aligned to the mould cavities. (G) The whole device was air-dried at room temperature or freeze-dried overnight. After drying, the dried, drug-filled polymer arrowheads connected to the metal shafts were removed from the mould. (H) Metal stoppers along the periphery of the patch were bent down. (b) Individual needles are shown from the front (i) and side (ii) (Chu and Prausnitz, 2011).

2.4.2.4.2. Dissolvable microneedles by micromoulding

In order to reduce biohazardous sharps waste, dissolvable microneedles have been developed. These microneedles undergo complete dissolution in the skin and are typically made primarily of water-soluble, inert, safe materials, such as sugars and polymers that dissolve once exposed to the skin (Kim *et al.*, 2012). The application of hollow microneedles does provide the advantage of acting as a physical enhancer for transdermal drug delivery. Nonetheless, the application is limited as its associated risk is needle breakage for the injection of a drug solution (Lee *et al.*, 2012). Thus, dissolving microneedles, intended for the painless transdermal release of encapsulated pharmaceutical agents after dermal insertion, were developed as a solution to the safety issue (Lee and Jung, 2012).

Dissolvable microneedles mainly deploy PDMS micromoulds similar as for the ceramic microneedles as previously mentioned, however they could be made from other materials or by other methods of manufacture as well, for example. The micromoulds are filled by solvent casting, where a liquefied polymer fills the mould and solidifies in the mould by solvent evaporation. In case where a liquid monomer is used, in-situ polymerization is used. Drawing methods of fabrication using polymer/sugar solutions and polymer/sugar melts have also been developed (Kim *et al.*, 2012). Various materials including dextran (Fukushima *et al.*, 2011), carboxymethyl cellulose (Raphael *et al.*, 2012), dextrin (Sullivan *et al.*, 2008), polyvinyl pyrrolidine (Sullivan *et al.*, 2008), chondroitin sulphate (Ito *et al.*, 2010), polyvinyl alcohol (Wendorf *et al.*, 2011), fibroin (You *et al.*, 2011), poly(lactic-co-glycolic) acid (Park *et al.*, 2006) and sugars (Martin *et al.*, 2012) have been dissolved in water. If the solutions or in some specific cases melts are filled into the mould, the additional use of centrifugal force and/or vacuum is sometimes warranted before drying.

Park and co-workers (2005) have fabricated biodegradable polymer microneedles based on micromoulding using polyurethane master structures or high aspect-ratio SU-8 epoxy photoresist to form PDMS moulds (Figure 2.8). To improve safety and manufacturability, the polymers used both had appreciable biocompatible and biodegradable properties. An advanced fabrication method was therefore developed using an in situ lens-based lithographic approach in which tapered-cone microneedle were produced in addition to the adaption of MEM masking and etching to produce bevelled- and chisel-tip microneedles. The permeability of human cadaver skin to bovine serum albumin and calcein were shown to increase up to three orders of magnitude. The geometry of the formulated microneedles has been shown by Park and co-workers (2005) to have an effect on the release kinetics of the compounds depending upon the geometry employed. By increasing skin permeability by at least two to three orders of magnitude, the polymer microneedles described therefore sought to overcome the current limitations associated with the use of silicon and metal.

(a)

A. Coating of SU-8

Silicon substrate

UV 365 nm

SU-8 (Epoxy)

B. UV exposure, and development

C. Sacrificial polymer layer between SU-8 cylinders

Cross-linked SU-8 cylindrical structures

D. Metal deposition

E. Second mask patterning

F. Ion etching

G. Removal of sacrificial layer

Master structure

(b)

Silicon

A. Create Si₃N₄ layer

B. Photolithography and reactive ion etching

C. KOH wet etching

D. SU-8 photolithography

E. PDMS filling

F. Reactive ion etching

G. Preparing master structure from micromold

Figure 2.8: Schematic of processes to fabricate (a) beveled-tip microneedles (b) chisel-tip microneedles (Park *et al.*, 2005).

Lee and co-workers (2011) also used drawing lithography as the technique for the fabrication of dissolving microneedles containing maltose as the structural matrix (Figure 2.9). Drawing lithography uses extensional deformation in which 2D viscous polymer materials are directly extended to a 3D polymer structure whilst utilizing the in the glass transition history of the material (Lee and Jung, 2012). Maltose was chosen as the triple-state (in liquid, glassy, solid) as the viscosity was able to be easily regulated by temperature manipulation (Lee *et al.*, 2011). Sulforhodamine B was encapsulated into the prepared dissolving microneedles and the patch was inserted into the shaved dorsal skin of brown guinea pigs. The cross-sectional image of the penetration site confirmed that no microneedle breakage occurred and that the prepared microneedles were successfully applied.
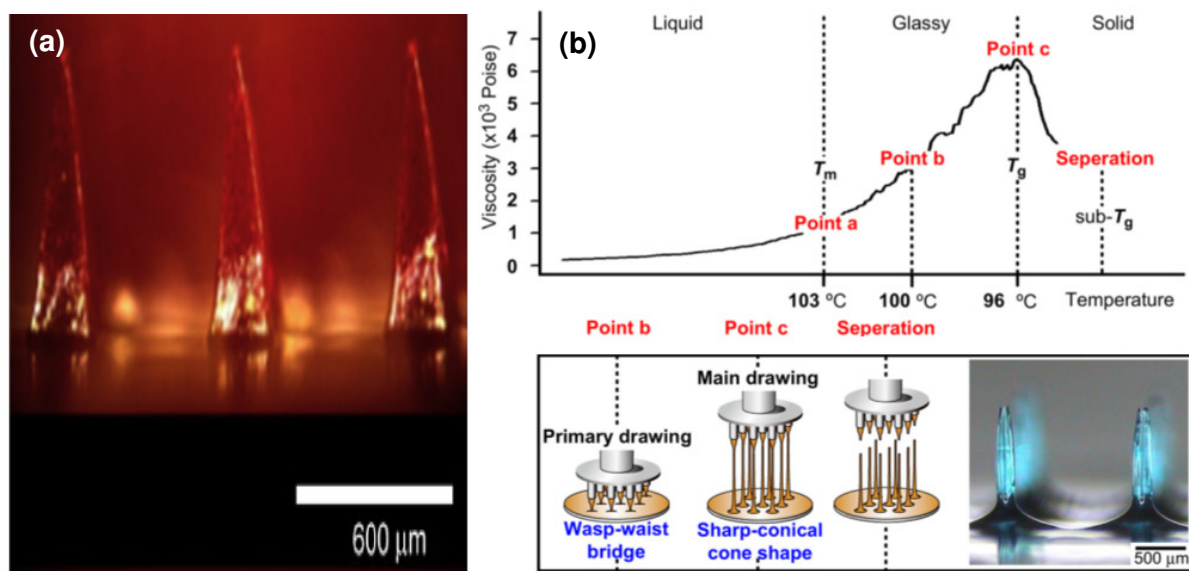
Figure 2.9: (a) The dissolving microneedle as developed by Lee and co-workers (2008) (b) Sharp-conical cone shapes were fabricated by stepwise controlled drawing, primary drawing at drawing point b and main drawing of drawing point c (Lee *et al.*, 2011).

2.4.2.4.3. Hybrid electro-microneedles

Lee and Jung (2012) discussed a specific drawing lithography as a unique additive process to fabricate microneedles (Figure 2.10) combining drawing lithography with a metal base plate. A noteworthy end-product by this type of fabrication is a hybrid electro-microneedle (HEM). Following insertion of the microneedle, the HEM's electrode facilitates cutaneous release from the encapsulated reservoir by generating electric field pulses following a poke and controlled release approach to transdermal delivery. The Hybrid electro-microneedle is produced in a manner similar to that in Figure 2.9b, the only difference is that the needle is produced on top of an electrode. To date this type of microneedles have not been further developed.
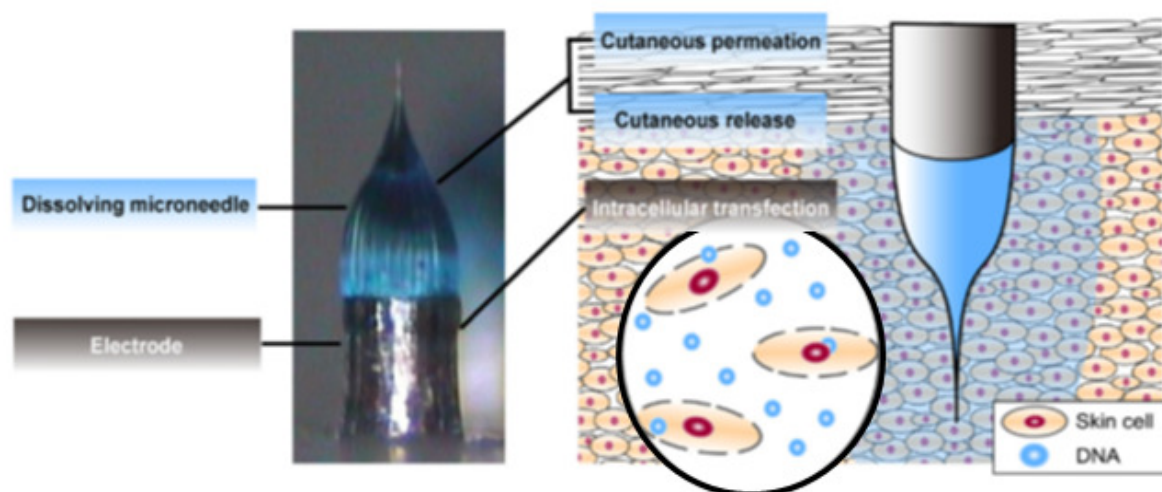
Figure 2.10: Schematic of the monolithic hybrid assembly of a dissolving microneedle and an electrode to produce a hybrid electro-microneedle and the stepwise-aligned cutaneous permeation, cutaneous release, and intracellular transfection using the HEM (Lee and Jung, 2012).

Lee and co-workers (2008) purport that microneedles intended for dissolution and safe use *in vivo* should be guided by certain criteria:

- Sufficient mechanical strength allowing for enhanced skin insertion
- Controlled drug release profiles for bolus or sustained delivery
- The use of gentle fabrication techniques to avoid damaging of sensitive biomolecules
- Enhanced rapid dissolution of prepared microneedles formulated with the use of safe, non-toxic materials

Further research conducted by Lee and co-workers (2008), describes a microneedle design consisting of encapsulated molecules within microneedle shafts which leave no sharp biohazardous medical waste upon exhaustion of drug release. Their fabrication process for the dissolving needles was developed by casting a viscous aqueous solution into a micro-fabricated mould containing biocompatible amylopectin or carboxymethylcellulose formulations during centrifugation. Micromoulds were fabricated using moulding processes and photolithography using a master mould that was structured in SU-8 photoresist. The microneedle matrix material was prepared from a viscous hydrogel solution comprising of amylopectin, bovine serum and ultra-low viscosity carboxymethylcellulose. The microneedle shafts were selectively loaded, providing bolus release of drug upon microneedle dissolution inside porcine cadaver skin.

2.4.2.4.4. Droplet-born air blowing

A method of microneedle fabrication has been proposed by Kim and co-workers (2013) which has the added advantage of controlling the loaded drug amount without significant drug loss. Conventional methods of fabrication methods have led to inactivity of drug due to UV assisted fabrication and heat. The DAB method (Figure 2.11), in which the polymer droplet is shaped to the microneedle via air blowing, allows for gentle fabrication conditions without the use of UV irradiation or heat. In addition, by utilizing a single polymer drop per microneedle allows direct control over the droplet size and concentration and thus for drug loading without drug loss. The process takes approximately 10 minutes and has been used to fabricate insulin loaded dissolving microneedles which have successfully reduced blood glucose levels after application to diabetic mice (Kim *et al.*, 2013). Liu and co-workers (2012) have further developed insulin delivery through the utilization of insulin-loaded microneedles fabricated from Hyaluronic acid. The microneedles were successful in systemic delivery avoiding serious skin damage.
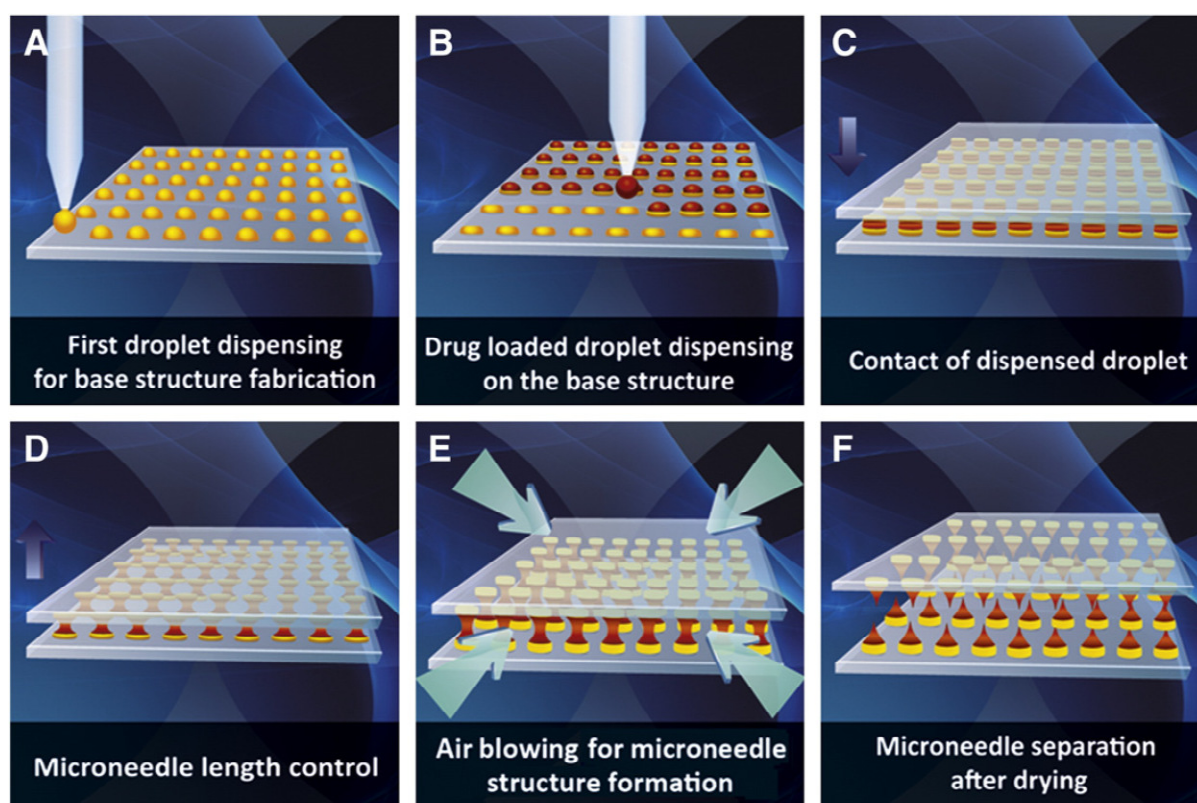
Figure 2.11: Schematic illustration of dissolving microneedle fabrication via droplet-born air blowing method. (A) Biopolymer dispensing on the flat surface for base structure fabrication. (B) Dispensing of drug-containing droplet over the base structure. (C) Contact of dispensed droplet by downward movement of upperplate. (D) Control of microneedle length. (E) Air blowing-mediated solidification of droplet to shape microneedle structure. (F) Separation of two plates producing dissolving microneedle arrays on upper and lower plates (Kim *et al.*, 2013).

2.4.2.4.5. Layer-by-layer assembly onto microneedles for vaccine delivery

Recently, Layer-by-layer (LbL) assembly has been gaining interest in vaccine delivery. This highly versatile deposition process was first suggested by Iler (1966) and Kirkland (1956) and relies on the alternate deposition of interacting species on a substrate with an intervening rinsing step following each deposition (Ariga *et al.*, 2014). DeMuth and co-workers (2012) have proven the application of poly(lactide-co-glycolide) (PLGA) microneedle arrays on mice, coated with multilayer films via LbL assembly of a biodegradable cationic poly(β-amino ester) (PBAE) and negatively charged interbilayer-crosslinked multilamellar lipid vesicles (ICMV) loaded with the protein antigen ovalbumin (OVA) and the molecular adjuvant monophosphoryl lipid A, were shown to rapidly be transferred from microneedle surfaces into the tissue within 5 minutes. In addition, enhanced DNA vaccination using the LbL polymer multilayer method was achieved by DeMuth and co-workers (DeMuth *et al.*, 2013)], utilizing rapid implantation of vaccine-loaded polymer films carrying biodegradable polycations, immune-stimulatory RNA and DNA, and into the epidermis with microneedles coated with releasable polyelectrolyte LbL multilayers. The advantages of using such method to enhance vaccine delivery allows for less costly but more effective distribution and vaccine storage due to the fact that the multilayer stabilized formulations can be stored easily without refrigeration until rehydration upon microneedle insertion into the target tissue.

2.4.2.5. Commercialization of microneedle transdermal delivery systems

Due to the limitations of other transdermal systems, the search for novel, more effective ways to administer potentially significant therapeutic compounds has resulted in the rapid movement of microneedle applications to commercialization. While other active transdermal systems exist, the efficiency of biopharmaceutical delivery is compromised and delivery can be burdensome to the patient. In the scientific literature, generally, microneedles have proven to be an efficient delivery system both in the delivery of drugs and other hormones and compounds. Currently, several systems employing microneedles are under development at a variety of commercial players, such as Microstructured Transdermal System (3M), Microinfusor (BD), Macroflux® (Alza), Microneedle Therapy System (MTS Roller™; Clinical Resolution Lab) and, Micro-trans™ and h-patch™ (Valeritas) and already were included in clinical trial phase testing. The MicronJet, is the most advanced hollow microneedle device currently available, developed by NanoPass Technologies, studies have demonstrated equivalent or superior immunogenicity to standard delivery using only 20% of the flu vaccine dose. In addition, Intanza® was the first influenza vaccine administered intradermally by micro-injection and was produced by Sanofi Pasteur MSD Limited (Figure 2.12).
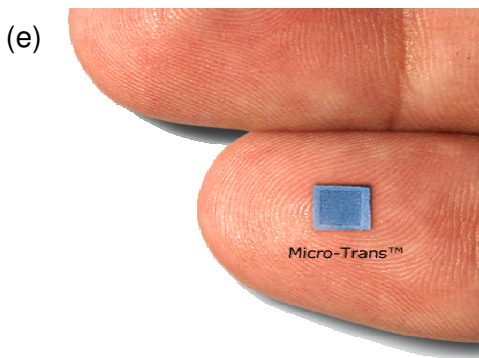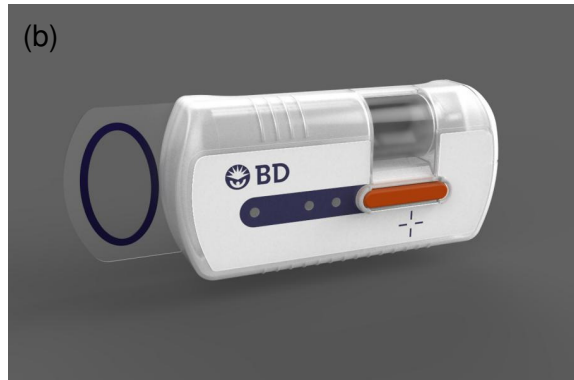
Figure 2.12: Current microneedle devices. (a) Microstructured Transdermal System (MTS) (b) Microinfusor (c) Macroflux® (d) Microneedle Therapy System (e) Micro-trans™ (f) h-patch™ (g) MicronJet (h) Intanza®.

The 3M MT system allows for the improved delivery efficiency of some drugs and vaccines thereby resulting in quicker onset of action, the system has the potential to generate a unique pharmacokinetic profile. Skin punch biopsies of porcine skin concluded that 3M's MTS can be used to provide rapid delivery of lidocaine for up to 90 minutes (Zhang *et al*., 2012).

The Microinfusor, developed by Becton Dickinson (BD) Technologies is a micro-needle containing drug delivery device capable of facilitating intradermal injections. Having a capacity of 0.2 to 15 mL, a wide range of therapeutic drugs can be delivered subcutaneously in a time ranging from a few seconds to several minutes. The hands-free system is designed for the automated delivery of high volume and/or highly viscous biotech drugs in clinical settings or at home. Preclinical studies on the Microinfusor have exhibited the successful intradermal delivery of an influenza vaccine with the same effectiveness of a conventional intramuscular injection (Alarcon *et al*., 2007).

Alza/Johnson & Johnson has developed Macroflux$^®$ for the enhanced delivery of biopharmaceuticals in a controlled, reproducible manner which ultimately improves bioavailability and efficacy without significant discomfort for the patient. Macroflux$^®$ technology involves use of a drug-coated titanium microprojection array covering an area of 8 cm^2 containing approximately 300 microprojections/cm^2. The drug-coated microprojections were shown to penetrate through the SC releasing drug into the microcapillaries (Ameri *et al*., 2006). According to Matriano and co-workers (2002), studies demonstrated that the patch allows for reproducible control of skin penetration depth and penetrated uniformly across the entire treated skin surface area to an average depth of 100µm. Control of intracutaneous OVA delivery by the microprojection array was achieved by varying the coating solution concentration, wearing time, and system size.

The patented MTS Roller™ is a FDA-approved supplemental medical tool. Developed for cosmetic purposes, the device is ideal for non-ablative and non-surgical treatment of various skin conditions such as hyperpigmentation, aging and scarring (acne, surgical). Clinical studies have shown the device to be more effective than ablative treatments like, dermabrasion laser resurfacing, and chemical peel and just as effective as non-ablative treatments in stimulating collagen and elastin production to smooth scars and erase wrinkles.

Micro-Trans™ Microneedle Array Patch technology (Valeritas) enables drug delivery into the dermis without skin characteristics or drug kinetics effecting the delivery. The arrays are

optimized to penetrate only the shallow layers of the skin, allowing for painless delivery. The *h*-Patch™ is a fully disposable, simple to use, controlled delivery technology platform designed to subcutaneously deliver drugs and can accommodate point-of-care fill or pre-filled liquid for lyophilized medications while leveraging standard filling processes.

Clinical trials on the developed microneedle array devices have been conducted. Studies were conducted on the effects of using Macroflux® to administer teriparatide [human PTH 1-34 (TPTD)] in comparison to Macroflux® placebo and injectable TPTD in postmenopausal osteoporotic women (Cosma *et al*., 2010). This study was performed in 13 centers in three countries and consisted of 165 postmenopausal women aged 50–81 whose last menstrual period was at least 1 year earlier. Results from the study concluded that the TPTD delivered by Macroflux® significantly increased bone mineral density against the placebo device in a dose-dependent manner. The Macroflux® device increased total hip bone mineral density compared to both the placebo device and the commercial injection. In addition, no prolonged hypercalcemia was observed and the treatments were well tolerated (Cosma *et al*., 2010).

The *h*-Patch™ has also been tested as a means to compare patient preference against insulin needle and syringe or pen as an insulin administration device for the treatment of Type 1 or 2 diabetes. The endpoint of this study was no longer deemed significant and has thus been terminated (http://clinicaltrialsfeeds.org/clinical-trials/show/NCT00453934). The other previously mentioned devices have not yet reach the clinical trial phase.

2.4.2.6. Future perspectives and recent advances in stimuli-responsive materials

With the development of microneedles, comes the need for the safety. When fabricated from metals, there is a possibility of the microneedles leaving traces of metals beneath the skin which may lead to erythema, irritation and other adverse effects. The microchannels created by the microneedles may be prone to microbial infection or toxin entry even though the channels may heal in a shorter time period than hypodermic needles. In this aspect, the use of microneedles for ocular delivery maybe welcomed. Advancements in PCA device developmental strategies are underway. The following highlights some possibilities in which this may be achieved:

2.4.2.6.1. Utilizing electrosensitive polymer materials for carbon nanotubes

To date, there have been numerous developments in the field of electro-responsive delivery using electro-sensitive polymers. This development is a stepping stone to the development of PCA using electro-responsive delivery. Nevertheless, the application of transdermal drug delivery systems is limited due to the low electro-conductivity and -sensitivity of polymers

(Kuila *et al.*, 2012) thus the incorporation of conducting materials, such as carbon based nanomaterials, in polymeric networks have been proposed as a strategy to enhance the electro-sensitivity of polymeric materials (Kuila *et al.*, 2012). Multi-Walled (MWNTs) or Single-Walled (SWNTs) Carbon Nanotubes (CNTs) not only reinforce hydrogels but also act as a means to increase the electric conductivity and thermal stability of the resulting composites (Yun *et al.*, 2011). Significant applications of CNTs as determined by Im and co-workers (2010) and Giri and co-workers (2011) respectively are: (1) an electro-sensitive transdermal drug delivery system consisting of a semi-interpenetrating polymer network of MWNTs composed of pentaerythritol triacrylate and polyethylene oxide MWNTs have been used as a component of an electro-sensitive system. The candidate drug used was (S)-(+)-ketoprofen, a NSAID with analgesic and antipyretic effects. It was shown that drug release increased with enhanced applied potentials, which was attributed to the higher electrical conductivity of CNTs; (2) composites of carboxymethyl guar gum and Multi-Walled Carbon Nanotubes (MWCNTs) used as potential devices for sustained transdermal release of Diclofenac sodium salt.

A study by Yun and co-workers (2011) investigated the use of electro-spun PVA/PAA hydrogel nanofibers containing MWCNTs as an electro-conducting component (Figure 2.13a). MWCNTs are purported to improve both the hydrogel's mechanical strength and electrical conductivity. Researchers concluded that the electro-responsive drug release from the nanofibers was a result of the variation of ionization of functional groups in the polymer matrices.

In a study by Spizzirri and co-workers (2013) a composite electro-conductive hydrogel based on a natural protein containing MWNTs was developed (Figure 2.13b). The composite was aimed at modulating the electro-responsive release of diclofenac sodium salt Gelatin/CNT hybrid hydrogels were fabricated by a straight forward synthetic strategy based on modified grafting approach. Resultant successful nanosized and uniformly dispersed spherical hybrid hydrogels with enhanced electrical properties, thermal stability and biocompatibility are depicted in Figure 2.13c.
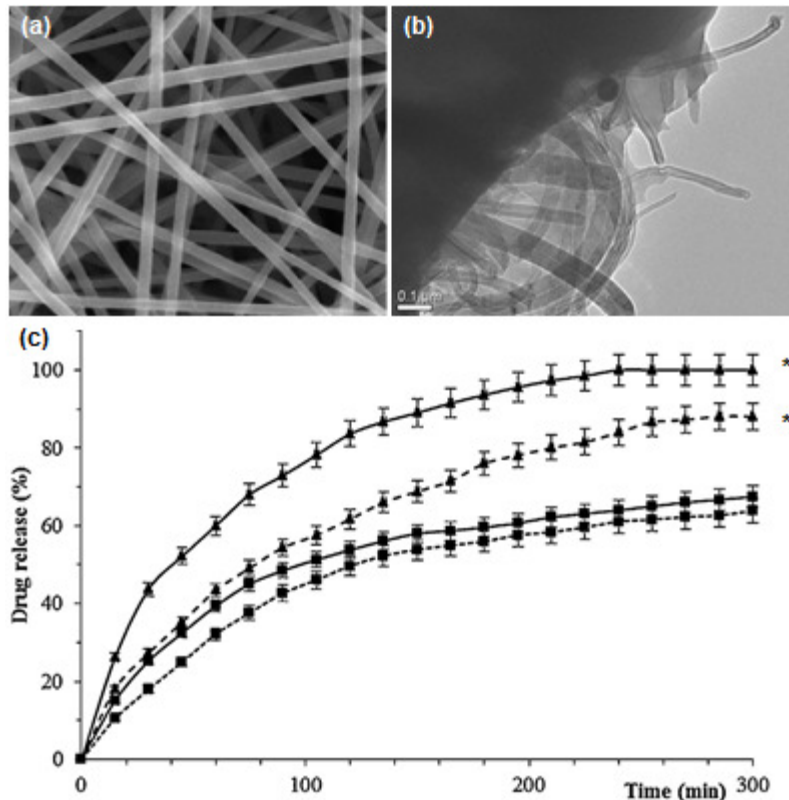
Figure 2.13: (a) SEM image of PVA/PAA nanofibers (1μm; Yun *et al*, 2011) (b) Transmission electron micrograph highlighting the presence of MWNTs into the polymeric network of the hydrogel. (c) DSS release as a function of time for differing microspheres in the absence (*) and in the presence of a 9-V direct current voltage (**) (0.1μm; Spizzirri *et al*, 2013).

2.4.2.6.2. Electric-field responsive microsystem applications

Microfabrication techniques facilitate the production of miniaturized electro-mechanical and mechanical elements; it is from this that novel MEMS based drug delivery devices have been developed. Liu and co-workers (2011) presented a MEMS based drug delivery device, which consisted of a metallic contact array (Figure 2.14). The MEMS device was based on an electro-active hydrogel matrix that responds through the de-swelling of the matrix to an electrical stimulus, which ultimately enables the release of Hematoxylin- the hydrophilic model drug selected. This MEMS based drug delivery device has the potential to facilitate advancements in the fields of PCA.
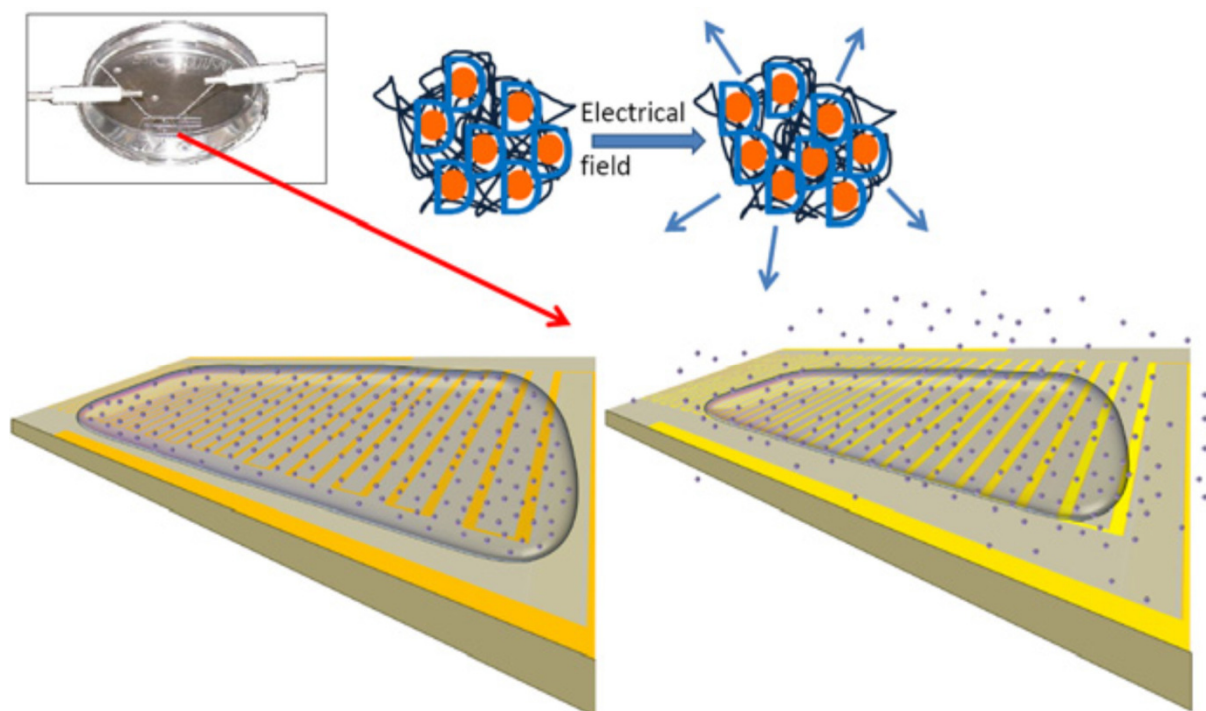
Figure 2.14: Polymer de-swelling drug delivery device as developed by Liu and co-workers (2011).

2.4.2.6.3. Electro-conductive hydrogels

Hydrogels are a three-dimensional network composed of cross-linked hydrophilic polymers which swell yet remain insoluble in water and are thus able to imbibe large amounts of biological fluids or water (Rodriguez *et al.*, 2003; Bhattarai *et al.*, 2009). Owing to their open network structure, polymer hydrogels have the ability (i) to sequester nanoparticles and (ii) to dramatically change their dimensions or phase transitions under an assortment of environmental stimuli such as changes in pH, ionic strength or temperature (Tumarkin and Kumacheva, 2009). In addition to their role as a simple drug reservoir, they may be used as site-specific targeting agents for the delivery of a variety of therapeutic agents (Rodriguez *et al.*, 2003; Bhattarai *et al.*, 2009).

Owing to their unique potentials, an electric current can also be used as an environmental signal to induce responses of hydrogels (Qiu and Park, 2001). ECHs are composed of polyelectrolytes or electro-active polymers (EAPs) such as polyaniline (PANi) and undergo shrinking or swelling in the presence of an applied electric potential (Qiu and Park, 2001; Bajpai *et al.*, 2009; Guiseppi-Elie A. 2010). There are various EAPs, which may be used as conducting polymers, such as polypyrrole (Geetha *et al.*, 2006; Chen *et al.*, 2012) polythiophene (Chen *et al.*, 2012), PDMS (Chen *et al.*, 2012), poly(methyl methacrylate) (Small *et al.*, 1997; Posadas and Florit, 2004), poly(3,4-ethylenedioxythiophene) (PEDOT) (Balci *et al.*, 1995) and PVA (Chen *et al.*, 2012). These single component polymers have

found a wide variety of applications in MEMS devices (Chen *et al.*, 2012). Drug release mechanism from the ECH is responsive to the electric field, but is not modulated. Future development of an iontophoretic patch would thus remove the need for the conventional IV or epidural PCA resulting in lower cost implications and improved patient acceptability.

Even though controlled drug delivery based on electro-sensitive hydrogels is still in its initial stages(Qiu and Park, 2001) a possible device consisting of a transdermal electro-responsive MNA patch promises to revolutionize the field of medicine, vaccination and disease treatment through an essentially pain-free, ultra-minimally invasive delivery mechanism. Hydrogel formulations will allow for daily or weekly dosage replacement using the same iontophoretic device as they can be designed as a unit dose-type drug-loaded hydrogel patch (Banga and Chien, 1993). The only way in which the hydrogel may be disadvantageous is that under long-term occlusion, the hydrogel can absorb sweat secretions which may become irritating (Banga and Chien, 1993).

2.5. Concluding Remarks

In pain management, the concept of patient-controlled analgesia was a remarkable development. In addition to providing better analgesic delivery, patient-controlled analgesia has improved our understanding of pain and suffering. As life expectancy increases, so does the incidence and morbidity of acute and chronic pain, ultimately placing a higher level of emphasis on pain management as an issue of patient's quality of life. Responding to this trend, iontophoresis-based MNA patches as modified transdermal delivery methods should be exploited for the systemically indicated electro-activated and modulated controlled delivery of drugs. A proposed electro-activated and modulated patch device could potentially result in painless and more convenient drug administration and delivery. The device will offer an extensive range of biomedical applications such as targeted drug delivery, delivery to the eye and diabetes treatment.

The future of drug delivery will be significantly influenced by microfabrication technologies with the optimization of drug delivery through human skin becoming more important in modern therapy. Even though transdermal micro-needle devices promise to revolutionize the field of medicine, vaccination and disease treatment, it is still a novel technology to be fully exploited. More research therefore needs to be conducted into the effectiveness and properties of microneedles as well as the polymer materials used in there fabrication to ensure their therapeutic safety for patients. Improvement into this technology will thus result in the evolution of new devices for the delivery of a wide range of biomedical compounds

presumably also reducing the amount of dosages and thus possible side effects of a drug. The use of microneedle systems especially in the administration of actives traditionally unattainable in conventional drug delivery techniques can therefore create a true paradigm shift the field of drug delivery.

CHAPTER 3

IDENTIFICATION OF THE ELECTRO-ACTIVE SPECIES FOR INCORPORATION INTO THE ELECTRO-MODULATED HYDROGEL

3.1. Introduction

Controlled-release formulations of opioid analgesics are widely assumed to be less subject to abuse than their immediate-release counter-parts in their ability to provide better quality of pain relief (Fisher, 2004). Drug delivery has been defined by Flynn (1979) as 'the use of whatever means possible, be it chemical, physicochemical or mechanical, to regulate a drug's access rate to the body's central compartment, or in some cases, directly to the involved tissues". Accounting for the carrier, the target and the route of administration, drug delivery has advanced into a plethora of devices or processes that are designed to make therapeutic agents more efficacious through modified release, augmented therapeutic index and bioavailability, and enhanced patient acceptance and patient compliance. Advancements in drug delivery technology have thus proven to bring commercial and therapeutic value to drug delivery products.

Due to their unique biocompatibility, amongst other advantages, hydrogels can provide similar properties to biological tissue constructs due to their scaffold-like structure and yet still maintain their structural integrity. When swollen, the flexibility capability provides a superior drug delivery vessel in some cases (Hamidi *et al.*, 2008). In an EMH, the essential EAP is incorporated within a crosslinked tri-dimensional polymer-based hydrogel network. The electrically-tunable properties, the water insolubility and the shape stability of the hydrogel are determined by the EAP and the three-dimensional network structure (Percec and Bera, 2001; Lee and Mooney, 2001).

Although controlled drug delivery systems focused on electro-responsive hydrogels is still in its infant stages, the combination of the hydrogel's swelling capabilities and the EAP's conductive properties, makes hydrogels versatile for various biomedical and therapeutic application, having the ability to permit delivery at a daily or weekly basis, allowing for patient-administered drug release into the target area (Qiu and Park, 2001; Rodriguez *et al.*, 2003; Luiz and de Torresi, 2005; Bhattarai *et al.*, 2009). EAPs have been intensively researched for their unique electrical and/or optical and electrochemical properties as they undergo swelling or deswelling in the presence of an applied electric field (Qiu and Park, 2001; Vanbever and Preat, 1999; Bajpai *et al.*, 2008; Guiseppi-Elie, 2010).

In order to further advance the EAP, a polymer blend or electro-active species was identified in this chapter. The blending of polymers facilitates an attractive means to combine individual polymer component desired properties with a concomitant enhancement of selected properties. Preliminary studies were performed on formulations of various combinations of polymers, crosslinking agents and methods, as well as on the electro-stimulus applied. These formulation variables, their respective quantities, and their formulation effects were subsequently tabulated to support the formulation variables chosen later in this chapter. Furthermore, all processing variables, successful and unsuccessful, required for the synthesis of the novel hydrogel formulation and a summary of the effects reflected in the preformulation studies are discussed in this chapter. Preliminary formulation studies involved, initially selecting and evaluating various monomers for their gel-forming properties, crosslinking agents for their coupling properties and polymers for their electro-responsive properties. Subsequently, other additives and formulation modifications were included so as to result in the desired drug release from the formulation. This chapter concludes with the identification of the most significant variables with their respective maximum and minimum parameters for optimization of the EMH using a Box-Behnken design model.

3.2. Materials and Methods

3.2.1. Materials

Hexamethylenediamine (M_w=116.2g/mol) and n-hexane were purchased form Merck Chemicals (Pty) Ltd. (Darmstadt, Germany), sebacoyl chloride (M_w=239.1g/mol), polyvinyl alcohol (PVA) (M_W=89,000-98,000g/mol), polyaniline (PANi) (M_w=20,000g/mol), gluteraldehyde solution (grade I, 25%), indomethacin (≥99%), acrylic acid (anhydrous, 99%), *N*, *N′*-Methylenebisacrylamide (≥99.5%) and potassium persulfate (≥99.0%) were all purchased from Sigma-Aldrich® (St. Louis, MO, USA). Polystyrene sulfonate (M_w=70,000g/mol) was purchased from Scientific Polymer Products, Inc. (Ontario, New York). Diethyl acetamidomalonate (DAA) was purchased from Fluka Chemie AG, Buchs, Switzerland. De-ionized water was obtained from a Milli-Q water purification system (Milli-Q, Millipore, Billerica, MA, USA). All other reagents used were of analytical grade and were employed as purchased.

3.2.2. Preparation of the preliminary hydrogel formulation and evaluation of the electro-responsive behavior

Many polymers such as polyamide 6,10 (PA 6,10), polystyrene sulfonate (PSS), polyaniline (PANi), poly (ethyleneimine) (PEI), and 1-vinylimidazole (VI) were employed in this study as candidate EAPs. For the synthesis of the hydrogel, acrylic acid (AA) and polyvinyl alcohol (PVA) were studied as monomers, N, N′-Methylenebisacrylamide, diethyl acetamidomalonate (DAA) and gluteraldehyde (GA) were employed as chemical crosslinking agents. N, N, N′, N′-Tetramethylethylenediamine (TEMED) and potassium persulfate (KPS) solution were employed as initiators in the crosslinking process of AA. The different combinations and quantities of these employed polymers are outlined later in Sections 3.2.5-3.2.7.

3.2.3. Preparation of polyamide 6,10

The PA 6,10 utilized in this study is a novel polymer synthesized by Kolawole and co-workers (2007). Briefly, hexamethylenediamine (1.75g) was dissolved in deionized water (100mL) i.e. the aqueous solution. The solution was neutralized by the addition of sodium hydroxide (NaOH; 0.1g). Separately, the non-aqueous solution comprising hexane (40mL), cyclohexane (40mL) and sebacoyl chloride (0.63g) was prepared. The non-aqueous solution was gradually added to the aqueous solution forming two immiscible phases that were stirred with a glass rod under a fume hood. Stirring continued until the formed white gel-like mass could no longer absorb solvent. The mass was then thoroughly rinsed with deionized water (100mL) 3 consecutive times and was then placed on filter paper to remove excess solvent. Following this, the mass was dried at 50°C±0.5 for 72 hours in an oven (Memmert 854, Schwabach, Western Germany). The polymer was powdered for use using a laboratory blender (CG 100, Kenwood Ltd, Cambridge UK) and then passed through an automatic granulating sieve of 1mm aperture size (Erweka AR 400; Optolabor (Pty) Ltd.) to ensure size uniformity.

3.2.3.1. Preparation of the polyamide 6,10 -polystyrene sulfonate polymer blend

The polymer blend composite prepared as an EAP constituted of varying ratios of PA 6,10 and PSS and was evaluated for electro-conductivity for institution into the electro-responsive drug delivery system. Each polymer was dissolved in $5\%^{v}/_{v}$ H_2SO_4 solution to facilitate the dissolution of the water-soluble PSS and the non-water-soluble PA 6,10 polymer. The blend solutions were dialyzed for 48 hours. Films were produced by drying the blends at 40°C±0.5 for 24 hours in an oven (Memmert 854, Schwabach, Western Germany). The polymer blends was powdered for further use. The blends were assessed for conductivity employing

a conductivity meter (TDSTest™ Kit Model WD-35661-70, Oakton® Instruments, Vernon Hills, IL, United States) and an average for each blend was recorded.

3.2.4. Investigation of preformulation variables for incorporation into a Box-Behnken design

3.2.4.1. Formulation and synthesis validation of sodium indomethacin

Indomethacin is observed to be a hydrophobic drug resulting in solubility difficulties with common aqueous based solvents (Liu *et al.*, 2013). In order for the solubility difficulties to be alleviated, the hydrophilic sodium salt of indomethacin was prepared. An appropriate solvent for indomethacin was determined using aqueous NaOH. Synthesis validation of sodium indomethacin was performed using Fourier Transform Infrared (FTIR) Spectroscopy. Briefly, 500mg of indomethacin was dissolved in 1M NaOH (100mL). The drug solution was frozen at -75°C for 48 hours and subsequently lyophilized. A homogenous, pale yellow powder resulted which was then crushed to obtain a uniform particle size. FTIR spectra of both sodium indomethacin and indomethacin were collected using a PerkinElmer® Spectrum 100 Series FT-IR Spectrometer fitted with a universal ATR Polarization Accessory (PerkinElmer Ltd., Beaconsfield, UK). The samples were placed on a diamond crystal and processed for the FTIR spectrum series at a resolution of $4cm^{-1}$. Samples were analyzed at wave numbers ranging from $650\text{-}4000cm^{-1}$. Further validation of the modified drug was determined using quantitative X-ray diffraction (XRD). Profiles were determined using an X-Ray Diffractometer (Rigaku Miniflex 600, Rigaku Corporation, Matsubara-cho, Akishima-shi, Tokyo, Japan) at room temperature. Integrated X-ray Powder Diffraction software (PDXL 2.1, Rigaku, Tokyo, Japan) was employed for sample analysis. The parameters employed are outlined in Table 3.1.

Table 3.1: X-ray diffraction parameters employed.

Parameter	Settings
Soller (inc.)	2.5°
Incident Height Slit (IHS)	10mm
Divergence Slit (DS)	1.25°
Solar Slit (SS)	13mm
Soller (rec.)	2.5°
Receiving Slit (RS)	13mm
Filter	None
Monochromater	None
Start	3°
Stop	140°
Step	0.1°
Speed	30°/minute
Scan axis	Theta/2-Theta
Scan mode	Continuous

3.2.4.2. Construction of calibration curve for the determination of sodium indomethacin release from the Electro-Modulated Hydrogel

An Ultraviolet (UV) spectrophotometric scan was run to determine the maximum wavelength for sodium indomethacin absorption in phosphate buffered saline (PBS). Using UV spectroscopy and a series of known concentrations (0.2-1.0mg/mL) of sodium indomethacin in PBS (pH 7.4; 37℃), a calibration curve was constructed. The linear curve was plotted with the observed absorbance of sodium indomethacin as the dependent variable and the concentration of sodium indomethacin as the independent variable. A statistical representation of the degree at which the function correlates the set of values (R^2 value) was computed for the curve.

3.2.4.3. Identification of optimization variables through in vitro release studies

The hydrogel formulations were synthesized using various polymer combinations and concentrations. The formulations were subsequently dried for 24 hours and were immersed in 20mL of PBS (pH 7.4; 37℃). The electro-stimulus was applied to the corresponding formulations using a potentiostat/galvanostat (PGSTAT302N, Autolab, Utrecht, Netherlands), where a platinum electrode (5mm) served as the cathode and a gold electrode (5mm) as the anode. PBS aliquots (0.1mL) were sampled at 30 minute time intervals before and after electro-stimulation over a 3 hour period. This was undertaken to determine the

effect of multiple electro-stimulations on sodium indomethacin release. The aliquots were removed and were replaced prior to and after the application of the electrical stimulation in order to maintain sink conditions. Filtered samples were diluted (1:19) and thereafter analyzed for sodium indomethacin content using UV spectroscopy (Implen Nanophotmeter^{TM}, Implen GmbH, München Germany) (Figure 3.1).
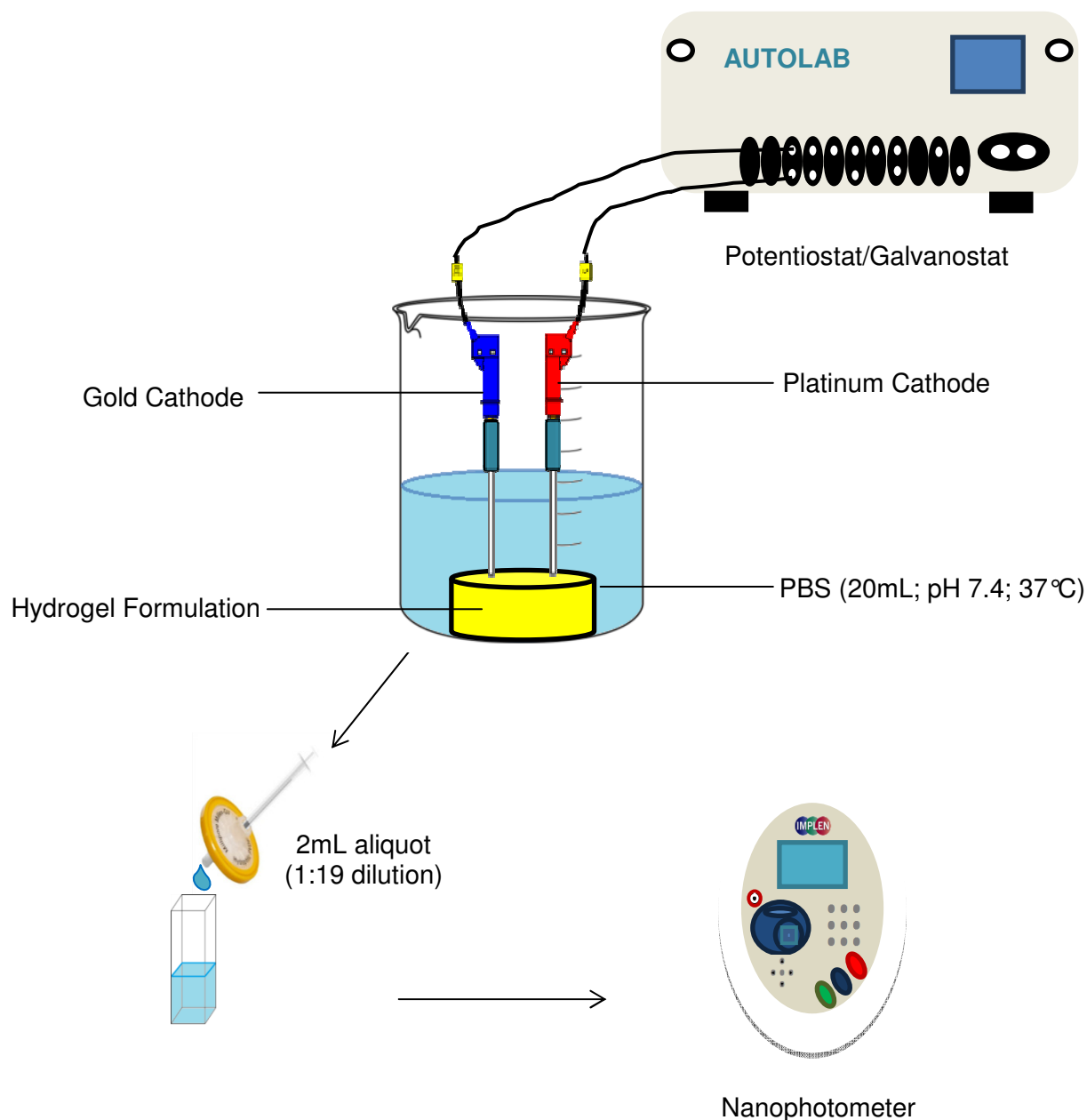
Figure 3.1: Schematic of the *in vitro* release studies employed.

3.2.5. Selection of an appropriate monomer for incorporation into the Electro-Modulated Hydrogel

Hydrogel synthesis consisted of three fundamental components: the monomer; initiator; and crosslinking agent, all of which impart certain characteristics when the quantities were varied. Table 3.2 outlines the two types of monomers used in the synthesis of the hydrogel and the subsequent effects on the formulation following variations in quantity.

Table 3.2: Monomer variables required for the Electro-Modulated Hydrogel synthesis and their formulation effects.

Variable	Variable Range	Formulation Effect
PVA*	0-600mg	Poor viscosity No brittleness
	600-1000mg	Appreciable viscosity Low brittleness
AA**	0-600mg	Low viscosity No brittleness
	600-1000mg	Appreciable viscosity Brittleness
PVA:AA Combination	0-600.0mg: 0.2mL	Low strength and viscosity of gel composite
	600-1200.0mg:0.6mL	Appreciable strength and viscosity of gel composite

*PVA- poly(vinyl alcohol) **AA - acrylic acid

3.2.6. Investigation of crosslinking agents to be employed in the synthesis of the Electro-Modulated Hydrogel

In addition to preventing burst release tendencies of a formulation, crosslinking allows for the extended release of drug from the formulation (Tanaka *et al.*, 2006). Table 3.3 outlines the crosslinking agents investigated for use in the synthesis of the hydrogel formulation.

Gelation rate of the hydrogel formulations was characterized using gelation time in the search for an appropriate crosslinking agent. Gelation time was measured as the time at which the mixture no longer flowed when the vial was tilted at an angle (Patenaude *et al.,* 2014). A visual assessment of the monomer and crosslinking agent was conducted prior to the *in vitro* drug release studies. A gelation time that allows for the transfer of the hydrogel into a mold was preferred in terms of processing (Chapter 7). The prepared hydrogel formulations were allowed to equilibrate to the desired gelation temperature for 3 minutes.

Table 3.3: Crosslinking agent variables and their formulation effects for the synthesis of the Electro-Modulated Hydrogel.

Variable	Variable Range	Formulation Effect
GA*	0-80mg	Crosslinking occurred
		Suspension formed
		Poor electro-modulated drug release
DAA**	0-100mg	Crosslinking occurred
		Robust gel composite formed
		Poor electro-modulated drug release
N,N′-Methylenebisacrylamide	0-100mg	Appreciable viscosity
		Robust gel composite formed
		Appreciable electro-modulated drug release
	100-500mg	High viscosity
		Brittle gel composite formed
		Poor electro-modulated drug release

* GA – gluteraldehyde **DAA - diethyl acetamidomalonate

3.2.7. Determination of the electro-active species for incorporation into the Electro-Modulated Hydrogel

In order to achieve electro-modulated drug release from the hydrogel formulation, polymers were investigated to identify their electro-responsive properties (if any). Table 3.4 summarizes the various polymer combinations utilized in order to achieve an EAP blend that resulted in the electro-responsive release.

Table 3.4: Electro-active polymer variables required for the Electro-Modulated Hydrogel synthesis and their formulation effects.

Variable	Variable Range	Formulation Effects
PA 6,10[a]:PSS[b]	10:90*** 30:70*** 50:50** 70:30* 90:10*	Incorporated blends displayed varying degrees of electro-modulated drug release Precipitation/ poor solubilities with increasing amounts of PA 6,10
PANi[c]	1-5%$^w/_w$	Appreciable electro-modulated drug release Poor hydrophilicity
PEI[d]	0-1mL	Appreciable electro-modulated drug release Low viscosity of gel composite Appreciable mechanical strength
	>3mL	Appreciable electro-modulated drug release High viscosity of gel composite Appreciable mechanical strength
VI[e]	<0.1 mL	Poor electro-modulated drug release Appreciable solubility Appreciable mechanical strength
	>1mL	Appreciable electro-modulated drug release Poor solubility Appreciable mechanical strength

[a]PA 6,10- polyamide 6,10 [b]PSS- polystyrene sulfonate [c]PANi- polyaniline [d]PEI- poly (ethyleneimine) [e]VI- 1-vinylimidazole ; ***good conductivity **; **appreciable conductivity; *poor conductivity

3.2.8. Investigation of the effects of the applied electro-stimulus for delivery of therapeutic levels of the active agent

In order to attain electro-modulated delivery of therapeutic levels of drug, the stimuli-responsive factors dictating the release requirements were determined through the variation in strength of the applied voltage to the hydrogel formulation (Table 3.5).

Table 3.5: Variations in applied voltage required for modulated drug release from the Electro-Modulated Hydrogel.

Variable	Variable Range	Formulation Effects
Applied voltage	0-5V	Differing electro-modulated drug release dependent on EAP (blend) employed

3.3. Results and Discussion

3.3.1. Electro-active / responsive capabilities of hydrogels

Stimuli-responsive hydrogels are described as intelligent or smart as they have the ability to dramatically modify their phase transitions or dimensions according to various environmental stimuli such as change in ionic strength, pH, or temperature (Chaterji *et al.*, 2004; Tumarkin and Kumacheva, 2009; Jagur-Grodzinski, 2010) and may be classified based on the structural factors that affect their "smartness". The increase in "responsiveness" of these superporous smart hydrogels is achieved by the increase in the size and interconnectivity of the water-swollen pores at equilibrium swelling. In addition to their unique potential, the electric field can be used as an environmental signal in the induction of a required hydrogel response (Qiu and Park, 2001). Furthermore, to support this study, the exponential growth in the amount of literature available on the use of electric currents *in vivo*, in the form of electroporation and iontophoresis, in the field of dermal and transdermal drug delivery already exists (Delgado-Charro and Guy, 2001; Vanbever and Preat, 1999) with the safe limits of electric field strengths determined for topical application (Murdan, 2003).

3.3.2. Synthesis validation of sodium indomethacin

For both compounds (Figure 3.2a), FTIR spectra (Figure 3.2b) revealed, strong bands observed at $600\text{-}800\text{cm}^{-1}$, indicating the presence of the alkyl halide (C-Cl). Sodium indomethacin displays a defined peak at 3211cm^{-1} indicating Carboxyl OH stretching which is absent in the FTIR spectra of indomethacin. The presence of an O-H band at 1760-

1690cm^{-1} is also indicative of a carboxyl group. The strong absorbance for sodium indomethacin at 1427cm^{-1} in this region is mainly due to the asymmetric stretching of the carboxylate anion COO^{-}. The symmetric stretching of the anion is observed at 1304cm^{-1} for indomethacin. The absorption band at 1560cm^{-1} pertaining to sodium indomethacin is assigned to the asymmetric carboxylate stretch by analogy to assignment for the ammonium salt of benzoic acid (Silverstein *et al.*, 2005). XRD profiling (Figure 3.2c) revealed the lower peak intensities of sodium indomethacin in comparison to indomethacin. Contrary to the peaks concluding crystalline structure of indomethacin, unsymmetrical, broad peaks were observed in the XRD profile of sodium indomethacin indicating the amorphous nature of the modified drug. It can thus be concluded that the salt of the drug was formed (Tong and Zografi, 1999).

(a)

(i)

(ii)
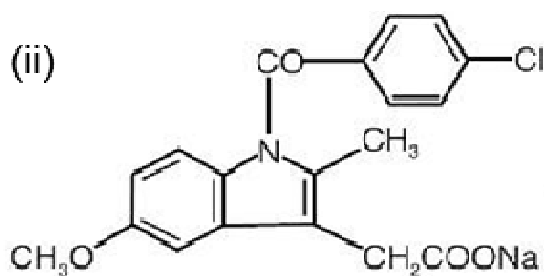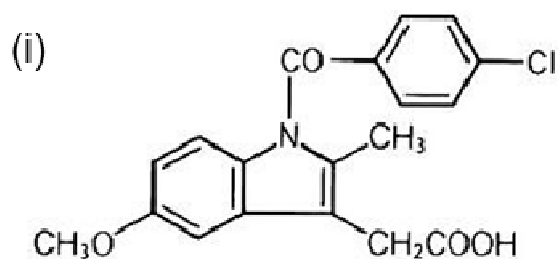
(b)
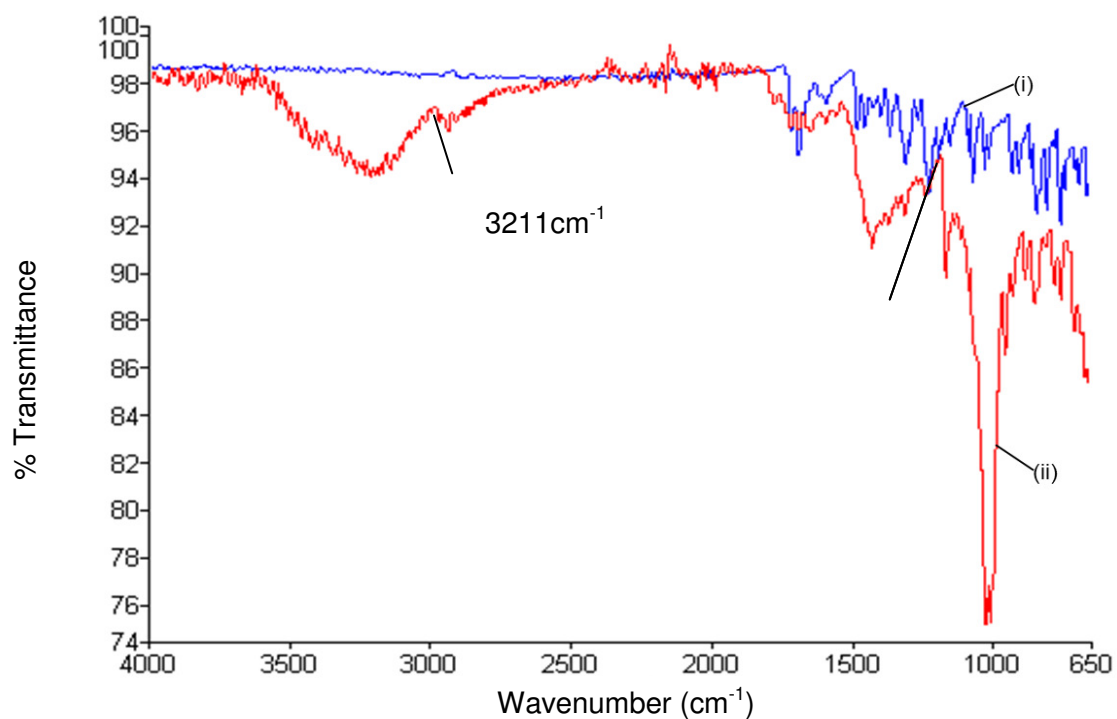
(c)
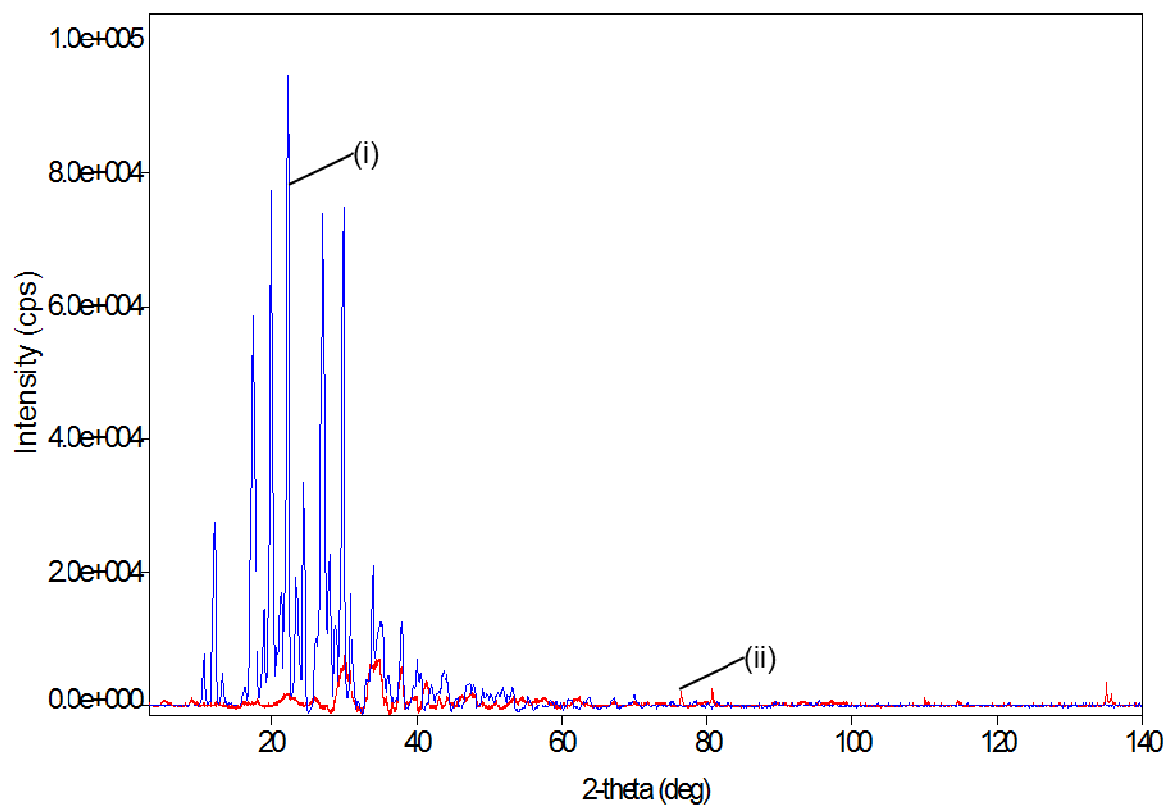
Figure 3.2: (a) Chemical structure of (i) indomethacin and (ii) sodium indomethacin. (b) FTIR spectra of (i) indomethacin and (ii) sodium indomethacin. (c) XRD profile of (i) indomethacin and (ii) sodium indomethacin.

3.3.3. Construction of a calibration curve for the ultraviolet spectrophotometric determination of sodium indomethacin

Figure 3.3a displays the spectrophotometric scan of sodium indomethacin in PBS (pH 7.4, 37°C). Using UV spectroscopy, it was found that indomethacin exhibits a maximum wavelength at λ_{320}, consistent with the literature published on indomethacin absorption peak of 318-321nm (Forster *et al.*, 2001; Anoopkumar-Dukie, 2003; Kamal *et al.*, 2008). Using a series of known concentrations (0.2-1mg/mL) of sodium indomethacin in PBS, a calibration curve at λ_{320} was constructed (Figure 3.3b). The linear curve was plotted with the observed absorbance of indomethacin as the dependent variable and the concentration of indomethacin as the independent variable (Figure 3.3b). The obtained R^2 value of the calibration curve was 0.99 (Figure 3.3b), indicating a perfect correlation.

(a)

Wavelength (nm)
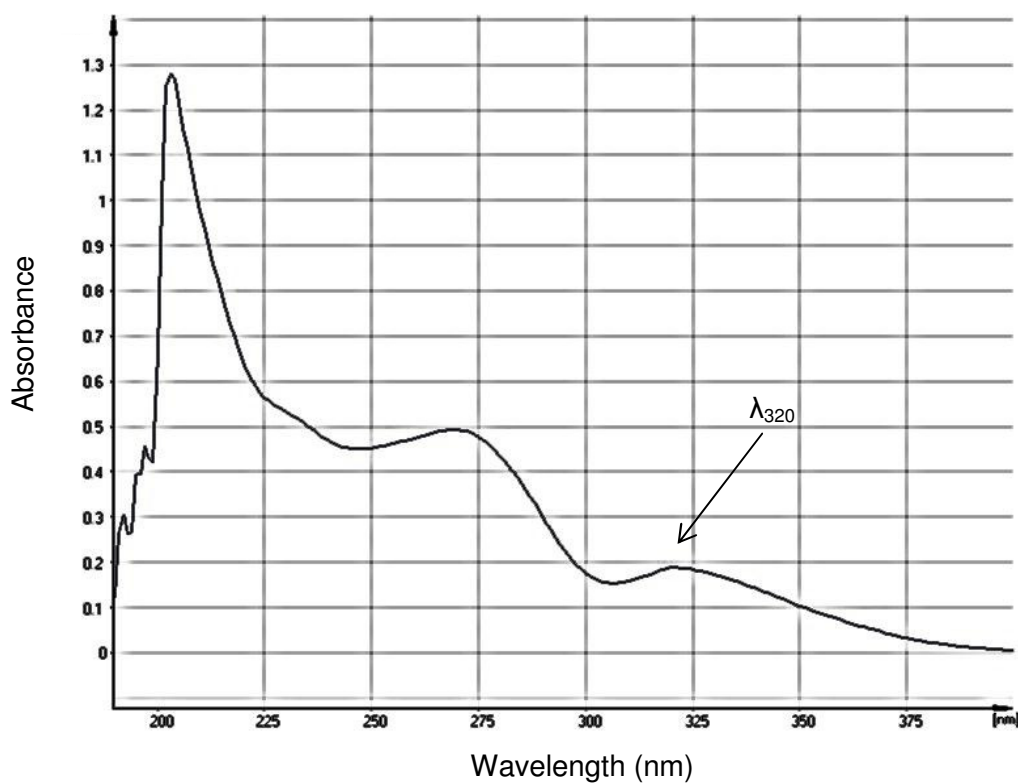
(b)
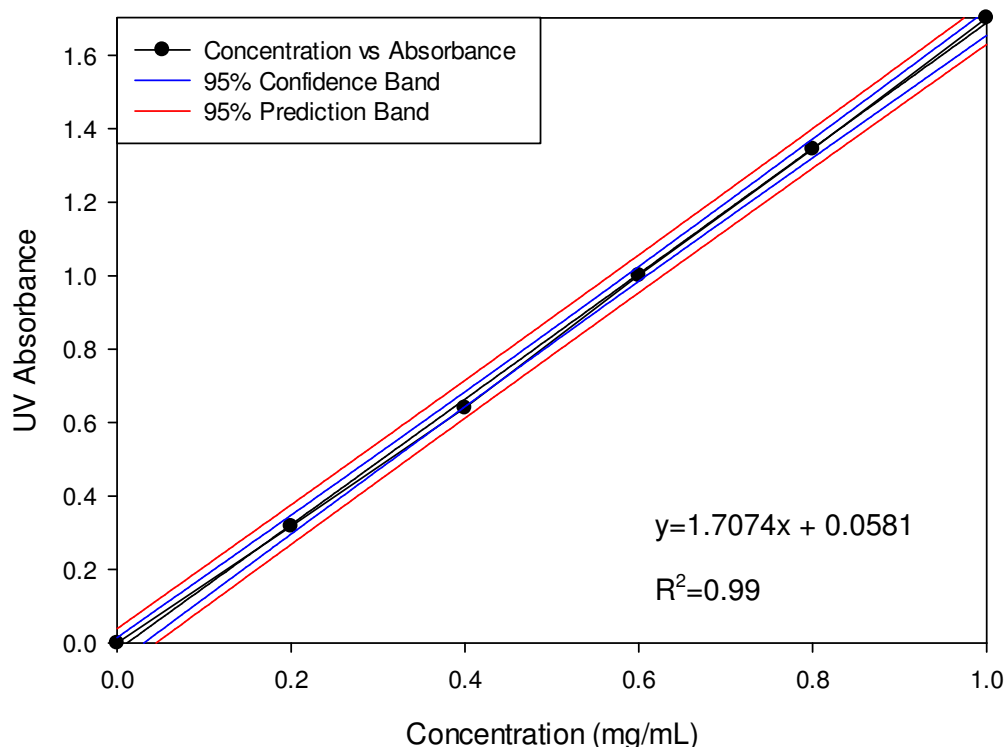
Figure 3.3: (a) UV Spectra of sodium indomethacin in PBS [WinASPECT, Version 1.6.13.0, 2002, Analytik Jena AG, Germany] (b) Calibration curve of sodium indomethacin in PBS at λ_{320}.

3.3.4. Design criteria and therapeutic considerations for the Electro-Modulated Hydrogel in drug delivery

As for any formulation, design criteria such as material selection, are crucial for both drug delivery and its mathematical modeling. These criteria are essential in governing the mode and rate of drug release from hydrogel matrices. Prior to hydrogel fabrication and drug-loading, these criteria have to be evaluated. These criteria include transport properties such as physical properties and drug molecule diffusion as well as structural properties and stimuli-responsiveness, and biological properties such as biocompatibility (Lin *et al.*, 2006). For a formulation comprising of an electro-responsive species within a hydrogel matrix, three design criteria are apparent: drug release; degree of matrix swelling; and matrix resilience. These criteria will be further elaborated on in Chapter 4.

The EMHM device is designed for a once daily application requiring the hydrogel component to maintain therapeutic levels of indomethacin throughout the day in order to provide effective pain treatment. Literature states that indomethacin has a therapeutic window of 0.5-5mg/mL in adult humans with lower amounts being sub-therapeutic and higher levels being toxic (Katzung, 2007). The apparent volume of distribution of indomethacin has been stated

to be approximately 18L with a plasma half-life ($t_{1/2}$) of 2.4 hours, which when utilized to calculate the elimination constant (k_e) of indomethacin (Equation 3.1) gives a k_e value of 0.28875. This value is of importance to accurately determine the plasma concentration levels of indomethacin at any point throughout the day to ensure therapeutic treatment for the patient.

$$t_{1/2} = \frac{0.693}{k_e}$$ **Equation 3.1**

Where $t_{1/2}$ is the plasma half- life of the drug and k_e is the elimination constant

The calculated k_e value was subsequently used in Equation 3.2 to determine the decrease in plasma indomethacin levels per hour to calculate the required indomethacin release from the hydrogel to maintain therapeutic drug levels as well as the initial spike to allow for therapeutic effectiveness.

$$A_b = A_0 . e^{-ket}$$ **Equation 3.2**

Where A_b is the plasma concentration at a specific time, A_0 is the plasma concentration at time 0, k_e is the elimination constant and t is the number of hours

It was determined that an initial drug spike of 54mg and a maintenance dose of 13mg every hour will be required to maintain therapeutic effectiveness, ultimately requiring an approximately loading dose of 370mg to maintain therapeutic effectiveness. Whilst the human adult contains approximately 6L of blood, it was thus chosen that three hydrogels could be incorporated into a single device allowing for each hydrogel to dose 6L of volume with indomethacin that could be correlated with other drugs. As a result, this led to a revised initial spiking concentration of 18mg with a maintenance dose of 4mg each hour to cater for indomethacin elimination (Figure 3.4). Due to the each being changed every day, the maintenance dose would cease to occur at hour 18 to allow for a drop in plasma levels prior to the next initial spike which prevent toxic concentrations being reached. The loading dose of each hydrogel would therefore approximately 100mg indomethacin, in line with the preformulation studies conducted (Katzung, 2007).
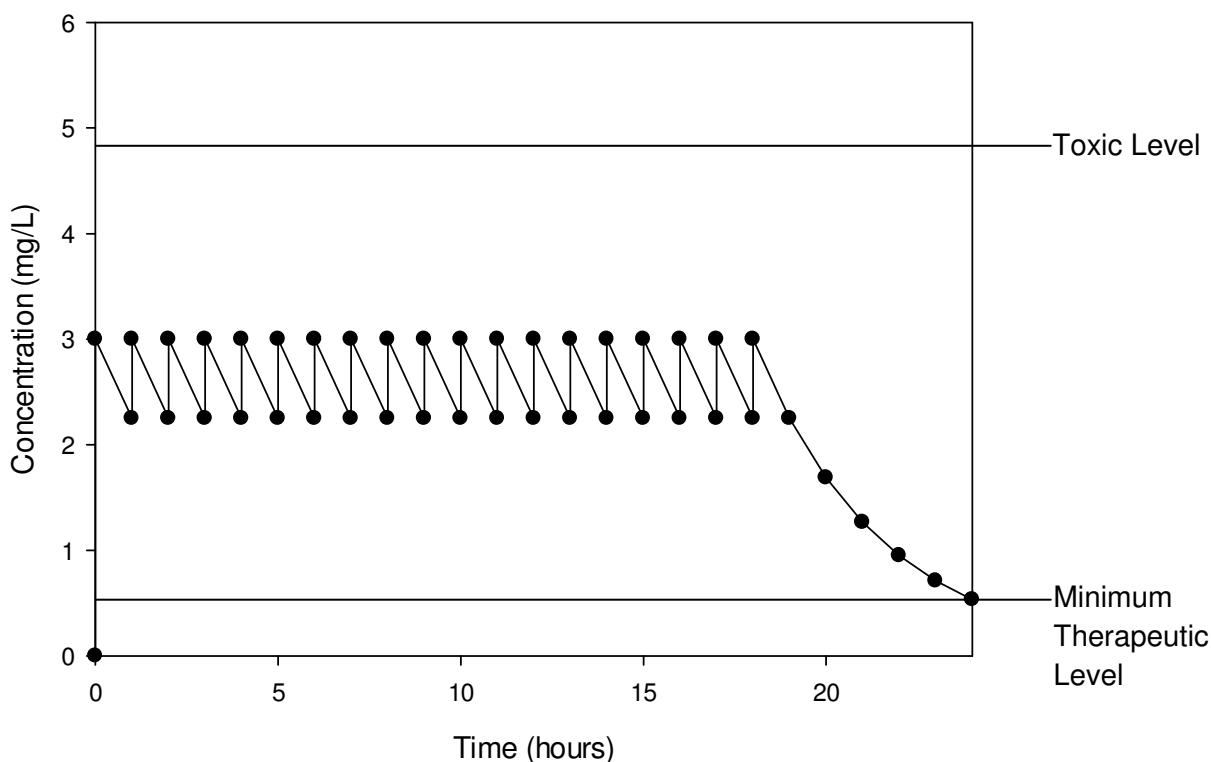
Figure 3.4: Theoretical therapeutic profile of sodium indomethacin.

3.3.5. Analysis of electro-responsive capability of the hydrogel formulation using *in vitro* release studies

3.3.5.1. Analysis of the polyamide 6,10 -polystyrene sulfonate blend as the electro-responsive polymer blend

When evaluated for conductivity, the polymer blends had lower conductivities than the individual polymers; with the conductivity measurement results proportional to the PSS concentration (Table 3.6). The lower conductivity of the blends as compared to their single polymer counterparts may be attributed to the formation of a neutralized polyelectrolyte complex, decreasing the availability of the sulphonate (SO_3^-) and ammonium (NH_3^+) to interact with charge. This is accounted for the fact that PSS is an ionomer, constituting of a polymer backbone with a small mole fraction of ionic groups (O'Connell *et al.*, 1996). The enhanced physical properties as compared to those of the unmodified parent polymer are because of the phase separation of the ionic groups into ionic microdomains. These aggregates, or ionic domains, act as reinforcing fillers and physical crosslinks (Galambos *et al.*, 1987).

Table 3.6: Formulation parameters of polyamide 6,10 -polystyrene sulfonate composites.

Blend Formulation	PA 6,10/PSS Ratio	Conductivity (µS)
PA 6,10*	100	383
PSS**	100	394
A	10:90	263
B	30.70	265
C	50:50	260
D	70:30	255
E	90:10	244

*PA 6,10- polyamide 6,10 **PSS- polystyrene sulfonate

Polymer Blend B, the most conductive blend was further evaluated against a control where no electro-stimulation was delivered to the hydrogel formulation (Figure 3.5). Polymer Blend B was also evaluated at voltages of 0.3, 1.5 and 5V to determine electro-responsive release (Figure 3.6). Conducting the release test with a control system verifies the ability of the blend to impart electro-responsive properties, as demonstrated by the substantial increase in drug release after electro-stimulation. In addition, the polymer blend does not impart electro-responsive properties to the hydrogel system, but rather electro-conductive properties. Although conductive in nature, it cannot be ignored that the release in relation with respect to diffusion is greater than that after electro-stimulation.
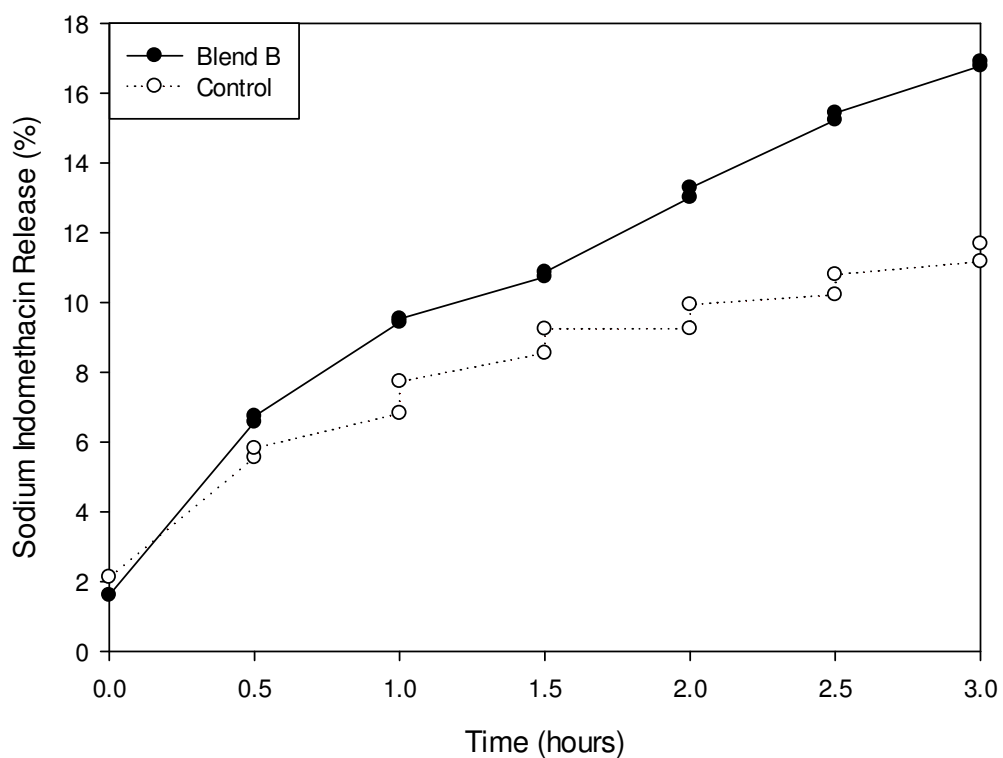
Figure 3.5: Drug release profiles of electro-stimulated formulation at 1.5V in relation to the control formulation.
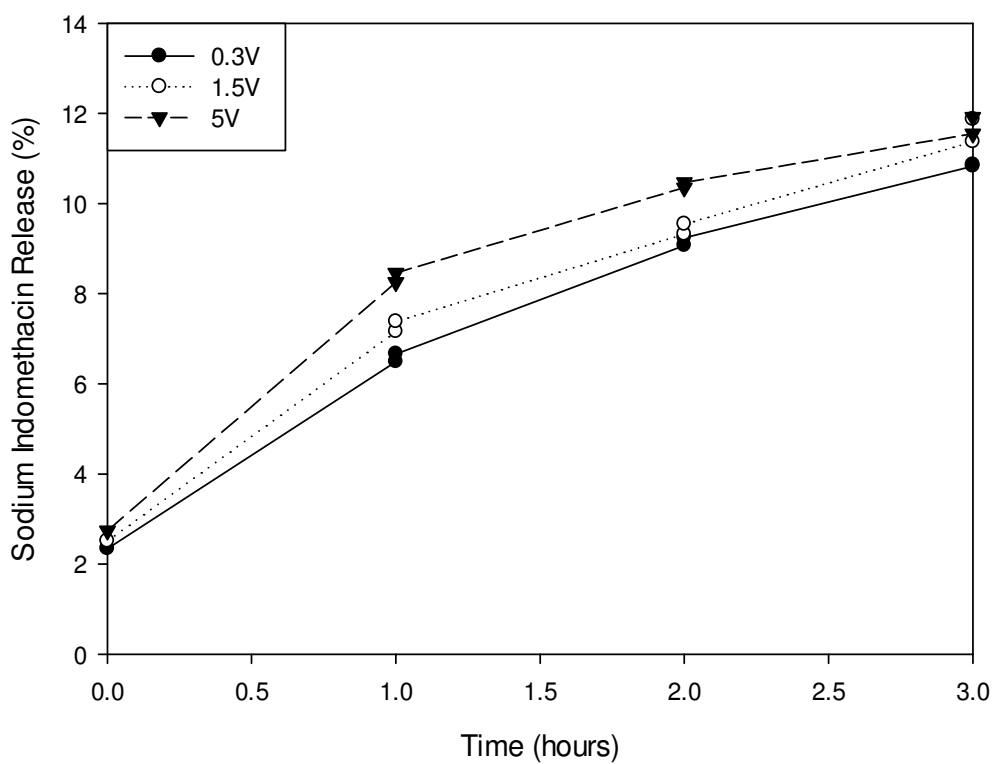
Figure 3.6: Drug release profile of polymer blend B at 0.3, 1.5 and 5V.

3.3.5.2. Incorporation of polyaniline as the electro-responsive polymer blend

Based on the work of Tsai (2011) in the design and development of an electro-actuated device for prolonged therapeutic management of moderate to severe chronic pain, PANi was investigated as a possible electro-active polymer. The hydrogel formulation was structurally too robust and the PANi too large in terms of particle size to either coat or be delivered through a MNA. The formulation (Figure 3.7a) was also seen to dramatically alter its structural integrity upon electro-stimulation with a fragmented network seen (Figure 3.7b).
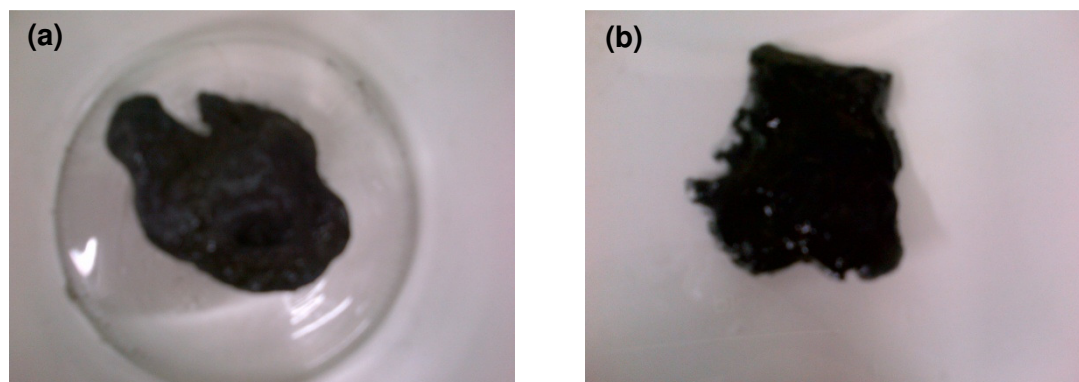
Figure 3.7: Images of the polyaniline containing hydrogel (a) prior to electrical stimulation and (b) after 4 electro-stimulations.

3.3.5.3. Analysis of the electro-responsive capability of poly(ethyleneimine)-1-vinylimidazole polymer blend

PEI and VI were incorporated as electro- responsive component in the hydrogel formulation. A preliminary investigation into their possible electro-responsive properties had indicated the required release response with release of 2.49-3.00% at each electro-stimulus spike (Figure 3.8). This electro-responsive blend was further investigated for incorporation into the hydrogel (Chapter 4).
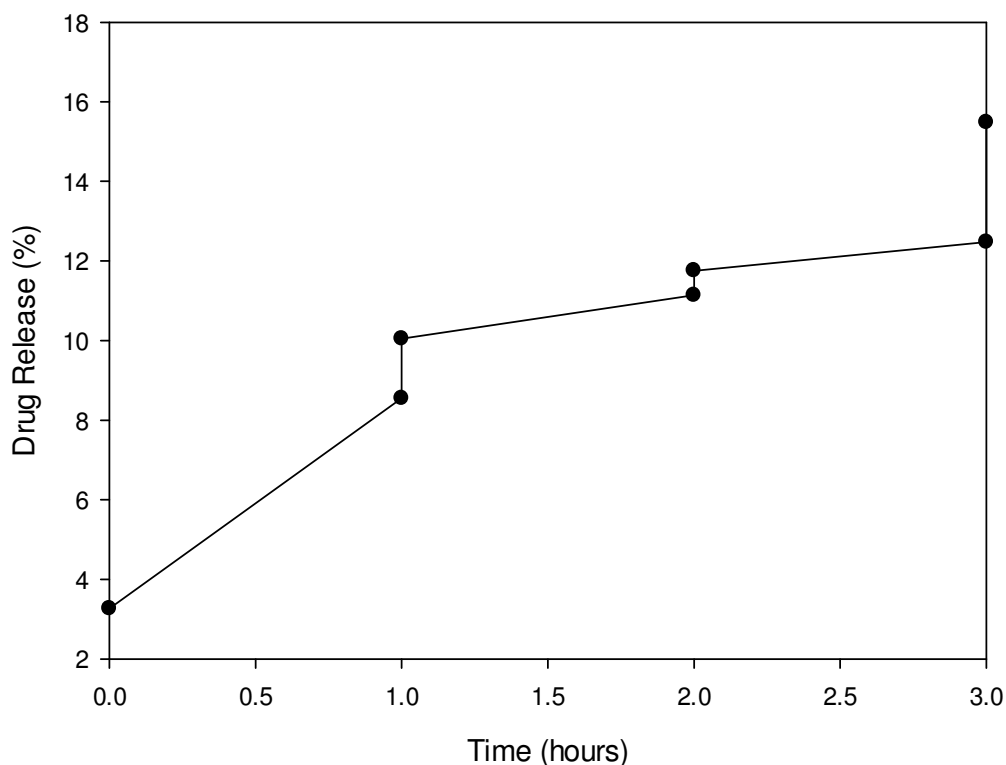
Figure 3.8: Drug release profile of the poly(ethyleneimine)-1-vinylimidazole containing hydrogel.

3.3.6. Evaluation of crosslinking agents for incorporation into the Electro-Modulated Hydrogel using gelation kinetics

The presence of crosslinks prevents dissolution of the polymer chains and thus segmentation of the hydrogel network. In addition, crosslinking maintains the structural integrity of the hydrogel through the formation of covalent bonds between the crosslinking agent and the polymeric chains. In theory, hydrogels that are highly cross-linked tend to swell less than hydrogels than their less-crosslinked counterparts. The solubility and mobility of the polymer network is reduced due to slower chain relaxation within the polymeric network upon hydration, hence retarding drug release (Hennink and van Nostrum, 2002).

The hydrogel formulation was designed to be homogeneous and have quick gelling kinetics without premature gelling. Gelation kinetics is a fundamental parameter in designing homogeneous gels for effective drug loading prior the formation of the gel (Moreira *et al.*, 2014). As previously discussed, subsequent gelation after the comfortable transfer of the hydrogel into a mold was required. Gelation of PVA using GA resulted in a hydrogel with poor structural integrity and a very low viscosity even after a 24 hour period. Although a homogenous structure was formed, gelation was a slow process. Higher GA concentrations were not employed due to the crosslinker's toxic nature (Hassan and Peppas, 2000). The

use of DAA resulted in almost immediate gelation, yet after subsequent drying of the gel; the hydrogel was rigid and did not conform to a uniform structure. It is evident from the results (Figure 3.9), that although DAA provided greater drug release, the release was not proportional to the applied voltage. The same was also seen using GA. This can be attributed to the crosslinking strength of the crosslinkers, with GA being relatively stronger in comparison to DAA. When N, N' methylenebisacrylamide was used to crosslink AA, an intermediate gelation time (±5 minutes) was observed. The resultant hydrogel was rigid having appreciable structural integrity. Heat was used as a catalyst in order to decrease the gelation time to ±3 minutes. PAA gelation was evident within seconds after using the N, N' methylenebisacrylamide and TEMED in conjugation with a thermal initiator. However, as a result, the gelation time decreased significantly making transfer into the MNA mold difficult. As result, TEMED was removed from the formulation process. Consequently, the PAA solution polymerized within a few minutes after being allowed to rest at ambient temperature. The PAA gel proved to be ideal gel as the solution has the ability to penetrate the molds and then undergo polymerization (Chapter 7).
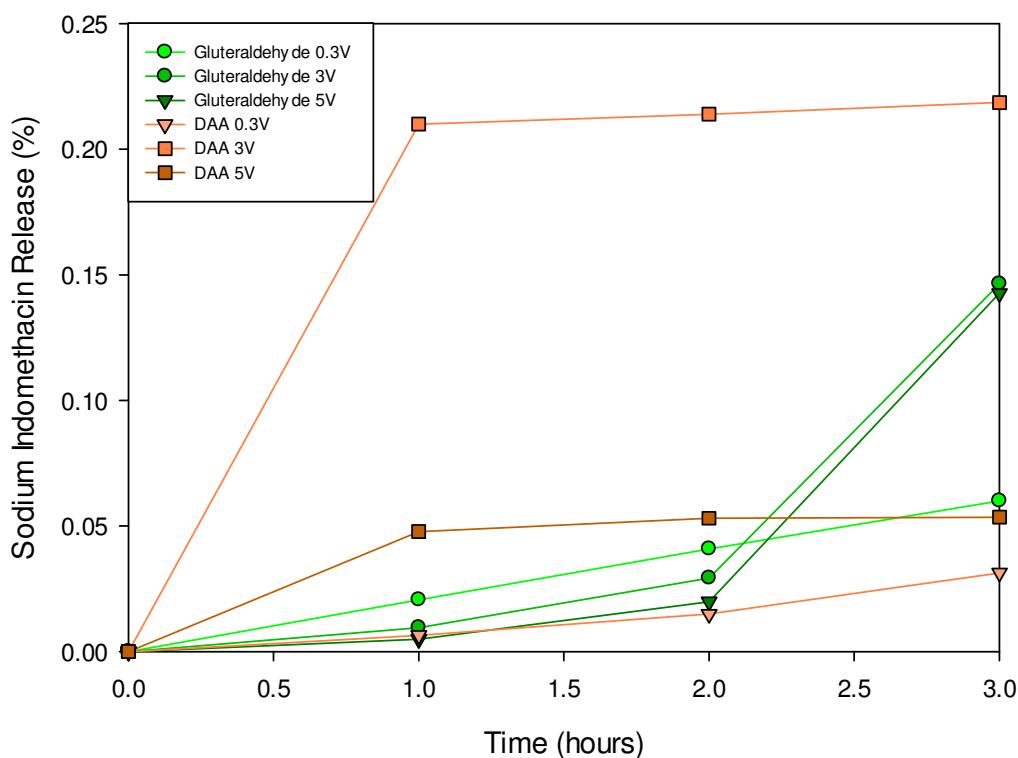
Figure 3.9: Drug release profiles comparing gluteraldehyde and diethyl acetamidomalonate.

PVA is a simple structure containing a pendant hydroxyl group that can be crosslinked with difunctional crosslinking agents such as gluteraldehyde (Hassan and Peppas, 2000). Even though GA solutions are highly toxic to physiological tissues, they are commonly used to crosslink PVA (Figure 3.10) where detoxification and other post-treatment methods of are required to prevent the toxic effects of residual GA involving the chemical bonding of the hydroxyl groups present in PVA with the aldehyde groups of GA (Tang *et al.*, 2010).
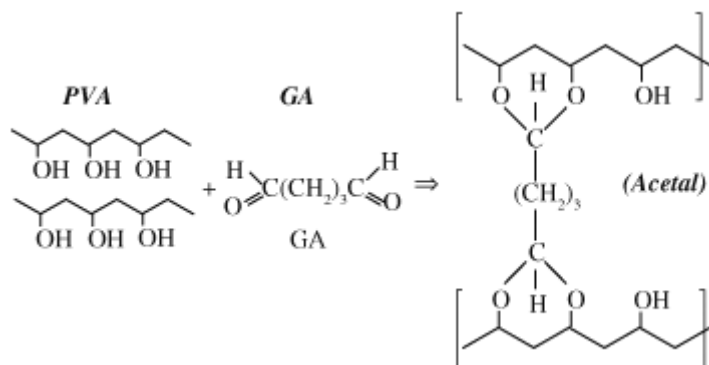
Figure 3.10: Mechanism of polyvinyl alcohol and glutaraldehyde crosslinking (dos Reis *et al.*, 2006).

In the formulation of the hydrogel, PVA was crosslinked using GA with the resultant gel being of very low viscosity and poor mechanical strength thus, the PVA remains un-crosslinked in the final delivery system. In order to produce the semi-IPN and thus requires no additional extraction of the toxic residues.

Once acrylic acid was selected as the second component of the semi-IPN, N, N' methylenebisacrylamide was chosen as the crosslinking agent in order to facilitate vinyl addition polymerization with the polymer network structure being varied through the adjustment of the monomer and crosslinker concentrations. Acrylic acid is the deamidation product of acrylamide and will co-polymerize with acrylamide and N,N' methylenebisacrylamide conferring ion exchange properties to resultant gel formed. In the initial preformulation studies, TEMED and KPS solution were used to initiate the reaction. TEMED accelerates the formation of free radicals by KPS which catalyzes polymerization. The persulfate free radicals convert the acrylamide monomers into free radicals. These free radicals then react with unactivated monomers to begin the polymerization chain reaction (Shi and Jackowski, 1998). The elongating polymer chains are randomly crosslinked by N, N' methylenebisacrylamide, resulting in a gel (Figure 3.11).

N, N' methylenebisacrylamide

CH$_2$=CH   +   CH$_2$=CH $\longrightarrow$ —CH$_2$—CH—CH$_2$—CH—CH$_2$=CH—
| | | | |

C=O   C=O   C=O   C=O   C=O

NH$_2$ NH   NH$_2$ NH$_2$ NH

                   CH$_2$ CH$_2$

                   NH   NH

                   C=O   NH$_2$ NH$_2$ NH

                   CH$_2$=CH   C=O   C=O   C=O

                                                 —CH$_2$—CH—CH$_2$—CH—CH$_2$—CH—

Acrylamide   Polyacrylamide
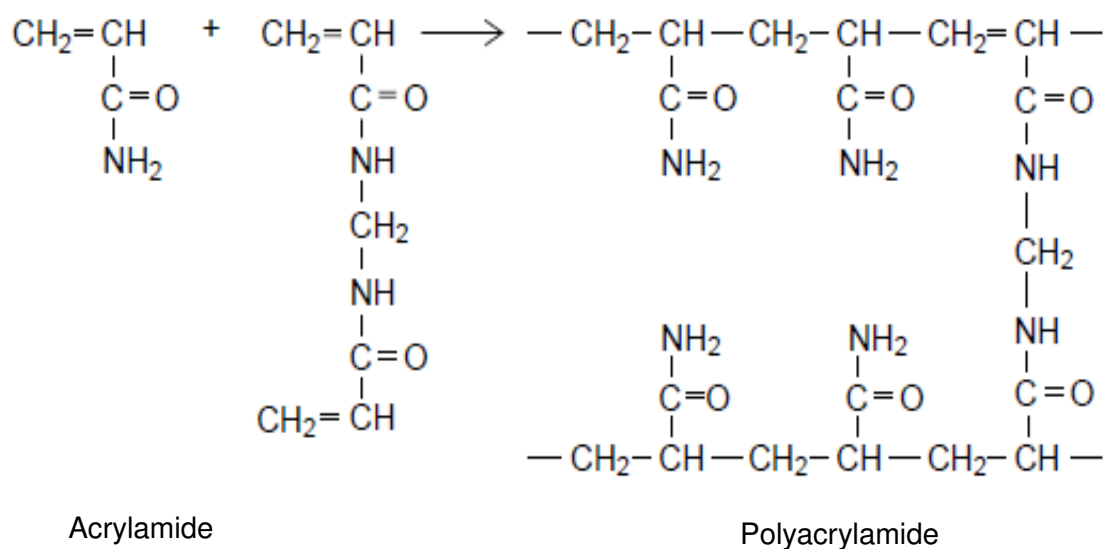
Figure 3.11: Polyacrylamide gel polymerization (BioRad Electrophoresis tech note 1156).

PVA is known for its robustness and AA for its conducting ability (Hassan and Peppas, 2000), each initially as individual monomers chosen per its respective inherent qualities. When combined, so as to allow for synergy between both individual characteristics of the individual components, the hydrogel possessed the required mechanical strength and homogeneity. N, N' methylenebisacrylamide was used to polymerize AA and thus form a second hydrogel network within the pre-polymerized PVA, ultimately forming the SEMI-IPN (Hoare and Kohane, 2008). Semi-IPNs are advantageous in that they allow for relatively dense hydrogel matrices to be produced, allowing for controllable physical properties, strengthened mechanical properties, and more efficient drug loading in comparison to conventional hydrogels (Mohamadnia *et al.*, 2007). A progressive increase in drug release from the hydrogel was observed as the applied potential difference increased even though the release at the spiking intervals was not consistent (Figure 3.12). The initial burst release observed in all the formulations is attributed to the weakly bound highly hydrophilic sodium indomethacin on the surface of the hydrogel. The changes in drug release entail that the controlled release of the therapeutic dose of sodium indomethacin at specific intervals is possible by selecting an optimal applied potential difference. Although the drug release from the hydrogel is small, the release is however electro-responsive and not solely dependent on diffusion alone.
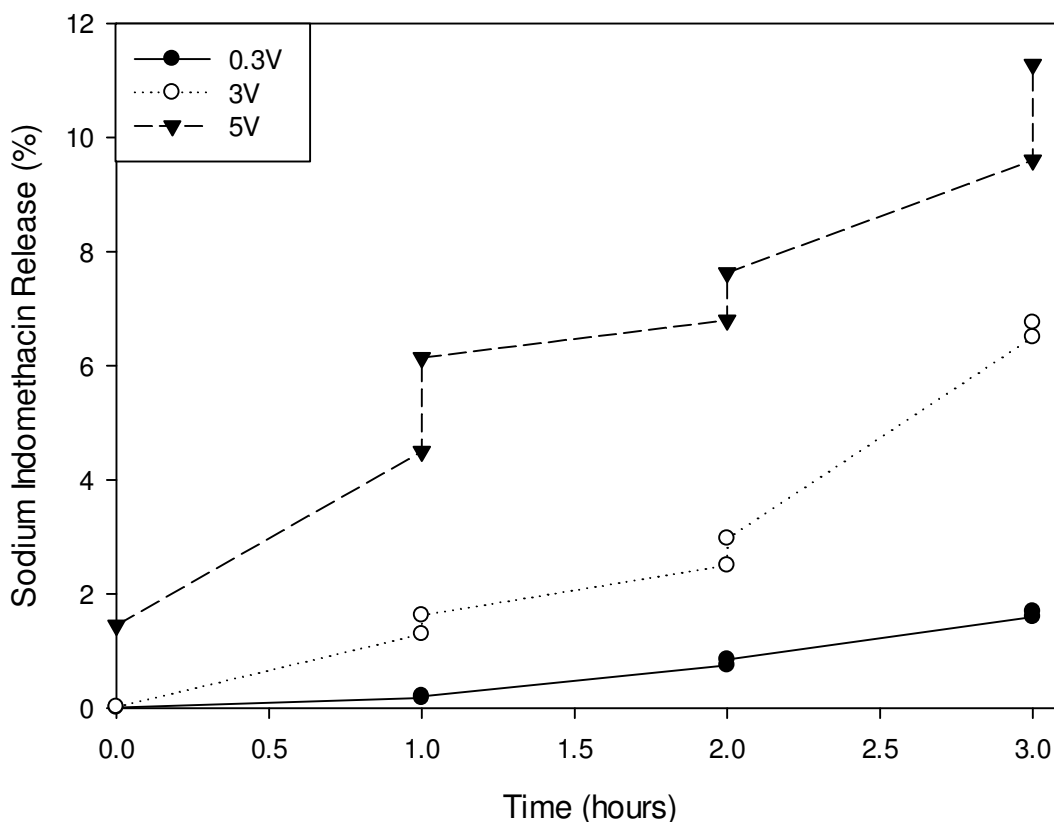
Figure 3.12: Drug release profiles of sodium indomethacin from UV analysis showing the influence of various potential differences on the poly(ethyleneimine)-1-vinylimidazole containing hydrogel.

3.3.7. Identification and selection of optimization variables for institution into a Box-Behnken design

The use of PVA and AA as individual monomers was proven to be too flaccid and rigid, respectively. Hence the combination resulted in a polymer network with appreciable mechanical strength. From the obtained results in this study, it can be concluded that a blend of PSS and PA 6,10 possess the property of enhanced conductive capabilities with the conductivity of the blend being proportional to the PSS concentration. The PEI-VI blend imparted the desired electro-responsive properties to the hydrogel. As per studies undertaken for the determination of the variables required for incorporation into the Box-Behnken design, Table 3.7 outlines the selected variables and minimum and maximum parameters:

Table 3.7: Variables to be employed for incorporation into the Box-Behnken design.

Variable Name	Lower Limit	Upper Limit
Voltage	0V	5V
1-Vinylimidazole	0.1mL	1mL
Poly(ethylene)imine	1mL	3mL

3.4. Concluding Remarks

Preliminary studies have concluded the rational selection and identification of the formulation variables most suited for the development and further optimization of the EMH, namely:

- Voltage level
- 1-Vinylimidazole volume
- Poly(ethylene)imine volume

The hydrogel constituents and formulation technique were selected on the basis that the EMH could be formulated from a relatively simple process that ensures the possibility of scale-up and reproducibility. In addition, toxic solvents and materials were avoided. The primary outcome of identifying an electro-responsive species was obtained in the form of poly(ethyleneimine) and 1-vinylimidazole with a electro-responsive release of at least 2.49-3.00%. The most significant variables of the candidate formulation along with their respective maximum and minimum parameters for optimization were identified. Chapter 4 details the Box-Behnken design for further optimization of the EMH.

CHAPTER 4
DESIGN, DEVELOPMENT AND OPTIMIZATION OF THE ELECTRO-MODULATED HYDROGEL

4.1. Introduction

The design criteria required for the ideal EMH formulation include transport properties, such as molecular diffusion, structural properties such as electro-responsiveness and matrix integrity, and biological properties such as biocompatibility (Figure 4.1; Lin *et al.*, 2006). For a formulation comprised of an electro-responsive species within a hydrogel matrix, three design criteria are apparent: electro-modulated drug release, degree of swelling, and matrix resilience. The use of an electro-responsive polymer blend offers a means to combine the desired and useful properties exhibited by the individual native polymers in the EMH with a simultaneous enhancement of selected properties. As a result, an investigation of a new strategy for the preparation of an EMH, with optimization through a Box-Behnken experimental design is reported on in this chapter.
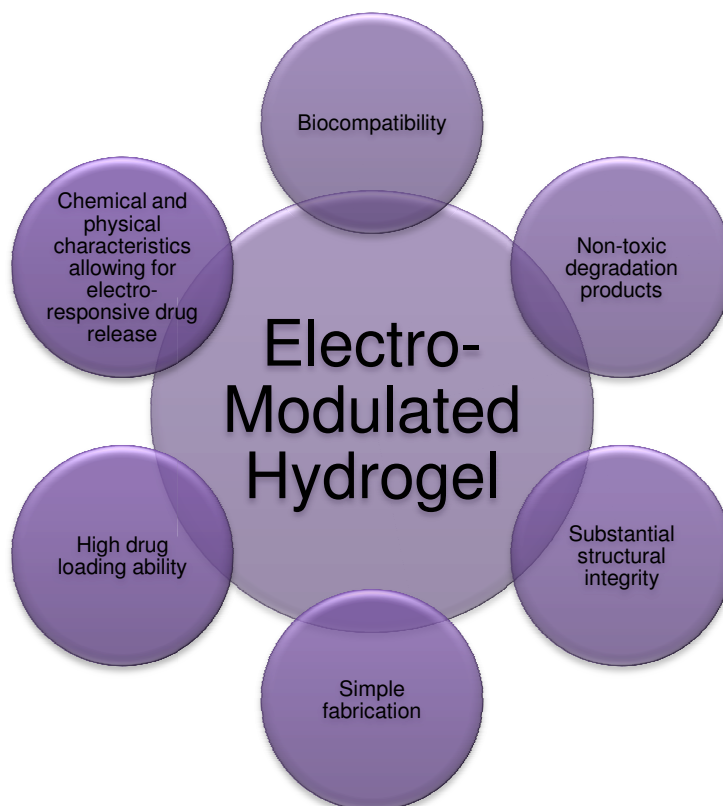
Figure 4.1: Design criteria for the Electro-Modulated Hydrogel.

Box and Behnken (1960) devised a statistical-based experimental design where multiple variables may be changed simultaneously whilst determining its influence on the outcome of a controlled experiment. The construction of a Box-Behnken design model was employed for the systematic optimization of the hydrogel composition and comprised of three variables, viz. PEI volume; VI volume; and applied voltage, critical to the success of the formulation. *In vitro* release studies as well as extensive physicochemical and physicomechanical properties of the formulations of the experimental design were also studied and are detailed herein.

4.2. Materials and Methods

4.2.1. Materials

Poly(ethyleneimine) solution (M_w=750,000g/mol; 50%^{w}/$_v$) 1-vinylimidazole (≥99%), indomethacin (≥99%), poly(vinyl alcohol) (M_w=89,000-98,000g/mol, 99+% hydrolyzed), acrylic acid (anhydrous, 99%), *N,N′*-Methylenebisacrylamide (≥99.5%) and potassium persulfate (≥99.0%) were all purchased from Sigma-Aldrich® (St. Louis, MO, USA). All other ingredients were of analytic grade and were used as received.

4.2.2. Preparation of the electro-modulated poly(ethyleneimine)-1-vinylimidazole-polyacrylic acid hydrogel formulations

For the electro-responsive release hydrogel, a 6%^{w}/$_v$ PVA-1M sodium hydroxide solution was prepared, to which the poly(ethyleneimine) solution and 1-vinylimidazole was added. Subsequently, sodium indomethacin was dissolved into the mixture. Acrylic acid was added. *N*, *N′*-Methylenebisacrylamide (100mg) was then added to facilitate the formation of the semi-IPN, instituting vinyl addition polymerization to increase the interconnectivity of the matrix.

4.2.3. Synthesis validation of the Electro-Modulated Hydrogel using Fourier Transform Infrared Spectroscopy

FTIR utilizing a Spectrum 100 FTIR Spectrometer (Perkin-Elmer, Beaconsfield, BUCKS, UK) was used to detect the vibration characteristics of chemical functional groups in the EMH samples. FTIR was performed on the native polymers involved in the blend as well as the hydrogel formulation as a means of validating the synthesis of the EMH. Samples were processed at a resolution of 4cm^{-1} and were analyzed at wave numbers ranging from 650-4000cm^{-1}.

4.2.4. Construction of calibration curve for the ultraviolet spectrophotometric determination of sodium indomethacin release from the Electro-Modulated Hydrogel

A calibration curve for sodium indomethacin was constructed in PBS (pH 7.4; 37°C) using a known series of concentrations of sodium indomethacin as detailed in Chapter 3, Section 3.2.4.2.

4.2.5.1. Determination of the effect of an enhanced conductive environment on the drug release profiles of the Electro-Modulated Hydrogel

The effect of aluminum foil as an enhanced electro-conductive environment was evaluated as part of the method modulation component of this study. This was due to aluminum foil being electro-sensitive thereby providing a constant surface area for an enhanced electro-conductivity. This evaluation was undertaken through *in vitro* drug release studies on a hydrogel formulation as mentioned in Chapter 3, Section 3.2.4.3, both with and without the use of the aluminium foil.

4.2.5.2. Determination of the effect of lyophilization on the electro-modulated drug release on the Electro-Modulated Hydrogel

In vitro drug release studies on the hydrogel were performed using lyophilized and air-dried (for 24 hours) EMH samples to determine the effect of lyophilization on the electro-modulated drug release profile of EMH. The release studies were carried out as detailed in Section 4.2.5.1 with aluminum foil covering the hydrogel samples on which the two electrodes were directly placed.

4.2.6. Experimental design and constraint optimization of the Electro-Modulated Hydrogel

A model-independent approach (Minitab® V15, Minitab Inc., PA, USA) was used to optimize the EMH. Statistical optimization using a Box-Behnken design model was employed to ascertain the ideal combination of electro-responsive polymeric species (X_{1+2}), as well as the ideal voltage (X_3) required capable of attaining desirable drug release, swelling and matrix resilience efficiencies. Table 4.1 summarizes the factor combinations of the fifteen experimental runs studied and their translation of the coded levels to the experimental units employed during the study.

Table 4.1: Statistically generated formulations obtained via the Box-Behnken design.

Formulation	Voltage (V)	1-Vinylimidazole (mL)	Poly(ethyleneimine) (mL)
1	1	1	2
2	5	0.1	2
3	3	0.55	2
4	3	0.1	1
5	3	1	3
6	5	0.55	3
7	5	1	2
8	3	0.55	2
9	3	0.55	2
10	3	1	1
11	1	0.55	1
12	1	0.1	2
13	1	0.55	3
14	3	0.1	3
15	5	0.55	1

4.2.6.1. Determination of the electro-responsive release per electro-stimulated spike interval using in vitro studies

In order to optimize for therapeutic levels of sodium indomethacin, the average amount of drug released per electro-stimulation for each formulation was determined using *in vitro* release studies as detailed in Chapter 3, Section 3.2.4.3.

4.2.6.2. Determination of the swelling capacity of the Electro-Modulated Hydrogel

The hydrogel samples were analyzed using the Karl Fischer Titrator (Mettler Toledo V30 Volumetric KF Titrator, Mettler Toledo Instruments Inc., Greifensee, Switzerland), where a methanol-water solution is used as the standard and water is quantified using electrical conductivity. The endpoint of the analysis is indicated by the conductivity difference of the solution when any unreacted Karl Fischer reagent. The employed parameters are detailed in Table 4.2.

Table 4.2: Parameters employed in the quantification of water using Karl Fischer titrimetric methods.

Parameter	Setting
Indication	DM143-SC Electrode
Temperature	25°C

The water content from the samples was determined at 0 and 24 hours after submersion in PBS (pH 7.4; 37℃). The hydrogel samples were removed from the PBS and the surface water removed with blotting paper. Gravimetric analysis, as a comparative method, was also used to determine the degree of swelling of the hydrogel and was also conducted, where: the gel sample was weighed before submersion into PBS and then again after 24 hours. The hydrogel was taken out and surface water removed followed by the determination of equilibrium swelling ratio. The equilibrium swelling ratio (ESR) was calculated using Equation 1:

$$\text{ESR} = \frac{(W_1 - W_0)}{W_0} \times 100 \qquad\qquad\qquad \textbf{Equation 4.1}$$

Where W_0 is the weight of the dried hydrogel and W_1 is the weight of the superabsorbent hydrogel.

4.2.6.3. Determination of the physicomechanical properties of the Electro-Modulated Hydrogel using textural analysis

Matrix Resilience (MR) was determined from various textural profiles generated for each hydrogel formulation using a Texture Analyzer (TA.XT.*plus Texture Analyser*, Stable Microsystems®, Surrey, UK). Computations of MR for the samples were performed using Force-Time profiles (N=3) and was employed as a measure of the cohesiveness of the polyelectrolyte matrices and referred to the ability of the matrices to recover to their original dimensions after a compressive stress was applied by the textural probe. The MR (%) was assessed according to the PEI and VI content at 25℃. Typical textural parameters for determining the MR of the formulations of the experimental design are listed in Table 4.3.

Table 4.3: Textural analysis parameter settings for determining the matrix resilience.

Parameter	Setting
Test Mode	Compression
Pre-Test Speed	1.0mm/sec
Test Speed	1.5mm/sec
Post-Speed Speed	1.5mm/sec
Target Mode	Strain
Strain	10%
Trigger Type	Force
Trigger Force	0.05N
Probe type	10mm cylinder

4.2.7. Response surface analysis of the responses employed

Minitab® statistical software (V15, Minitab Inc., PA, USA) was employed to carried out the response surface analysis of the various response variables. The results were demonstrated using response surface and contour plots derived for the measured responses (electro-modulated drug release, degree of swelling and matrix resilience), based on the experimental model.

4.2.8. Evaluation of the surface morphology of the Electro-Modulated Hydrogel samples using Scanning Electron Microscopy

In order to observe surface structures and morphology more accurately, SEM images of the EMH samples were taken using a FEI Phenom™ G2 Pro Desktop Scanning Electron Microscope SEM (Eindhoven, The Netherlands). SEM images of the EMH prior to and after electro-stimulation, in a buffer of pH 7.4, were taken for surface comparison. Prior to imaging, the samples were submerged into the buffer and the optimal voltage applied of 3.63V. EMH samples were then submerged in liquid nitrogen to maintain the integrity of the matrix.

4.3. Results and Discussion

4.3.1. The selection of independent variables for incorporation into a Box-Behnken design

4.3.1.1. Poly(ethyleneimine) as the electro-active species

PEI characteristically is a highly branched aliphatic polyamine (Abu-Saied *et al.*, 2013). The polycation is currently being used in various biochemical and biomolecular studies in addition to its polyelectrolyte properties such as electron transfer and redox reactions (Giménez-Martín *et al.*, 2007; Lojou and Bianco, 2007). The polymer (Figure 4.2a) has a repeating C_2H_5N unit and with a branch for every 3-3.5 nitrogen atoms in a linear unit (Maketon and Ogden, 2009). The high amine content allows for the ability to chelate metal ions and donate electrons.

4.3.1.2. 1-Vinylimidazole as the dual functioning plasticizer and electro-active species

1-Vinylimidazole has advantageous complexing properties due to the electron donor nitrogen in the imidazole ring and is very active in donor-acceptor binding and hydrogen bonding (Figure 4.2b). This weak basic polyelectrolyte that has been already used as a model to be used in various studies (Annenkov *et al.*, 2004). In addition to imparting

plasticizer-like properties, the polymer's vinyl moieties have electro-active capabilities even though there is limited literature on the VI polymers. It is important to note that even the copolymerization of acrylic acid with vinylimidazoles was reported by Davies and co-workers (1973) to be complicated by side reactions.

(a)

(b)
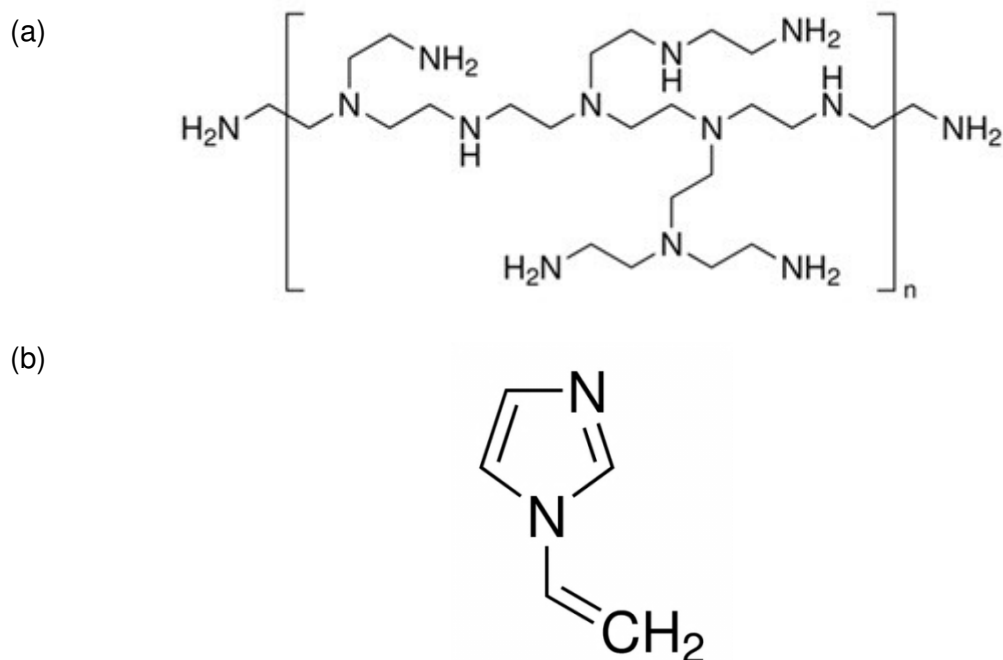
Figure 4.2: Chemical structure of (a) poly(ethyleneimine) and (b) 1-vinylimidazole.

4.3.1.3. Externally applied electric current for stimuli-responsive release

Electro-modulated drug release differentiates the EMH from other types of hydrogels, in order to attain electro-modulated therapeutically relevant levels of drug from the formulation, the stimuli-responsive factor dictating the release requirements were determined through the variation in strength of applied voltage to the hydrogel formulation. *In vitro* electro-stimulation was achieved using the potentiostat/galvanostat (PGSTAT302N, Autolab, Utrecht, Netherlands).

4.3.2. Validation of the crosslinked Electro-Modulated Hydrogel formulation

The shifts and changes in the peak intensity as indicated by the FTIR spectra (Figure 4.3) of the polymer blend in relation to the native polymers specified that chemical interactions and/or electrostatic interactions did occur in the polyelectrolyte matrices. The FTIR spectra of VI revealed the vibrations of imidazole cycles at $1543cm^{-1}$, $1420cm^{-1}$, $1279cm^{-1}$, and $1232cm^{-1}$, bands of azole C–H at $1085cm^{-1}$, and deformational vibrations of the heterocycle at $923cm^{-1}$ and $827cm^{-1}$. The bands observed at $1638cm^{-1}$, $1011cm^{-1}$, $954cm^{-1}$ and $874cm^{-1}$ are indicative of the presence of the vinyl group.

The basicity of polymeric imidazoles (pK_b=5-6) lies between that of very weakly basic amides and ethers and that of stronger bases such as amines (Annenkov *et al.*, 2004). Distinct from amines, imidazole units do not completely become protonated at low pH, but are very active in donor-acceptor and hydrogen binding (Pekel *et al.*, 2002).

The main functional groups of PEI are CH_2, NH and NH_3^+, the presence of protonable amino nitrogen at every third atom of the polymeric backbone imparts the highly positive charge to the polymer. The repeating ethylamine units of PEI confers its highly water-soluble property (Yang *et al.*, 2006). The IR spectrum of PEI shows a peak at $1456cm^{-1}$ which corresponds to the in plane bending of CH_2. The bending vibration of the NH group and the stretching vibration of the C–N groups of PEI can be seen at $1555cm^{-1}$ and $1119cm^{-1}$, respectively (Choosakoonkriang *et al.*, 2003). Peaks indicated by $1638cm^{-1}$ and $1680cm^{-1}$ are attributed to a secondary amine group. An aromatic secondary amine (CN stretch) is seen at $1350–1280cm^{-1}$.
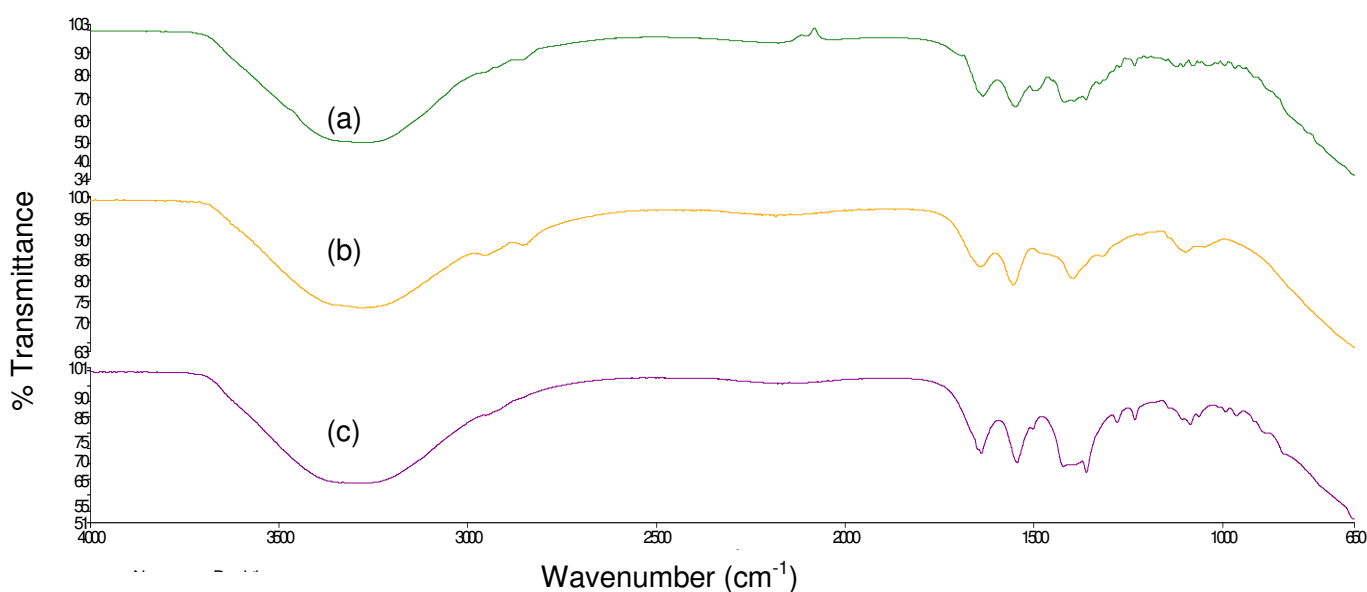
Figure 4.3: FTIR spectra of (a) the polymer blend (b) poly(ethyleneimine) and (c) 1-vinylimidazole.

From the FTIR spectra of the individual IPN components (Figure 4.4), the presence of amine groups was substantiated by a broad band from 2946.68 to $3327.16cm^{-1}$ and 2162.33 to $3367.95cm^{-1}$ signifying NH_2 stretching pertaining to PVA and the semi-IPN, respectively (Bawa *et al.*, 2011). PVA is defined by bands located at wavenumbers larger than $3000cm^{-1}$ belonging to the OH group (Arndt *et al.*, 1999). The observed peak at $1535.06cm^{-1}$ was assigned to NH_2 deformation. PVA lacks C=O stretching vibrations. The $1589.83cm^{-1}$ peak

observed in the FTIR spectra of the semi-IPN is also attributed to NH_2 deformation. For PAA, the peaks around 1634.78cm^{-1} and 1616.81cm^{-1} can be assigned to the amide I and II bands, respectively (Kumar *et al.*, 2012). It is clearly indicated that the anhydride formation occurs connected with the growth of the respective bands of the C-O-C stretching vibrations at 1032.19cm^{-1} and the C=O stretching vibrations, characteristic for the anhydride formation, at 1729.52cm^{-1}. Simultaneously the C=O stretching vibration of the acid in the semi-IPN at 1697.68cm^{-1} decreases.
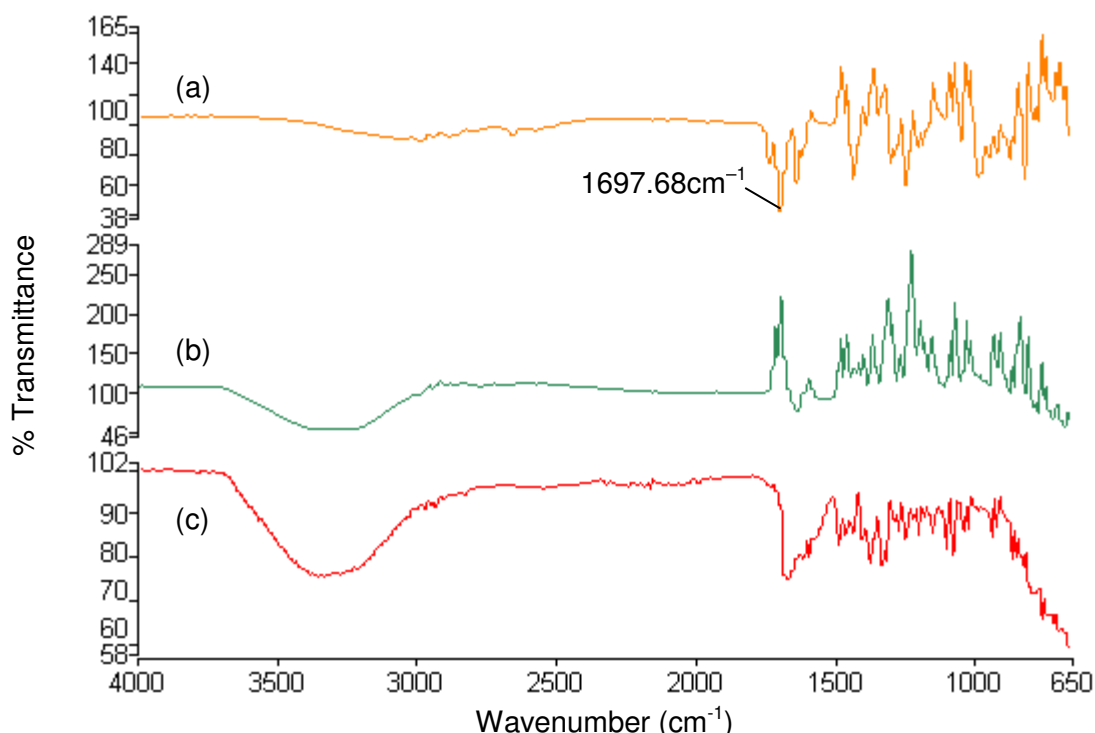
Figure 4.4: FTIR spectra of (a) polyacrylic acid (b) poly(vinyl alcohol) and the (c) semi-IPN.

4.3.3. *In vitro* drug release analysis

When the aluminum foil was placed above the electro-modulated formulation, enhanced electro-modulated drug release was seen in comparison to the formulation contacting a foil ring (Figure 4.5). This observed increase in electro-responsive release (≤1.5%) is possibly due to the foil acting as a conductor, resulting in a greater surface area exposed to electro-stimulation. The hydrogel formulation was proven to be electro-responsive in comparison to the control, with electro-responsive releases of ≤0.6% and ≤1.5%, respectively.
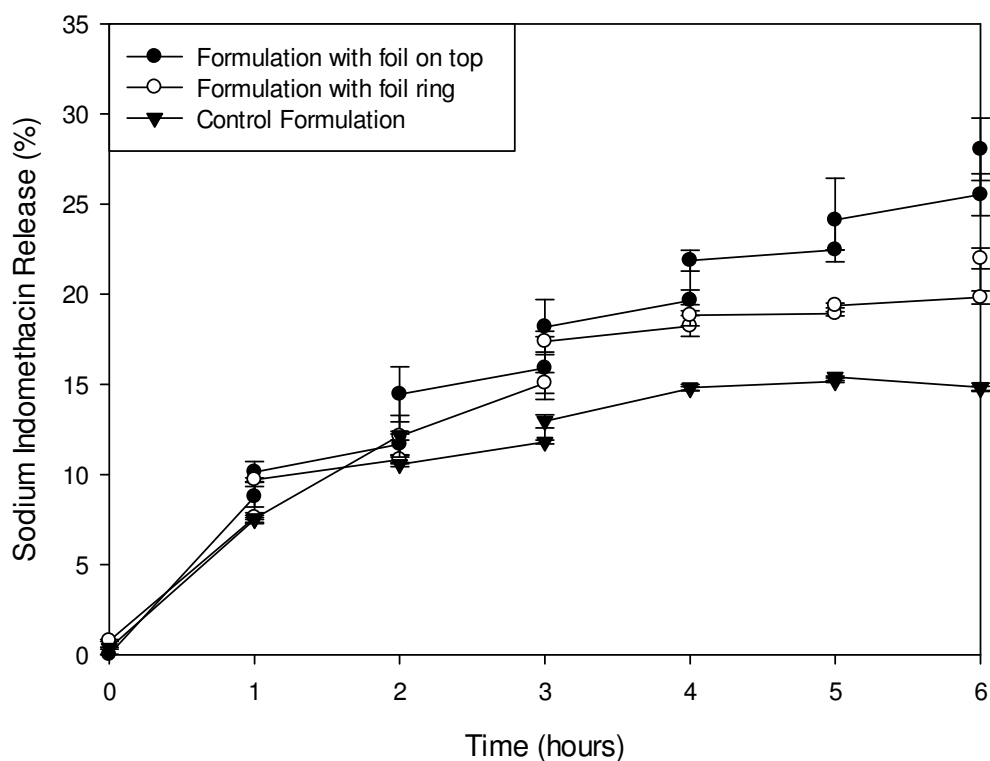
Figure 4.5: Drug release profiles indicating the effect of aluminum foil on the Electro-Modulated Hydrogel formulation (N=3; SD≤1.52 in all cases).

The lyophilized formulation, although displaying a greater increase in drug release, is no longer electro-responsive from hour 3 (Figure 4.6) indicating possible conformational changes of the hydrogel matrix induced by the process of dehydration (Ru *et al.*, 1998). The initial display of an increase in release is due to the osmotic effect of the liquid penetrating the hydrogel matrix due to the concentration gradient. The enhanced release seen with the lyophilized formulation is due to the larger diffusion gradient caused by lyophilization and subsequent rehydration in solution. Compared to the lyophilized formulation, the air-dried formulation does, however, display continuous electro-responsive ability, possibly as a result of the osmotic gradient created by the IPN's semi-crosslinked nature, allowing for the crosslinked PAA to act as a membrane-like barrier.
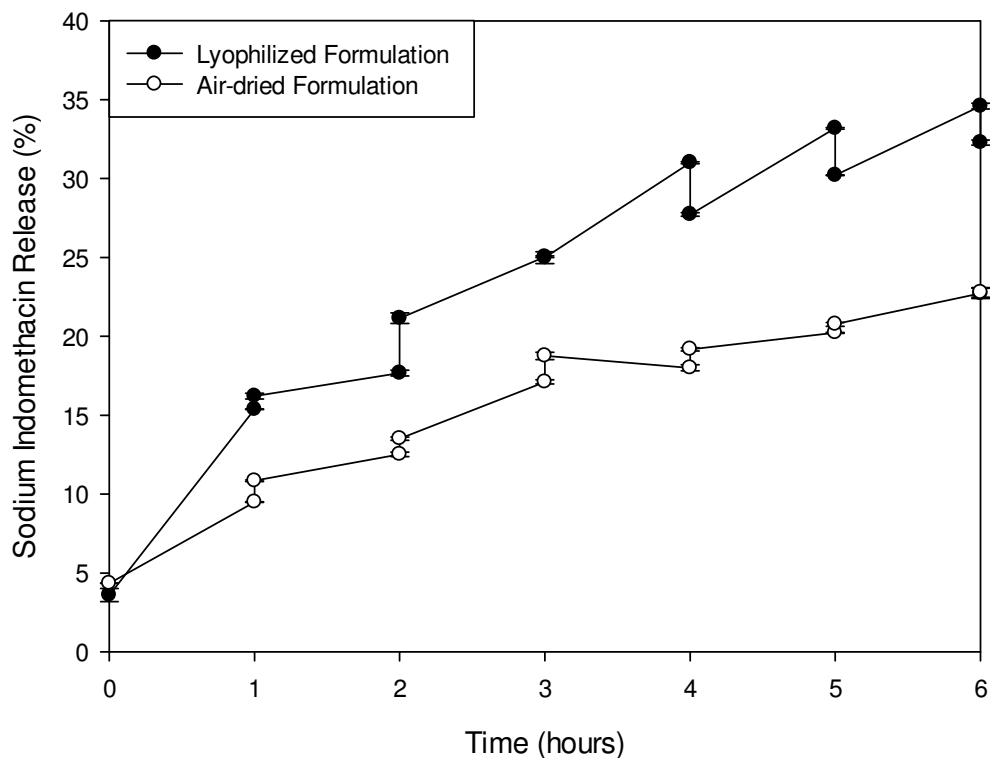
Figure 4.6: Drug release profiles indicating the effect of lyophilization on the Electro-Modulated Hydrogel formulation (N=3; SD≤0.34 in all cases).

The drug release profiles from the *in vitro* studies on the design formulations are depicted in Figure 4.7. Notably composition of Formulations 5 and 6 as well as and Formulations 7 and 8 are similar yet display different swelling abilities. This is attributed to the different voltages applied to the formulations, initiating structural changes accordingly. Average drug release values per electro-stimulation are given in Table 4.4. All formulations displayed electro-responsive behavior. A further discussion is indicated in the surface plot analyses in Section 4.3.6.
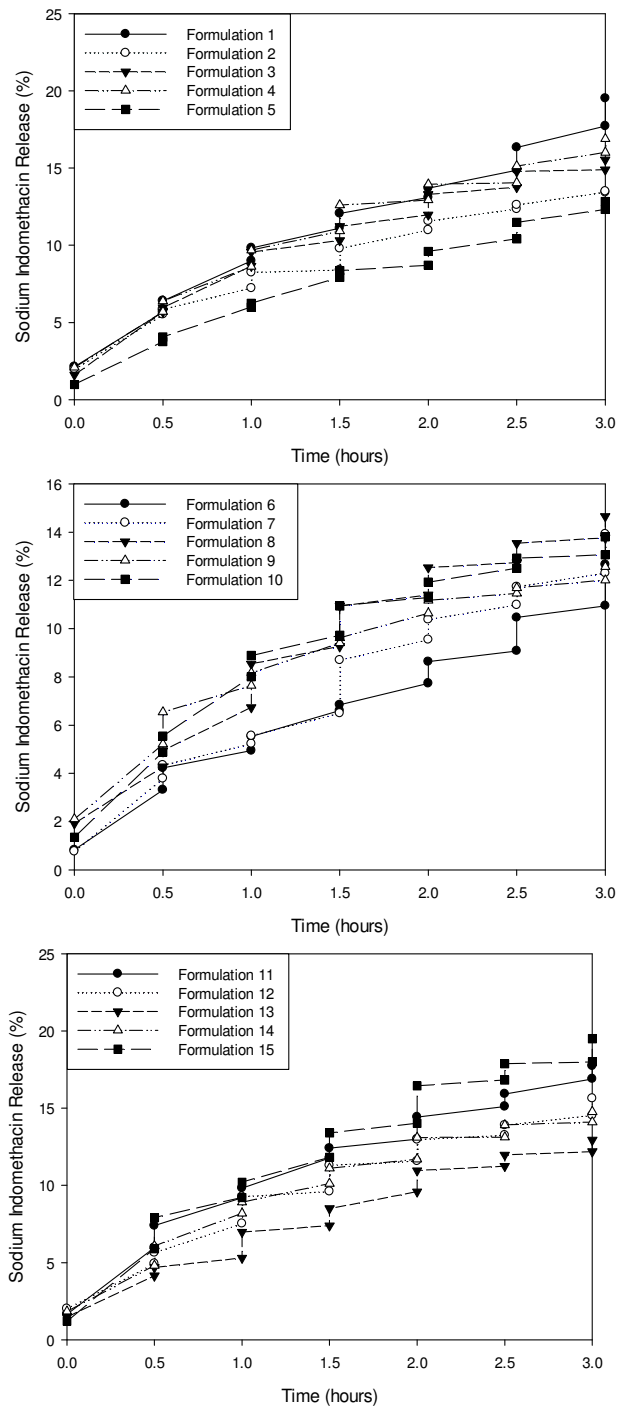
Figure 4.7: Drug release profiles of Box-Behnken design formulations (SD≤2.23 in all cases).

The results indicated that formulations of an electro-responsive nature were produced. The formulations were more structurally stable, not being electro-sensitive and being unaffected by electro-stimulation as opposed to previous research in which a polymer that dissolved in the presence of electricity was utilized.

Table 4.4: Average drug release (per electro-stimulation; N=3) values obtained after electro-stimulation as per Box-Behnken design.

Formulation No.	Average Drug Release (mg)
1	1.66 (±0.42)
2	0.91 (±0.22)
3	1.04 (±0.18)
4	1.35 (±0.31)
5	0.73 (±0.16)
6	0.99 (±0.12)
7	1.07 (±0.22)
8	1.20 (±0.19)
9	1.09 (±0.18)
10	1.19 (±0.23)
11	1.21 (±0.13)
12	1.23 (±0.15)
13	1.24 (±0.22)
14	1.37 (±0.27)
15	1.73 (±0.36)

4.3.4. Influence of moisture content as determined by titrimetric studies

Figure 4.8 indicates the water content of the hydrogel samples at 0 and 24 hours as well as the net change in water content. All design formulations displayed a net increase of ±1-24% in hydration with time. This can be as a result of the protonation of the PEI amine groups which results in an influx of counter-ions and a lowering of the osmotic potential ultimately facilitating osmotic swelling. Formulation 5 displayed a decrease in water content. If the volume of VI is increased in the hydrogels, the water sorption rate is decreased. This may be due to the partly hydrophobic characteristics of the VI polymer, which as a monomer is neutral. VI interaction with water molecules may also result, and water sorption may be slow. In the PAA/PVA EMH, PAA serves as the ionic polymer and PVA, the neutral polymer. As the voltage is applied, electrons repel the carboxylic anions in the gel, thus facilitating swelling. When ionized, the fixed carboxyl ions repel each other, leading to network swelling. The extent of swelling depends on the concentration of functional ionizable groups on the network.

The formation of carboxylic anions in the semi-IPN may be another possible reason for this decrease in water content. Normally, strong electrostatic forces contribute to network expansion and develop as a result of the formation of these carboxylic anions (Elliott *et al.*, 2004). As a result of the attraction due to strong electrostatic forces, the ionic concentration

inside the copolymer is greater than the concentration outside. This concentration difference results in an osmotic pressure gradient resulting in the influx of water. The water absorption properties are thought to result from osmotic pressure as well as due to the interaction through the hydrogen bonding of the water molecules and the carboxylic groups of the copolymer.

Figure 4.9 displays the comparison between the degree of swelling using the KF Titrator method and gravimetrical analysis method displays. The correlation coefficients (R^2) obtained for the KF Titrator method and gravimetrical method were 0.105 and 0.065 respectively. The KF method provides a more accurate result as the gravimetric method is subject to variability in terms of weighing the sample on the scale and removing excess fluid.
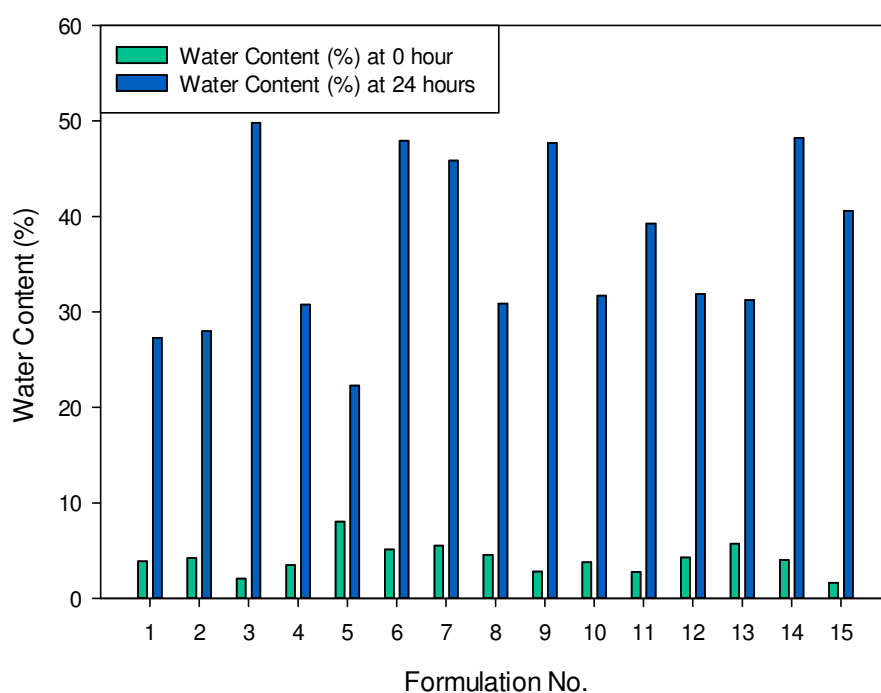
Figure 4.8: Changes in water content as determined by Karl Fischer titrimetric methods.
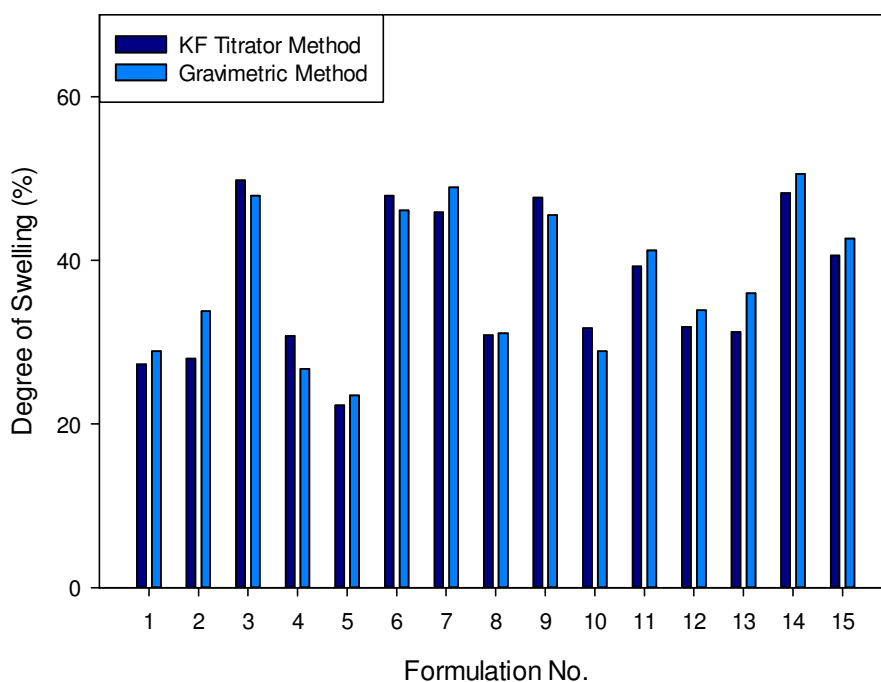
Figure 4.9: Comparison between water content using the Karl Fischer titrimetric method and gravimetrical analysis method.

4.3.5. Assessment of the physicomechanical properties of the Electro-Modulated Hydrogel formulation

Matrix Resilience (MR) refers to the ability of the hydrogel to revert to its original structure after the application of a deforming force and is represented as a percentage of the ratio between the Area Under the Curve (AUC) of anchors 1 and 2 (AUC_{1-2}), and 2 and 3 (AUC_{2-3}). A typical Force-Time profile generated for computation of the EMH MR is shown in Figure 4.10. This figure pertains to F11 of the experimental design.

The effect of polymer blend ratios cannot be ignored as they imparted various intricate physicomechanical characteristics. Textural profile analysis revealed that the PEI/VI blend did not have a significant impact on the robustness of the hydrogel formulations as the MR varied. MR increased with relatively harder matrices, invalidating matrix plastic deformation. The matrices absorbed less impacting energy with harder matrices and therefore the matrix resilience was high.

Densely networked matrices have compact matrices that are resistant to applied mechanical stress. Compact matrices confer lower MR and have the ability, upon hydration, to encompass and retain a notable quantity of drug for longer durations (Choonara *et al.*,

2008). Compact matrices are beneficial in applications where controlled release is desired. Porous matrix structures impart higher matrix resilience as they are less resistant to an applied stress. The porous structure allows for the entry of liquid media, resulting in subsequent rapid release and erosion. Porous matrix structures are thus not be suitable for entrapping lower molecular weight drugs. A relationship between matrix resilience and drug release properties was not clearly defined.
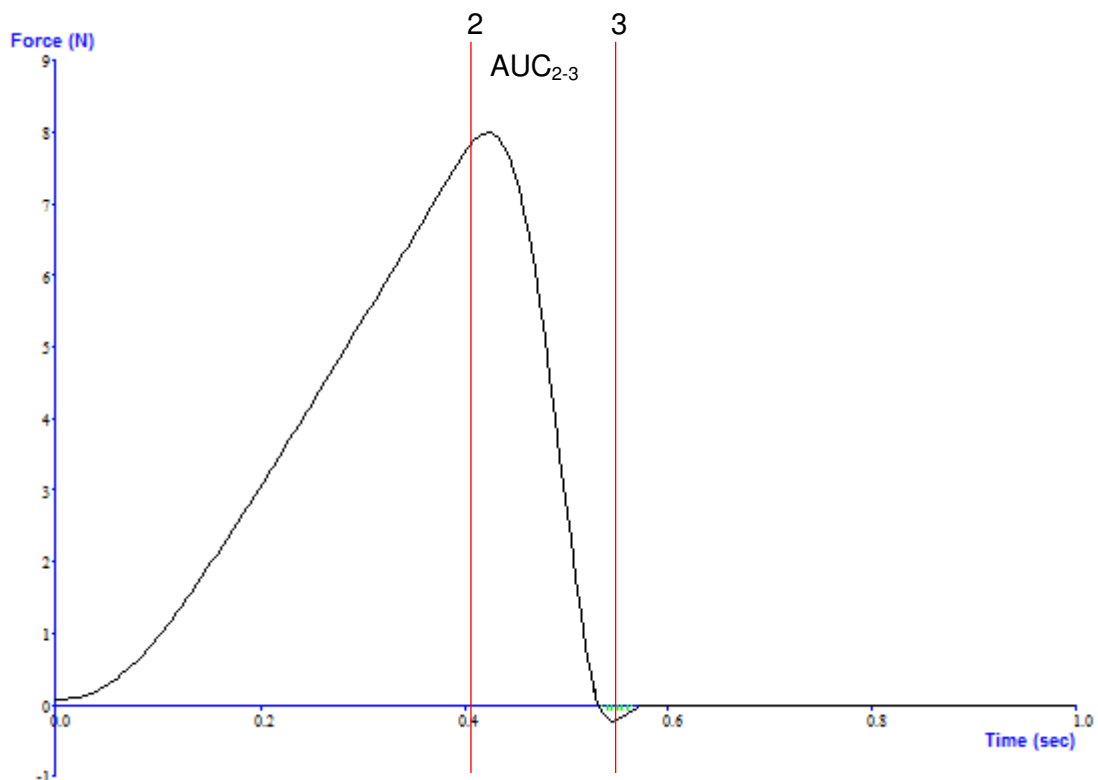
Figure 4.10: Force-Time profile of an Electro-Modulated Hydrogel formulation.

4.3.6. Response surface analysis of the Box-Behnken design

In order to determine the relationship between the response variables and the predictor variables, a full ANOVA analysis was undertaken of the measured formulation responses (Figure 4.11, Table 4.5), electro-responsiveness drug release, swelling and matrix resilience. The suitability of the multiple regression models were assessed through residual analysis. Residual plots for electro-responsiveness drug release, swelling and matrix resilience are depicted in Figure 4.11. The assumptions of a multiple linear regression model is that the response variables are independent and normally distributed, random variables with constant variance and means depending linearly on the explanatory variables (Larsen and McCleary, 1972). Strong linear relationships were observed for all response variables as

indicated by the narrow clustering of the partial residuals. The scatter plot of the residual, where the residuals were plotted against the model predications, is fairly uniform and radiate around zero. They generally showed random scatter i.e. no trends, indicating none of the underlying assumptions of the multiple regression analysis were grossly violated; some outliers as well as some fanning was observed indicative of a degree of nonconstant variance (du Toit *et al.*, 2013). The normal probability plots of the residuals fell on a straight line indicating the data to be normally distributed with no evidence of unidentified variables. Apparent patterning was not observed in any of the variable plots, indicating non-violation of the assumptions of zero means and constant variance of the regression model despite the presence of few outliers in these plots. Deviation could have resulted from experimental error. The obtained histograms for electro-responsive drug release and matrix resilience were generally symmetrical hence supporting the probability plots of uniform distribution. The obtained histogram for swelling displays a lack of symmetry indicative of a random error of the data set. The scatter plot, residual versus observation order, indicates the performance of the model. Scatter points remained in constant magnitude indicating non-random error. A full ANOVA was carried out and is depicted in Table 4.5.

Table 4.5: ANOVA analysis for the measured responses.

	p-values		
Response variable	**EMDR**	**Swelling**	**Matrix Resilience**
Voltage	0.961	0.502	0.702
1-Vinylimidazole	0.552	0.213	0.731
Poly(ethylene)imine	0.949	0.472	0.778
Voltage*voltage	0.481	0.681	0.147
1-Vinylimidazole*1-Vinylimidazole	0.947	0.178	0.683
Poly(ethylene)imine* Poly(ethylene)imine	0.707	0.679	0.924
Voltage*1-Vinylimidazole	0.682	0.299	0.767
Voltage* Poly(ethylene)imine	0.251	0.640	0.179
1-Vinylimidazole* Poly(ethylene)imine	0.444	0.154	0.743

The complete regression equations generated for electro-modulated drug release (EMDR), swelling and matrix resilience are indicated below, where voltage is denoted by x_1, 1-vinylimidazole by x_2 and poly(ethyleneimine)] by x_3:

$EMDR = 1.057 + 0.015[x_1] + 0.759[x_2] + 0.046[x_3] + 0.029[x_1]^2 - 0.053[x_2]^2 + 0.061[x_3]^2 - 0.071[x_1 * x_2] - 0.096[x_1 * x_3 - 0.272[x_2 * x_3]$

Equation 4.2

$Swelling = 17.454 - 6.236[x_1] + 50.116[x_2] + 15.714[x_3] + 0.494[x_1]^2 - 35.043[x_2]^2 - 1.989[x_3]^2 + 5.593[x_1 * x_2] + 1.083[x_1 * x_3 - 16.223[x_2 * x_3]$

Equation 4.3

$Matrix\ Resilience = 96.818 + 9.671[x_1] + 35.332[x_2] - 16.613[x_3] - 5.353[x_1]^2 - 26.784[x_2]^2 + 1.256[x_3]^2 - 4.178[x_1 * x_2] + 9.383[x_1 * x_3 - 9.261[x_2 * x_3]$

Equation 4.4
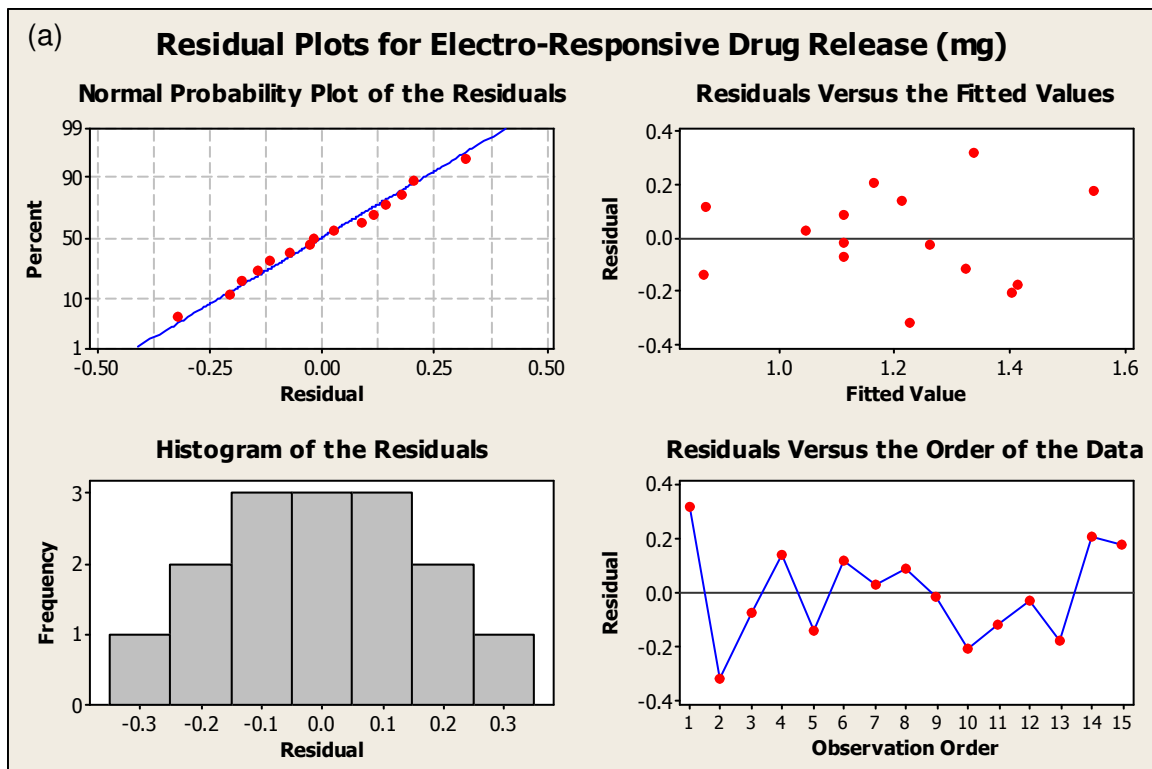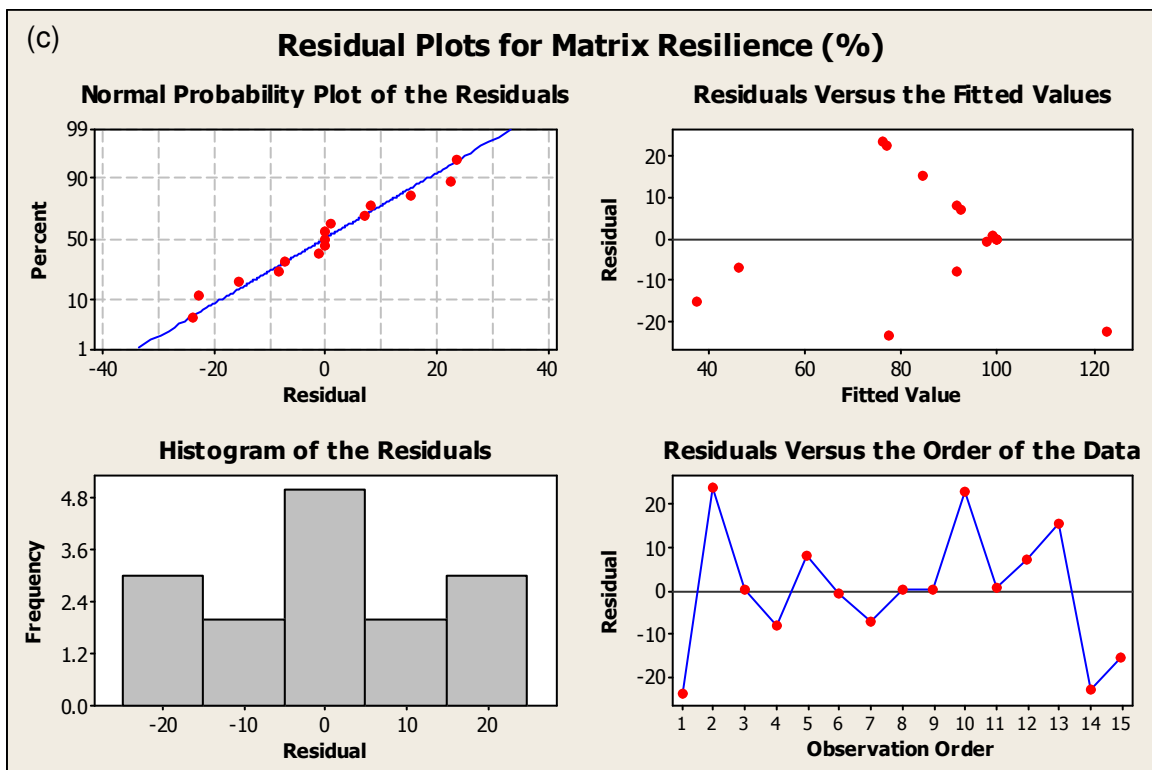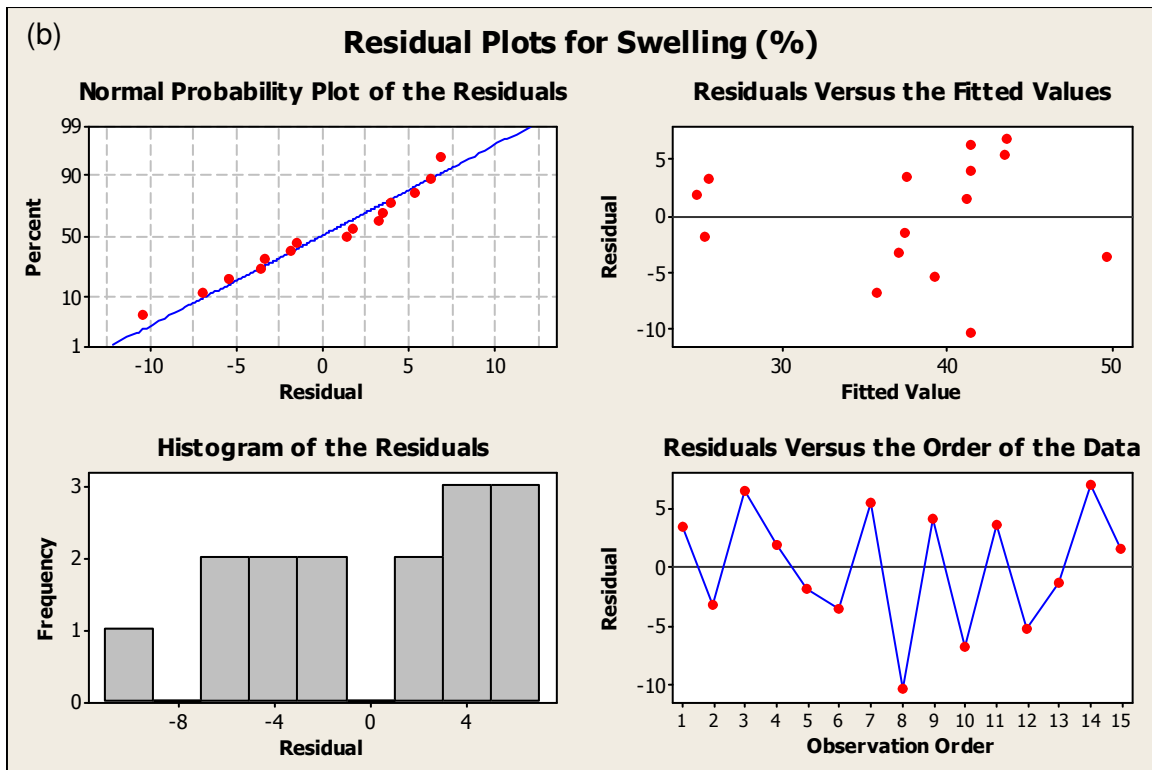
Figure 4.11: Residual plots for the responses (a) electro-modulated drug release (b) swelling and (c) matrix resilience.

Drug release, polymer swelling and matrix erosion are important factors impacting on the observed drug release profile from polymeric matrices. The synchronization between these erosion and diffusion fronts may produce the desired zero-order drug release kinetics. Plots were used to represent the functional relationship between the experimental variables and the responses achieved. The effects of the PEI and VI polymer blend on electro-modulated drug release (EMDR) are depicted in Figure 4.12. Increased volumes of PEI (>2.6mL) and VI (>0.7mL), resulted in ideal therapeutic electro-modulated drug release (0.8mg). Increasing the volume of the polymer results in an increase in the bulk volume of the hydrogel matrix thereby resulting in a decrease in drug release as drug is then required to release from a greater size of the EMH network. Lower amounts of PEI and amounts of VI ranging from 0.20-0.74mL result in a smaller volume of EMH produced and thus a smaller polymer network for drug to release and diffuse from and as a result, is consistent with greater than 1.6mg of drug release per stimulation, pertaining to a possible toxic dose in terms of the therapeutic window of indomethacin (Katzung, 2007).
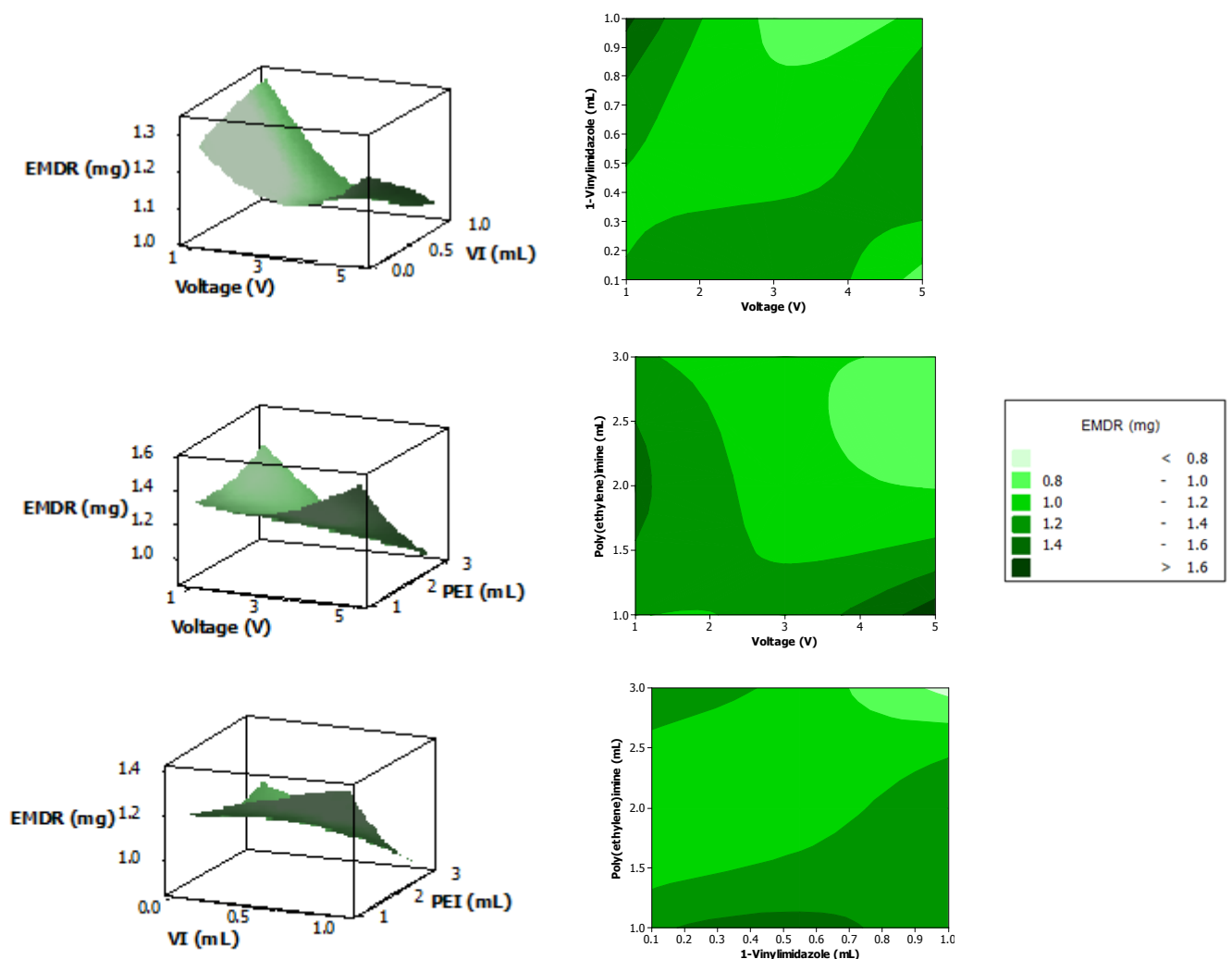
Figure 4.12: Response surface and contour plots depicting the effects of poly(ethyleneimine) and 1-vinylimidazole on electro-modulated drug release.

Minimal swelling is seen with 1.0-1.6mL of PEI and less than 0.15mL of VI (Figure 4.13), attributed to the decrease in chain entanglements of the PEI and VI resulting in the rigidity of the PAA network. VI has added function of imparting plasticizer-like qualities to the EMH and thus reduces its swelling capabilities. Though minimal swelling is required, the obtained statistical values are inappropriate when compared to their corresponding electro-responsive release values. The obtained values for VI and PEI as per the Box-Behnken design, are 0.55-1.00mL and 1.0-3.0mL, respectively, indicating swelling of <25-45%, which is consistent with swelling data.
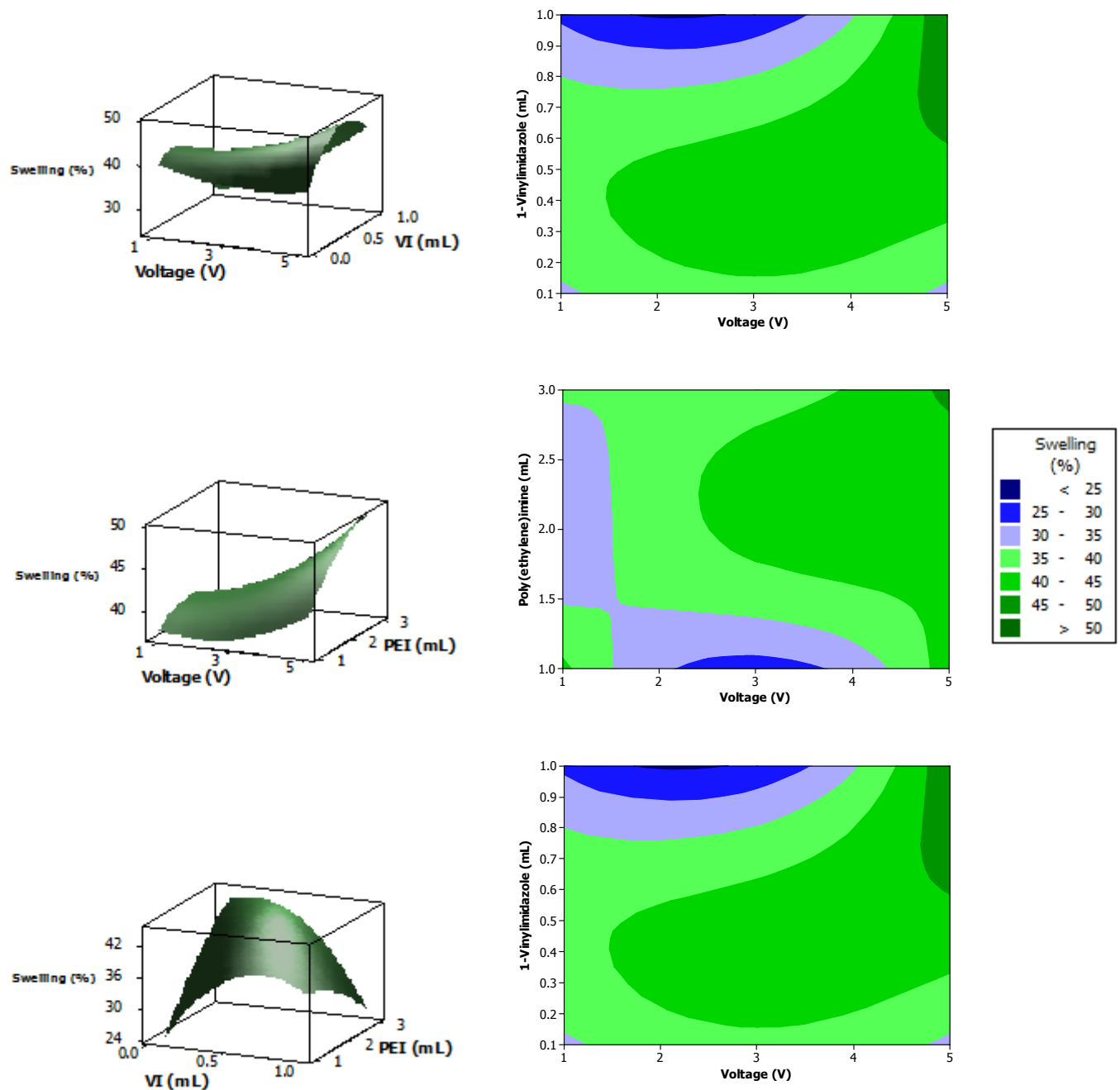
Figure 4.13: Response surface and contour plots depicting the effects of poly(ethyleneimine),1-vinylimidazole and voltage on swelling.

In terms of resilience (Figure 4.14), moderate PEI ranges of 1.75-3.00mL and low VI ranges of 0.9-1.0mL are indicative of a high resilience capability. This is consistent with the plasticizer-like properties that VI imparts to the EMH formulation. Voltage ranges from 2.6-3.5V display greater resilience allowing the formulation to revert to its initial form.
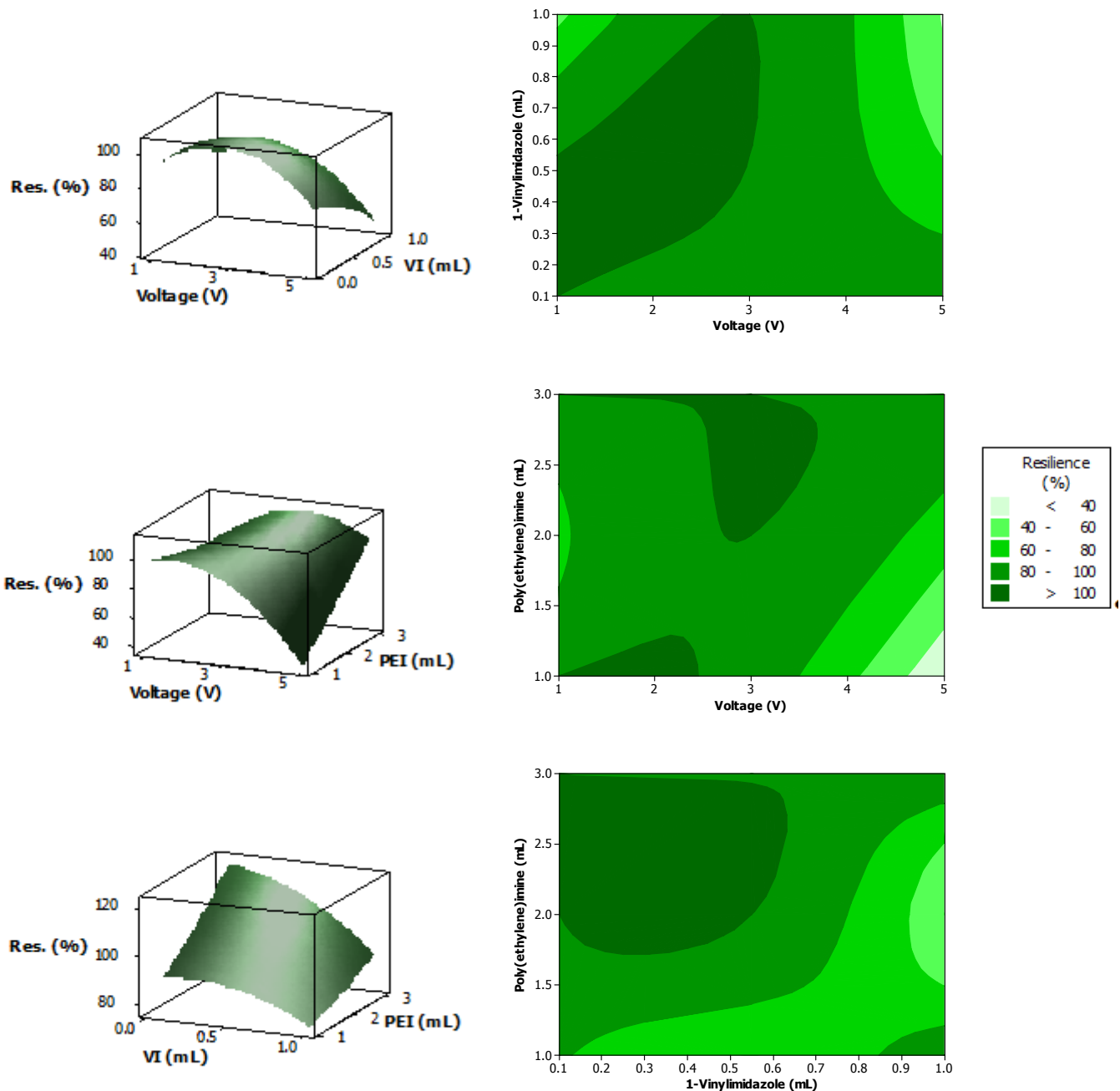
Figure 4.14: Response surface and contour plots depicting the effects of poly(ethyleneimine),1-vinylimidazole and voltage on matrix resilience.

4.3.7. Main and interaction effects on the formulation responses

Interaction effects represent the combined effects of factors on the dependent measure. The impact of one factor depends on the level of the other factor when an interaction effect is present. The plot displays both the levels and mean of each level of one variable on the X axis, ultimately testing the moderation. A "main effect" is the effect of one the independent variables on the dependent variable, ignoring the effects of all other independent variables (Dawson, 2014).

The main effects plots (Figures 4.18a, 4.19a and 4.20a) depict a horizontal line drawn at the grand mean. The effects of the variables on the formulation are represented by the differences between the mean and the reference line. PEI and to a lesser extent, voltage had a more definite effect on the electro-responsive capability of the hydrogel formulation (Figure 4.15a). This can be accounted for by the VI polymer having the dual feature of imparting electro-responsive capabilities and plasticizer–like effects to the formulation. In all interaction plots, disordinal interactions were observed, indicating that the interaction effect between the variables is significant. The greater deviations imply higher degrees of interaction. Electro-modulated drug release displays an interaction between PEI and VI at 0.10-0.55mL of the imidazole polymer (Figure 4.15b). Interactions between PEI and the applied voltages occurred at 1V and 5V (Figure 4.15c). An interaction at 1V is seen with VI (Figure 4.15d).

(a)
Main Effects Plot (data means) for Electro-Modulated Drug Release (mg)
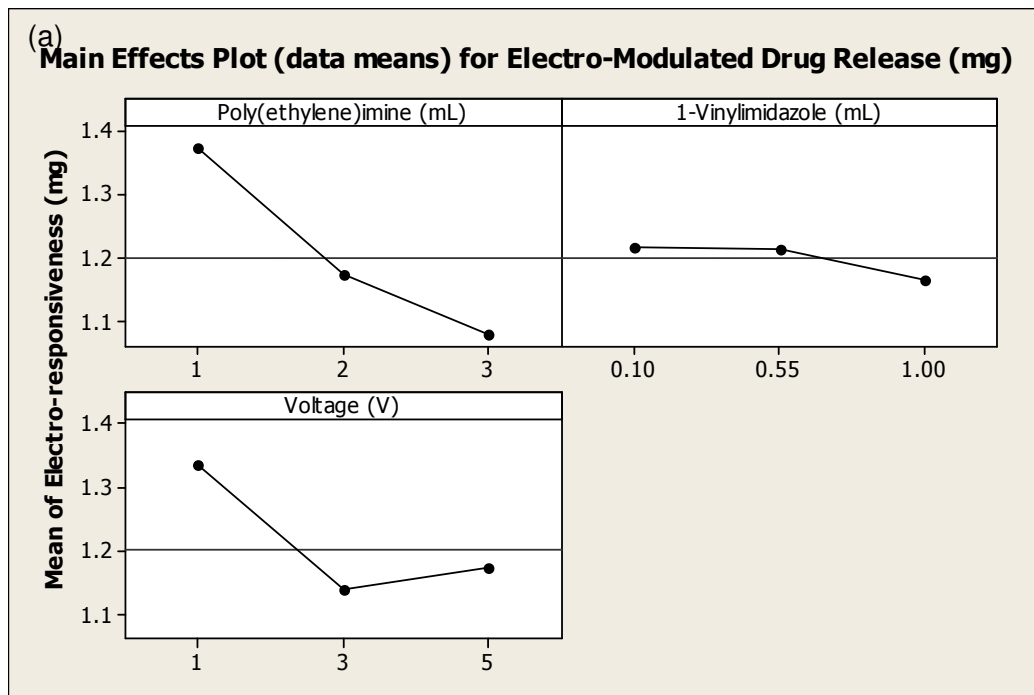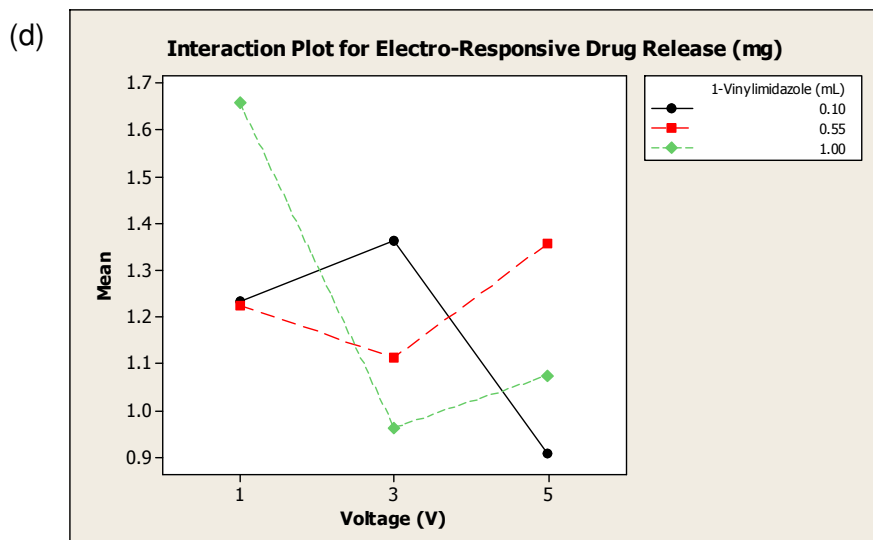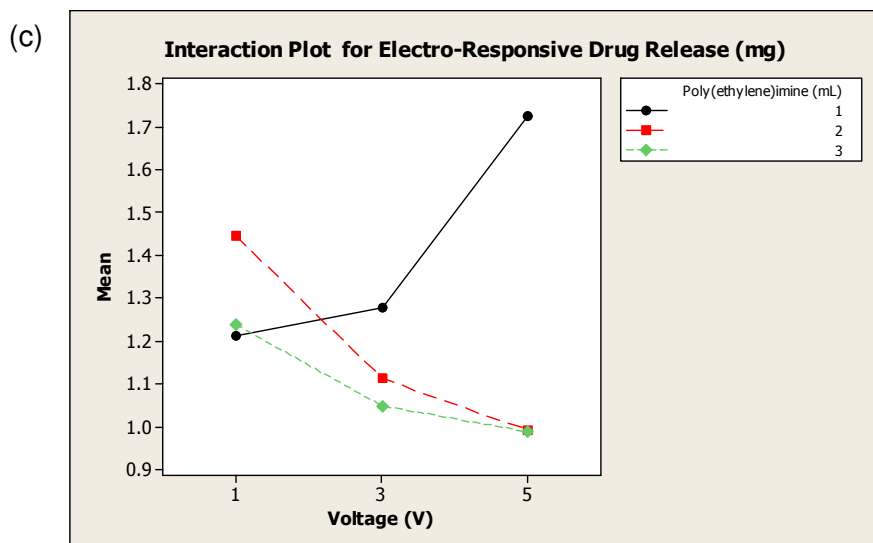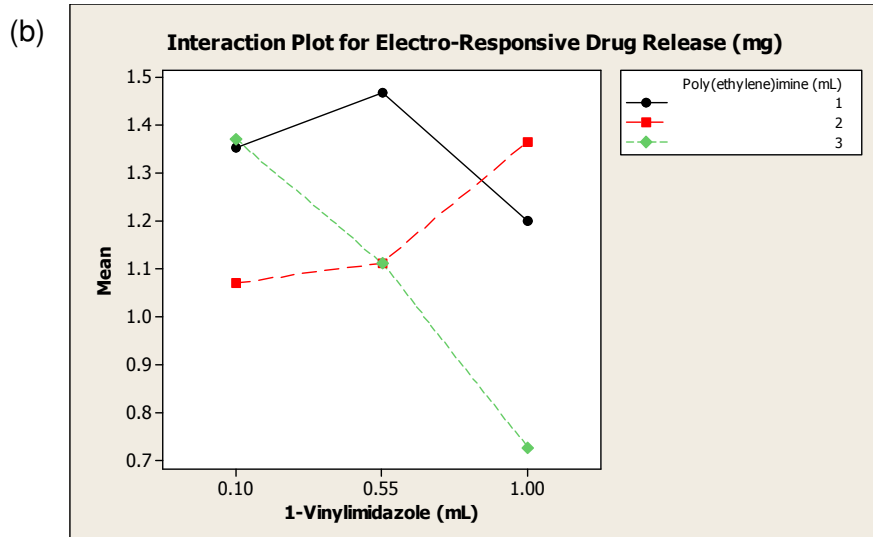
Figure 4.15: (a) Main variable effects plot for electro-modulated drug release. Interaction plots of (b) poly(ethyleneimine) and 1-vinylimidazole (c) poly(ethyleneimine) and voltage (d) 1-vinylimidazole and voltage on electro-modulated drug release.

Regarding the swelling ability of the EMH, the applied voltage and VI effects the fluid intake of the hydrogel to a greater extent than PEI (Figure 4.16a). An interaction between PEI and VI is seen at 0.55mL (Figure 4.16b). Applied voltages at 2V and 4V indicate interactions with PEI (Figure 4.16c). Figure 4.16d indicates interactions of VI at 3.5 and 4V.
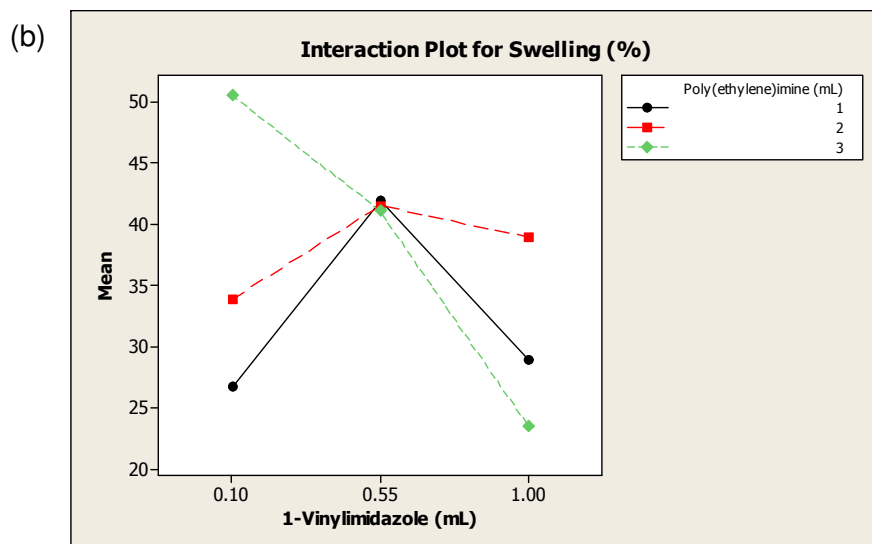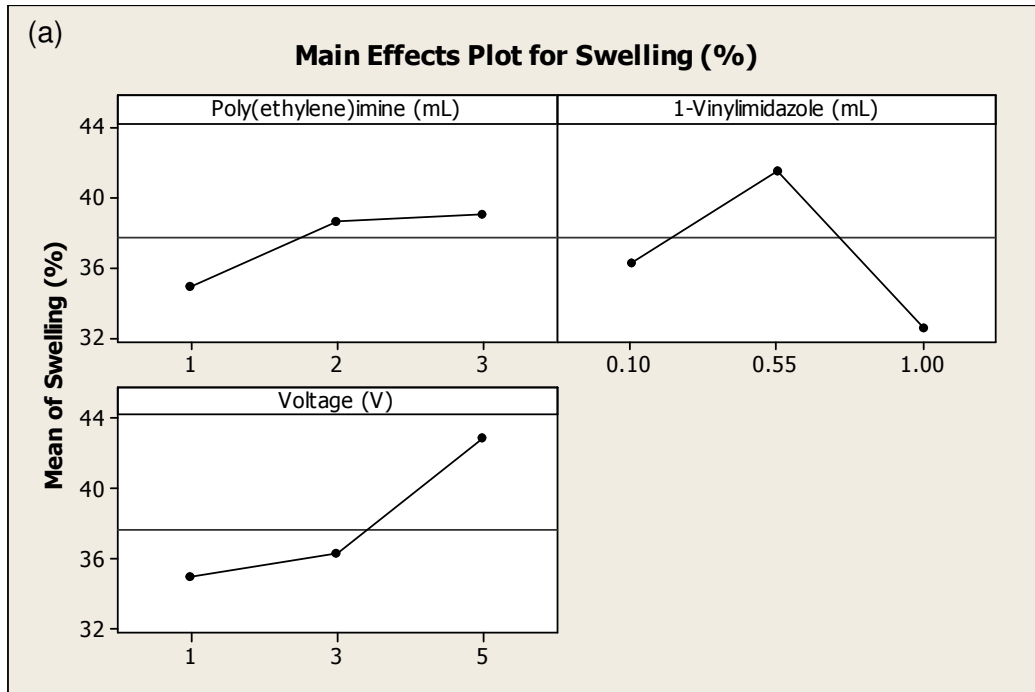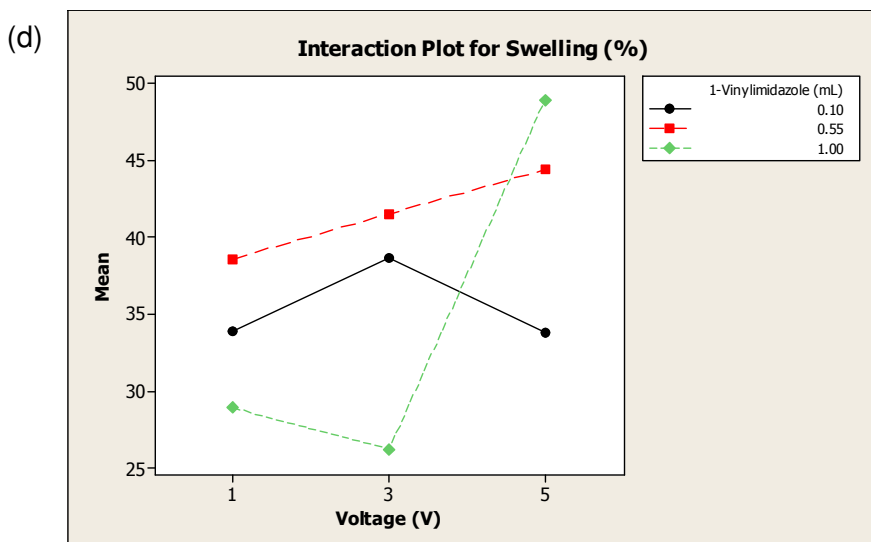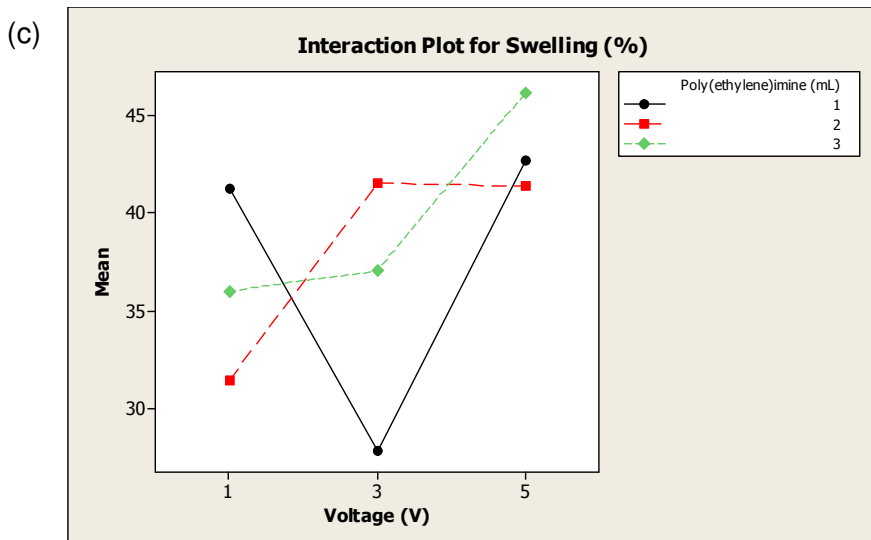
Figure 4.16: (a) Main variable effects plot for swelling. Interaction plots of (b) poly(ethyleneimine) and 1-vinylimidazole (c) poly(ethyleneimine) and voltage (d) 1-vinylimidazole and voltage on swelling.

Voltage regulates the opening and closing of the polymer network thus facilitating the release of drug, this is detailed in Chapter 5, Section 5.3.13. VI maintains the network's structural integrity-limiting network expansion and destruction of the formulation. Matrix resilience is mainly affected by the two electro-responsive polymers and to a lesser degree, the applied voltage (Figure 4.17a). The effect of the polymer blend imparts various intricate physicomechanical characteristics as determined by the textural profile analysis. Figure 4.17b depicts interactions occurring with PEI and VI at 0.1, 0.55 and 1mL. PEI was shown to interact when exposed to voltages of 1V, 3V and 5V (Figure 4.17c). VI interacts with voltages of 1V and 3V (Figure 4.17d).

(a) Main Effects Plot for Matrix Resilience (%)

(b) Interaction Plot for Matrix Resilience (%)

(c) Interaction Plot for Matrix Resilience (%)

(d)

Interaction Plot for Matrix Resilience (%)

1-Vinylimidazole (mL)
- 0.10
- 0.55
- 1.00
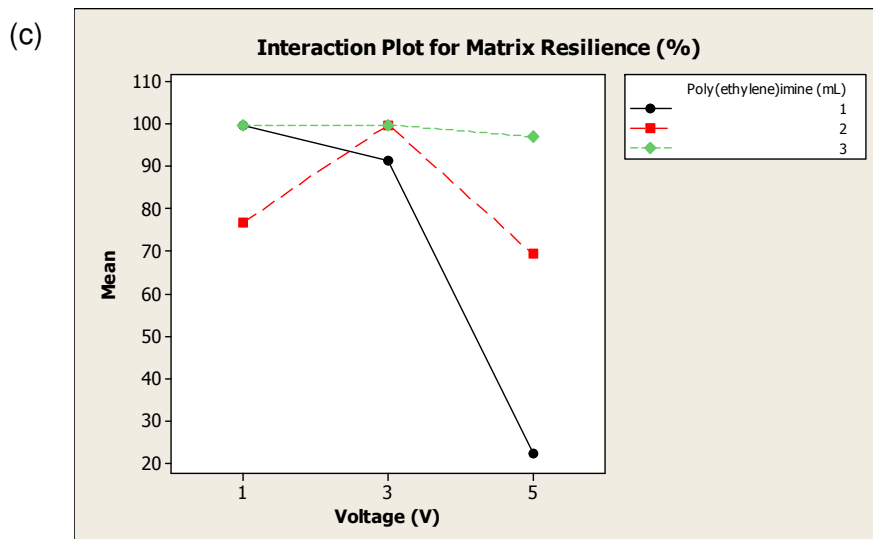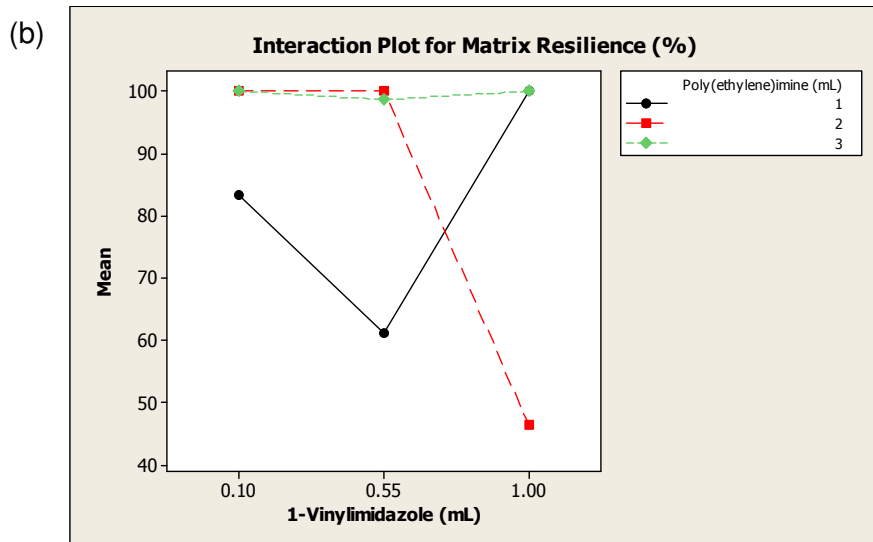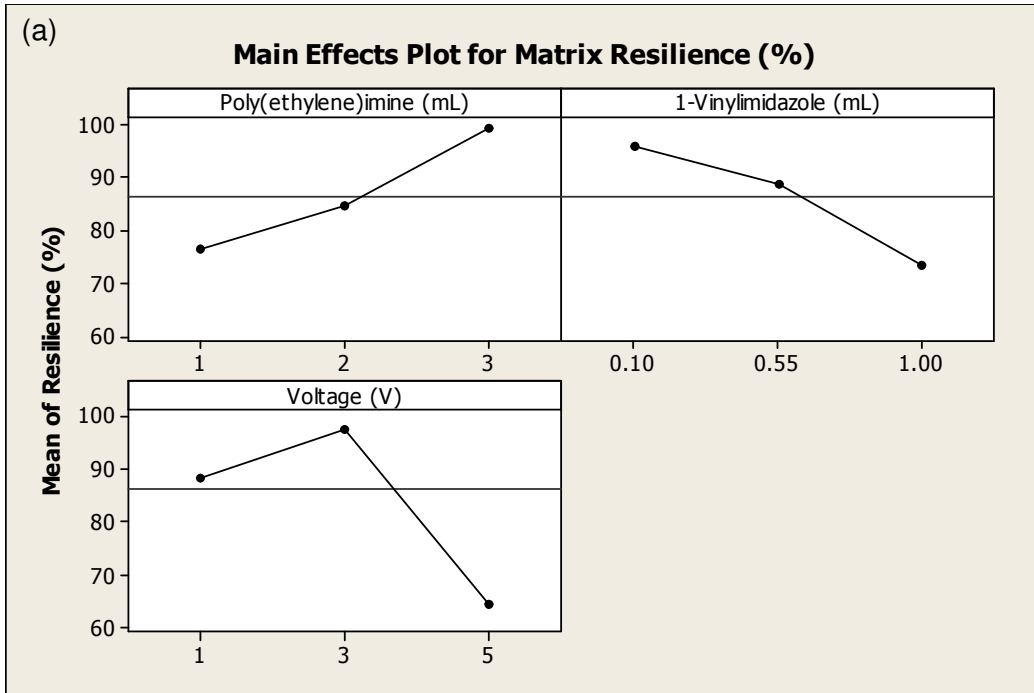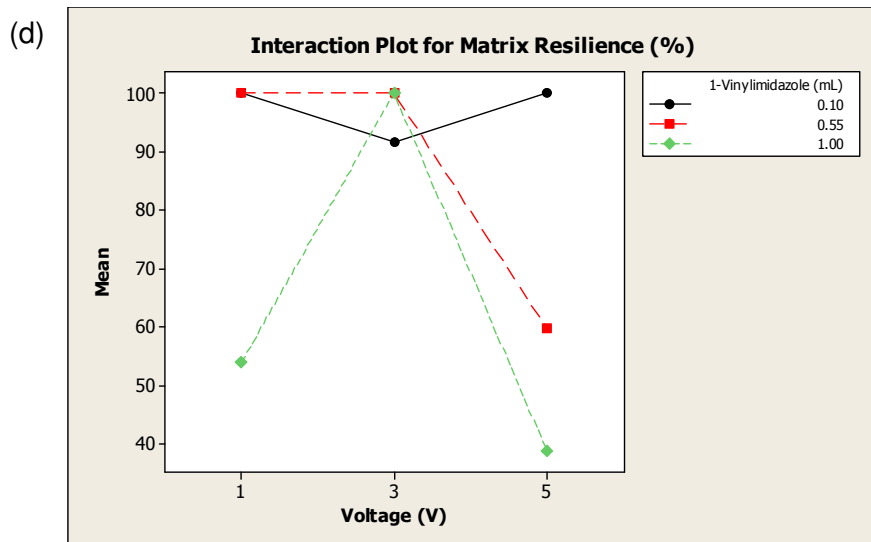
Figure 4.17: (a) Main variable effects plot for matrix resilience. Interaction plots of (b) poly(ethyleneimine) and 1-vinylimidazole (c) poly(ethyleneimine) and voltage (d) 1-vinylimidazole and voltage on matrix resilience.

4.3.8. Surface morphology of the Electro-Modulated Hydrogel

Scanning electron micrographs of the EMH prior to electro-stimulation are depicted in Figure 4.18a. Pores in the EMH become noticeable after electro-stimulation facilitating drug release (Figure 4.18b), indicating formulation stability and electro-induced structural changes in polymer conformation.
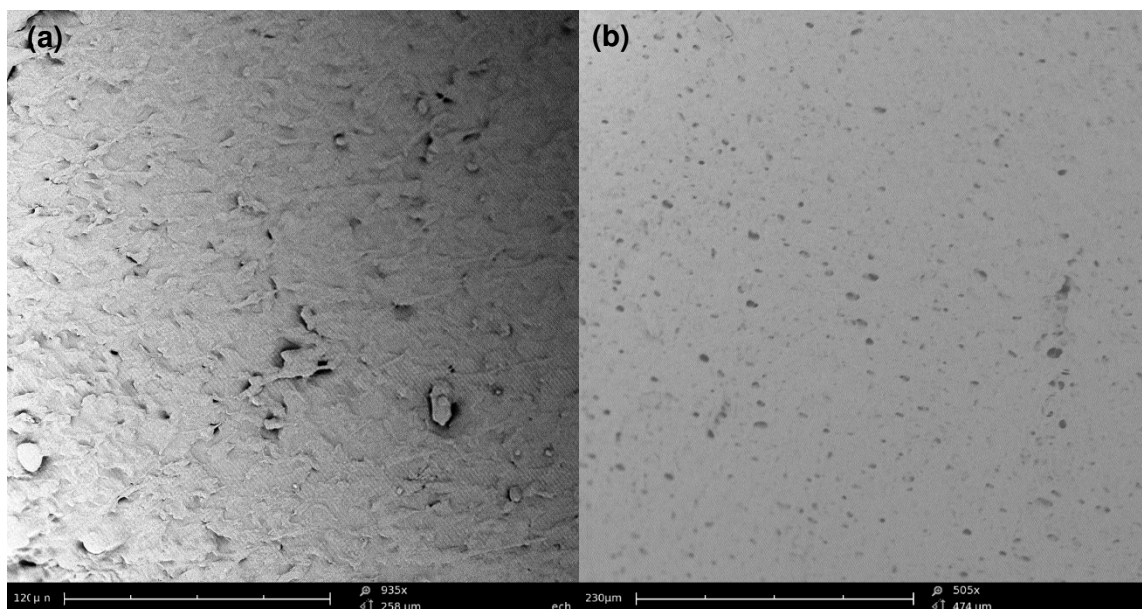
Figure 4.18: Scanning electron micrograph images of the surface morphologies of the Electro-Modulated Hydrogel (a) prior to and (b) after electro-stimulation.

4.3.9. Response optimization of the Electro-Modulated Hydrogel

Response optimization procedure (MINITAB®, V15, Minitab, USA) was used to obtain the preferred levels of the selected formulatory components. An optimal formulation was developed following simultaneous constrained optimization of matrix resilience, swelling properties, and electro-modulated drug release. Maximization of matrix resilience, minimization of swelling properties and an electro-modulated drug release were used for response optimization. The optimized levels of the independent variables and their predicted responses were then determined. The optimal levels of the independent variables as well as the constraint settings utilized that would achieve the desired drug release, swelling and matrix resilience characteristics are listed in Table 4.6. The optimized levels of the independent variables, the goal for the response, the predicted response, y, at the current factor settings, as well as the individual and composite desirability scores are shown in Figure 4.19. Based on the statistical desirability function, it was found that the composite desirabilities for the formulation was 1.0.

Table 4.6: Formulation constraints utilized for response optimization.

Responses	Parameters
Drug Release	0.8mg/electro-stimulation
Swelling	Minimize
Matrix Resilience	Maximize
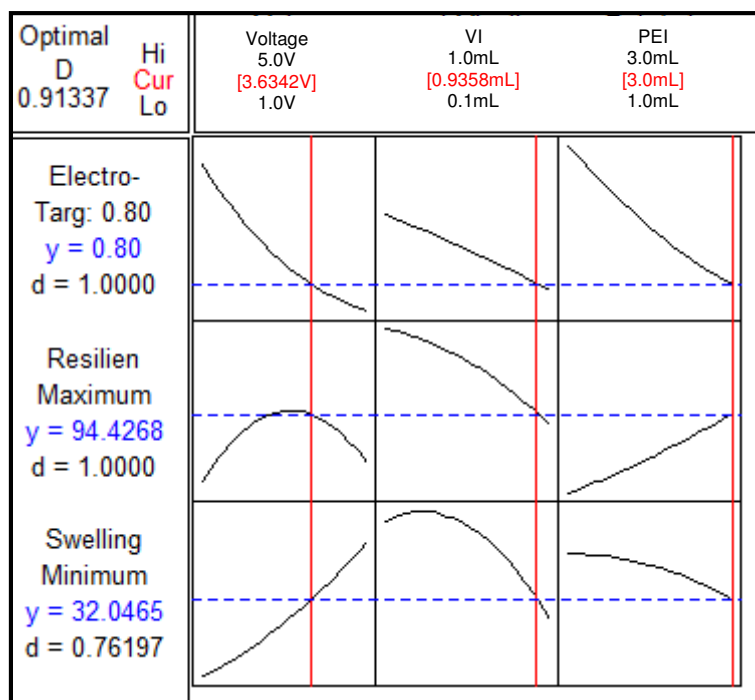
Figure 4.19: Desirability plots representing the levels of poly(ethyleneimine) , 1-vinylimidazole and voltage required to synthesize the optimized formulation.

4.4. Concluding Remarks

This chapter described the utilization of a PEI and VI polymer blend to formulate an electro-conductive hydrogel with electro-responsive release. The results were demonstrated using three variables, namely amount of PEI; amount of VI; and voltage, derived for the measured responses .i.e. electro-modulated drug release, degree of swelling and matrix resilience. Volumes of PEI (>2.6mL) and VI (>0.7mL), resulted in ideal therapeutic electro-modulated drug release of 0.8mg per electro-stimulation for sodium indomethacin. Lower amounts of PEI and amounts of VI ranging from 0.2-0.74mL are consistent with >1.6mg release per stimulation. Moreover, the relative ratios of PEI to VI polymer significantly influenced the degree of electro-modulated drug release and subsequently the matrix resilience of the hydrogels. Textural profile analysis of the various matrices revealed the crosslinked hydrogel matrices were notably resilient. Swelling and water content determination studies were consistent with the predicted results from the response surface analyses, indicating swelling of <25-45%, which is consistent with swelling data (R^2=0.98).

Following the formulation optimization described in this chapter, further characterization of the EMH through physicochemical and physicomechanical characterization is described in the following chapter as a step to determine the efficacy of the design and development of the EMH for eventual *in vivo* studies.

CHAPTER 5

PHYSICOCHEMICAL AND PHYSICOMECHANICAL CHARACTERIZATION OF THE OPTIMIZED ELECTRO-MODULATED HYDROGEL

5.1. Introduction

The principal aim of pharmaceutical research is to ensure that effective, safe and reproducible drug delivery systems elicit the required therapeutic response both *in vitro* and *in vivo*. In order to fulfill these requirements, it is necessary prior to *in vivo* studies, to undertake extensive *in vitro* and *ex vivo* studies. Since the physicomechanical properties of a drug delivery system may have a significant effect on drug release behavior, the effects of such characteristics on physicochemical and drug release performance requires assessment (Tiwari and Rajabi-Siahboomi, 2008). Due to the intricacy and novelty of the EMH, the primary focus of this chapter was to assess the overall pertinent structural characteristics of the EMH formulation on the drug release potential in addition to the stability of the formulation.

In order to gain an in-depth understanding of the electro-modulated function instigated to the hydrogel, a computational investigation of the molecular mechanical electrosimulations was undertaken generated by the standard bond lengths and angles of PAA, PEI and VI. Due to the complexity of a hydrogel of this nature, this chapter focuses on the affects of electro-stimulation to assess the physicochemical and physicomechanical properties of the formulation. Swelling capabilities were assessed in buffers of different pH, thus determining the ionic properties related to swelling of the hydrogel matrix. Fourier Transform Infrared Spectroscopy and X-ray Diffraction analysis were undertaken for structural profiling, Differential Scanning Calorimetric studies for thermal properties, porosity analysis, Scanning Electron Microscopy and Magnetic Resonance Imaging for evaluation of the surface morphology and characteristics. *In vitro* pharmacokinetic analysis, the pertinent electrical properties pertaining to the EMH as well as the electroactive capabilities of the EMH employing cyclic voltammetry were also evaluated.

Additionally, as part of this chapter, the versatility of the EMH is also investigated by incorporating various potent analgesics such as morphine HCL, fentanyl citrate and celecoxib. These formulations were also subjected to physicomechanical assessment and are detailed herein. This chapter therefore provide for the detailed *in vitro* characterization of

the optimized EMH as well as the versatility of the system prior to the conduction of *ex vivo* and *in vivo* studies.

5.2. Materials and Methods

5.2.1. Materials

Poly(ethyleneimine) solution (M_w =750,000g/mol), 1-vinylimidazole (≥99%), indomethacin (≥99%), poly(vinyl alcohol) (M_w= 89,000-98,000g/mol, 99+% hydrolyzed), acrylic acid (anhydrous, 99%), *N,N'*-Methylenebisacrylamide (≥99.5%) and potassium persulfate (≥99.0%) were all purchased from Sigma-Aldrich® (St. Louis, MO, USA). All other ingredients were of analytic grade and were used as received. Morphine HCL, celecoxib, and fentanyl citrate were purchased from their respective manufacturers.

5.2.2. Preparation of the optimized Electro-Modulated Hydrogel

A three-factor, Box-Behnken design was employed for the optimization of the electro-responsive formulation. Statistical optimization was employed using a model-independent approach (Minitab® V15, Minitab Inc., PA, USA) to ascertain the ideal polymeric and external stimulus combination with the desired physicochemical properties capable of attaining desirable electro-modulated drug release, swelling and matrix resilience efficiencies. Detailed analysis of the model is discussed in Chapter 4 of this thesis,

As per the design, 6%$^w/_v$ PVA-1M sodium hydroxide solution was prepared, to which the poly(ethyleneimine) solution (3mL) and 1-vinylimidazole (0.9358mL) was added. Subsequently, sodium indomethacin (100mg) was dissolved into the mixture. Acrylic acid was added (0.6g). *N, N'*-Methylenebisacrylamide (100mg) was then added to facilitate the formation of the semi-IPN.

In addition, formulation multifunctionality was assessed through the substation of sodium indomethacin with morphine HCL, celecoxib, and fentanyl citrate, allowing for a variety of drugs to be incorporated into the EMH and subsequently the development of the drug delivery system as a platform.

5.2.3. Construction of a calibration curve for quantification of the active agents employed in the electro-responsive release from the Electro-Modulated Hydrogel

A calibration curve for sodium indomethacin was constructed as detailed in Chapter 3, Section 3.2.4.2. A UV spectrophotometric scan was run prior to *in vitro* drug release analysis to determine the maximum wavelength for morphine HCL, celecoxib, and fentanyl citrate

absorption in PBS (pH 7.4; 37℃). It was found that morphine HCL exhibits a maximum wavelength at λ_{278}, celecoxib at λ_{208} and fentanyl citrate at λ_{203}. Using a series of known concentrations (0.2-1.0mg/mL for morphine HCL and celecoxib, and 0.2-1.0µg/mL for fentanyl citrate) of drug in PBS, a calibration curve at the aforementioned wavelengths were constructed for morphine HCL ($\varepsilon=3.020x$), celecoxib ($\varepsilon=1.678$), and fentanyl citrate ($\varepsilon=0.0984$). The linear curves ($R^2=0.99$) were plotted with the observed absorbance of drug as the dependent variable and the concentration of drug as the independent variable.

5.2.4. Determination of the Drug Entrapment Efficiency of the Electro-Modulated Hydrogel

In order to validate the drug content of the optimized formulation, the Drug Entrapment Efficiency (DEE) was determined. A hydrogel sample of a known weight of 22mg was immersed in PBS (pH 7.4; 37℃). The sample solutions were homogenized for a period of 10 minutes followed by sonication (Vibra-Cell^{TM}, Sonics® Sonics & Material Inc., Newtown, CT, USA) at amplitude of 80% for 15 minutes. Sodium indomethacin content (mg) was assessed in triplicate and determined by UV spectroscopy (Implen Nanophotometer^{TM}, Implen GmbH, München, Germany) at λ_{320} against the calibration curves.

5.2.5. Synthesis validation of the optimized Electro-Modulated Hydrogel using Fourier Transform Infrared Spectroscopy

FTIR Spectroscopy was used to detect the vibration characteristics of chemical functional groups in the hydrogel samples and was carried out as detailed in Chapter 4, Section 4.2.3.

5.2.6. Investigation of the electro-responsive drug delivery of the optimized formulation using *in vitro* drug release analysis

5.2.6.1. Preparation of artificial sweat

The composition of human sweat is shown in Table 5.1 (Shimamura *et al.*, 2004). Artificial Sweat (AS 3) was prepared to simulate transdermal conditions where the concentration of the positive ions was the same as the median value of the cation concentrations in human sweat. NaOH (0.1M) was used to adjust the pH of the AS to the median value (5.4) of human sweat which ranges from pH 4.5 to 6.3.

Table 5.1: Composition of human sweat and artificial sweat.

Human Sweat		Artificial Sweat - AS (3)*	
Ion	**Concentration (mEq/L)**	**Salt**	**Concentration (g/L)**
Sodium	9.7-94.1	NaCl	2.92
Calcium	0.2-6	$CaCl_2$	0.166
Magnesium	0.03-4	$MgSO_4$	0.12
Iron	0.022-0.068	KH_2PO_4	1.02
Copper	0.002	pH	5.4
Manganese	0.001-0.003		
Zinc	0.016-0.052		
Chloride	0-65.1		
Phosphorus	0.003-0.014		
Sulphur	0.022-0.231		
Bromide	0.002-0.006		
Fluoride	0.011-0.095		
Iodine	0.043-0.096		
Potassium	4.3-10.7		

*milliequivalents of calcium ion

5.2.6.2. In vitro release studies conducted at pH 7.4

In vitro drug release studies on the optimized hydrogel as well as the formulations containing morphine HCL, celecoxib, and fentanyl citrate were performed as mentioned in Chapter 3, Section 3.2.4.3.

5.2.6.3. In vitro release studies using artificial sweat

The release study was performed as described in Chapter 3, Section 3.2.4.3 to determine whether the electro-responsiveness of the hydrogel be affected should sweat enter the EMHM device. The study could not be undertaken under the ideal conditions pertaining to volume due to the volume of sweat being so small. In order to account for consistency, the volume used was 20mL.

5.2.7. Determination of physicomechanical properties of the polymeric components of the Electro-Modulated Hydrogel and their synergistic effects

Texture analysis involving gel strength, matrix resilience and hardness number analyses were performed to determine the effect of electro-stimulation on the physicomechanical behavior of the optimized hydrogel samples and those containing the potent, scheduled drugs. Indentation hardness was represented by the Brinell Hardness Number (BHN)

derived through the textural profiling analysis. Typical textural parameters for determining the physicomechanical behavior of the formulations are outlined in Table 5.2.

Table 5.2: Textural analysis parameter settings employed.

Parameter	Matrix Resilience	Matrix Hardness	Gel Strength
Pre-Test Speed	1.0mm/sec	1mm/sec	1mm/sec
Test Speed	1.5mm/sec	0.5mm/sec	1mm/sec
Post-Speed Speed	1.5mm/sec	10mm/sec	10mm/sec
Target Mode	Strain	Distance	Distance(5mm)
Compression Strain	50%	N/A	N/A
Compression Force	N/A	40N	N/A
Strain	10%	50%	N/A
Trigger Type	Auto	Auto	Auto
Trigger Force	0.05N	0.05N	0.05N
Probe type	Delrin cylinder probe (10mm)	Spherical (5mm)	Radius cylinder (0.5")

5.2.7.1. Matrix resilience

Matrix resilience (MR) was determined from various textural profiles generated for each hydrogel formulation using a Texture Analyzer (TA.XT.*plus Texture Analyser*, Stable Microsystems[®], Surrey, UK) as detailed in Chapter 4, Section 4.2.6.3.

5.2.7.2. Matrix hardness

Matrix hardness (MH) was calculated in terms of the BHN (M/mm^2) using a calibrated texture analyzer (TA.XT plus Stable Microsystems, Surrey. UK) fixed with a ball probe indenter of diameter 4.981mm. The indentation diameter was employed at 2.311mm with a 5kg load cell for all readings. The indentation hardness was represented by a conversion to the BHN (Equation 5.1).

$$BHN = \frac{2N}{\pi D(D - \sqrt{D^2 - d^2})}$$
Equation 5.1

Where, N =applied force (kgf), generated from indentation (N), D =diameter of indenter (mm) (4.981mm) and d = diameter of indentation depth (2.311mm).

5.2.7.3. Gel strength

The gel strength (often expressed as Bloom) is the mass in grams necessary to depress a standard plunger of 4mm diameter into the gel at a gelatin concentration of 6.67% after 17 hours at 10°C. A 0.5" radius cylinder probe was employed for the determination of gel strength. Typical Force-Time profiles were generated for computation of the gel strength using a Texture Analyzer (TA.XT.*plus Texture Analyser*, Stable Microsystems®, Surrey, UK).

5.2.8. Characterization of thermal transitions using Differential Scanning Calorimetry

In order to ascertained phase change temperatures, melting points, chemical reaction temperatures, and glass transitions (T_g) of the EMH, the EMH underwent DSC testing employing a Temperature Modulated or Advanced DSC (TMDSC/ ADSC) (Mettler Toledo DSC-1 STARe System, Schwerzenback, ZH, Switzerland) to further assess the thermal behavior of the constituents.

Thermal transitions were assessed in terms of the T_g measured in response to variation in the magnitude of the crystallization temperature (T_c) and melting temperature (T_m) peaks corresponding to the total heat flow (ΔH). Calibration of temperature and enthalpy on the instrument were undertaken using indium. The thermal transitions of native PEI and VI hydrogel films were compared to a physical mixture of PEI and VI as well as ground samples of the EMH. Samples (±10mg) were accurately weighed into standard 40μL aluminum open pans and hermetically sealed in perforated 40μL aluminum pans. Samples were then heated from -20-100°C and held at 100°C for 3 minutes so as to evaporate any moisture present in the sample, to eliminate any thermal history and to determine the T_g. The pans were then ramped at 10°C/minute between a temperature gradient of -20-400°C under a constant purge of an inert N_2 atmosphere (100mL/minute) in order to diminish oxidation. The melting point (T_m) obtained from the melting point depression was determined according to the peaks generated on the experimental DSC curves.

5.2.9. Porositometric analysis of the Electro-Modulated Hydrogel in the presence of buffers of differing pH

Porosity analysis employing the BET isotherm of nitrogen was conducted as an investigation to determine the presence of pores and pore size within the optimized formulation prior to and after electro-stimulation as well as the optimized samples at pH 5.5 and 7.4 after electro-stimulation. An ASAP 2020 Porositometer (Micromeritics Instrument Company (Pty) Ltd., Norcross, GA, USA) equipped with research grade ASAP 2020 V3.01 software was employed to determine the quantifiable aspects of the hydrogel's porous nature, such as surface area, pore diameter, total pore volume, and bulk and absolute densities. Briefly, the

pieces of the hydrogel (100mg) were evacuated with Nitrogen gas (N_2) (hard-sphere diameter=3.860Å; molecular cross-section=0.162nm^2) for the removal of surface moisture and gas particles prior to analysis. Table 5.3 lists the parameters and settings employed under standard conditions of temperature and pressure (STP: 0°C and 760torr). The samples were weighed (±100mg) and placed in a cylindrical sample tube. To reduce the total free space, increase the capacity of the vacuum pressure and thus allow for timely degassing, a glass filler rod was inserted with within the sample tube. The samples were covered in an isothermal jacket and were degassed for approximately 18 hours. The degassed samples were transferred to the analysis port and immersed in liquid nitrogen prior to analysis. The Barrett, Joyner and Halenda (BJH) and BET adsorption and desorption relationships were subsequently generated.

Table 5.3: Parameters employed for the evacuation and heating phases during degassing of the Electro-Modulated Hydrogel samples.

Parameter	Rate/Target
Evacuation Phase	
Temperature ramp rate	10°C/minute
Target temperature	40°C
Evacuation rate	50mmHg/second
Unrestricted evacuation from	30mmHg
Vacuum set point	500µmHg
Evacuation time	60 minutes
Heating Phase	
Temperature ramp rate	10°C/minute
Hold temperature	30°C
Hold time	1320 minutes

5.2.10. Characterization of morphological transitions using Scanning Electron Microscopy

SEM images of the EMH both before and after electro-stimulation, in buffers of pH 5.4 and 7.4, were taken for surface comparison. Prior to imaging, the samples were submerged into their respective buffers and the optimal voltage (3.63V) applied. The samples were subsequently blot-dried and submerged in liquid nitrogen in order to maintain matrix integrity.

5.2.11. Qualitative characterization of the optimized Electro-Modulated Hydrogel formulation under different pH using Magnetic Resonance Imaging

A Magnetic Resonance Imaging (MRI) system with digital MARAN-i System configured with a DRX2 HF Spectrometer console (Oxford Instruments Magnetic Resonance, Oxon, UK) was employed for the viewing of the mechanical behaviors of the hydrogel matrices. The MRI was equipped with a compact 0.5 Tesla permanent magnet stabilized at 37°C and a dissolution flow through cell. After duly configuring, optimizing the shims and probe tuning, the cone-like lower part of the cell was filled with glass beads to provide laminar flow at 16mL/minute of the solvents employed. The hydrogel samples were placed in position each time within the cell which in turn was positioned in a magnetic bore of the system and magnetic resonance images were acquired every 3 minutes with MARAN-i version 1.0 software

The image was acquired after setting the frequency offset and testing gain employing RINMR version 5.7 under continuous solvent flow conditions. MARAN-i software comprises image acquisition software and image analysis software. The image acquisition parameters are depicted in Table 5.4.

Table 5.4: Image acquisition parameters applied during magnetic resonance imaging using MARAN-i.

Sample No.	Parameter	Value
1.	Imaging protocol	FSHEF
2.	Requested gain (%)	4.17
3.	Signal strength	68.92
4.	Average	2
5.	Matrix size	128
6.	Repetition time (ms)	1000.00
7.	Spin Echo Tau (ms)	6.80
8.	Image acquired after	60 minutes
9.	Total scans	64

5.2.12. Determination of the degree of crystallinity employing X-Ray Diffraction analysis

Quantitative X-ray diffraction patterns were performed for the determination of the crystalline or amorphous nature of the optimized EMH. The XRD profiles were recorded using an X-Ray Diffractometer (Rigaku Miniflex 600, Rigaku Corporation, Matsubara-cho, Akishima-shi, Tokyo, Japan) at room temperature. Integrated X-ray Powder Diffraction software (PDXL 2.1, Rigaku, Tokyo, Japan). The measurement conditions are outlined in Chapter 3, Section 3.2.4.1, Table 3.1.

The finely pulverized sample (±20mg) was loaded into a glass sample holder. The intensity values at the main interplanar distances (diffraction peak angles) were determined for the pure PEI and VI as well as the PEI: VI mixture. The diffractogram of pure indomethacin was instituted as a reference for qualitative representation of the degree of crystallinity.

5.2.13. Assessment of the influence of electro-modulation on the swelling capabilities of the Electro-Modulated Hydrogel

The EMH samples were analyzed for water content determination using the Karl Fischer Titrator (Mettler Toledo V30 Volumetric KF Titrator, Mettler Toledo Instruments Inc., Greifensee, Switzerland). The test was conducted on a control as well as an EMH sample to which the optimized electric field of 3.63V was applied. The hydrogel samples were removed from the PBS (37°C; pH 7.4) and the water content determined at 0, 0.5, 1, 1.5, 2, 2.5, 3 and 24 hours.

5.2.14. Pharmacokinetic analysis of *in vitro* drug release

Quantitative evaluation of the drug transport process occurring across the skin necessitates selection of a suitable pharmacokinetic model for fitting of the concentration-time data. Appropriate model selection required the use of diagnostics such as the Akaike's Information Criterion (AIC), Schwarz's Bayesian Criterion (SBC) correlation coefficient, sum of squares of residuals (SS) and standard error of weighted residuals (SE). AIC and SBC hold the most significance (Zhang *et al.*, 2010) as they are a measure of goodness of fit based on maximum likelihood and were conducted.

Models employed include Zero order, Zero order with T_{lag}, First order, First order with T_{lag}, Higuchi, Hixson-Crowell, Makoid-Banakar, Korsmeyer-Peppas and the Quadratic model. The model associated with the smallest value of AIC or SBC in models of a given set of data is regarded as giving the best fit. Lower values are indicative of the preferred model, i.e., the one with the fewest parameters that still provides an adequate fit to the data, although it is

not the actual value but rather the difference between the values in a set. The value that is the lowest in the set represents the best fit. In this case each set is the different kinetic model. Thus the variation between the values among different sets is not a consideration (du Toit, 2013).

5.2.15. Investigation of the electro-active capabilities of the Electro-Modulated Hydrogel using cyclic voltammetry

Cyclic voltammetry was employed in order to assess the electroactive capabilities of the EMH using the three-electrode method as the electrical potential of a reference does not change easily during the measurement. Hydrogels containing the native PEI and VI as well as the optimized EMH was dissolved in PBS (pH 7.4) which served as the conducting solvent (Raoof *et al.*, 2009). The sample solutions were homogenized for a period of 10 minutes followed by sonication (Vibra-CellTM, Sonics[R] Sonics & Material Inc., Newtown, CT, USA) at amplitude of 80% for a period of 15 minutes. Prior to cyclic voltammetric assessment, the solutions were purged with nitrogen gas for 3 minutes. The conventional three-electrode system was used with a saturate Ag/AgCl (3.0M KCl) electrode serving as the reference electrode, a platinum auxiliary electrode and a glassy carbon electrode (5mm) as the working electrode. The vertex potential range used was -2V to +2V and -4V to +4V, the scan rate, 0.1V/second and the step potential, 0.00244V.

5.2.16. Conductivity and resistance measurements of the Electro-Modulated Hydrogel

A conductivity meter (SevenMulti™, Mettler-Toledo, Zurich, Switzerland) was employed to determine the ionic conductivity and resistance of hydrogels containing the native PEI and VI as well as the optimized EMH dissolved in PBS (pH 7.4). An average of 3 readings was recorded.

5.2.17. Computational investigation of Molecular Mechanics Electrosimulations and Electromimetic modeling

Molecular Mechanics (MM) Computations in vacuum and hydrated system were performed using the HyperChem™ 8.0.8 Molecular Modeling System (Hypercube Inc., Gainesville, Florida, USA) and ChemBio3D Ultra 11.0 (CambridgeSoft Corporation, Cambridge, UK). The PEI, PAA and VI was generated from standard bond lengths and angles employing polymer builder tools using ChemBio3D Ultra in their syndiotactic stereochemistry as 3D model. The individual polymer models were initially energy-minimized using MM+ force field and the resulting structures were again energy-minimized using the Amber 3 (Assisted Model Building and Energy Refinements) force field.

The conformer having the lowest energy was used to create the polymer-polymer and polymer-protein complexes. A complex of one polymer molecule with another was assembled by disposing the molecules in a parallel way, and the same procedure of energy-minimization was repeated to generate the final models: PAA, PEI, PAA-PEI, and PAA-PEI-VI (different ratios). Full geometry optimization was carried out in vacuum employing the Polak–Ribiere conjugate gradient algorithm until an RMS gradient of 0.001 kcal/mol was reached. For molecular mechanics calculations in vacuum, the force fields were utilized with a distance-dependent dielectric constant scaled by a factor of 1. The 1-4 scale factors were electrostatic 0.5 and van der Waals 0.5 (Kumar *et al.*, 2011).

To generate the final models in solvated system the MM simulations were performed for cubic periodic boxes with the polymer/polymer at the center of the cubic box and the remaining free space filled with water molecules and the same procedure of energy-minimization was repeated to generate the solvated models except that the force fields were utilized with a distance-independent dielectric constant with no scaling (Table 5.5). The MM electrosimulations were performed under the influence of an external electric field along all the three coordinates x, y, and z at various filed strengths of 0.00 a.u., 0.1 a.u., 0.3 a.u., and 0.5 a.u. to generate the final models listed later in Table 5.9. Full geometry optimizations were carried out in solvated system employing the Polak–Ribiere conjugate gradient method until an RMS gradient of 0.001 kcal/mol was reached. Additionally, the Force field options in the AMBER (with explicit solvent) were extended to incorporate cutoffs to Inner and Outer options with the nearest-image periodic boundary conditions and the outer and inner cutoffs were to ensure that there were no discontinuities in the potential surface (Table 5.5; Choonara *et al.*, 2011).

Table 5.5: Computational parameters used to construct aqueous-phase model building and simulations.

Parameter	Description
Periodic box dimensions	$20 \times 15 \times 25 A^{\circ 3}$
Cut-offs	Switched
Dielectric (epsilon)	Constant
1-4 Scale factors	Electrostatic: 0.5 van der Walls: 0.5
Outer radius	7.5 A°
Inner radius	3.5 A°
Water molecules	248
Solvent/Polymer distance	2.3 A°

The molecular mechanics simulation was carried out in various consecutive steps to generate the final electrosimulation model as follows:

Step 1:   Individual molecules viz PAA, PEI and VI were generated in vacuum followed by geometrical stabilization.

Step 2:   Molecular complexes such as $PEI\text{-}PAA_2$ (two PAA molecules in complexation with one PEI molecule) and $PEI\text{-}PAA_2\text{-}VI_4$ ($PEI\text{-}PAA_2$ molecule in complexation with four VI molecules) were generated in vacuum using parallel disposition and were geometrically optimized.

Step 3: $PEI\text{-}PAA_2\text{-}VI_4$ was geometrically optimized under periodic boundary conditions with water as the solvent phase.

Step 4:   The solvated $PEI\text{-}PAA_2\text{-}VI_4$ was subjected to electric field in x, y, and z co-ordinate directions at electric field values of 0.1 a.u., 0.3 a.u., and 0.5 a.u. Geometrical optimization was carried out under identical periodic boundary conditions with water as the solvent phase.

5.3. Results and Discussion

5.3.1. Construction of calibration curves for the ultraviolet spectrophotometric determination of active agent release from the Electro-Modulated Hydrogel

A calibration curve for sodium indomethacin was constructed in PBS (pH 7.4; 37°C) using a known series of concentrations of sodium indomethacin as detailed in Chapter 3, Section 3.2.4.2. An ultraviolet spectrophotometric scan was run to determine the maximum wavelength for morphine HCL absorption in PBS. Using UV spectroscopy, it was found that morphine HCL exhibits a maximum wavelength at λ_{278} (Appendix 11.3.1) consistent with the literature published on the morphine HCL 285nm absorption peak (Morales *et al.*, 2004; Morales *et al.*, 2011). The linear curve was plotted with the observed absorbance of morphine HCL as the dependent variable and the concentration of morphine HCL the independent variable. A statistical representation of the degree at which the function correlates the set of values (R^2 value) was computed for the curve (Appendix 11.3.1).

Similarly, calibration curves (Appendices 11.3.2 and 11.3.3) for celecoxib and fentanyl citrate were carried out at λ_{208} (Frank *et al.*, 2004) and λ_{203} (Almousa *et al.*, 2011), respectively.

5.3.2. *In vitro* release studies

The principle in the design of the electro-responsive polymeric matrix was to ensure that it responds by releasing the incorporated analgesic agent in a manner responsive to an electro-responsive stimulus. As depicted by Figure 5.1a, the EMH responded in the desired manner. At pH 7.4, the EMH displays more consistent electro-responsive release than at pH 5.4, where the electro-responsive properties of the drug are greatly reduced. The moisture content is increased, resulting in increased swelling in the simulated sweat buffer (Section 5.3.9). Exposing the EMH to different pH and electro-stimuli reiterates the fact that PAA's large number of free carboxylic moieties increases sensitivity to pH and electrical stimuli (Cai and Gupta, 2012).

Further *in vitro* studies were carried out on the optimized formulation containing morphine HCL, celecoxib and fentanyl citrate in order to determine the versatility of the formulation (Figure 5.1b-d). The drug release studies were carried out as previously mentioned. All EMH formulations displayed electro-responsive release with various spikes, possibly as a result of the different solubilities of the analgesic agents.
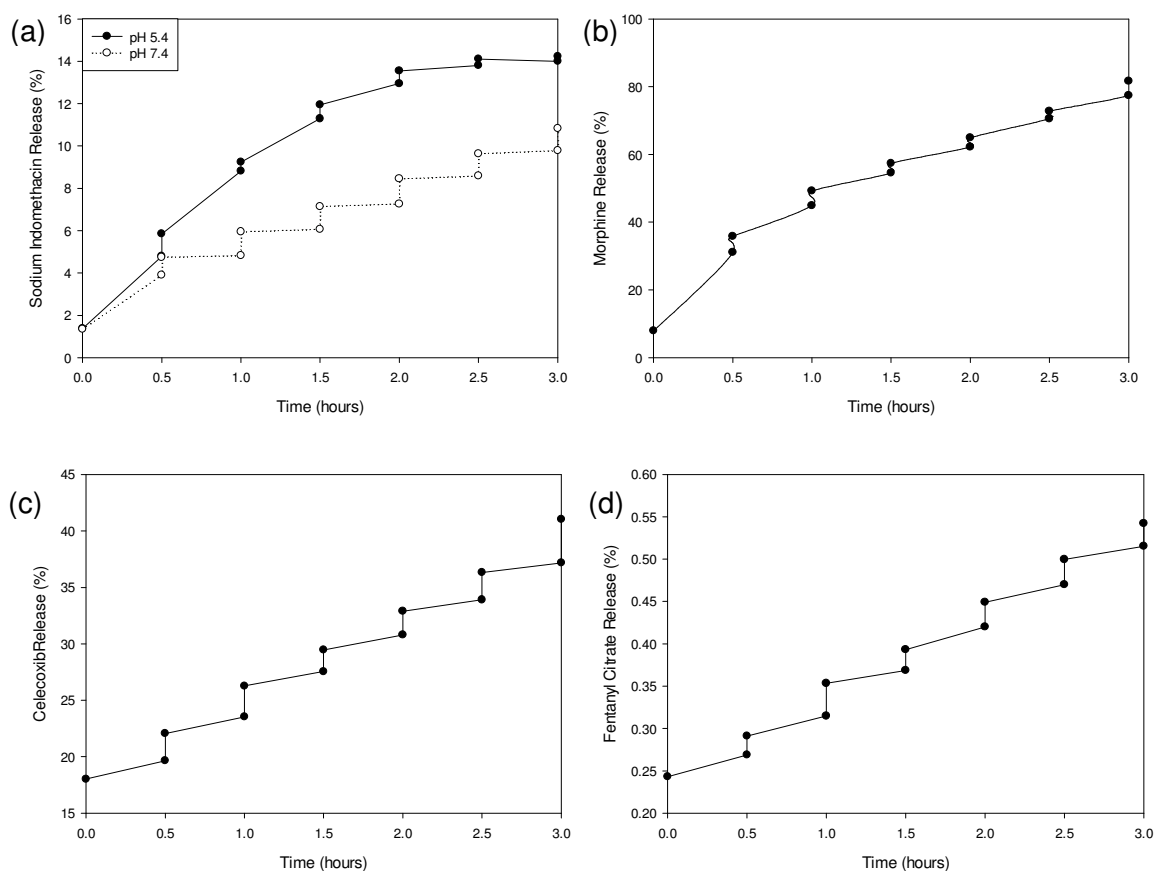
Figure 5.1: Drug release profiles of the optimized Electro-Modulated Hydrogel containing (a) sodium indomethacin at pH 5.4 and pH 7.4 (b) Morphine HCL (c) Celecoxib and (d) Fentanyl citrate.

In addition digital images of the EMH containing sodium indomethacin were taken at consecutive intervals following electro-stimulation so as to visually depict the loss of indomethacin from the EMH matrix. After stimulation, the EMH displayed a color change from a uniform dark yellow to lighter colors. In addition, the color change is more apparent at the outer rims of the EMH, which consecutively increase in accordance with electro-stimulation (Figure 5.2).

| 0 hours | ES 1 | ES 2 | ES 3 | ES 4 | 3 hours |
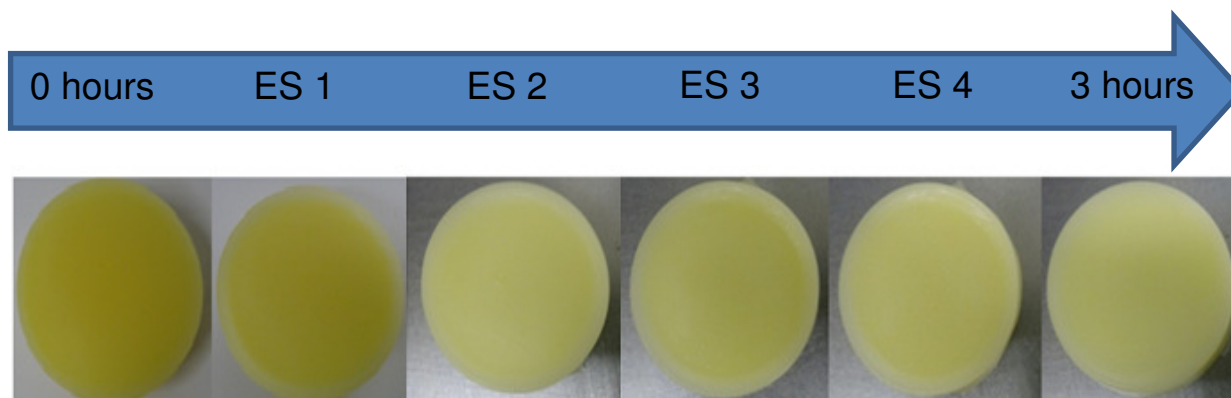
Figure 5.2: Digital images depicting the color change from the Electro-Modulated Hydrogel after electro-stimulations at pH 7.4.

5.3.3. Synthesis validation of the optimized Electro-Modulated Hydrogel

FTIR analysis of the optimized EMH revealed the omission of the VI peak at 2176.88cm^{-1} (Figure 5.3). The, peak corresponding to presence of nitrogen is absent possibly as a result of crosslinking. All other observed peaks are as detailed in Chapter 4, Section 4.3.2.
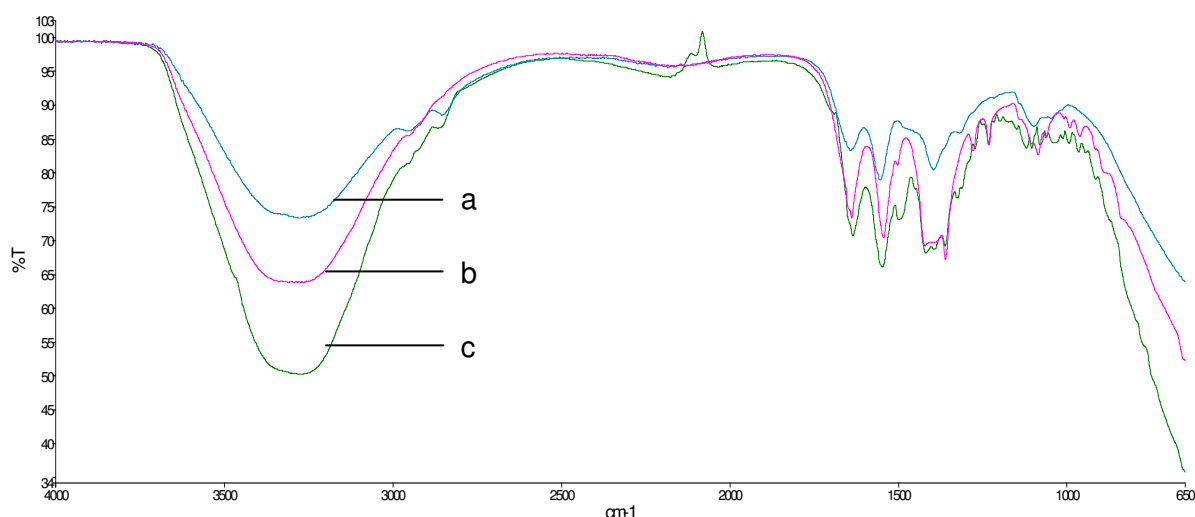
Figure 5.3: FT-IR spectrum of the (a) poly (ethyleneimine) and (b) 1-vinylimidazole-containing Electro-Modulated Hydrogel. (c) The optimized Electro-Modulated Hydrogel.

5.3.4. Analysis of the physicomechanical behavior

Textural profile analysis in terms of BHN and gel strength revealed that the integrity of the EMH samples declined after electro-stimulation. MR remained constant and was unaffected by the electro-stimulation. Figure 5.4a-c depicts the Force-Time and Force-Distance profiles of the EMH prior to and after electro-stimulation. In all cases, N=3. MR for the EMH containing sodium indomethacin was calculated to be 95.16% which correlates to that of the optimized EMH (±4.85). MR for the control EMHs containing morphine, fentanyl and celecoxib were calculated to be 87.62%, 96.73% and 92.46% respectively (±3.27). MR after electro-stimulation was calculated to be 90.23% for the optimized EMH containing sodium indomethacin (±5.38), and 84.21%, 89.13% and 87.96% for morphine, fentanyl and celecoxib respectively (±4.13). This decline in MR could be as a result of the notable formation of pores in the matrix as depicted in Figure 5.8b (ii). The BHN of the EMHs were also seen to decrease following electro-stimulation from 0.076 to 0.000 for sodium indomethacin, 0.091 to 0.008 for morphine, 0.156 to 0.004 for fentanyl and from 0.290 to 0.008 for celecoxib (SD≤0.048 in all cases). Gel strength of the EMH decreased after electro-stimulation, the most common method to enhance the hydrogel strength is by increasing the crosslink density and the hydrophobic nature of the hydrogel. The monomer concentration and crosslink density has remained constant throughout the study. Gel strength ranged from 4.98N to 3.32N for sodium indomethacin, 3.14N to 0.35N for morphine, 6.23N to 0.57N for fentanyl and from 13.98N to 2.13N for celecoxib, prior to after electro-stimulation (SD≤1.92 in all cases). A significant reduction in gel strength was seen with morphine, reduced from 14.14N to 2.95N after electro-stimulation (SD≤0.87). If correlated with the respective drug release profiles (Figure 5.1) it can be seen that the release of drug is greater in gels having lower gel strength. The phenomenon can be explained by the fact that the incorporated drug contributed to the strength of the network and subsequent release weakened the EMH matrix (Choonara *et al.*, 2008). Notably all textural profiles of the electro-stimulated matrix display slightly increased results as compared to their control counterparts affected by the incorporated drug (Namdeo *et al.*, 2010).
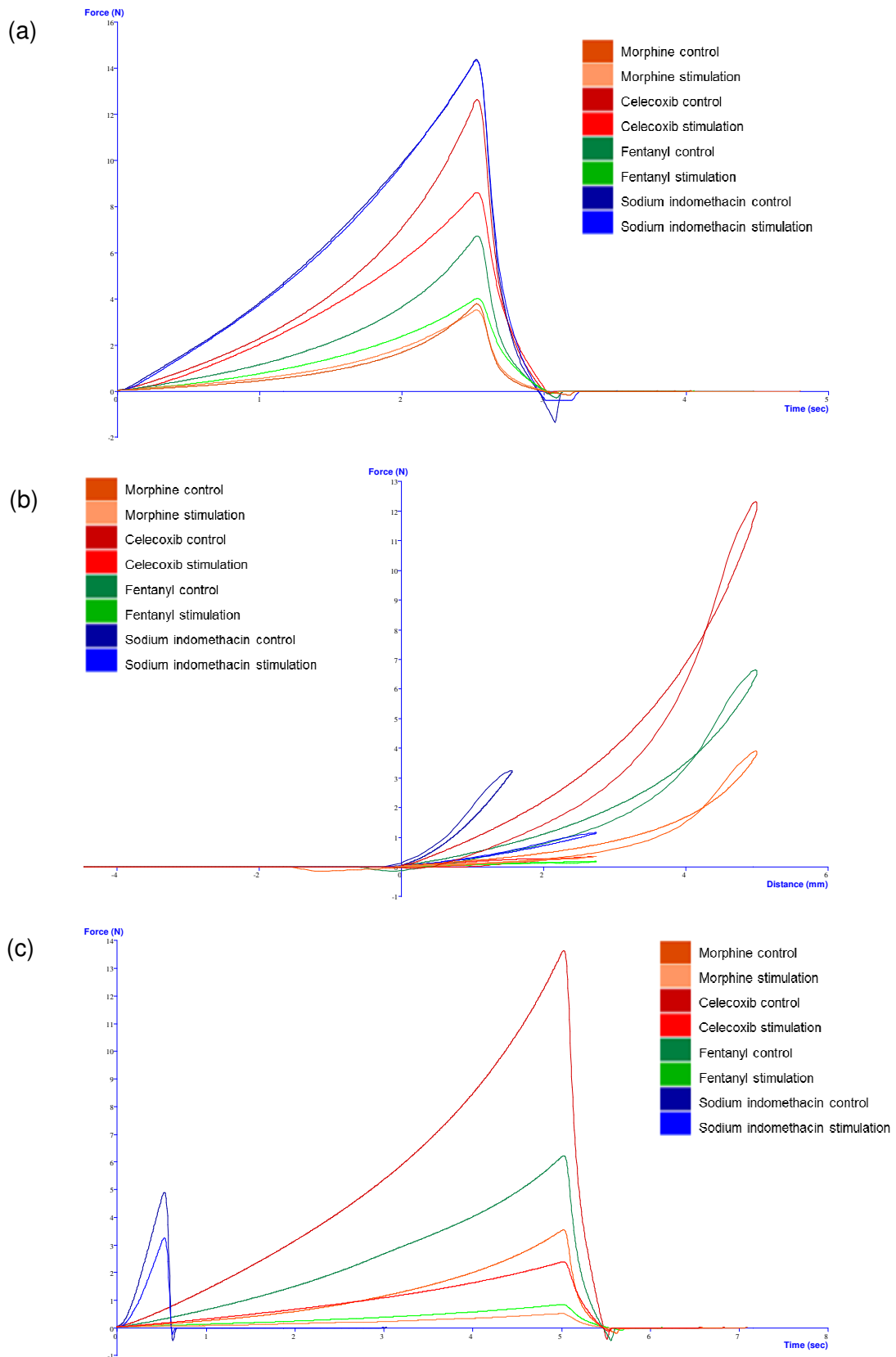
Figure 5.4: Profiles depicting the (a) matrix resilience (b) hardness and (c) gel strength of the Electro-Modulated Hydrogel prior to and after electro-stimulation.

Sodium indomethacin-containing EMH samples were evaluated using the afore-mentioned physicomechanical tests at pH 5.4 and 7.4 in order to determine pH responsive changes (Figure 5.5).
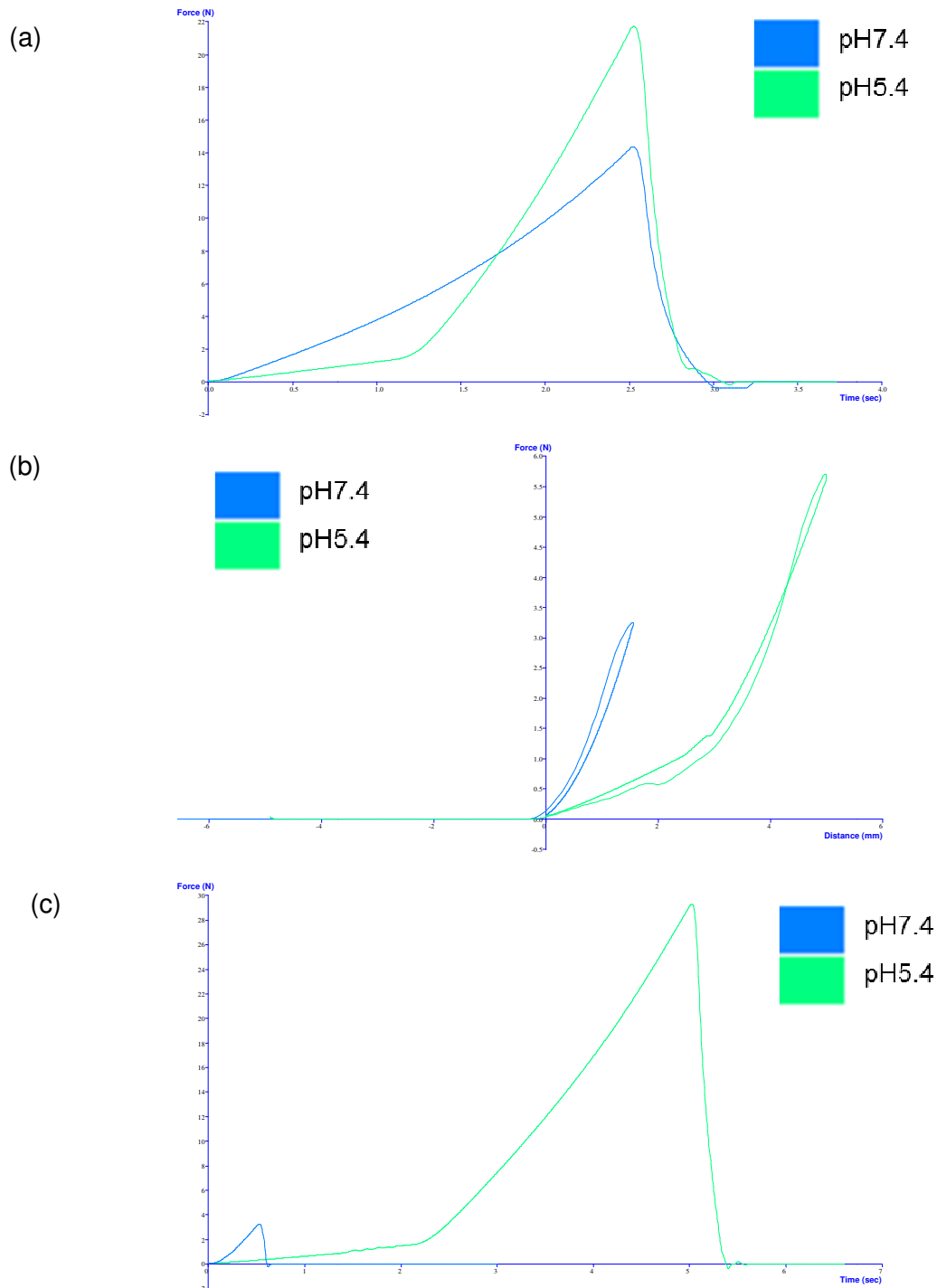
Figure 5.5: Profiles depicting the (a) matrix resilience (b) hardness and (c) gel strength profiles of the Electro-Modulated Hydrogel containing sodium indomethacin at pH 5.4 and pH 7.4.

The calculated MR for the EMH at pH 5.4 and pH 7.4 were calculated to be 94.32% and 98.54% respectively (SD≤1.40). BHN values were calculated to be 0.131 and 0.026 respectively (SD≤0.50). Gel strength was determined to be 29.83N and 4.93N respectively (SD≤4.47). The increase in strength at a lower pH is due to the decrease in polymeric chain flexibility. Conversely, the strength at pH 7.4 is lower due to the chain becoming more flexible.

5.3.5. Thermal profile analysis of the optimized Electro-Modulated Hydrogel formulation

A single glass transition temperature (T_g) for the EMH semi-IPN was observed indicating that both parent semi-IPN polymer components (PAA/PVA) have excellent miscibility and that strong interactions due to hydrogen bonding exist between the two networks of this semi-IPN (Figure 5.6). Should the semi-IPN polymer components have been immiscible, two T_g peaks corresponding to the parent polymers would have been observed. When two networks of a semi-IPN are compatible, the semi-IPN possesses a single T_g (Zhang *et al.*, 2004; Yue *et al.*, 2008).Exothermic peaks were displayed by all the EMH samples. Melting was observed at 100-140°C. The EMH containing the blend and the hydrogel containing VI displayed oxidation peaks at 250-270°C and 190-210°C respectively. After characterizing the thermal properties of the native PEI and VI as well as the physical mixture it was found that the T_g of PEI, VI and the EMH occurred in the range of 30-50°C, 50-60°C and 30-40°C respectively, consistent with the fact that T_g generally increases according to increasing ionic group concentration (Weiss *et al.*, 1985); this event is seen at 125°C for the EMH. For VI, an endothermic event, typically due to hydration, occurred in the range of 140-160°C and 200-210°C. An exothermic event at 300-330°C for the EMH was seen.

Figure 5.6: Differential Scanning Calorimetry thermogram of (a) Electro-Modulated Hydrogel (b) poly (ethyleneimine) and (c) 1-vinylimidazole.

5.3.6. Simultaneous qualitative and quantitative analysis of the Electro-Modulated Hydrogel surface morphology and porosity

Porositometric analysis on the EMH samples were conducted as it facilitates drug release at rates determined by their diffusion coefficient through the EMH matrix (Jagur-Grodzinski, 2010). The BJH and BET characteristics observed in the porositometric analysis of the EMH are outlined in Table 5.6.

Table 5.6: Surface area and porosity characteristics of the Electro-Modulated Hydrogel samples.

Parameter		Dry EMH	pH 5.4	pH 7.4
Surface area	BET Surface Area	5.0300m²/g	-2.5076m²/g	-2.3530m²/g
	BJH Adsorption average pore width (4V/A by BET)	28.0128Å	-19.0650Å	-33.2319Å
Pore Volume	BJH Adsorption average pore diameter (4V/A)	51.432Å	46.074Å	41.674Å
	BJH Desorption average pore diameter (4V/A)	48.088Å	41.157Å	39.603Å

The BET surface area plot and the isotherm log plot for the EMH prior to and after electro-stimulation at pH 5.4 and 7.4 are depicted in Figure 5.7. The BET surface area of the EMH was calculated to be 5.0300m²/g, -2.5076m²/g and -2.3530m²/g respectively. The average pore width of the EMH prior to electro-stimulation was calculated to be 28.0128Å (2.80128nm) with the average adsorption and desorption pore diameters being 51.432Å (5.1432nm) and 48.088Å (4.8088nm) respectively. The average pore width of the EMH at pH 5.4 was calculated to be -19.0650Å (1.90650nm) with the average adsorption and desorption pore diameters being 46.074Å (4.6074nm) and 41.647Å (4.1647nm) respectively. Type H3 hysteresis was observed in all plots (Figure 5.7) and thus do not exhibit any limiting adsorption at high p/p_0. This behavior can for instance be caused by the existence of non-rigid aggregates of plate-like particles or assemblages of slit-shaped pores (Thommes, 2010).

The larger pore volume of the EMH at pH 5.4 after electro-stimulation accounts for the increase in drug diffusion from the EMH matrix (Figure 5.1a) resulting in inappropriate release. The average pore width of the EMH at pH 7.4 was calculated to be -33.2319Å (3.32319nm) with the average adsorption and desorption pore diameters being 41.674Å

(4.1674nm) and 39.603Å (3.9603nm) respectively. The pore volume of the EMH at pH 7.4 is smaller in comparison to the control EMH. However, does prove to be highly efficient in electro-responsive release. This is beneficial as the release of the therapeutic agent can be controlled over longer periods of time resulting in an extended duration of action, desirable patient compliance, a decreased burden of care and ultimately a positive therapeutic outcome.
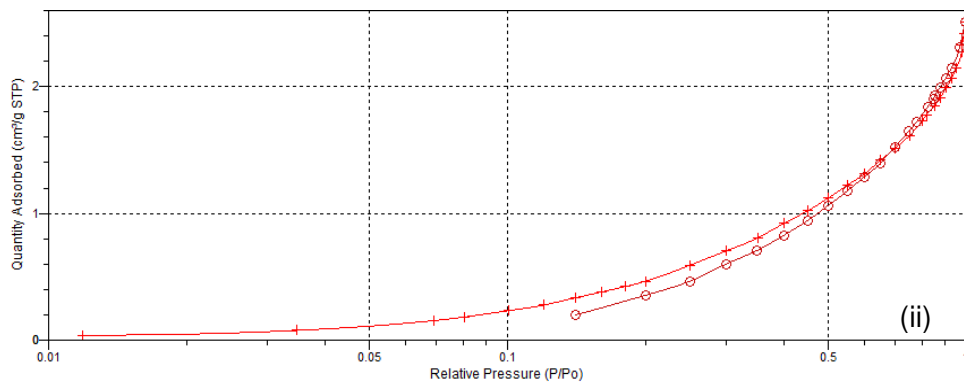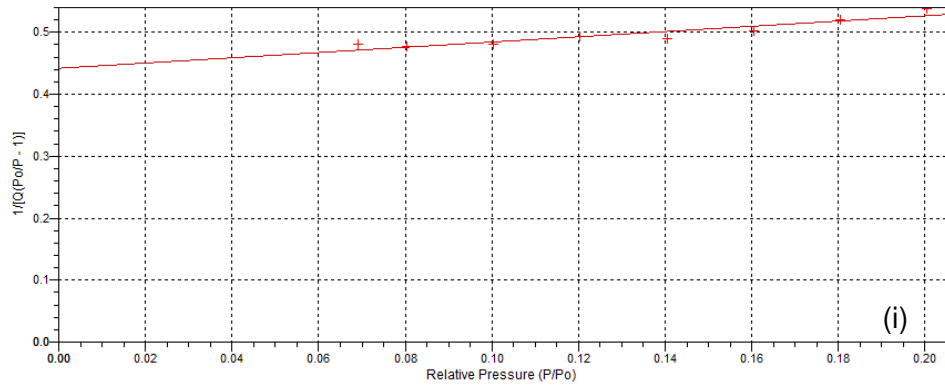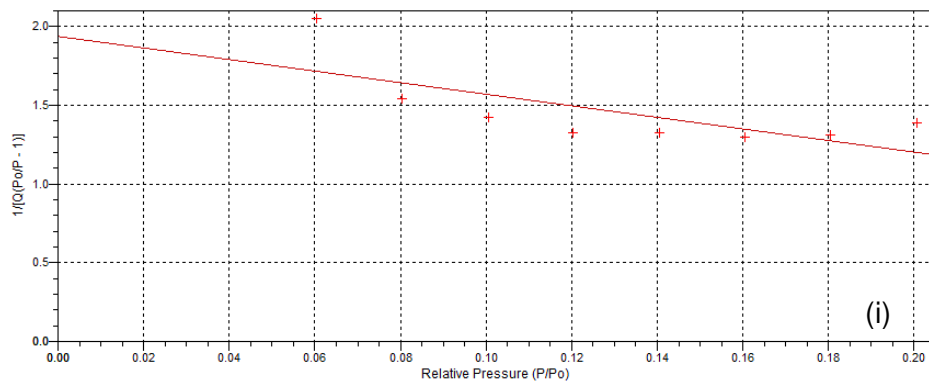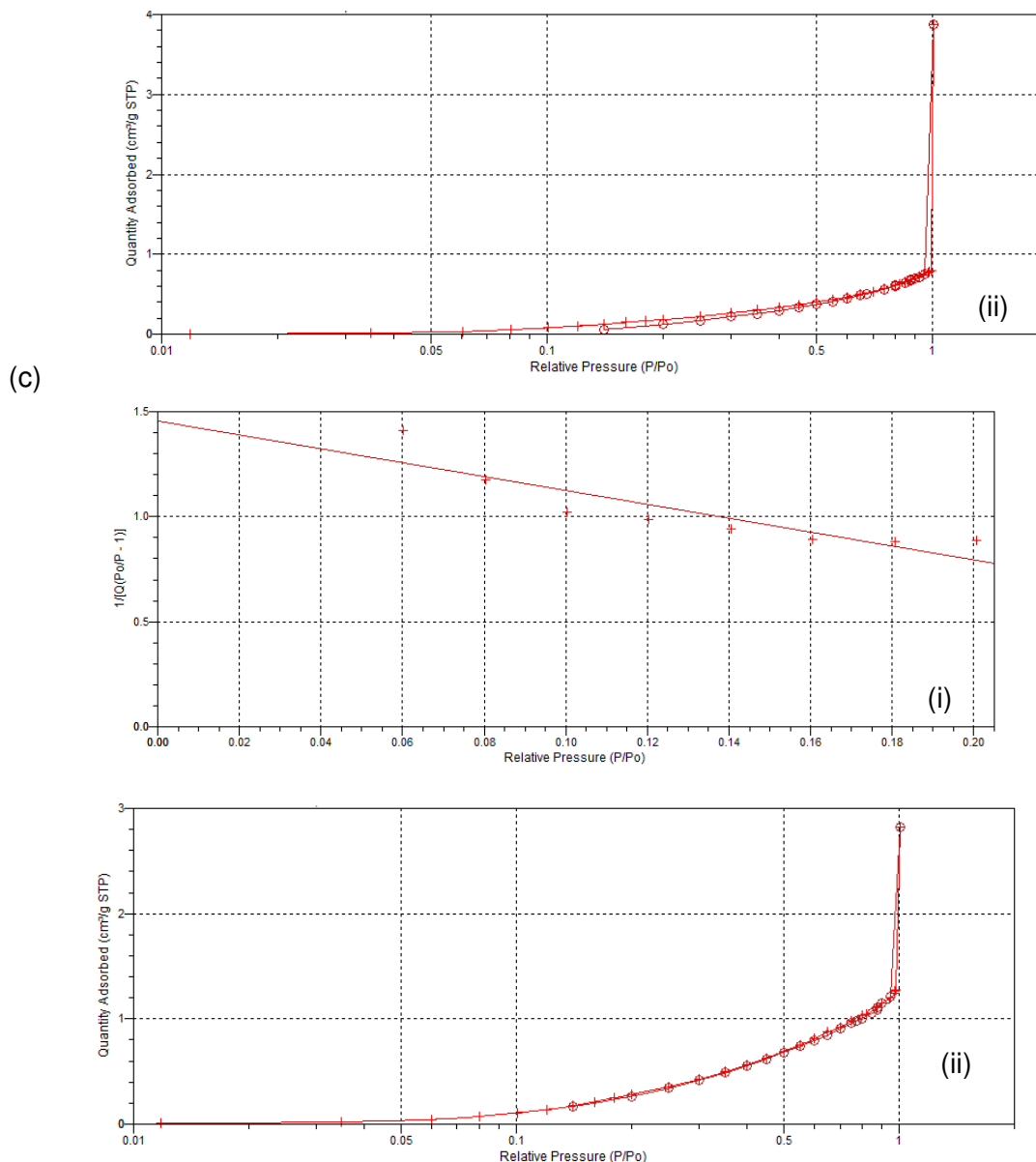
Figure 5.7: (i) BET surface analysis plot and (ii) isotherm log plot of the (a) Electro-Modulated Hydrogel control (b) Electro-Modulated Hydrogel at pH 5.4 (c) of the Electro-Modulated Hydrogel at pH 7.4.

Due to the high degree of entanglement and the shorter inter-gel strand lengths, in effect, equilibrium swelling decreases. In addition to the distribution of crosslinks, the chain length between crosslinks within a gel can be highly variable (Pakravan *et al.*, 2011). At low concentrations of the monomer, a small number of longer strands poorly connect the gels (Pakravan *et al.*, 2011). High monomer concentrations result in a greater number of shorter strands that are more extensively entangled than the inter-gel strands formed at low monomer concentrations (Pakravan *et al.*, 2011).

SEM revealed that with exposure to simulated transdermal conditions, alterations were observed in the surface morphology of the EMH (Figure 5.8). Pores were present in the EMH after stimulation at both pH values (Figure 5.8b). The pores were not present in the EMH prior to stimulation (Figure 5.8a(i)). Considering that electro-stimulation was the only change in the environment, it can be concluded that the pores were as a result of the polymer network opening in response to the applied field, proving the electro-responsive ability of the EMH system. The porosity data further validates this as the average pore width of the EMH prior to electro-stimulation was calculated to be 28.0128Å (2.80128nm) as compared to the average pore width of the EMH after electro-stimulation which was calculated to be -33.2319Å (3.32319nm). After allowing the sample to return to its native state, the average pore width of the EMH was calculated to be 27.1218Å (2.71218nm).
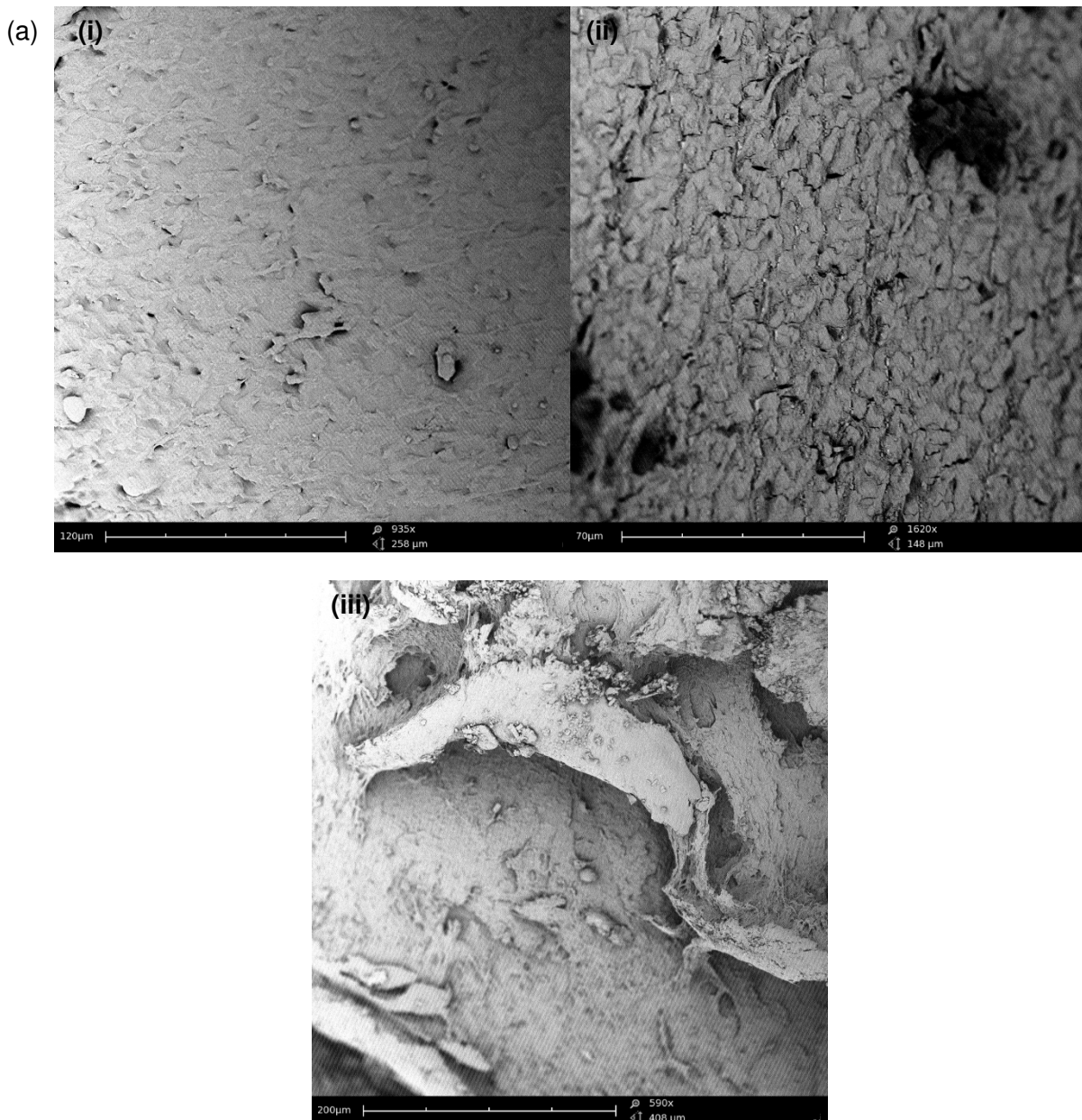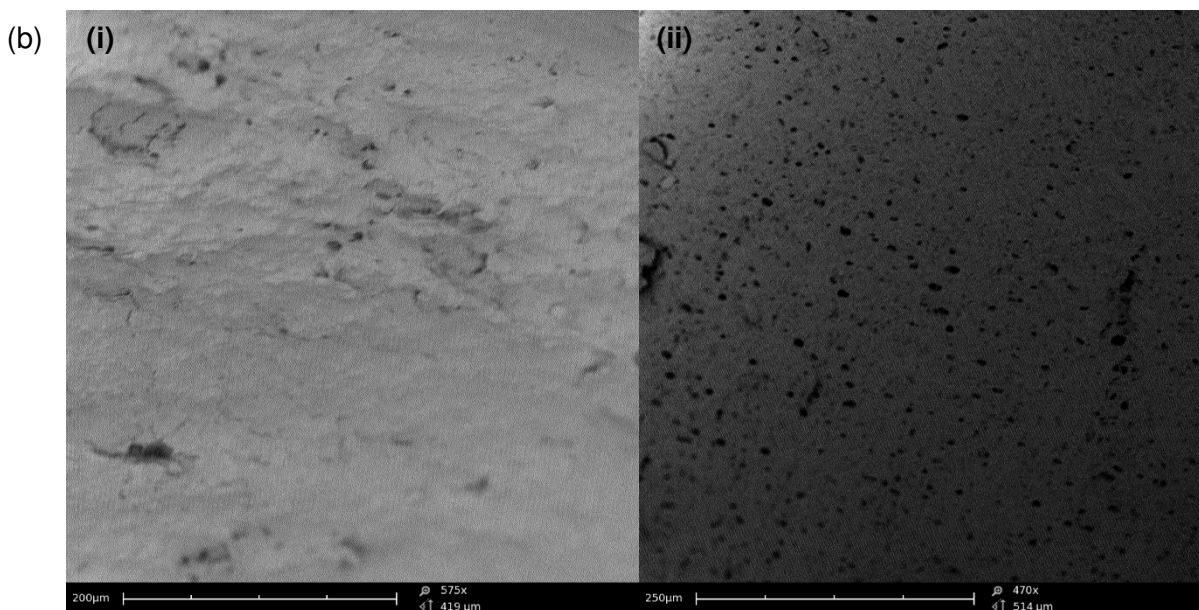
Figure 5.8: (a) SEM images of the surface morphologies of (i) the Electro-Modulated Hydrogel prior to electro-stimulation (ii) poly (ethyleneimine) (iii) 1-vinylimidazole. (b) SEM images of the Electro-Modulated Hydrogel after electro-stimulation at (i) pH 5.4 (ii) pH 7.4.

5.3.7. Analysis of the degree of crystallinity of the Electro-Modulated Hydrogel

The X-ray diffractograms for sodium indomethacin, PEI, VI and the EMH are illustrated in Figure 5.9a (i-v). Stereoregularity or symmetry as depicted by narrow and symmetrical peaks indicates that the indomethacin is crystalline in structure (du Toit *et al.*, 2013). On the contrary the native polymers and the EMH are dominantly amorphous in nature due to the absence of this characteristic. Amorphous polymers contain a randomly orientated entangled chain that generally prevents crystallization (Vassal *et al.*, 2000). The EMH does however display slight symmetry ($2\theta=30\text{-}40°$) as a result of the incorporation of indomethacin into the gel. An amorphous nature of molecular dispersal or drug within the polymeric EMH matrix was indicated by the absence of complete crystallinity in the drug-loaded EMH. The broad peak observed indicates that the PVA/PAA semi-IPN is amorphous. Nonetheless, while the crystalline phase is non-conducting, there still is significant polymer chain flexibility existing in the amorphous phase. This characteristic can greatly enhance ionic conductivity.

When evaluated as a separate entity, using the Integrated X-ray Powder Diffraction software (PDXL 2.1, Rigaku, Tokyo, Japan), the polyelectrolytic EMH was found to contain N-(3-Nitrobenzylidine)phenylene-1,4-diamine (36%) and poly(ethylene 2,6-naphthalenedicarboxylate) (64%), which may contribute to the EMH's electro-responsive behavior due to the nitro moieties (Figure 5.9b).
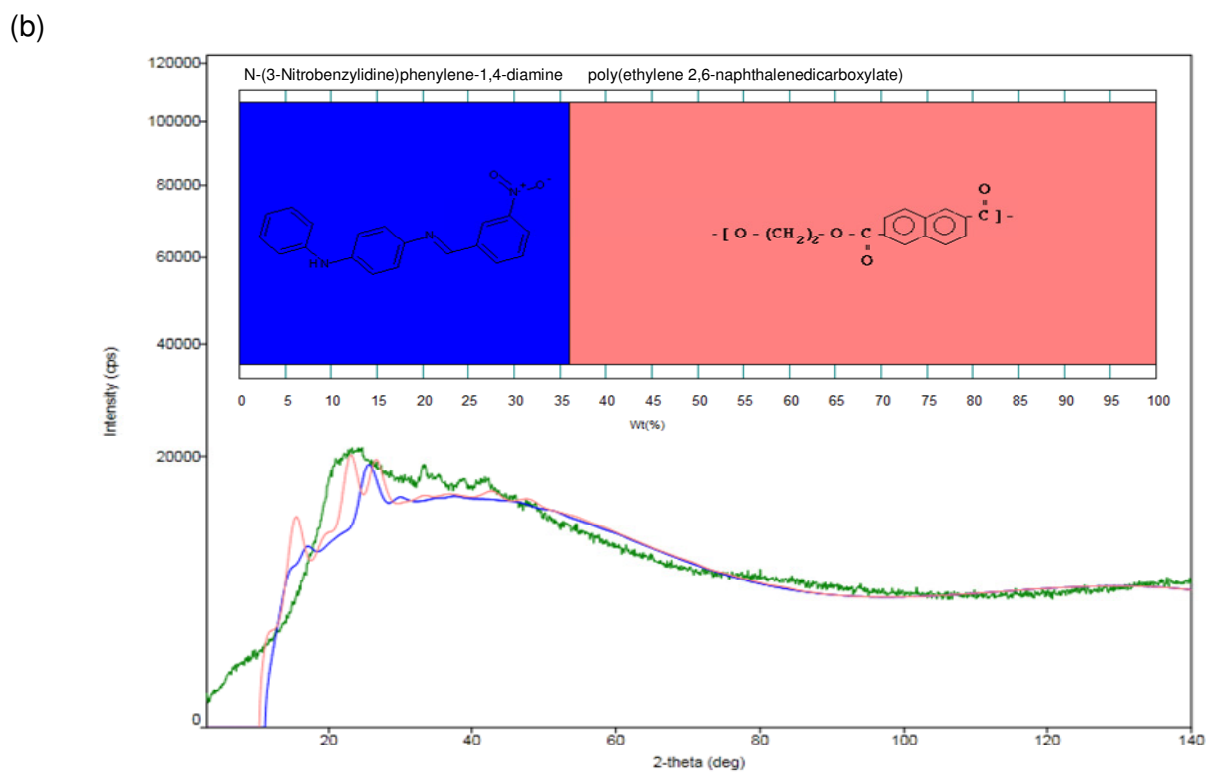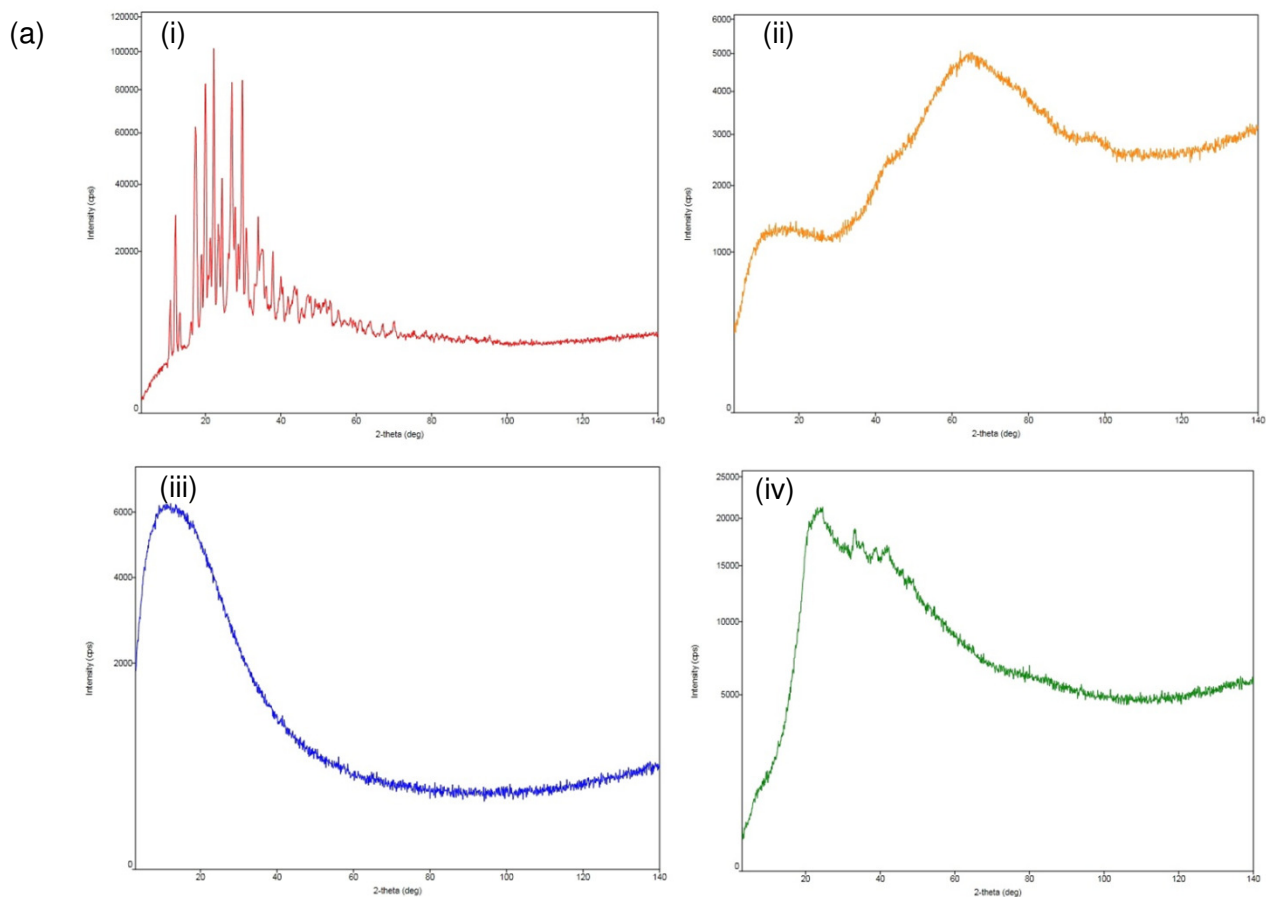
Figure 5.9: (a) XRD diffractograms of (i) sodium indomethacin (ii) poly(ethyleneimine) (iii) 1-vinylimidazole (iv) the Electro-Modulated Hydrogel (b) The components of the Electro-Modulated Hydrogel.

5.3.8. Assessment of the pH-responsive swelling properties through rheological analysis and Magnetic Resonance Imaging

The EMH hydrogel when exposed to PBS (pH 7.4) displayed constantly defined increases in width (Figure 5.10a) caused by the high concentration of charged ionic groups due to the ionization of the carboxylic acid groups (Lin and Metters, 2006). The polymer chains thus extend more in the higher pH as the ionic groups repel each other. The consistency in swelling can be inferred to the consistency in the observed uniform drug release (Figure 5.10b).

(a)
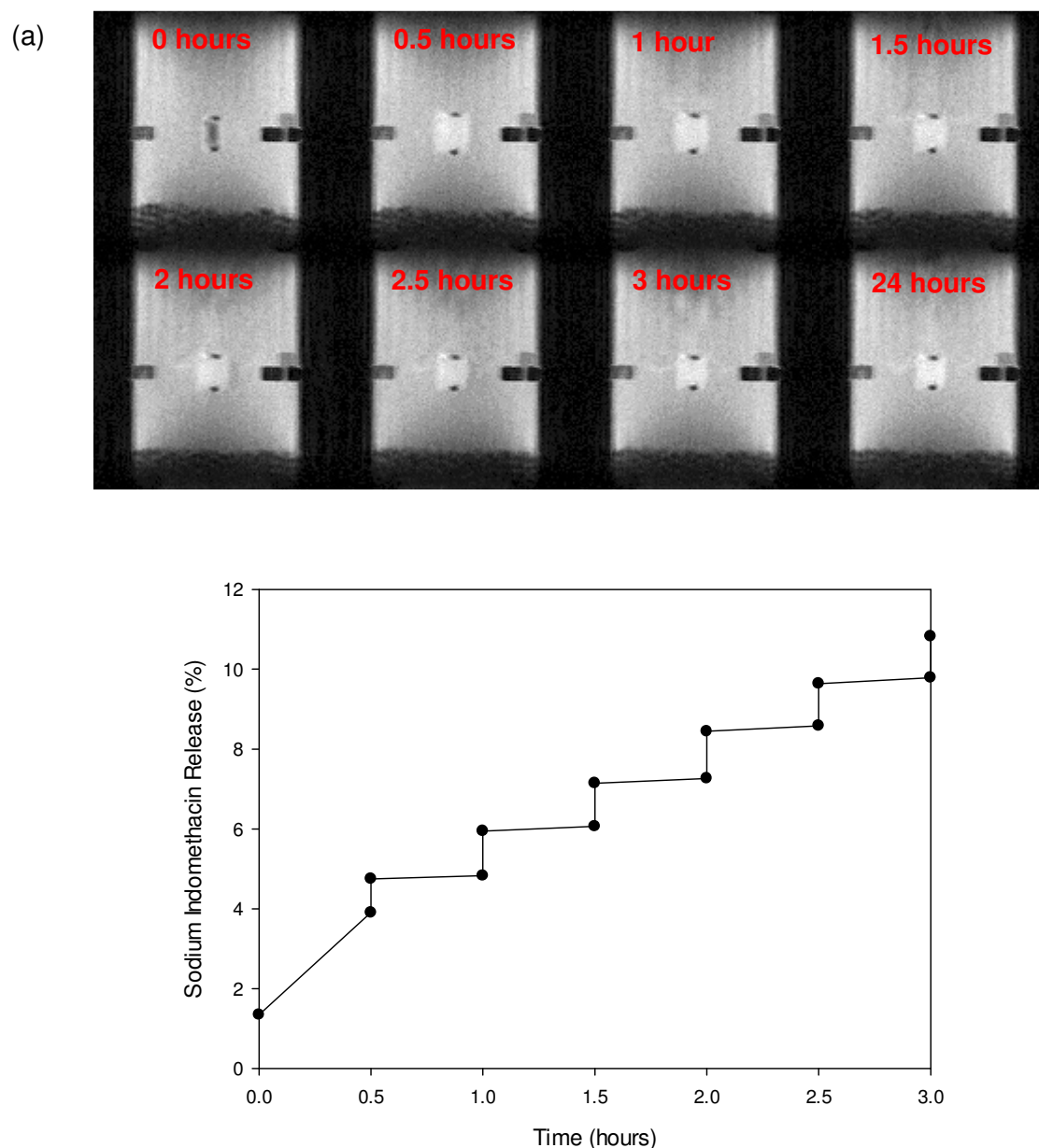
Figure 5.10: (a) Magnetic resonance images over a 24 hour period and the (b) drug release profile of the Electro-Modulated Hydrogel in PBS (pH 7.4).

The MRI images of the hydrogel in PBS (pH 5.4) displayed progressive increases in size over the 24 hour period (Figure 5.11a). It can be assumed that when exposed to PBS (pH 5.4); the degree of ionization of hydrogel bound groups is limited, restricting swelling (Lin and Metters, 2006). Here it is important that the hydrogel matches the modulus of the surrounding environment so as to avoid further unwarranted drug release. The inconsistent swelling to the hydrogel formulation it can be extrapolated to the inconsistent drug release observed at pH 5.4 (Figure 5.11b).

(a)
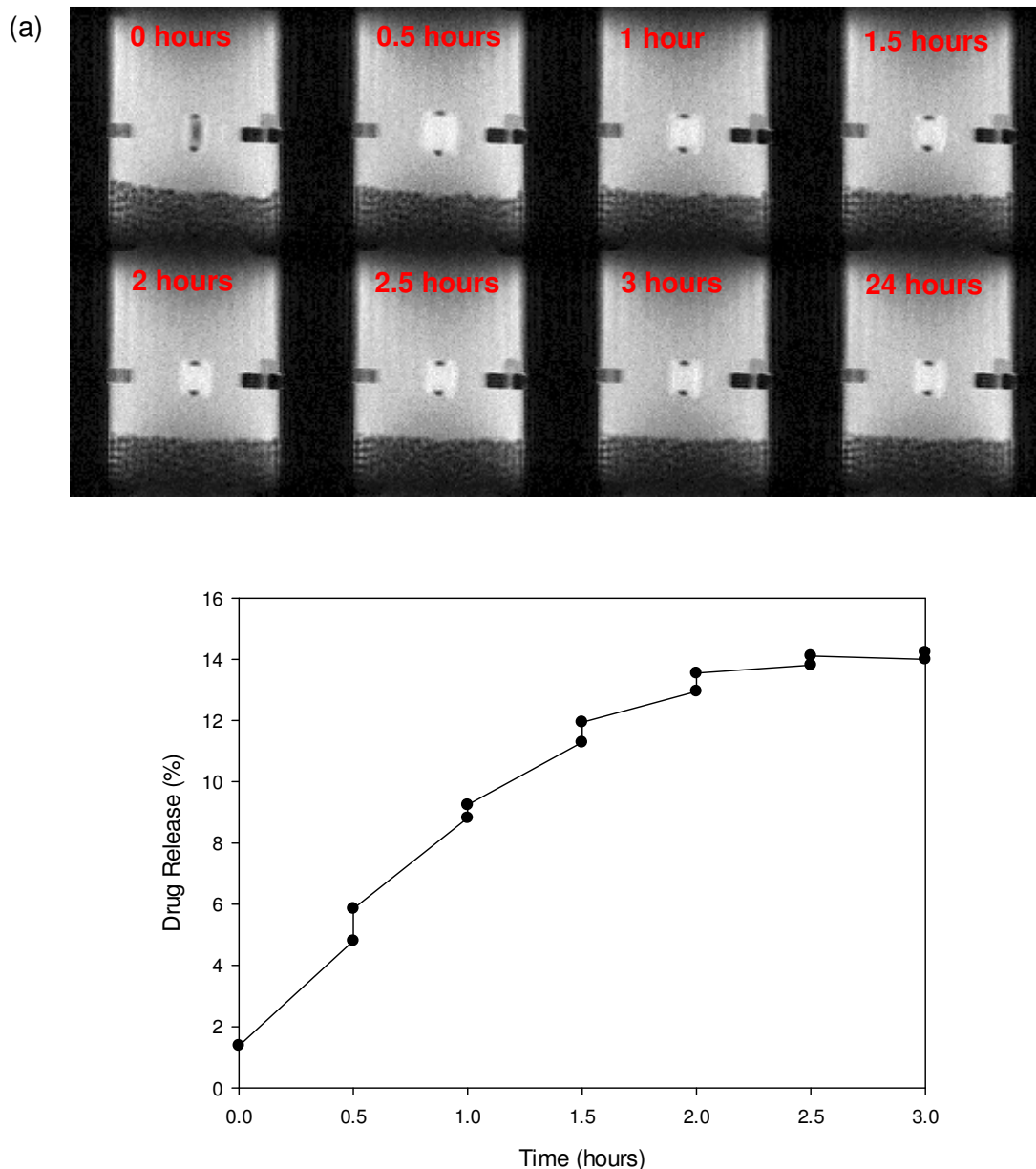
Figure 5.11: (a) Magnetic resonance images over a 24 hour period and the (b) drug release profile of the Electro-Modulated Hydrogel in PBS (pH 5.4).

5.3.9. Assessment of the influence of electro-stimulation on swelling capability

Hydrogels exhibit spatial gel inhomogeneity or an inhomogeneous cross-link density distribution (Okay *et al.*, 1998). Inhomogeneity decreases with the ionization degree of gels as a result of the effects of the mobile counter ions and electrostatic repulsion (Okay *et al.*, 1998) facilitating the open structure allowing for electro-modulated drug release. Hydrogel swelling is dependent on both functional group hydrophilicity and network space (Lin and Metters, 2006). When containing ionic moieties, swelling depends on the pH of the surrounding medium (Okay *et al.*, 1998; Lin and Metters, 2006). When the external pH is higher than the pKa of the ionizable groups bound to the polymer chains, anionic hydrogels tend to deprotonate and swell more. Cationic hydrogels tend to protonate and swell more when the external pH is lower than the pKb of the ionizable groups (Lin and Metters, 2006). The pH-dependent swelling curves exhibit one or more inflection points near the pKa/pKb of the ionizable groups, depending on the ionic monomers used to synthesize the gel, as shown in Figure 5.19 (Lin and Metters, 2006).
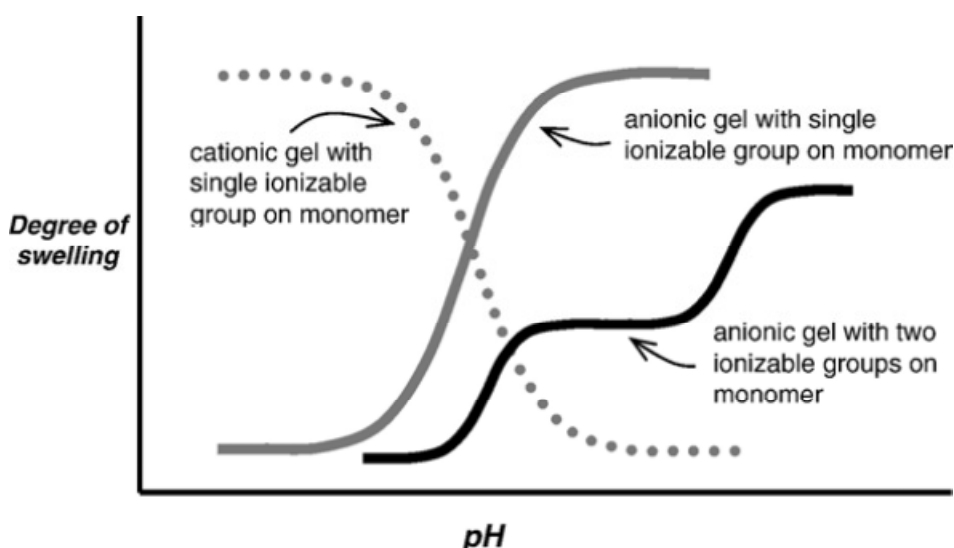
Figure 5.12: Schematic of relative ionic hydrogel swelling as a function of pH (Lin and Metters, 2006).

Hydrophilicity can be enhanced by the incorporation of ionizable functional groups, such as carboxyl groups. Acrylic acid is often a monomer employed in the fabrication of pH-sensitive hydrogels for their pH-sensitive -COOH group (Cai and Gupta, 2012).

In the PAA/PVA EMH, PAA serves as the ionic polymer and PVA, the neutral polymer. As the voltage is applied, the fixed carboxylic anions become ionized; the electrons then repel the carboxylic anions in the gel, thus facilitating network swelling. This is noted by the difference in water content in the EMH samples as compared to the controls (Figure 5.13).

The extent of swelling depends on the concentration of functional ionizable groups on the network.

The EMH shows less swelling when exposed to an applied electrical field at pH 7.4. The semi-IPN is a polyelectrolyte hydrogel comprising of ionizable weak acidic and weak basic groups, which can be ionized in basic and acidic environments respectively. Gels containing acidic moieties protonate in acidic conditions, leading to a decrease in the charge density and the content of mobile counterions which ultimately results in the shrinking of the gel. Polyelectrolyte gels generally deswell as water is syneresed from the gel when exposed to an electric field. The decrease in swelling at pH 7.4 may also be attributed to the formation of strong hydrogen bonds between the hydroxyl groups of PVA and water (Cai and Gupta, 2012; Jianqi and Lixia, 2012). The magnitude of the gel response often decreases with time and with increasing number of on-off cycles as the gel fatigues.

The observed increase in swelling at pH 5.4, denoted by the solid line, is as a result of ionic repulsion of carboxylic ions and the free water contents. As a result, there is dissociation of hydrogen bonds due to the decrease of bound water in the hydrogel. Complete ionization of almost all the carboxylic groups in the PAA backbone occurs at pH values lower than the pKa (approximately 4.28) of the PAA polymer (Jianqi and Lixia, 2012; Quintero, *et al.*, 2010). As the pH decreases below that of the pKa, hydroxyl (H^+) ionic strength increases, effectively suppressing polycarboxylic group ionization. Polymeric chain flexibility is low and the gel is neutral. Conversely, should the pH of the environmental solution rise above the pKa, the polycarboxylic groups within the network will undergo ionization thus replacing the H+ ions by attracting cations into the gel. The swelling pressure and swelling increases as the free ion concentration is thereby raised inside the gel. In order to maintain equilibrium, the gel expands to overcome the repulsion that exists between the ionized polycarboxylic groups. It has been found that the ionic strength of the swelling medium is inversely proportional to the equilibrium swelling of hydrogels that are capable of ionization. The successive pH increments ultimately lead to multiple acid–base equilibriums and thus the stepwise swelling of the polymer due to the –COOH/–COO⁻ groups being progressively ionized and neutralized (Jianqi and Lixia, 2012).
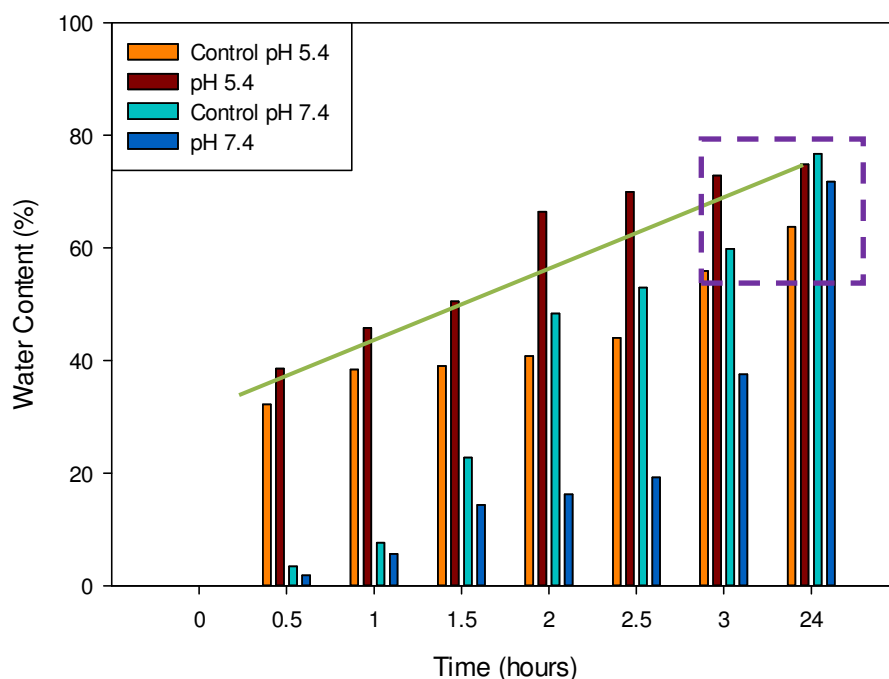
Figure 5.13: Water content determination of Electro-Modulated Hydrogel at pH 5.4 and 7.4.

Buffer solutions generally have low ionic strength; the absorption of few of the present mobile ions is required to balance the osmotic pressure and thus the swelling. Steric interactions among the charged polymer groups will occur inside the hydrogel due to the low ion concentration of the solution located inside the hydrogel, promoting increased hydrogel swelling. The osmotic gradient facilitates higher species diffusion into the hydrogel when exposed to solutions with higher ionic strength so as to balance the osmotic pressure and neutralize the carboxylate groups located on the PAA backbone. Subsequently, polymer network mobility is notably reduced due to the steric effects between the partially ionized carboxylic groups being shielded, due to the high content of electrolytes.

In a swollen hydrogel, there is an increase in the repulsion between the negatively charged PAA carboxylate ions. The free volume and capability to imbibe water thus increases. There is still however the possibility of buffer solution hydroxide ions diffusing into the hydrogel and reacting with the dissociated protons from the PAA carboxyl groups to form water and cause swelling of the hydrogel. PAA carboxyl group dissociation is much more significant when the pH is higher than its *pK*a, 4.7 therefore the EMH showed a greater effect at pH 7.4.

Interestingly, between hour 3 to 24, the EMH displays a retention of its swelling state (Figure 5.13), possibly indicating a superabsorbent ability. In addition, the retention may result due to the polymer network being 'closed' as it was not exposed to an electro-stimulus.

136

5.3.10. Cyclic voltammetric assessment of the electro-active function

Assessing cyclic voltammetry uses a reference electrode (RE), working electrode (WE), and counter electrode (CE), also called the secondary or auxiliary electrode (Figure 5.14a). In certain cases, potentiostats may also have a sense (S) electrode in addition to the WE. The applied potential is measured against the RE, while the CE closes the electrical circuit for the current to flow. The experiments are performed by a potentiostat that effectively controls the voltage between the WE and RE, while measuring the current through the CE, the WE is connected to the ground. Digital potentiostats cannot apply a true linear waveform due to the discrete nature of digital electronics thus, a scan is generated by a sequence of discrete steps, resulting in a staircase scan (Figure 5.14b). In the standard staircase method, the measurement time window is located at the very end of the interval time. The staircase scan is used as an approximation to a true linear scan. The staircase scan and thus the interval time t_{int} are defined by two parameters (Autolab Application Note EC07, 2011):

$$t_{int} = \frac{E_{step}}{\vec{V}}$$
Equation 5.2

Where $\vec{V}$ is the scan rate (V/s) and E_{step} is the step potential (V) and interval time, t_{int} defined in seconds.

Each potential step triggers the occurrence of a charging current or capacitive current, which decays exponentially, as:

$$i_c = \frac{E_{step}}{R_u} e^{\frac{t}{R_u C_{dl}}}$$
Equation 5.3

Where R_u is the uncompensated resistance and C_{dl} is the double layer capacitance. These values are often combined to express a characteristic time, τ, given by:

$$\tau = R_u C_{dl}$$
Equation 5.4

With typical values encountered in aqueous solutions, a characteristic time in the range of a few hundred µs is to be expected, implying that the charging current has all but decayed at the end of the interval time. Figure 5.14c shows an example of a waveform for a staircase potential scan.
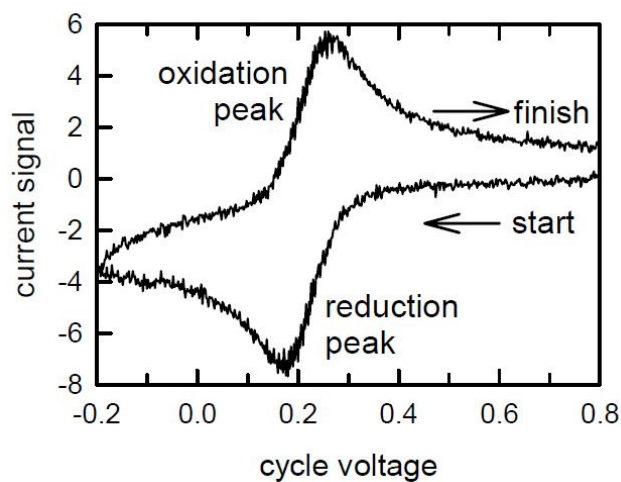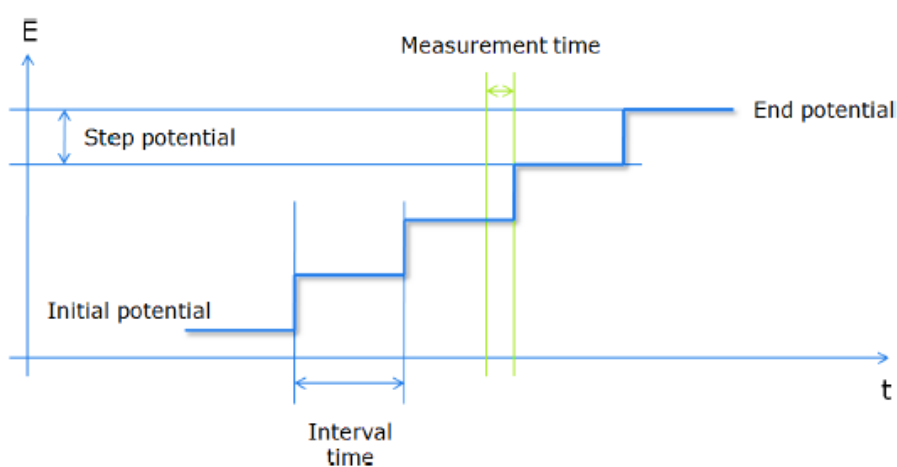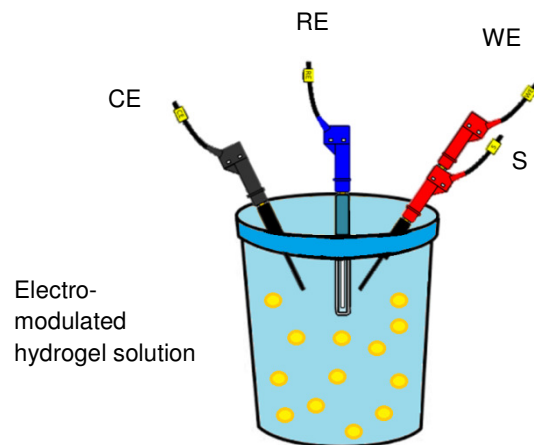
Figure 5.14: (a) Set up of cyclic voltammetry apparatus (adapted from Autolab Application Note EC07, 2011). Typical (b) staircase scan (c) staircase waveform.

Cyclic voltammetry was employed to assess the electroactive capabilities of the EMH. The resultant voltammograms (Figure 5.15a-d) depicts the presence of oxidation and reduction waves. Anodic (oxidation) peaks occurred in figures a-d at 0.7V, 0. 5V, 0.6V and 0.4V, respectively. Cathodic (reduction) peaks are observed in Figure 5.15d , at -2.8V and -1.3V.

Oxidation peaks in Figure 5.15a, b and d may be attributed to the oxidation of the imine moieties in PEI, and the peak in Figure 5.15c to the oxidation of the imidazole moieties. Reduction peaks may be attributed to the excess amino groups as well as the various ionic interactions occurring between the sample, electrode and electrolyte system interfaces. The bulk ionic conductivity of the EMH is lower in comparison to that of PBS resulting in a slower ion transfer rate. Polarization was observed when the ion transfer rate could not meet the reaction rate on the electrode-electrolyte interface and was revealed as a reduction of the distinct peaks and a small position shift against the potential axis.
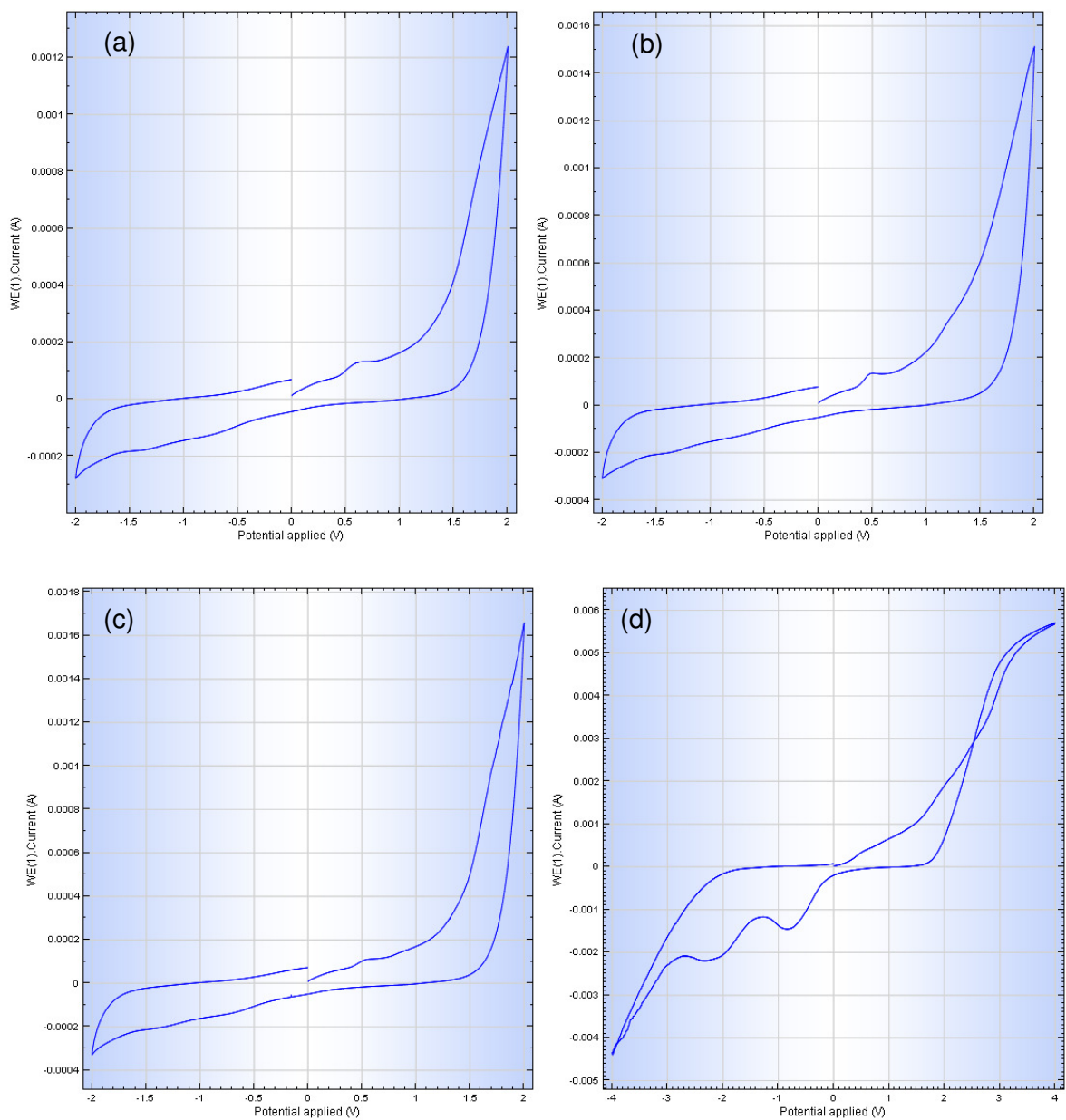
Figure 5.15: Voltammogram showing the electro-activity from -2V to +2V of (a) Electro-Modulated Hydrogel (b) poly (ethyleneimine) (c) 1-vinylimidazole and from -4V to +4V of (d) Electro-Modulated Hydrogel.

5.3.11. Conductivity and Resistance Measurements

The samples were found to have varying conductivity and resistance measurements (Table 5.7). Although the EMH had the lowest conductivity in comparison to the native polymers, the highest resistance was also observed. Cross-linking of the amino moieties may have led to the observed decrease in conductivity of the EMH.

Table 5.7: Conductivity and Resistance Measurements as per Electro-Modulated Hydrogel samples.

Sample	Conductivity (mS/cm)	Resistance (Ω/cm)
EMH	17.92	5.50
PEI	18.33	5.13
VI	18.02	5.29

5.3.12. Kinetic analysis of drug release from the optimum formulation

The kinetic models generated were in congruence with the electro-responsive capabilities of the device. The mechanistic models employed were the Highuchi, Hixson and Korsmeyer-Peppas. The Makoid-Banakar model was employed as an empirical model. Table 5.8 represents the degree to which each model describes the optimum formulation. All models displayed similar R^2 values of ±0.96 and relatively low AICs with the exception of the Higuchi mode, having a R^2 of 0.8345 and a high AIC of 20.8031. In terms of therapeutic treatment of diseases, zero order release is most desirable. The release kinetics of sodium indomethacin was best exemplified by the zero order model with a lag (Figure 5.16). A comparatively low AIC was obtained with a high R^2 of 0.9676. The Korsemeyer-Peppas model was employed to provide a prediction of the drug release mechanism. The Korsemeyer- Peppas release exponent (n) was observed between 0.45 and 0.89, which is indicative of anomalous (non-Fickian) diffusion (Ritger and Peppas, 1987).
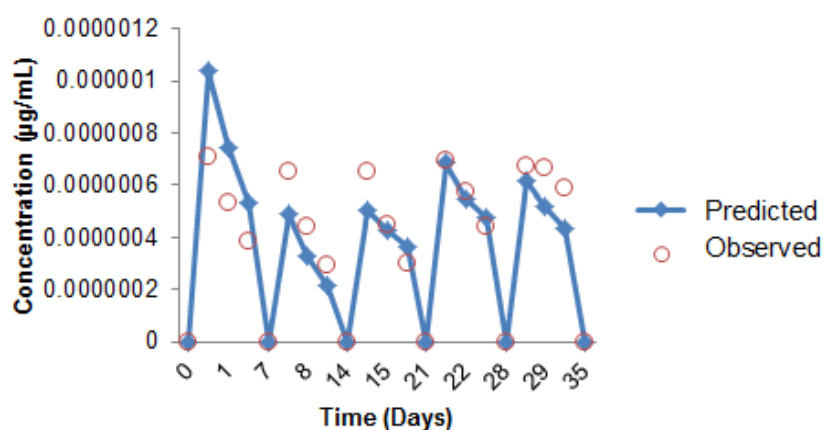
Figure 5.16: Results for extravascular pharmacokinetic analysis employing lag.

Table 5.8: Release parameters and statistical descriptors of the Electro-Modulated Hydrogel -Microneedle device.

	Zero order		
k_0 (h^{-1})		AIC	R^2
0.489		-3.5923	0.964
	Zero order with T_{lag}		
k_0 (h^{-1})		AIC	R^2
0.474		-2.1829	0.9653
	First order		
k_1 (h^{-1})		AIC	R^2
0.005		-3.4272	0.9636
	First order with T_{lag}		
k_1 (h^{-1})		AIC	R^2
0.005		-1.8978	0.9646
	Higuchi		
k_H $(h^{-1/2})$		AIC	R^2
1.072		20.8031	0.8345
	Hixson-Crowell		
H_{HC} $(h^{-1/3})$		AIC	R^2
0.002		-3.4858	0.9637

	Makoid-Banakar				
kMB	**n**	**k**	AIC		R^2
0.555	0.563	-0.108	-1.3160		0.9676

	Korsmeyer-Peppas		
kKP	**n**	AIC	R^2
0.470	1.023	-1.6712	0.9641

	Quadratic		
k_1 (h^{-1})	k_2 (h^{-1})	AIC	R^2
0.000	0.005	-1.8819	0.9646

k_0 (h^{-1})-zero order rate constant ; k_1 (h^{-1})- first order rate constant; k_H $(h^{-1/2})$- Higuchi rate constant; H_{HC} $(h^{-1/3})$-Hixon-Crowell rate constant; kMB- Makoid-Banakar rate constant; n- empirical parameter; k- empirical parameter, kKP- Korsmeyer-Peppas rate constant; k_2 (h^{-1})- second order rate constant; AIC- Akaike's Information Criterion; R^2-correlation coefficient

Even though similar high R^2 values that were obtained, the models employed may not provide a definite correlation to the *in vitro* release kinetics as the models operate by determining the constants at each individual time point and subsequently determines the working regression of those points not necessarily catering for the pulsatile-like response of the electro-responsive system. Thus a new model may need to be introduced for future kinetic analysis of stimuli-responsive systems.

5.3.13. Electromimetic Modeling

Firstly, considering the PEI-PAA$_2$-VI$_4$ molecular build-up in vacuum, the formation of PEI-PAA$_2$ complex accompanied with a stabilizing interaction of ≈-30kcal/mol (Table 5.9) wherein the van der Waals (vdW) forces played the major role in geometry stabilization with stabilization energy of ≈-30kcal/mol – meaning that the whole stabilization was brought up by hydrophobic forces in vacuum phase. Interestingly and more convincingly, the formation of PEI-PAA$_2$-VI$_4$ was companied with further stabilization of van der Waals component energy reaching to even negative values (≈-42kcal/mol) leading to a contribution of ≈88kcal/mol towards geometry optimization. In both the cases, the hydrophobic steric interactions (vdW) countered the torsional and stretching caused by the addition for vinyl imidazole leading to the formation of a well-fit geometrically-optimized energy-minimized BiPERG structure that acted as the template for further solvated studies under electric field.

Table 5.9: Inherent energy attributes representing the molecular assemblies modeled using static lattice atomistic simulations in vacuum and solvated phase.

Molecular complex	E(V_Σ)[a]	E(V_b)[b]	E(V_θ)[c]	E(V_φ)[d]	E(V_{ij})[e]	E(V_{hb})[f]	E(V_{el})[g]
PAA	76.02	8.87	43.21	10.63	13.42	-0.12	0.00
PEI	28.36	1.42	5.38	9.32	12.23	0.00	0.00
VI	15.68	0.05	15.05	~0.0	0.57	0.0	0.00
PEI-PAA$_2$	150.96	19.20	92.71	31.13	8.34	-0.41	0.00
PEI-PAA$_2$-VI$_4$	155.81	16.58	147.04	34.16	-41.96	0.00	0.00
PEI-PAA$_2$-VI$_4$-H$_2$O (0.0)	-2645.51	37.33	170.218	40.02	-67.58	-0.75	-2824.74
PEI-PAA$_2$-VI$_4$-H$_2$O (0.1x)	2250.91	336.831	975.802	47.44	9.30	-1.21	-2745.75
PEI-PAA$_2$-VI$_4$-H$_2$O (0.3x)	5051.92	1198.81	2788.45	41.58	94.02	-0.29	-3079.67
PEI-PAA$_2$-VI$_4$-H$_2$O (0.5x)	5766.877	5321.24	8349.21	44.18	151.34	-1.51	-4024.21
PEI-PAA$_2$-VI$_4$-H$_2$O (0.1y)	668.41	345.73	1010.36	41.68	3.09	-0.48	-2837.74
PEI-PAA$_2$-VI$_4$-H$_2$O (0.3y)	1853.85	1241.53	2900.71	44.19	49.79	-0.34	-3279.12
PEI-PAA$_2$-VI$_4$-H$_2$O (0.5y)	2956.49	5391.06	8426.01	49.36	159.74	-0.49	-4263.61
PEI-PAA$_2$-VI$_4$-H$_2$O (0.1z)	4141.08	348.47	1029.64	40.59	10.06	-0.59	-2922.53
PEI-PAA$_2$-VI$_4$-H$_2$O (0.3z)	8980.11	1232.85	2854.01	38.91	29.98	-0.41	-3231.63
PEI-PAA$_2$-VI$_4$-H$_2$O (0.5z)	45841.19	5409.57	8457.95	53.28	91.98	-0.44	-4233.49

[a] total steric energy for an optimized structure
[b] bond stretching contributions
[c] bond angle contributions
[d] torsional contribution arising from deviations from optimum dihedral angles
[e] van der Waals interactions
[f] hydrogen-bond energy function
[g] electrostatic energy

Furthering the study, presented are novel electrosimulations addressing a unique drug delivery phenomenon where the plasticized polymeric chains undergo intrinsic interactions as well as the electro-influenced adjustments as discussed below. Employing molecular mechanics simulations and subsequent energy/geometry minimizations, complex interactions and fascinating results were discovered between the polymeric molecules (PAA

and PEI) and between polymeric molecules and the plasticizer (PAA-PEI and VI) in presence of water molecules under the influence of electric field. To explain this complex behavior, a new theory, Pillay's Electro-influenced Geometrical Organization-ReOrganization Theory (PEiGOR Theory), is presented based on following assumptions and observations (Figure 5.17):

1. *The Organization* – Polymeric chains organize with respect to the direction and strength of electric field: Electric field application → polymer chains organization → increase in static energy due to electron transfer reaction → molecular alignment → planar structural conformation → reduced networking → electroresponsive drug release.

2. *The ReOrganization* – Polymeric chains in assumptions 1 reorganize with respect to surrounding polymer molecules/plasticizer/solvent molecules via "local oriental correlations (LOCs)": Intrinsic interactions → local oriental correlations → change in reaction co-ordinates → solvent relaxation → polymer chains reorganization → decrease in static energy values → increased networking → drug retention.
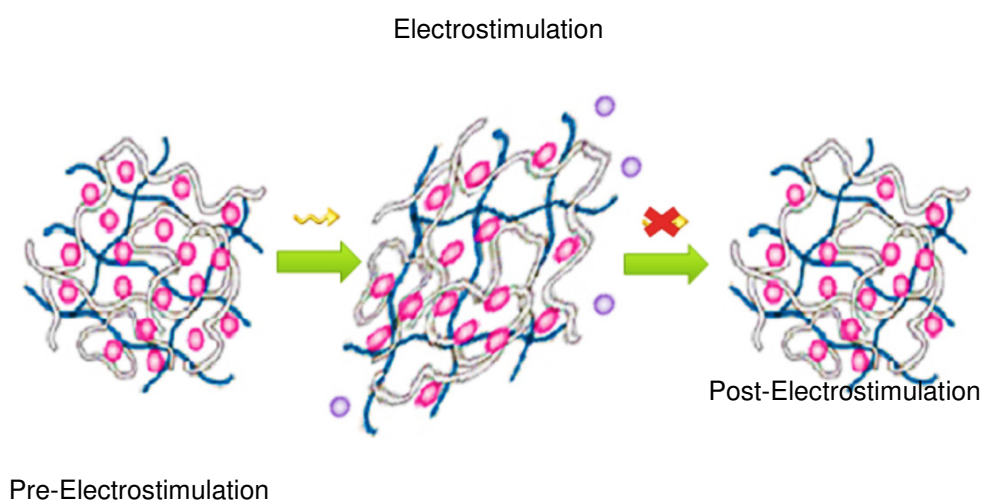
Figure 5.17: Graphical representation of the PEiGOR Theory. ⬤ Entrapped drug ◯ Released drug 〜 PEI 〜 PAA 〜➤ Electro-stimulation

The energy surfaces in Figures 5.18, 5.19, and 5.20 confirm the organization-reorganization theory to a great extent where the energy mapping generated for the directional optimization display the "fluctuation patterns" representative of the organization-reorganization pattern wherein organization caused a crest in the surface and reorganization resulted in trough formation. Additionally, it is clear from the energy maps shown in Figures 5.18, 5.19, and 5.20 and Table 5.9 that there is a positive relation between the stabilization energy and the

applied electric strength wherein an increase in energy from 2250kcal/mol to 5766kcal/mol (x direction); 668kcal/mol to 2956kcal/mol (y direction); and 4141kcal/mol to 45841kcal/mol (z direction) was observed in case of energy field application at the strengths of 0.1a.u. to 0.5a.u., respectively. As the electric potential increased; the stabilization energy also increased which may be due to increased alignment of the electric dipoles with a complete alignment resulting from the forces required to overcome the additional interfaces in the domain structure. With respect to the response of the bipolymeric interfacially plasticized EMH (a non-symmetrical structure) towards the direction of electric field application, the orientation of the approaching point charge with respect to the molecular complex played an important part. The shorter the distance between the point charge from the centre of the molecular complex, the stronger the interactions.
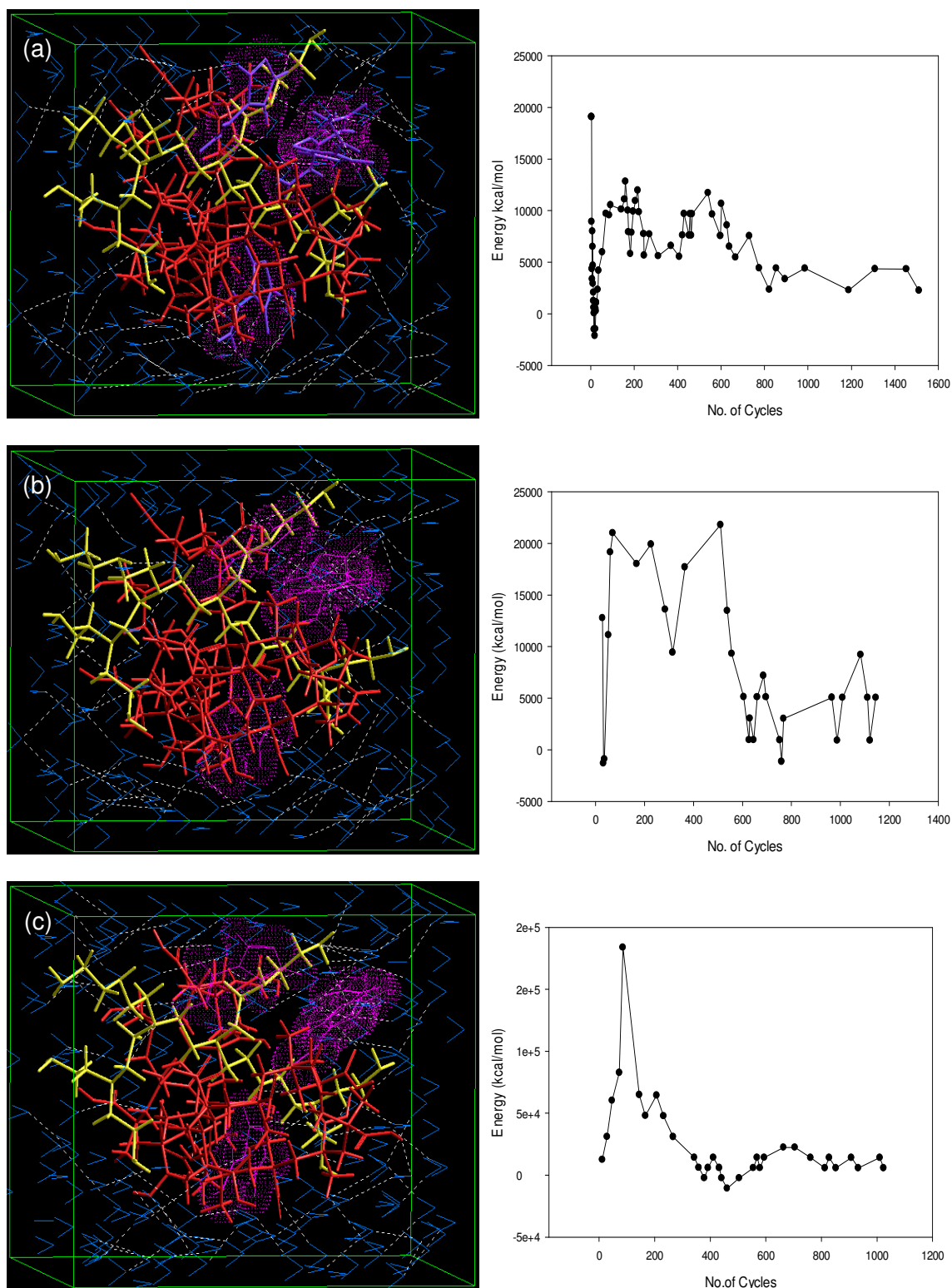
Figure 5.18: Visualization of geometrical preferences of (a) PEI-PAA$_2$-VI$_4$-H$_2$O (0.1x); (b) PEI-PAA$_2$-VI$_4$-H$_2$O (0.3x); and (c) PEI-PAA$_2$-VI$_4$-H$_2$O (0.5x) after molecular simulation in a solvated system under external electric field and the corresponding energy plot showing the geometrical optimization mapping over the iteration cycles.
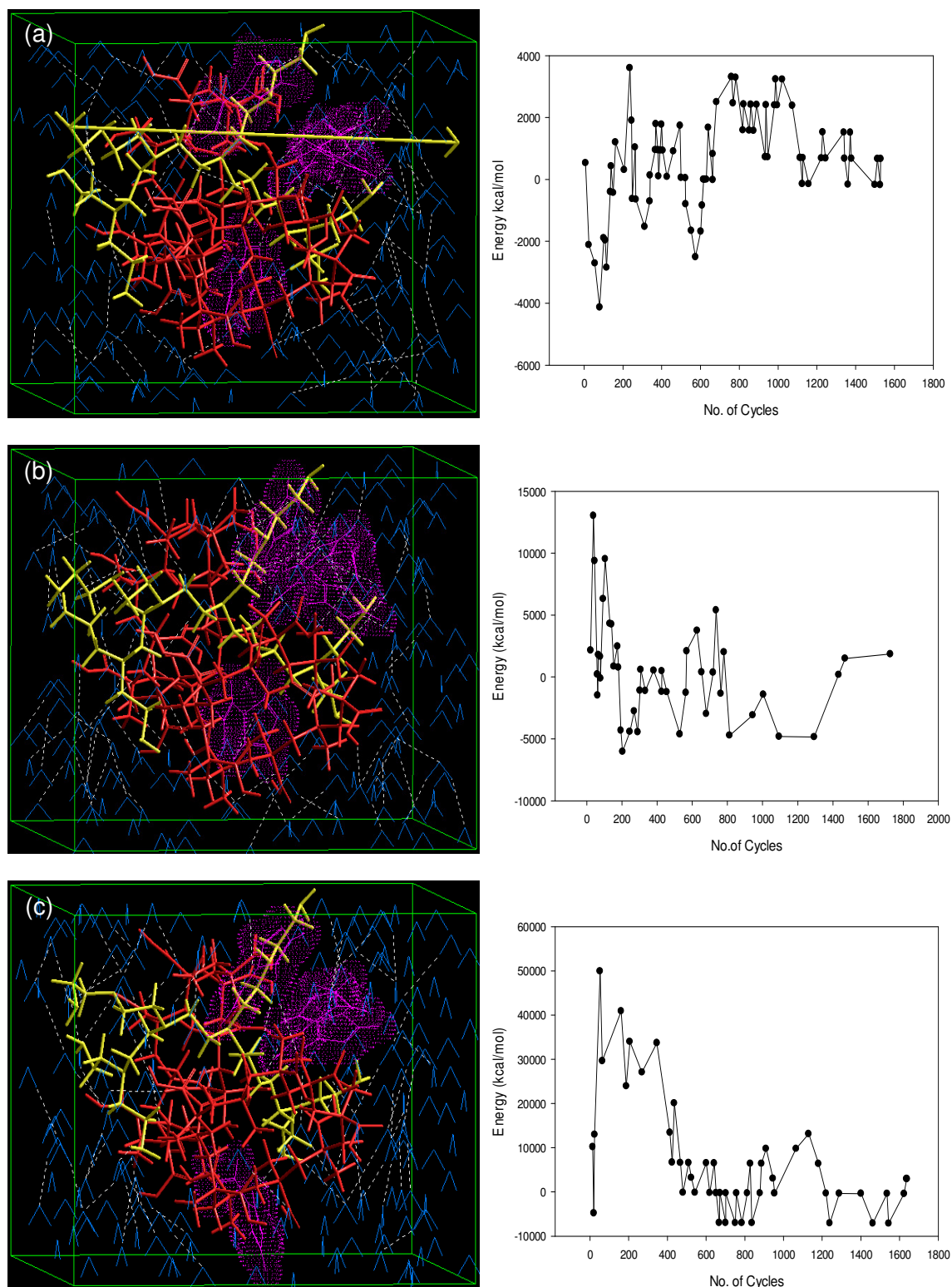
Figure 5.19: Visualization of geometrical preferences of (a) PEI-PAA$_2$-VI$_4$-H$_2$O (0.1y); (b) PEI-PAA$_2$-VI$_4$-H$_2$O (0.3y); and (c) PEI-PAA$_2$-VI$_4$-H$_2$O (0.5y) after molecular simulation in a solvated system under external electric field and the corresponding energy plot showing the geometrical optimization mapping over the iteration cycles.
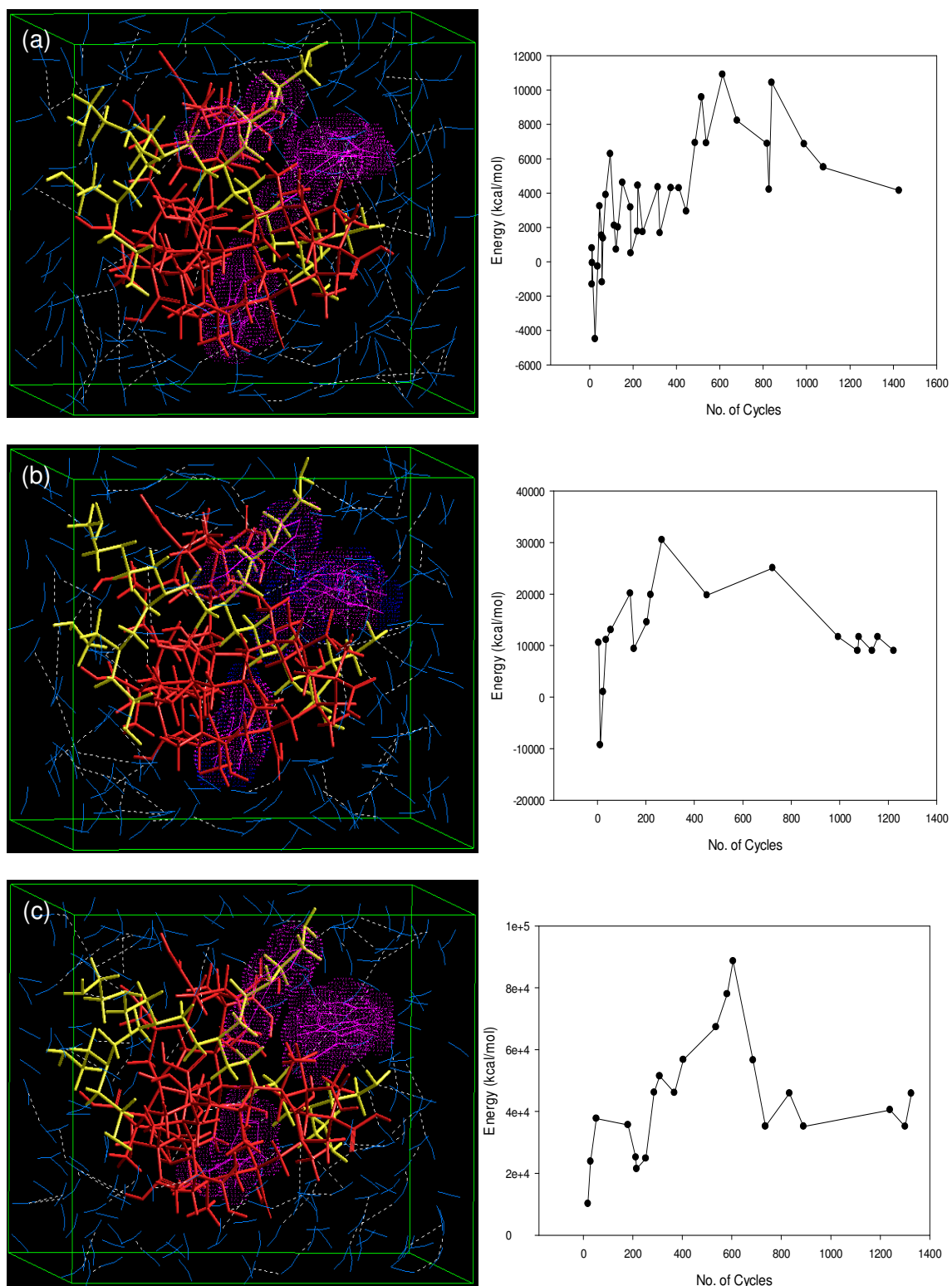
Figure 5.20: Visualization of geometrical preferences of (a) PEI-PAA$_2$-VI$_4$-H$_2$O (0.1z); (b) PEI-PAA$_2$-VI$_4$-H$_2$O (0.3z); and (c) PEI-PAA$_2$-VI$_4$-H$_2$O (0.5z) after molecular simulation in a solvated system under external electric field and the corresponding energy plot showing the geometrical optimization mapping over the iteration cycles.

The component energy terms additionally played a deciding role in the molecular simulation and modeling. The component energy values listed in Table 5.9 represent the average energy values of the fluctuation pattern and have no additive relation to the final optimized value. Considerable H-bonding interactions were observed during the vacuum phase stabilization of the PAA-PEI complex. As expected, the hydrogen bonding was not constant during the electrosimulation as it forms the part of environmental interaction through which the charge transfer occurs. However, it should be noted that the negative H-bonding values were retained throughout the electric direction and field options with values ranging from -1.51 to -0.29kcal/mol. The electrostatic interaction played a major role in energy stabilization of the final molecular complex with values on higher side of stabilized negative energy scale. Among the destabilization energy terms, all except torsional contribution fluctuated throughout the direction and strength range. From Table 5.9 it is evident that the spatial *Organization* might have resulted from the drastic changes in bond stretching and bond angle contributions with small but significant changes in torsional contributions arising from optimum dihedral angles and hydrophobic van der Waals forces with the *ReOrganization* resulting from hydrogen bonding and electrostatic forces as explained above.

The arrangement of plasticizer VI within polymer sheets resulted in the formation of an electroconductive imidazole ring network across the polymeric architecture of the bipolymeric interfacially plasticized EMHs. These plasticized microsites were balanced by torsional constraints within the intervening layer which attracted H_2O molecules to hydrate the region, leading to swelling of the hydrogel structure. Although electroconductive hydrogels have been studied and reported for several years, however not much work had been reported with regard to the mechanisms involved in experimental hydration and molecular diffusion of a plasticizer within polymer chains. The present molecular simulation study thus might be adjunctive to experimental work concerning the molecular interplay.

The molecular mechanics simulations under solvated phase displayed some basic similarities of molecular behavior in all nine cases. VI molecules appear not to rove around, but instead to tend to drift close to the hydrogen-bonding sites sunken inside the polymer structure. However, the molecules while moving, display a critical "jump diffusional behavior" - the polymer chains vibrate within a microenvironment for a short period, and then move to new micromolecular sites. These jump-motions are likely to be concentrated along varied locations in the vicinity of electrostatic charged spots attracting the water molecules. However, in contrast, the solvent molecules may exhibit incessant diffusion on the timescale of these simulations. While with no electric field in place; the molecular complex does not show the fluctuation flexibility wherein the molecular components demonstrate a differential

spatial variation leading to geometrically optimized and energetically minimized structures via two principle component interactions, one among the polymer/plasticizer molecules and the other among the complex and solvent molecules leading to a well organized and highly stable molecular architecture (Figure 5.21).
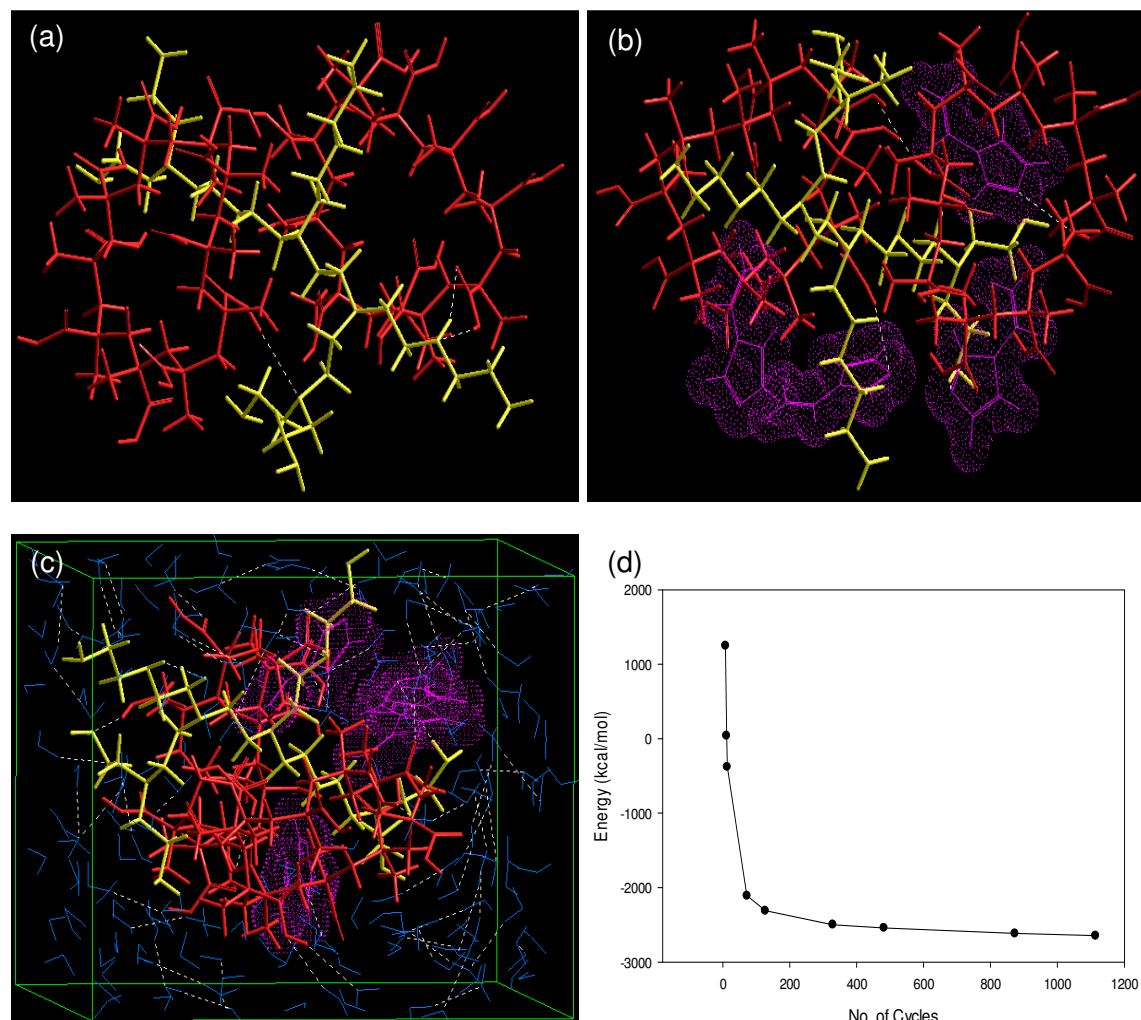
Figure 5.21: Visualization of geometrical preferences of (a) PEI-PAA$_2$ after molecular simulation in vacuum; (b) PEI-PAA$_2$-VI$_4$ after molecular simulation in vacuum; (c) PEI-PAA$_2$-VI$_4$-H$_2$O after molecular simulation in a solvated system under no external electric field; and (d) the corresponding energy plot showing the geometrical optimization mapping over the iteration cycles.

5.4. Concluding Remarks

A fast response of hydrogels to the external stimuli is also a requirement in many application areas of electro-responsive hydrogels. The PVA/PAA semi-IPN containing the PEI/VI blend has proven the electro-responsive capabilities. In addition, pH responsive behavior was observed as associated to the swelling capability of the EMH. Also observed, the EMH semi-IPN serves as a high ionic conductivity polyelectrolyte EMH. This chapter concluded that due to the ionic nature the EMH, the semi-IPNs displayed greater swelling ratios at pH 5.4 in comparison to pH 7.4. PVA is a neutral polymer. The results indicate that swelling increased as the pH decreased due to the counter-acting swelling abilities of the PAA and PVA. At room temperature, the EMH shows ionic conductivity as high as 17.92S/cm. significant differences depending on the ionic strength of the solution used was observed in the morphologies and pore sizes were observed in both the swollen and unswollen EMH. As depicted by the XRD results, due to the amorphous structure of the EMH, the polymer chain becomes more flexible for ionic transport, suggesting that the formulated EMHs are promising in the field of pH/ electro-responsive drug delivery. In addition, the EMHs may be used for a variety of applications as they are capable of showing suitable responses to electro-stimulation even when incorporated with different therapeutic agents and display considerable swelling factors in the pH range investigated here.

CHAPTER 6

DEVELOPMENT AND EVALUATION OF THE MICRONEEDLE ARRAY TO BE EMPLOYED IN THE ELECTRO-MODULATED HYDROGEL-MICRONEEDLE DEVICE

6.1. Introduction

The ceramic MNAs used as part of this device have been fabricated by a simple process in which alumina slurry is casted into a PDMS microneedle mold and is subsequently sintered. The simpler technique of ceramic micromoulding offers the advantage to ensure device production at low cost due to the potential of up-scaling the technology.

The idea of a nanoporous MNA is that it holds a defined volume of active for controlled release in its open pore volume including the backing plate, functioning similarly to the reservoir in a patch but enhancing the compound's permeability into the skin by mechanically breaching it. The nanoporous structure in the material seamlessly connects the viable epidermis via the microneedles with the main part of the drug-reservoir, the backing plate of the microneedles, atop of the skin (Figure 6.1). At the same time the slurry material maintains overall mechanical integrity of the microneedles during insertion into the skin and avoids the relatively complexity of manufacturing a cannulae through the microneedles, opting for flow-through of a compound injected from a reservoir into the skin.

(a)   **(b)**
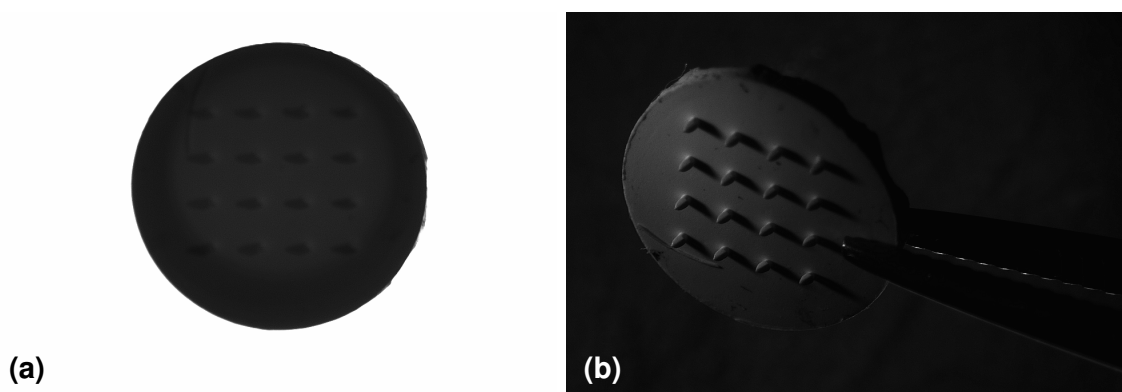
Figure 6.1: Overview of the sintered ceramic array also showing the (a) front and the (b) detailed view of the microneedle tips.

In addition to fabrication of the EMHM device, integration, dosing and many others issues are apparent from a pharmaceutical research point of view. To ensure the success of the device, this chapter thus illustrates the physicochemical testing of the MNAs for incorporation into the EMHM device for subsequent *ex vivo* and *in vivo* testing.

6.2. Materials and Methods

6.2.1. Materials

The Sylgard® 184 Base silicone elastomer and the Sylgard® 184 Curing agent silicone elastomer were procured from Dow Corning (Seneffe, Belgium). All other reagents were of analytical grade and were procured from Merck (Schiphol-Rijk, Netherlands).

6.2.2. Etching of the SU-8 master photoresist required for fabrication of the microneedle array

A PDMS solution consisting of the base and curing agent was prepared (10:1) and was subsequently degassed in a vacuum chamber (RV3, Edwards, Munich, Germany).

A low-pressure chemical vapor deposition (LPCVD) -silicon nitride covered 4-inch wafer of Si (silicon; 100) was patterned using photolithography techniques and $CHF_3 + O_2$ plasma (Figure 6.2). The Si wafer was further anisotropically etched using potassium hydroxide solution (KOH; 25%) through openings in the silicon nitride mask. Removal of the silicon nitride was facilitated by hydrogen fluoride (50%). As a result, an antireflective highly conformal titanium-silicide layer was formed. The titanium-silicide layer functions to prevent exposure of the SU-8 resist by the scattering of UV-light from the oblique faces of the Si-etched pyramids. Without the titanium-silicide layer, undesirable polymerization and thus defects in the microneedles tips would have resulted. This process resulted in the formation of the 1st PDMS mold. The length of the microneedles and the tips geometry were defined by patterning of the SU-8 thick layer (Bystrova and Lüttge, 2011).
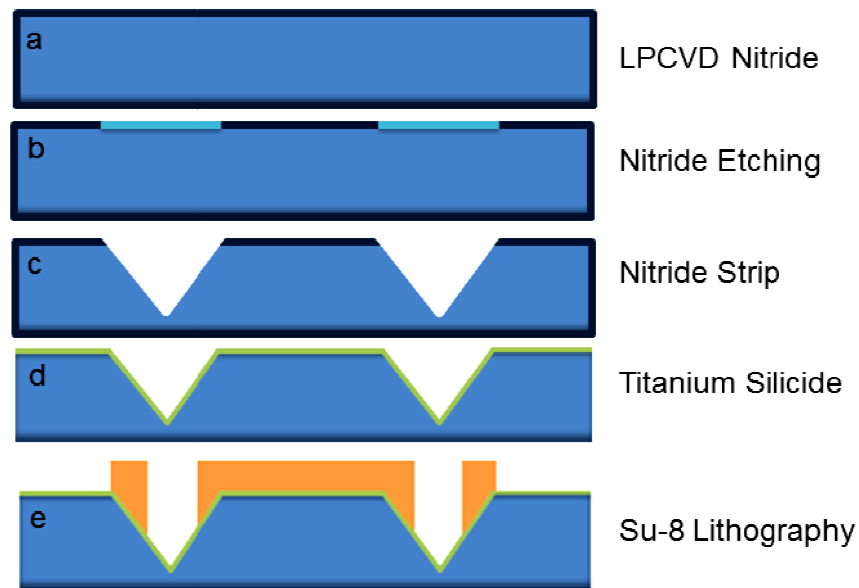
Figure 6.2: Process sketch for producing a Si-master (a) Silicon nitride deposition on Si wafer (b) Patterned silicon nitride (c) Anisotropically etched Si (d) Silicon nitride removed (e) Titanium silicide layer formed (f) SU-8 photoresist spinned on and patterned (Figure adapted with permission from Elsevier Ltd: Bystrova and Lüttge, 2011).

The SU-8 mask was cleaned with acetone and dried. Following the deposition of an anti-adhesion fluorocarbon layer onto the SU-8/Si master the 1st PDMS mold was replicated and released by placing the mask into an assembled casting tool (Figure 6.3). The PDMS solution was poured into the tool and subsequently degassed. The tool was cured at 80˚C for 24 hours after being degassed using a vacuum pump (RV3, Edwards, Munich, Germany). The second replication was achieved by repeating the fluorocarbon deposition and releasing the 2nd PDMS mold (production mold). This 2nd mold was used for casting of the ceramic slurry.
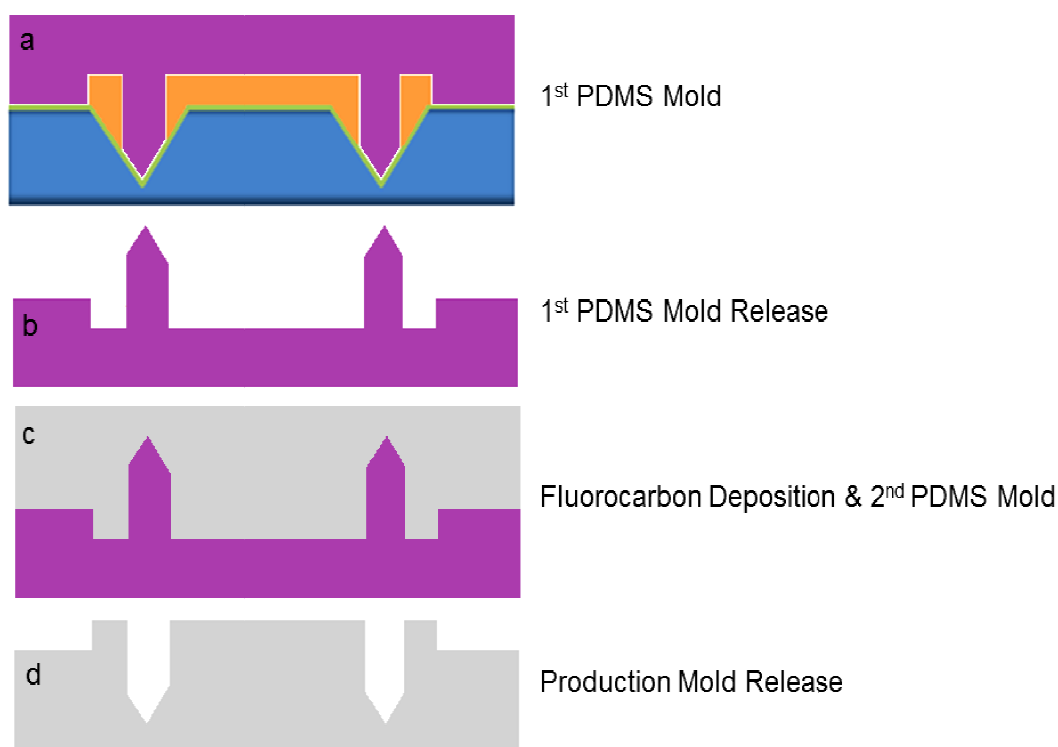
Figure 6.3: Process sketch for producing polydimethyl siloxane molds and ceramic microneedle arrays: (a) Fluorocarbon layer deposition, replication of the 1st polydimethyl siloxane mold; (b) Mold release; (c) Deposition of the fluorocarbon layer and replication of the 2nd polydimethyl siloxane mold; (d) The 2nd polydimethyl siloxane mold (Figure adapted with permission from Elsevier Ltd: Bystrova and Lüttge, 2011).

The PDMS mold was placed into an ethanol solution and cleaned prior to casting using ultrasonication for a period of 1hr at amplitude of 80%. After removal, the mold was dried at 60 °C for 1 hour. The mold was allowed to cool in a petri dish on a droplet of ethanol, which allows for good signal transmission into the slurry during ultrasonication.

6.2.3. Preparation of the ceramic slurry required for microneedle array fabrication

For ceramic casting, a slurry made of 43%$^w/_v$ alumina (AKP 30, Sumitomo) suspended in 46% $^w/_v$ ethanol containing 6.4% $^w/_v$ poly(vinyl butyral) (B-98, Tape Casting Warehouse) as a binder and 2.8%$^w/_v$ butyl benzyl phthalate (S-160, Tape Casting Warehouse) as a plasticizer, 1.0% $^w/_v$ kaolin as sintering agent and 0.8%$^w/_v$ Solsperse 20000 (Noveon Division Lubrizol Ltd.), was used as a dispersant (Verhoeven *et al.*, 2012).

PDMS molds were filled with the slurry and the air bubbles removed by placing the mold in an ultrasonic bath. Following removal, the slurry was allowed to air dry. After drying, the ceramic green body was released from the PDMS mold and MNAs with a diameter of 4.5mm were cut out. The MNA green bodies were then sintered in a controlled manner utilizing a

155

tube furnace at a maximum sinter temperature of 1500°C (Verhoeven *et al.*, 2012).Ceramic samples for the porosity measurements were prepared in the same way but molded on a flat piece of PDMS for reasons of convenience in the manufacture of test samples.

6.2.4. Casting of the ceramic slurry for production of the microneedle array

The ceramic slurry (15mL) was pipetted into the PDMS mold that was set in a petri dish. To further define the casting slurry volume, a PDMS ring with a height of ±7mm was set around the petri dish (Figure 6.4). The petri dish was sealed using parafilm to prevent ethanol evaporation as any air that is trapped in the slurry during the casting can cause microstructural defects. The casted slurry was then ultrasonicated for 30 minutes, to degas the slurry while simultaneously allowing for thorough filling of the mold.
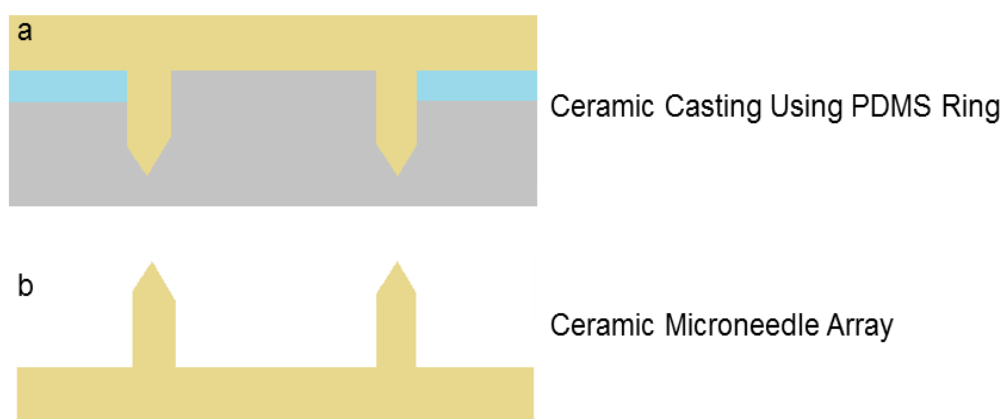
Figure 6.4: Process sketch for producing the polydimethyl siloxane molds and ceramic microneedle arrays. (a) Casting of ceramic slurry; (b) Sintered microneedle array.

6.2.5. Porositometric analysis of the ceramic slurry used in the fabrication of the microneedle arrays

Porosity analysis employing the BET isotherm of nitrogen was conducted as a supplementary investigation to determine the presence of pores and pore size within the dry ceramic MNA as well as the ceramic MNA after being immersed in the drug solution for 24 hours. Porositometric analysis was carried out using an ASAP 2020 Porositometer (Micromeritics Instrument Company (Pty) Ltd., Norcross, GA, USA) as detailed in Chapter 5, Section 5.2.9. The conditions employed were outlined in Chapter 5, Section 5.2.9, Table 5.3. The BJH and BET adsorption and desorption relationships were subsequently generated.

6.2.6. Method modulation of drug permeability of the ceramic microneedle array utilizing an apple skin model

A simulated study in order to determine the penetration and diffusion of a colored ink compound facilitated by MNA penetration through apple tissue was developed. The penetration through the apple skin under dry stagnant, moist and flow conditions were determined as outlined: the apple skin was cut into 1mm thick slices, and the array comprising of 16 microneedles was imprinted onto the apple skin. A drop of ink (1µL) was placed onto the microneedle imprint and the skin pieces were subsequently mounted onto inclined glass slides (Figure 6.5). Distilled water was used to simulate the moist and flowing conditions. The skins were exposed to their respective environments for 10 minutes before being viewed under a Leica DMI5000 M microscope (Wetzlar, Germany).
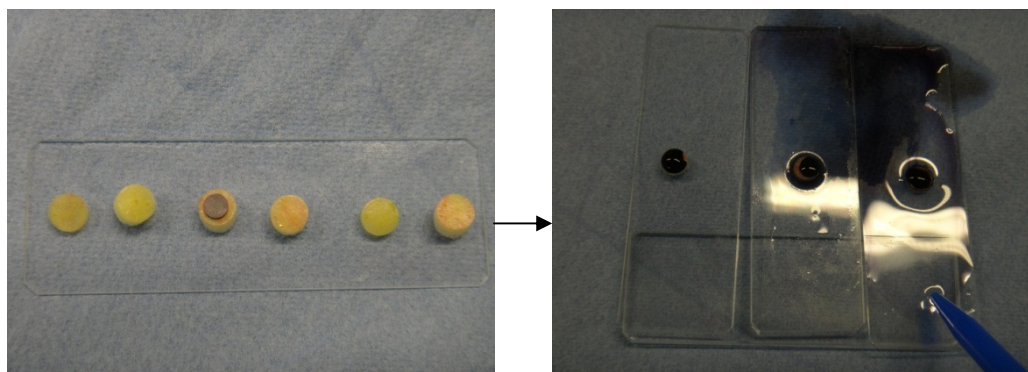
Figure 6.5: The experimental set-up of the modulated drug permeability method.

The above experiment was repeated using Hydro-Terephthalic Acid (HTA) as the fluorescent dye. A comparison study of the diffusion of the dye compound through the MNA and a hypodermic needle through the apple tissue at various time intervals was carried out. The dye (1µL) was injected into the apple tissue using the syringe. The MNA was pressed into the tissue and a drop of the dye (1µL) was placed onto the back plate of the array. The apple tissue samples were exposed to their respective environments for 20 minutes, 6 hours, 24 hours and 72 hours before being analyzed using a preconfigured USB4000-FL fluorescence spectrometer (Ocean Optics, Germany). The calibration curve of intensity versus concentration was constructed for a 2mmol/L HTA solution at the 420nm absorption peak (Chai *et al.*, 2009).

6.2.7. Synthesis of a microneedle array composed of the optimized Electro-Modulated Hydrogel

The optimized EMH formulation was prepared and pipetted (150µL) into various PDMS moulds in order to synthesize a single MNA composed of the optimized EMH (Figure 6.6). The hydrogel-laden molds were left for 48 hours at 25°C to allow for hydrogel polymerization. Topographical visualization of the MNAs was achieved with a stereomicroscope (Leica MZ10 F) connected to a digital camera (DFC365Fx) and image analysis system (Leica Application Suite; Switzerland).

VI   PEI

Preparation of the EMH   EMH   Pipetting of the EMH into the PDMS mould
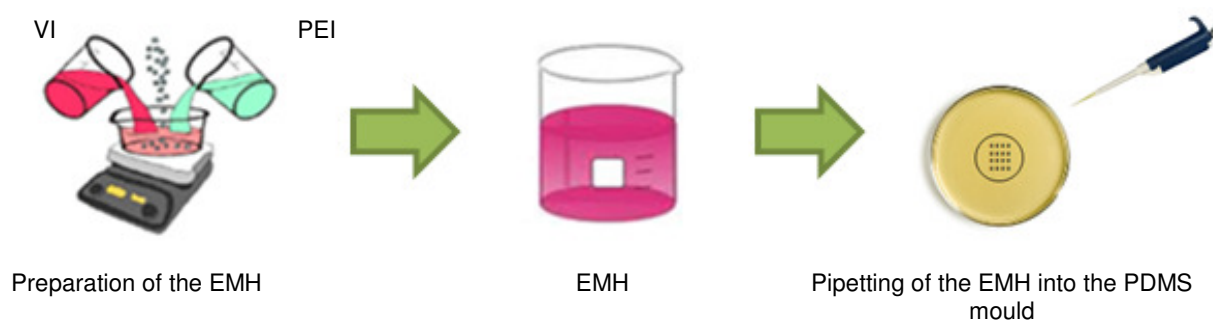
Figure 6.6: Schematic of the fabrication process for the Electro-Modulated Hydrogel microneedle array.

6.2.8. Formulation of microneedle array molds using an imprinting technique

In addition to the utilization of the PDMS mold, various other materials were investigated as possible molds. As an alternative, a prototype PDMS MNA obtained from MESA+ was used to initiate the formation of a direct mold by compressing the MNA into a polystyrene base. Briefly, the master MNA was placed onto the material being investigated and slight pressure applied to produce the microneedle shaft channels. This process was carried out with the aim of manufacturing microneedle molds with quicker production time. The polystyrene base was subsequently filled with the EMH that was allowed to polymerize over 24 hours. The polystyrene base was broken around the hydrogel disc and the EMH viewed under a stereomicroscope (Olympus® Model SZX7) connected to a digital camera and image analysis system (analySIS® Soft Imaging System, Japan).

6.3. Results and Discussion

6.3.1. Porositometric analysis of the ceramic material employed

The BET surface area plot and the isotherm log plot for the MNA prior to and after immersion in drug solution are depicted in Figure 6.7. The BET surface area of the MNA was calculated at 0 and 24 hours to be 10.4127m²/g and 9.0227m²/g, respectively (Table 6.1). The average pore width of the MNA prior to immersion was calculated to be 79.5676Å (7.95676 nm) with

the average adsorption and desorption pore diameters being 125.839Å (12.5839nm) and 129.612Å (12.9612nm), respectively. The average pore width of the MNA after immersion was calculated to be 87.139Å (8.7139nm) with the average adsorption and desorption pore diameters being 127.545Å (12.7545 nm) and 125.538Å (12.5538nm), respectively.

Porous materials allow for a relatively large amount of drugs to be the introduced into the dosage form. The increase in pore width may be as result of drug deposition into and removal from the ceramic. The reduced surface area is as a result of deposited drug into the pores. This is beneficial as the release of the therapeutic agent can be controlled over longer periods of time resulting in an extended duration of action, desirable patient compliance, a decreased burden of care and ultimately a positive therapeutic outcome.

(a)
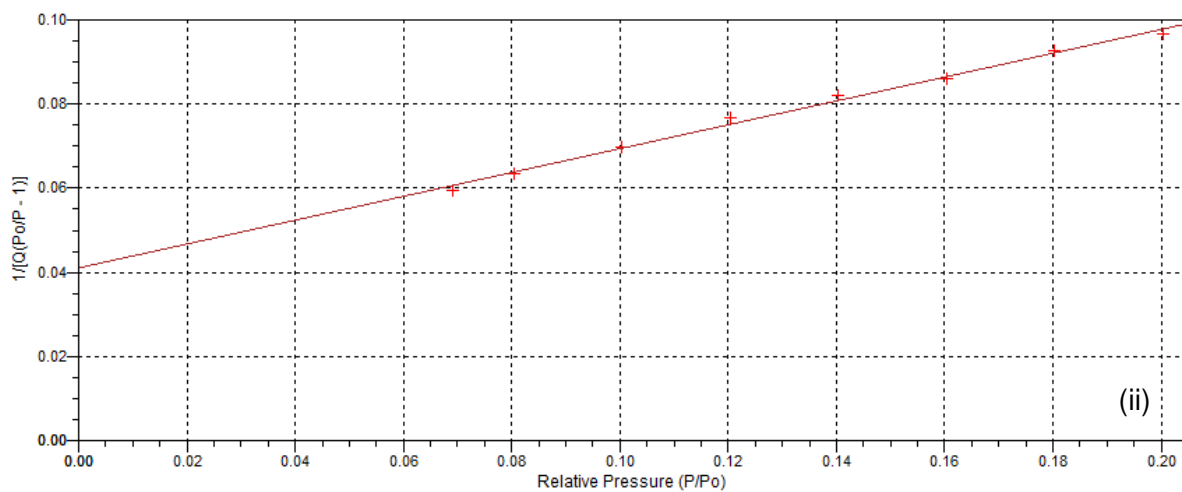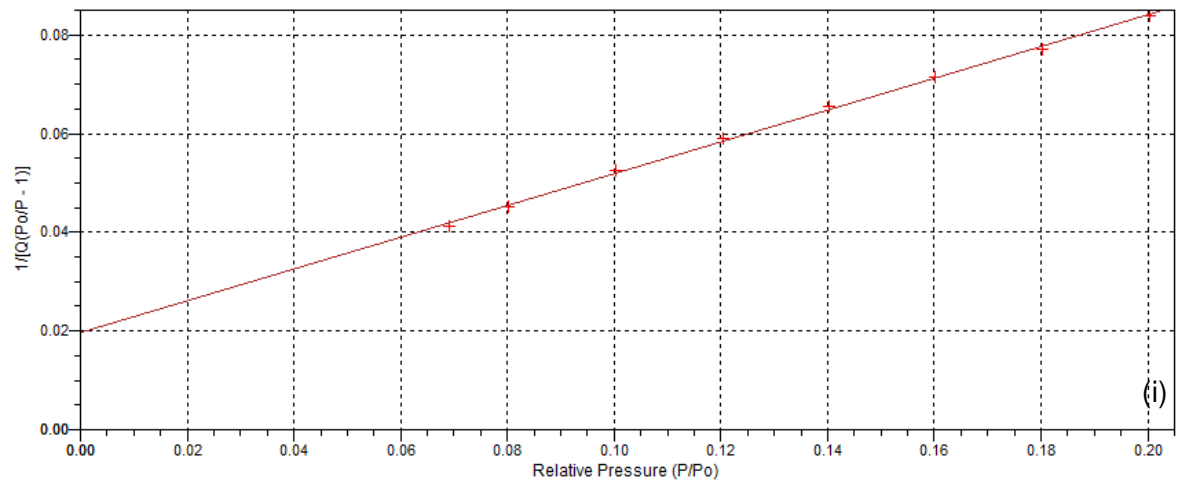
(b)
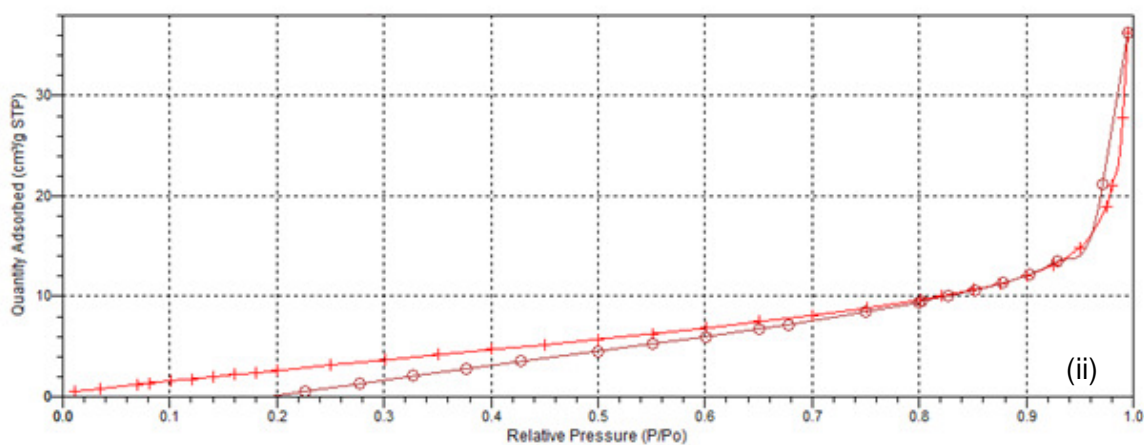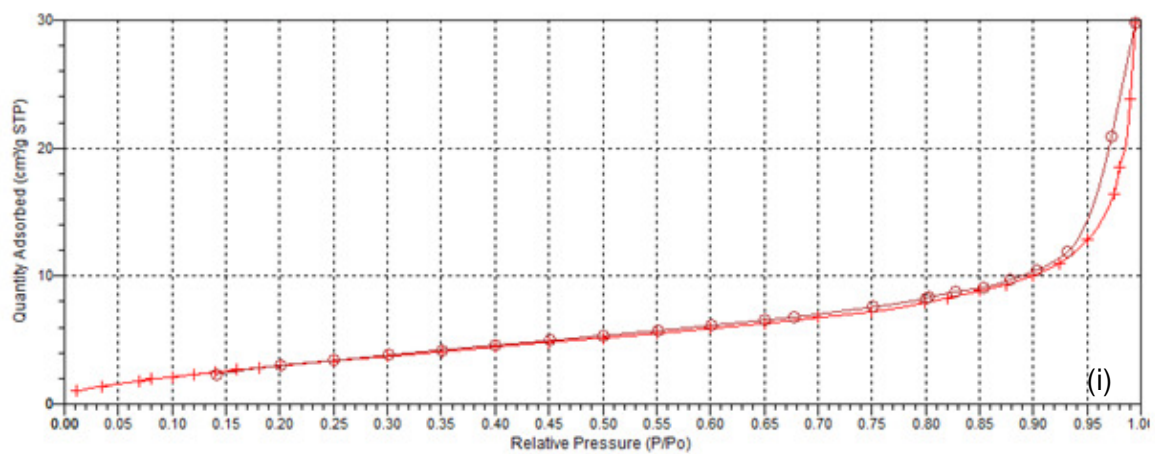
Figure 6.7: Brunauer-Emmett-Teller surface analysis plot (a) and isotherm log plot (b) of the (i) MNA$_{0 \text{ hours}}$ (ii) MNA$_{24 \text{ hours}}$.

Table 6.1: Surface area and porosity characteristics of the microneedle samples.

Parameter		MNA$_{0\ hours}$	MNA$_{24\ hours}$
Surface area	BET Surface Area	10.4127 m²/g	9.0227 m²/g
	BJH Adsorption average pore width (4V/A by BET)	79.5676 Å	87.139 Å
Pore Volume	BJH Adsorption average pore diameter (4V/A)	125.839 Å	127.545 Å
	BJH Desorption average pore diameter (4V/A)	129.612 Å	125.538 Å

6.3.2. Analysis of the modulated diffusion studies

Distinct changes were observed depending on the exposed environment. As can be expected, when exposed to dry conditions there was no to little ink diffusion. When exposed to moist and flow conditions more ink was present in the apple tissue (Figure 6.8).
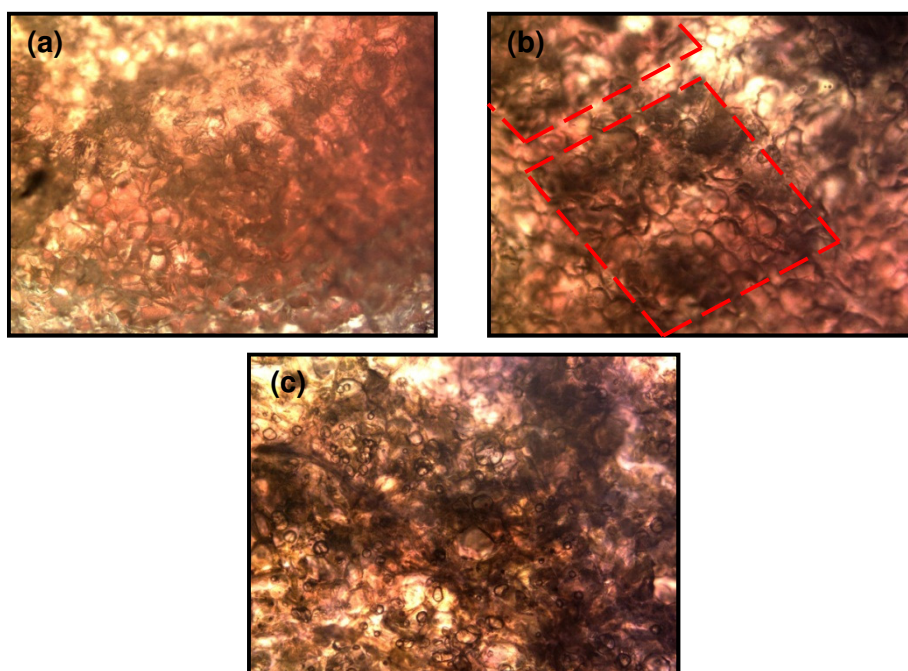
Figure 6.8: Ventral images of the apple skin under (a) dry stagnant conditions (b) moist stagnant conditions (c) conditions employing flow.

6.3.3. Construction of a calibration curve for the quantification of Hydro-Terephthalic Acid using fluorescence spectroscopy

Figure 6.9 depicts the calibration curves obtained for HTA at λ_{420}. HTA concentrations ranged from 0-2mmol/L, and a correlation co-efficient of $R^2=0.99$ was computed for the curve.
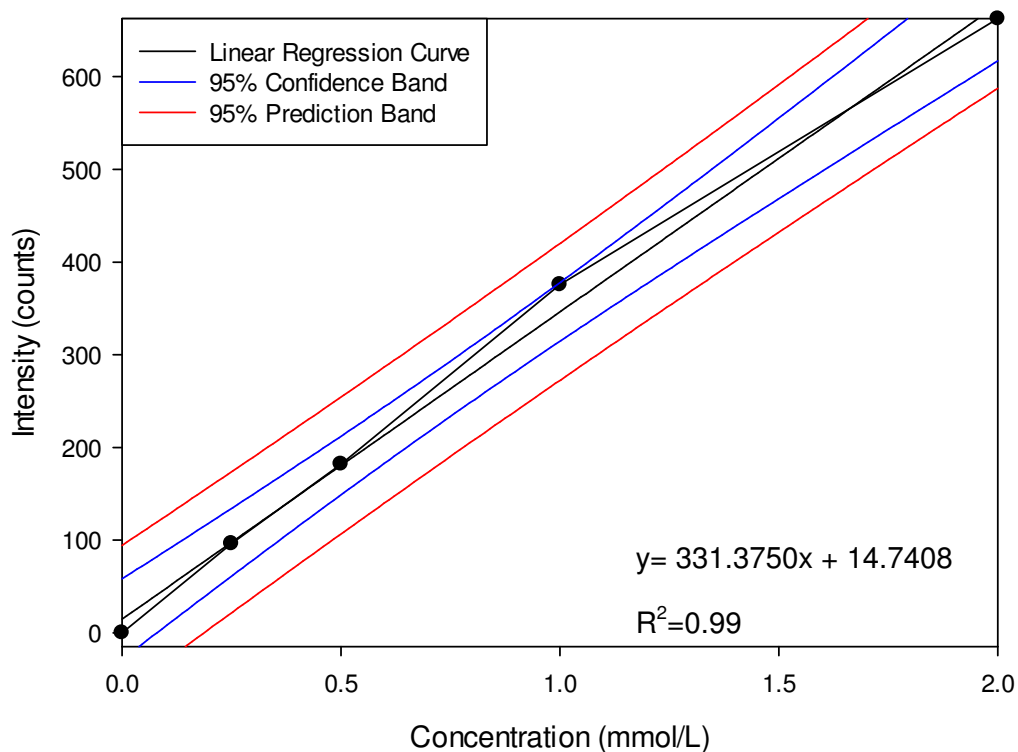
Figure 6.9: Calibration curve of Hydro-Terephthalic Acid at λ_{420}.

From Figure 6.10a HTA was present in the greatest quantity using the MNA at 72 hours (1.61mmol/L), indicating appreciable diffusion through the nano-porous ceramic material. An absence of the HTA peak in Figure 6.10b possibly indicates the presence of fluorescing constituents of the apple tissue, accounting for the noise seen.

(a)
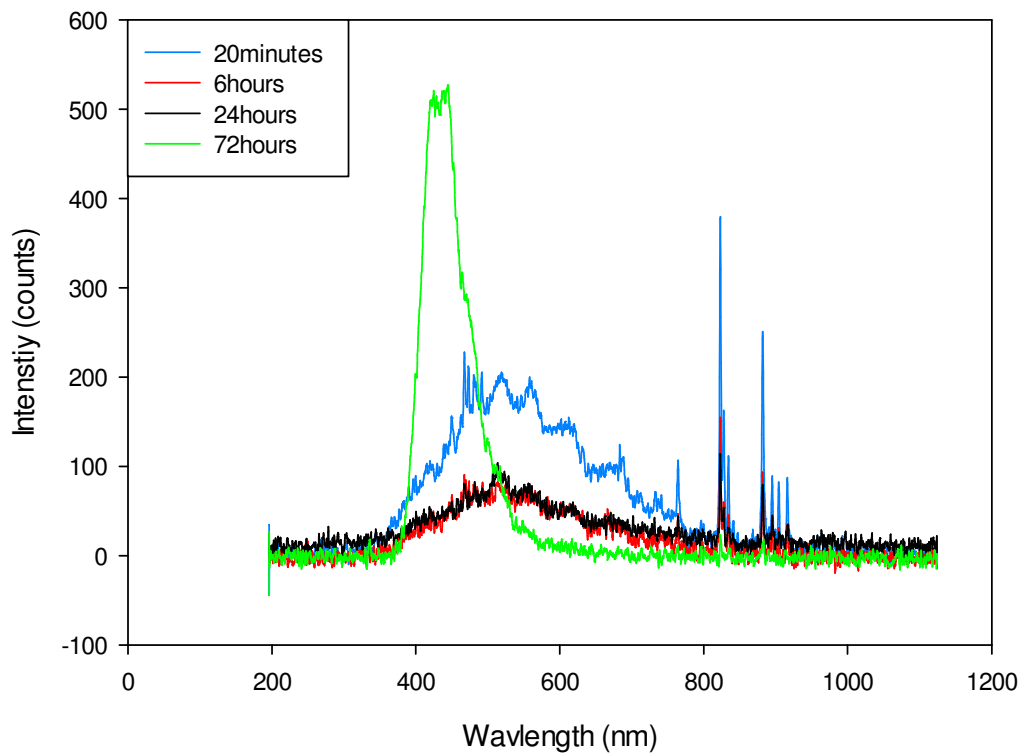
(b)
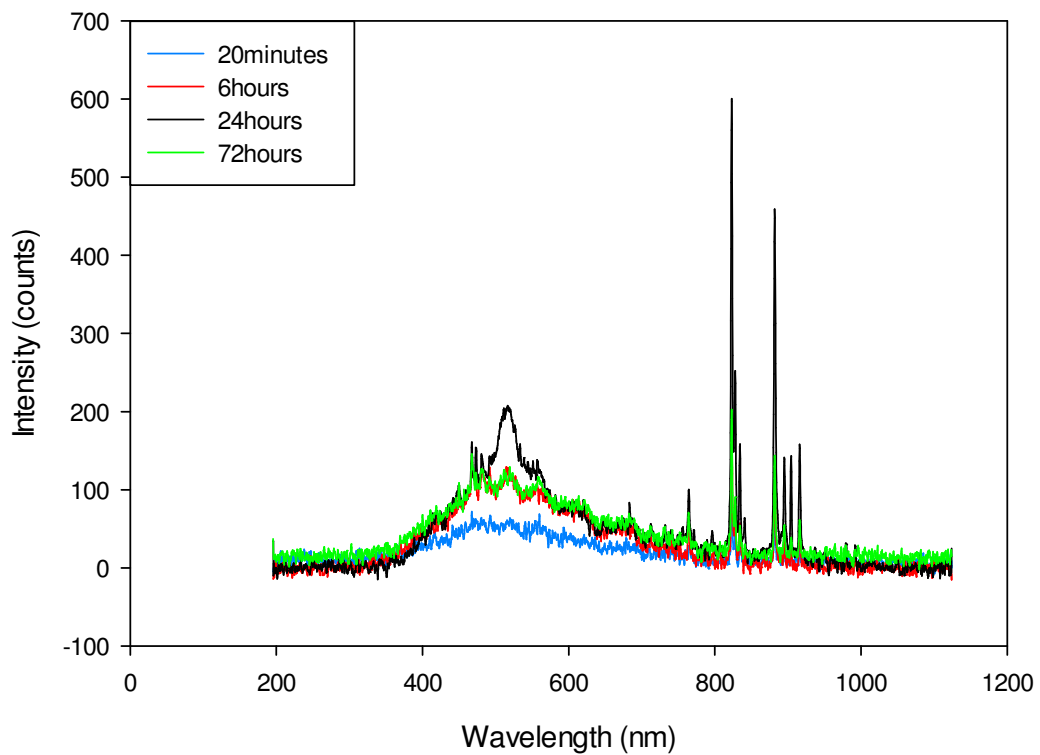
Figure 6.10: Fluorescence spectrum of the tissue permeation experiment using the (a) microneedle array (b) hypodermic needle.

6.3.4. Fabrication of a microneedle array composed of the optimized Electro-Modulated Hydrogel

Polystyrene was used as a material for microneedle mold manufacture. Although formation of micro-projections was facilitated, the projections were not of suitable size (Figure 6.11). The needles were unstable in terms of maintaining structural integrity and lacked proper formation. In addition, the microneedles melted when handled (37°C). A preliminary investigation had resulted in the polymerization of the hydrogel on the surface.
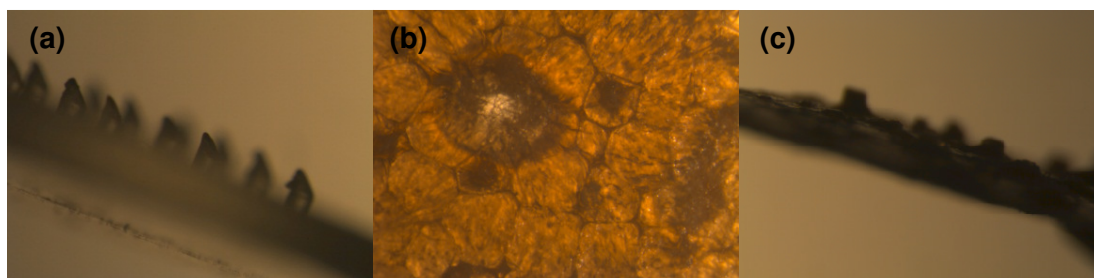
Figure 6.11: (a) Side view of the polydimethyl siloxane microneedle array prototype used in the mold manufacture (b) Dorsal surface of microneedle array projection produced from polystyrene base (c) Side view of microneedle array produced from polystyrene base.

The EMH, did however, polymerize when PDMS was sued as the material for the microneedle mold. Figure 6.12 depicts the chemical structure of PDMS. Due to its favorable physicochemical properties, PDMS is extensively used in the field of analytical chemistry (Seethapathy and Górecki, 2012). The translucent polymer is highly hydrophobic, non-toxic and does not bio-accumulate (Merkel *et al.*, 2000). PDMS consists of a flexible (Si–O) backbone and a repeating (Si(CH$_3$)$_2$O) unit, the number of which generally defines the molecular weight, and consequently its viscoelastic properties (Izuka *et al.*, 1992). In addition, the inert polymer matrix tends to swell least when exposed to water (Lee *et al.*, 2003).
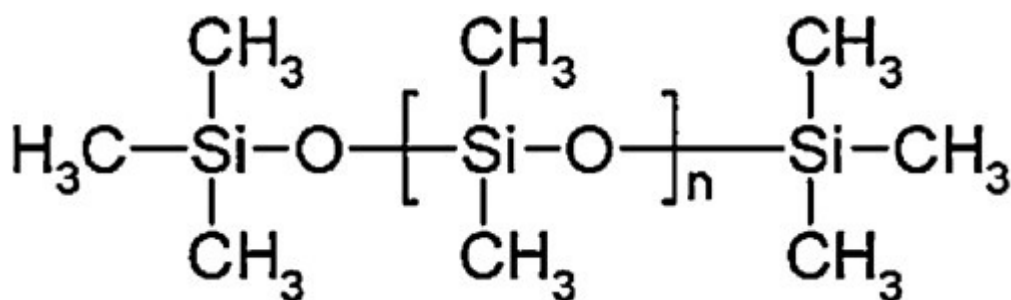
Figure 6.12: Chemical structure of polydimethyl siloxane (Seethapathy and Górecki, 2012).

Figure 6.13 depicts images of the top and side view of a MNA composed of pure EMH and is shown to have formed better in comparison to the other geometries.
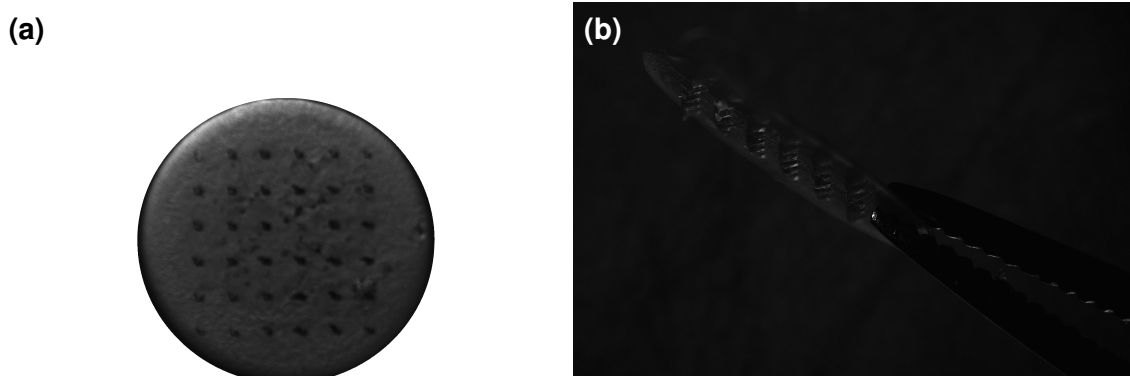
Figure 6.13: Microscope images of the (a) front and (b) side view of the microneedle composed of the Electro-Modulated Hydrogel.

6.4. Concluding Remarks

Evaluation of the ceramic MNAs revealed that the material was robust and porous in nature. Permeation studies using HTA proved the ability of the MNA to facilitate diffusion through the needles with the MNA, indicating appreciable diffusion through the nano-porous ceramic material. Whilst favorable results were achieved, testing specific to drug release kinetics can be undertaken for tailoring to specific therapeutic requirements. With the success of the formulated MNA, the MNA and the optimized EMH were incorporated into a single device that would allow for transdermal delivery. *Ex vivo* evaluation is undertaken in Chapter 7, where permeation and microbiological studies performed.

CHAPTER 7
EX VIVO EVALUATION OF THE TRANSDERMAL ELECTRO-MODULATED HYDROGEL-MICRONEEDLE DEVICE

7.1. Introduction

In addition to protecting the body from the external environment, the SC prevents microbial access to the skin and thus pathogenic disease. Moreover, it is a very effective barrier to the permeation of drug substances. Depending on their physicochemical properties, certain drug substances achieve a therapeutic effect solely through passive diffusion while other substances require additional permeation enhancement methods such as the use of microneedles. Although studies have been conducted on the ability of microneedles to effectively breach the SC, few reports exist on the physical penetration enhancer causing any skin or systemic infection (Prausnitz, 2004; Donnelly *et al.*, 2009) nor is there any available literature of such a device being developed. Thus, preliminary *ex vivo* tests were performed demonstrating the feasibility of the EMHM device for transdermal drug delivery *in vivo*. The studies allowed for the potential safety/toxicity profile to be determined and more importantly, an evaluation of the efficacy of the device prior to undertaking *in vivo* studies. In order to assess the microbial penetration through the skin after the application of a microneedle, three micro-organisms where selected correlating to the commensal inhabitants of human skin viz. *Staphylococcus epidermidis*, *Pseudomonas aeruginosa* and *Candida albicans.*

7.2. Microbial flora of the skin

The aerobic, Gram-positive cocci cluster of *S. epidermidis* is thought to comprise more than 90% of the aerobic resident flora (Cogen *et al.*, 2008). Often resistant to antibiotics, *S. epidermidis* has the ability to form biofilms on plastic devices which contributes towards the major virulence factor of the micro-organism. *S. epidermidis* is also one of the primary causes of implanted medical-device related infections (McCann *et al.*, 2008). *P. aeruginosa* is a Gram-negative, rod shaped bacteria and is an opportunistic pathogen causing disease mainly in patients with poor immunity (Sharma *et al.*, 2014). Commonly the cause of nosocomial infections, the pathogen is distinguished from other Gram-negative bacteria by its ability to produce fluorescent molecules such as pyoverdin or fluorescein, pyorubin and pyocyanin (Cogen *et al.*, 2008). The commensal, *C. albicans* is found on the mucosal surfaces of the gastrointestinal and genitourinary tracts, becoming pathogenic only when the body is immunocompromised and can infect a broad range of body sites (Hube, 2004;

Kumamoto, 2011). It is possible for *P. aeruginosa* and *C. albicans* to co-exist in the host with the attenuation of *P. aeruginosa* resulting in the growth of *C. albicans*.

7.3. Selection of appropriate animal model for *ex vivo* studies

The most relevant membrane to be employed in *ex vivo* studies is human skin. However, due to ethical reasons, a number of animal models such as porcine, rat, mouse, primates, and guinea pig models, have been suggested as suitable replacements for the evaluation of percutaneous permeation studies (Godin and Touitou, 2007). The most relevant animal model for human skin is the pig as both its biochemical and histological properties have been shown to repeatedly be similar to that of human skin (Gray and Yardley, 1975; Dick and Scott, 1992; Jacobi *et al.*, 2007). In addition, the follicular structure resembles that of humans, with hairs and infundibula extending deeply into the dermis (Godin and Touitou, 2007) with averages of 20 hairs/cm^2 present on porcine skin as compared to 14-32 hairs, except the forehead area, in humans (Jacobi *et al.*, 2007). Pig skin and human skin share similar microbiological colonization (Baird-Parker, 1962). Furthermore, the dermal collagen fiber arrangement and vascular anatomy, as well as the contents of SC ceramides and glycosphingolipids are similar in the domestic pig and the human (Simon and Maibach, 2000). Moreover skin resistance in the pig model is also similar (1.18kΩ/cm^2) to that of humans (3.94kΩ/cm^2) as compared to the rat (0.98 kΩ/cm^2), rabbit (0.35 kΩ/cm^2) and guinea pig (1.97 kΩ/cm^2) (Davies *et al.*, 2004).

7.2. Materials and Methods

7.2.1. Materials

Poly(ethyleneimine) solution (M_w =750,000g/mol), 1-vinylimidazole (≥99%), indomethacin (≥99%), poly(vinyl alcohol) (M_w =89,000-98,000g/mol, 99+% hydrolyzed), acrylic acid (anhydrous, 99%), *N*,*N'*-Methylenebisacrylamide (≥99.5%) and potassium persulfate (≥99.0%) were all purchased from Sigma-Aldrich® (St. Louis, MO, USA). All other ingredients were of analytic grade and were used as received. Stock cultures of *S. epidermis* (ATCC 2223), *C. albicans* (ATCC 10231) and *P. aeruginosa* (ATCC 27853), were obtained from Davies Diagnostics, Randburg, South Africa.

7.2.2. Preparation of the Electro-Modulated Hydrogel- Microneedle device

The optimized EMH was prepared as per the requirements detailed in Chapter 5, Section 5.2.2. The EMH was placed onto an MNA (Figure 7.1) containing a droplet of deionized water on its back plate which was allowed to dry for 24 hours to ensure adhesivity with minimal resistance to drug movement from the EMH through the MNA.
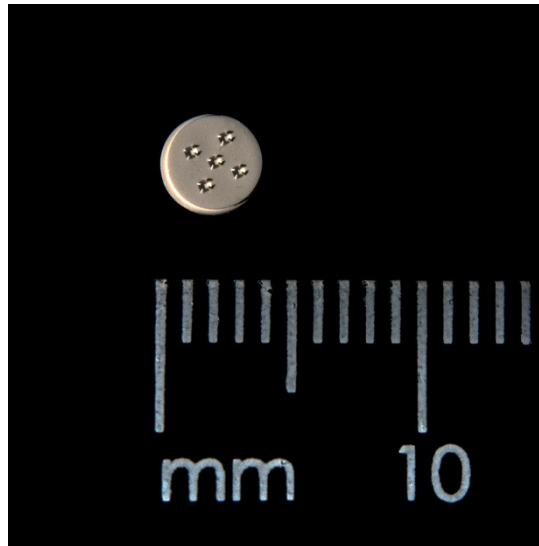
Figure 7.1: Image depicting the array containing microneedles.

7.2.3. Preparation of porcine tissue samples

Porcine skin tissue from the abdominal region was washed and the hair removed. The exogenous tissues and subcutaneous layers were carefully removed resulting in skin thickness of 400µm. The skin was stored at -80°C for a maximum of 2 weeks for future use. Frozen skin was thawed at room temperature for 3 hours prior to use.

7.2.4. Determination of porcine skin integrity

Confirmation of skin membrane integrity is an essential component for *ex vivo* analysis, as compromised skin membrane integrity during any preliminary tissue handling may falsify permeability results (Scott *et al.*, 1991). Skin membrane integrity was checked through ionic conductivity using a SevenMulti S40 pH/electrical conductivity meter (Mettler-Toledo, Zurich, Switzerland) prior to and after experimental procedures.

7.2.4.1. Ionic conductivity measurements

Ionic conductivity as a function of skin integrity was determined using a SevenMulti S40 pH/electrical conductivity meter (Mettler-Toledo, Zurich, Switzerland) prior to and after the experimental procedure.

7.2.4.2. Resistance reduction factor and permeation enhancement ratio

The Resistance Reduction Factor, *RF*, or the damage ratio, was calculated (Heylings *et al.*, 2001; Rachakonda *et al.*, 2008). It is defined as the ratio of the initial resistance value at time 0 to the resistance value of the sample obtained at time t, or:

$$RF = \frac{R0}{Rt}$$

<div align="right">**Equation 7.1**</div>

The permeability enhancement ratio, taken as the ratio of the permeability coefficient experimentally obtained to that of the control, was calculated as follows:

$$\text{Permeation Enhancement} = \frac{\text{Ptreated skin}}{\text{Po untreated skin}}$$

<div align="right">**Equation 7.2**</div>

7.2.4.3. Determination of skin tissue structural integrity using Fourier Transform Infrared Spectroscopy

FTIR Spectroscopy was used to detect the vibration characteristics of chemical functional groups in lyophilized porcine skin tissue samples and was carried out as detailed in Chapter 4, Section 4.2.3.

7.2.5. Isolation and stock maintenance of *Candida albicans, Pseudomonas aeruginosa* and *Staphylococcus epidermidis* cultures

All cultures were obtained from lyophilized bacterial stocks (Davies Diagnostics, Randburg, South Africa) and inoculated into 50mL sterile Tryptone Soya broth (TSB) and incubated at 37°C for 48 hours. TSB was prepared as per manufacturer specifications by adding 30g to 1L of distilled water and autoclaving at 121°C for 20 minutes. Purity studies were conducted by placing the autoclaved TSB at room temperature for 48 hours and purity determined through lack of microbial growth.

7.2.6. Determination of total viable colony count

Prior to the microbial *ex vivo* testing, the total viable colony count was determined for quality assurance by evaluating the total count of viable colonies in standardized inoculated carriers (Figure 7.2). In addition, determination of the colony count allowed for inspection and positive identification of the counted organism. Each of the three cultures was made to 20mL spore suspensions using sterile saline. Aliquots of the stock cultures (100µL) were made up to 20mL using sterile saline. The stock cultures were vortexed to ensure complete mixing. Aliquots (100µL) were further diluted in sterile saline using serial dilution (1:100) and were pipetted (100µL) onto Tryptone Soya agar (TSA) plates. The TSA plates were prepared using the spread technique and were incubated at 37°C for 24 hours for *S. epidermis* and *P. aeruginosa* and at 25°C 48 hours for *C. albicans.* Resulting microbial growth after incubation

was assessed by counting the number of viable colonies and extrapolating the number of colony forming units (CFU) found in the original suspension.
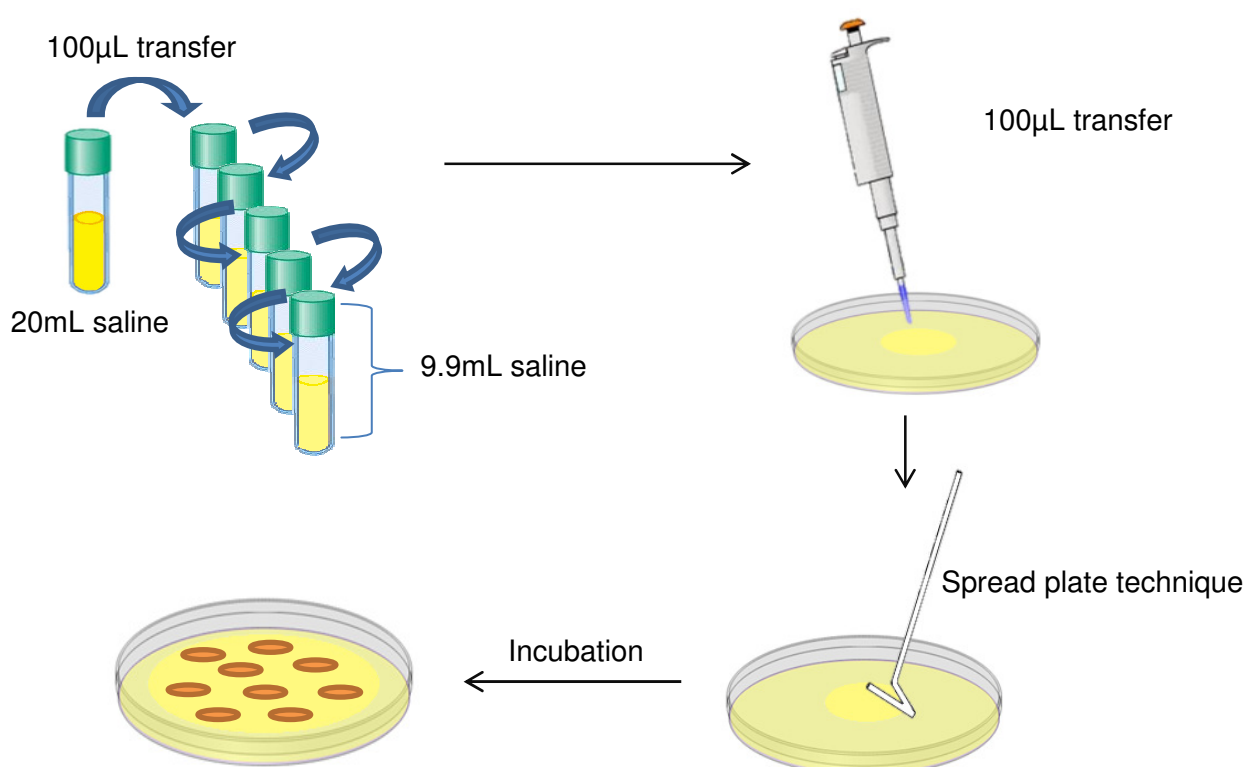
Figure 7.2: Schematic illustrating the serial dilution process.

7.2.7. Determination of the electro-modulated drug delivery using *ex vivo* studies

Ex vivo studies were conducted to ascertain the effectiveness of the EMHM device as well as the permeability of skin tissue to sodium indomethacin. The studies were carried out utilizing a Franz Diffusion Cell (FDC) apparatus (PermeGear Inc., Bethlehem, PA, USA) equipped with a 12mL receptor compartment, clamp, stirrer-bar and a thermostat controlled water jacket (Figure 7.3a). Excised porcine skin stored at -80°C was thawed prior to use. Porcine skin samples with a thickness of 3.5±0.5mm were placed between the donor and receptor compartments of the FDC. The indomethacin permeated the skin into the simulated plasma in the receptor compartment (PBS; 12mL; pH 7.4; 37°C). Samples (100µL) were withdrawn from the receptor compartment, at 30minute time intervals over a period of 3 hours.

Drug concentrations were determined using UV spectrophotometric analysis (IMPLEN Nanophotmeter™, Implen GmbH, München Germany).
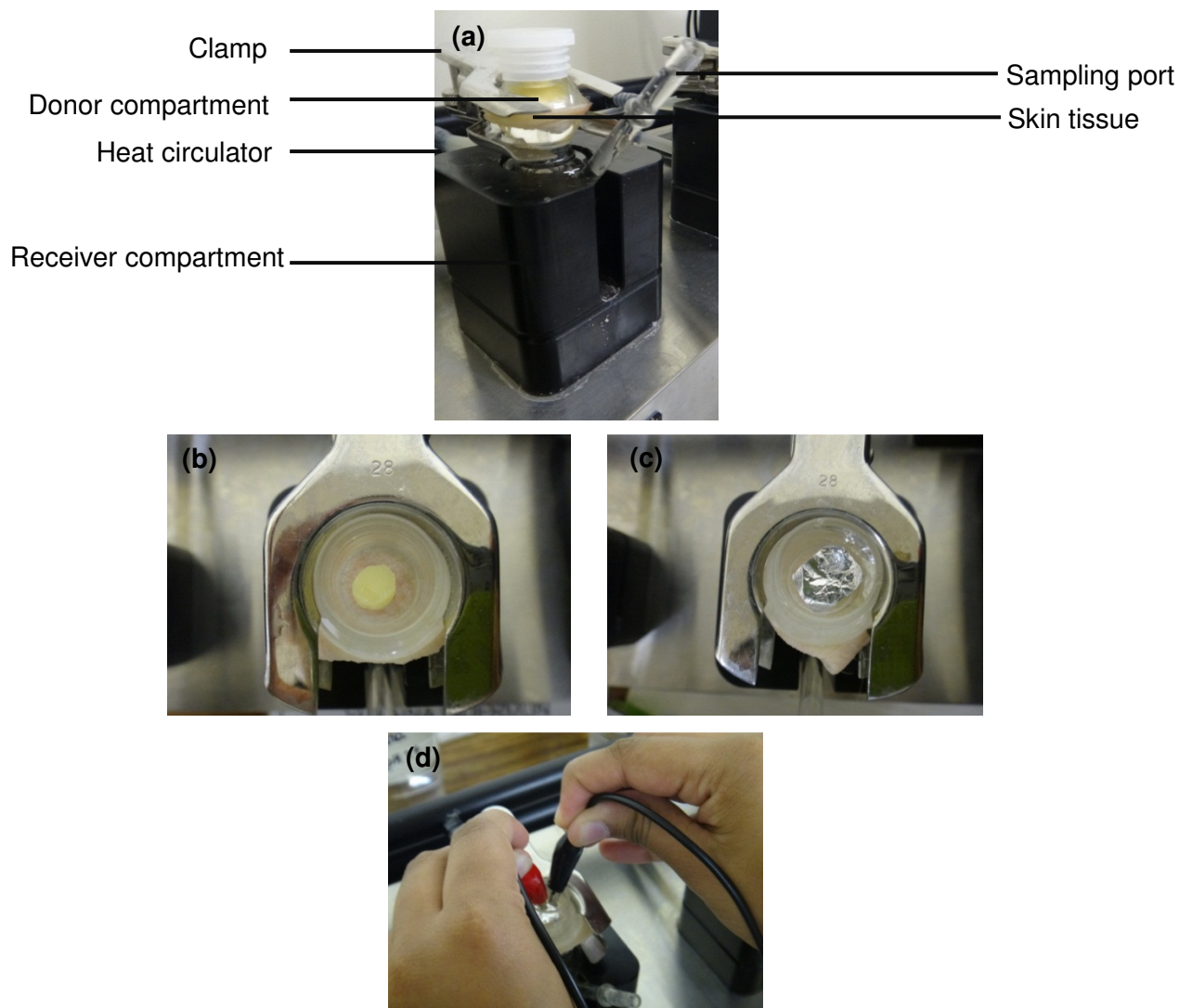
Figure 7.3: Digital image depicting the (a) Franz diffusion cell apparatus used (b) Electro-modulated hydrogel-microneedle device on the porcine tissue sample (c) Aluminum foil placed on the device and (d) Electro-stimulation of the device at 3.63V.

Initial analyses (Test A) were conducted to ascertain the permeability of sodium indomethacin through the excised porcine skin. This was done as to determine the effectiveness of the developed MNA against topically applied sodium indomethacin. This analysis was repeated using the ceramic MNA dummy (Test B) as a correlation against the topical administration of sodium indomethacin and the MNAs as well as a correlation with the results determined during *in vitro* drug release analysis and DEE tests. Once determined, the formulated EMH was analyzed without and with electro-stimulation (Test C and D respectively). Test D utilized aluminum foil, as per *in vitro* studies, which covered the EMH on which a current was applied. Results of this analysis would determine permeability of sodium indomethacin upon electro-stimulation with a control of no electro-stimulation added. Once completed, the EMHM device was analyzed with and without electro-stimulation (Test

E and F) to ascertain the effectiveness of the formulated system for a more complete comparison prior to possible future *in vivo* studies. Test G was carried out as a means of comparison between a MNA that was fully saturated with drug solution with Tests A and B. The various tests conducted are summarized in Table 7.1.

Table 7.1: Testing parameters employed in the *ex vivo* studies.

Test	Method of Delivery	Substrate	Electro-Stimulation
A	Indomethacin solution (20mg/mL)	Skin	No
B	Indomethacin solution (20mg/mL)	MNA dummy-skin	No
C	EMH	Skin	No
D	EMH	Skin	Yes
E	EMH	MNA-skin	No
F	EMH	MNA-skin	Yes
G	Saturated MNA	Skin	No

7.2.7.1. Determination of penetration ability using fluorescence

To visually assess the working ability of the EMH in conjugation with the MNA, an EMH was formulated using fluorescein dye coupled to the sodium indomethacin drug. Briefly, indomethacin and fluorescein were dissolved in a 1M NaOH solution. The solution was frozen at -75°C for 48 hours and lyophilized to form a free-flowing powder. The powdered compound was incorporated into the optimized hydrogel as the active agent. The EMH was placed onto an agarose ($1\%^w/_v$) plate and was subjected to electro-stimulation. The EMH was subjected to electro-stimulation both in the presence and absence of the MNA in order to prove device effectiveness. Digital images were taken of the experiments when exposed to UV- light.

7.2.7.2. Evaluation of drug permeability

The cumulative sodium indomethacin diffusion per unit area of skin tissue was ascertained in terms of drug permeability. The drug permeability coefficient (cm.h^{-1}) of drug across the skin tissue was calculated per unit area using Equation 7.3. (Lavon *et al.*, 2005):

$$P = \frac{C_2 \times V}{A \times t \times C_1}$$

Equation 7.3

Where: P [cm.h^{-1}]-permeability coefficient; V [ml]-volume of the receiver compartment (12mL); A [cm^2]-effective permeation area (1.767cm^2); t [h]-time interval; C_1 [mg.mL^{-1}]-concentration in donor compartment; C_2 [mg.mL^{-1}]-concentration in receiver compartment.

The permeation enhancement is the ratio of permeability coefficient of treated skin to permeability coefficient of untreated skin.

7.2.8. *Ex vivo* microbial evaluation of the Electro-Modulated Hydrogel-Microneedle device

Using the sterilized FDC apparatus, various microbial penetration assays were carried out using aliquots of microbial suspension containing 1.2×10^6 Colony Forming Units (CFU)/mL, 1×10^9 CFU/mL and 1.8×10^5 CFU/mL of *S. epidermis, P. aeruginosa* and *C. albicans* respectively. Sterilized porcine tissue that was not punctured (control) or punctured (test) were included in the study in one of three different ways: (i) punctured with a microneedle which was left in place for 24 hours for determination of complete penetration with a MNA interface (ii) punctured with a microneedle which was removed for determination of penetration through the MNA puncture sites (iii) punctured with a hypodermic needle (24G) which was removed for comparison against penetration through the MNA puncture sites. Aliquots (100µL) of the microbial suspension were placed into the donor compartment of the FDC cell and the assay was run using the conditions previously described. Sterilized lids were used to cover the donor compartments and prevent evaporation of the buffer. Samples (100µL) were withdrawn from the receptor compartment, at various time intervals over a period of 24 hours. The samples were plated onto TSA and were incubated at 37°C for 24 hours for *S. epidermis* and *P. aeruginosa* and at 25°C 48 hours for *C. albicans.* After 24 hours, the tissue was removed from the donor compartment and the remaining microbial content quantified from the samples and the tissue.

7.2.8.1. Assessment of microbial load on the needles employed in the ex vivo microbial tests

The microbial load from the hypodermic needle and microneedle after the application of the known concentration of microbial suspension onto the tissue was quantified. Both types of needles were placed into sterile PBS (10 mL) and vortexed for 2 minutes. Subsequently, serial dilutions (1:100) were performed, and the resulting suspensions plated and incubated as described in Section 7.2.6.

7.2.8.2. Determination of remaining load on the porcine skin tissue

Since bacteria have the ability to adhere to the skin, it was important to determine any adherence to the porcine tissue to validate the microbial permeation results. The porcine skin samples were removed immediately after the *ex vivo* studies. Using a surgical blade, both the layers containing the epidermis and SC was gently scraped (Figure 7.4). The load

was placed into 20mL saline, vortexed, diluted (1:100) and plated out. The samples were subsequently incubated as previously described in Section 7.2.6.
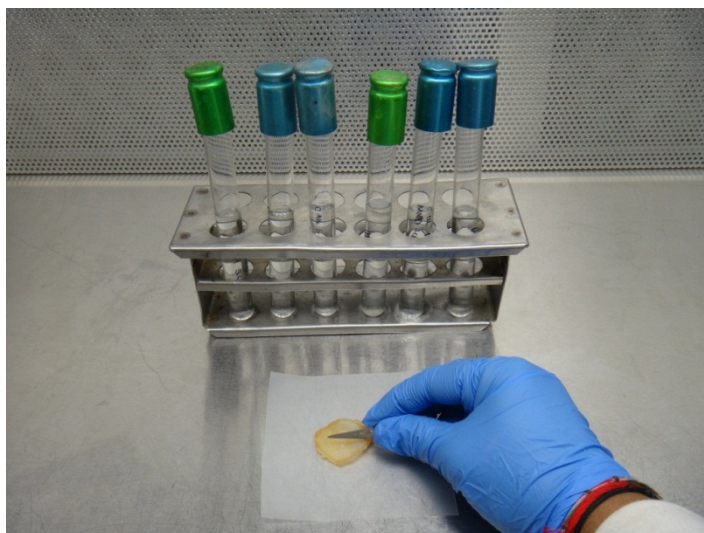
Figure 7.4: Image depicting the adherence test.

7.3. Results and Discussion

7.3.1. Assessment of the electro-modulated delivery as per *ex vivo* studies

Prior to assessing the permeation of sodium indomethacin through the porcine skin tissue, it is important to define the theoretical release from the EMH using a FDC (Figure 7.5). The entrapped lining against the inside wall of the EMH is released following electro-stimulation, in which the hydrogel polymer network opens. The drug molecules undergo subsequent diffusion through the both the network and the MNA and subsequently pass into the skin. C_p is the solubility of the drug in the EMH and C_m is the concentration at the skin-solution interface. C_s is the concentration of the drug in the solution at the polymer-solution interface, and is generally below the solubility of drug in polymer at the interface. There is a real difference between the solubility of the drug in the polymer and in the solution, although both exist at the interface. Finally, C_b is the concentration of the drug in the buffer solution in the receptor cell (Sinko *et al.*, 2010).
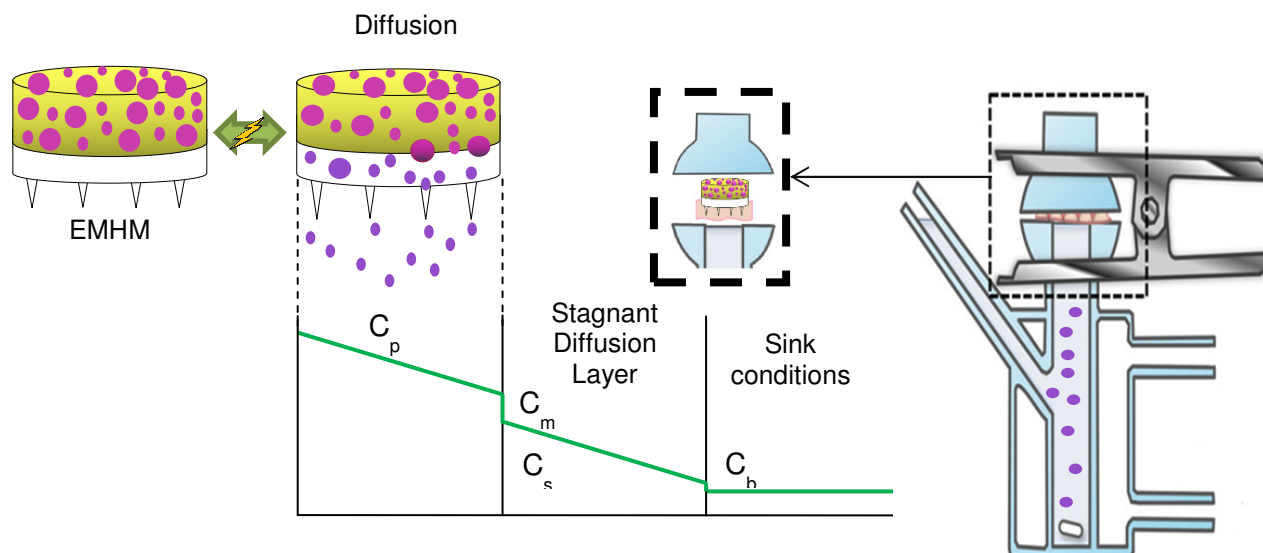
Figure 7.5: Diffusion of sodium indomethacin through the Electro-Modulated Hydrogel. Drug was contained in the hydrogel matrix and subsequently released following electro-stimulation. Drug diffusion through the Electro-Modulated Hydrogel and stagnant aqueous diffusion layer and into the receptor compartment at sink conditions (adapted from Sinko *et al.*, 2010 and Chen *et al.*, 2013).

Figure 7.6a clearly demonstrates the pronounced, yet erratic, enhancement of skin permeability to the sodium indomethacin solution (Test A and B). In addition, both tests revealed a plateau at 1.5 hours due to saturation of the skin tissue. A decrease in permeation (±3mg) was observed through the utilization of the MNA dummy (test B), indicating absorption of the drug solution into the ceramic material. Test G revealed lower drug permeation even though a saturated MNA was used. Permeation of less than 2mg can be accounted for by a lower surface area exposed to the skin tissue.

Application of the EMH onto the skin (Test C and D) have demonstrated more controlled release, with greater drug release (±0.24mg) after electro-stimulation of the EMH. The undertakings of Tests C and D with Tests E and F using MNAs has resulted in more favorable release. Test E demonstrated that without electro-stimulation, significantly less drug release is obtained (±0.45mg) as compared to Test F with electro-stimulation (±2.93mg). In addition, results from Test F revealed controlled release of the sodium indomethacin through the skin as compared to that of Test A using the drug solution (3% to 21%).

Permeation enhancement results from Figure 7.5b depicts that the control procedures has significantly lower permeation capabilities as compared to the corresponding experimental procedures. RF values from the Franz Diffusion studies showed similar behavior. Samples

with an initial resistivity of or above 20KΩ/cm^2 with PBS (pH 7.4) were used (Mitragotri *et al.*, 2000; Karande and Mitragotri, 2003; Lee *et al.*, 2006). The increased rigidity of the lipid bilayers accounts for higher skin resistance (Rachakonda *et al.*, 2008). Lower RFs are seen for tests A, B and D which may be as a result of the individual lipid molecules in the skin having a higher vibrational energy, making the lipid bilayers more fluidic.

(a)
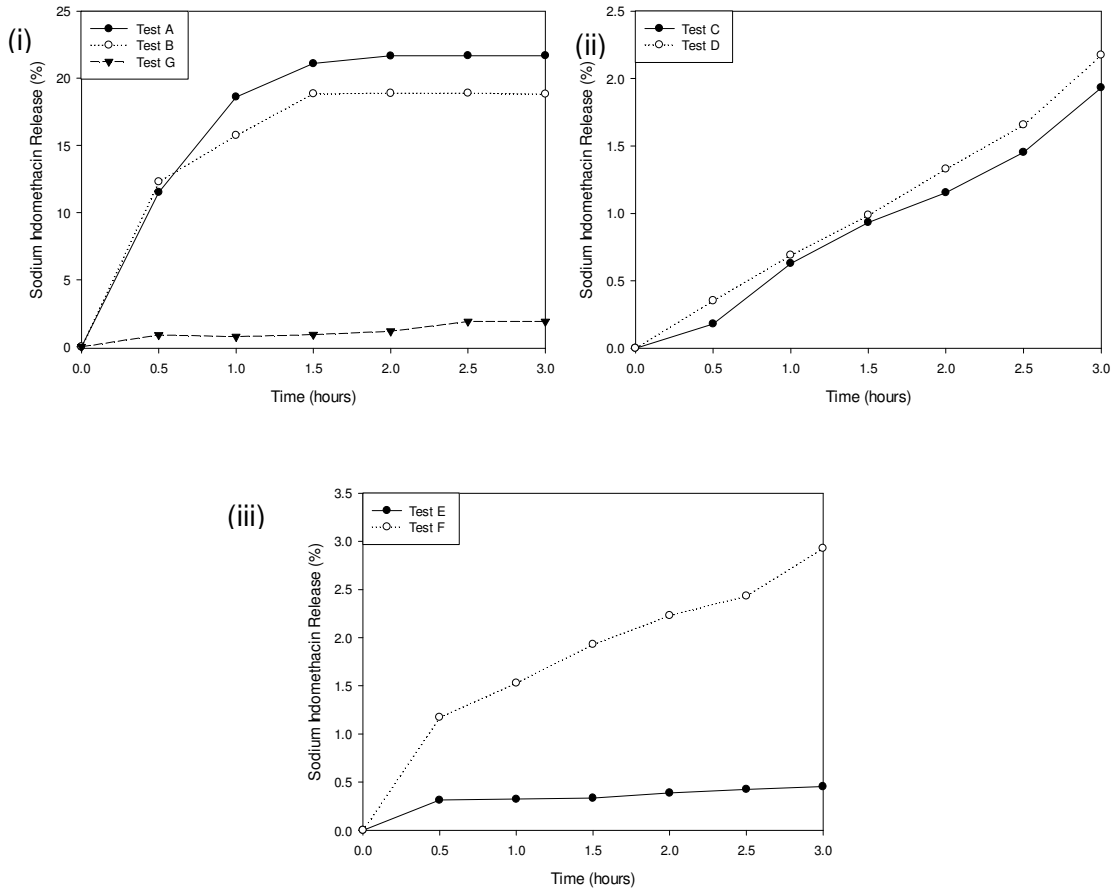
(b)
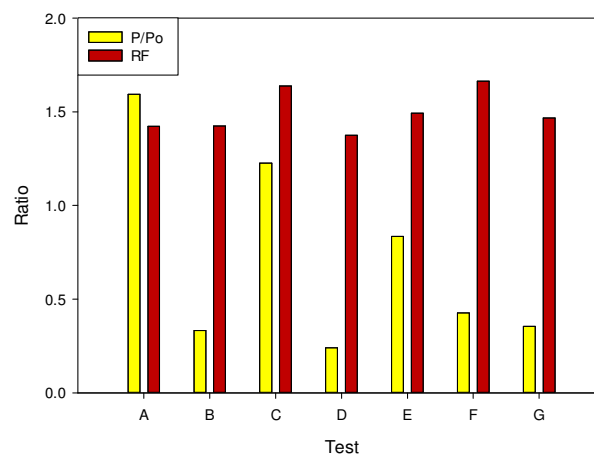
Figure 7.6: (a) Drug release profiles, (b) permeation enhancement and RF profiles as per *ex vivo* studies (N=3; SD≤0.34 in all cases)

Results from the fluorescence studies indicated that the hydrogel is stimuli-responsive, and releases the active agent after electro-stimulation (Figure 7.7a). Figure 7.7b depicts that greater permeation is achieved when using the microneedle, and hence demonstrates the success of the device.

(a)
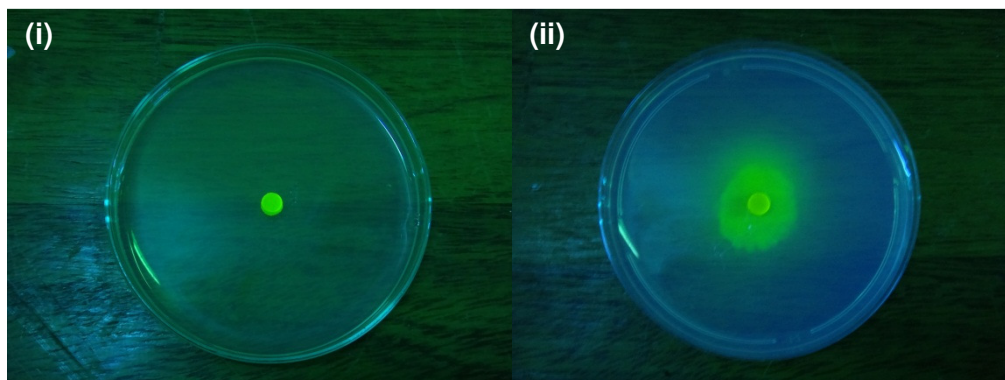
(b)
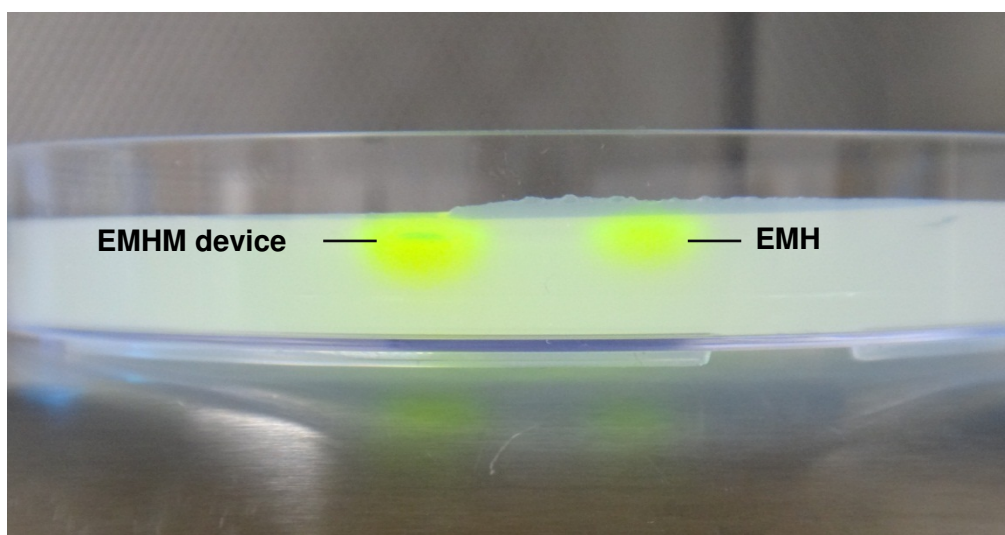
Figure 7.7: Digital images of the (a) Electro-Modulated Hydrogel (i) prior to and (ii) after electro-stimulation. (b) Effectiveness of the EMHM device in the permeation of fluorescent sodium indomethacin.

7.3.2. Influence of the *ex vivo* evaluation on skin integrity

FTIR characterization determined asymmetric and symmetric C-H vibrations obtained at 2920 and 2850cm^{-1}, respectively which have been ascribed to hydrocarbon lipid chains of the SC with the CH$_2$-scissoring bands providing information on the lateral packing of the lipid chains in the horny layer (Knutson *et al.*, 1985, Golden *et al.*, 1986; Babita *et al*, 2006; He *et al.*, 2009; Schwarz *et al.*, 2012). The obtained FTIR spectrum (Figure 7.8) displays peaks at 2922.76 and 2852.75cm^{-1}, demonstrating the presence of the intact SC in all samples, also

peaks around 1742.86cm^{-1} were present illustrating the C=O stretching vibration of lipid polar head groups (Babita *et al*, 2006). Strong water absorbance and amide bands are found in the region of 1500-1700 and 3000-3600cm^{-1}, respectively (Babita *et al*, 2006). The bands at 1639.77 and 1550.89cm^{-1} of the SC proteins have been suggested to arise from amide I and II stretching vibrations, respectively (Babita *et al*, 2006). The bands have been attributed to characterizing the secondary structure of keratin (He *et al*., 2009). The amide I band is due to C=O stretching vibration, while the amide II band is due to C-N stretching and N-H bending vibration of the amide group present in proteins (Babita *et al*, 2006). Both bands owe their origin primarily to proteins. A shift of the amide II vibration is often ascribed to permeation enhancing effects (He *et al*., 2009). In the study, slight shifts in the band to 1553.98cm^{-1} could be detected in regard to this absorption band.
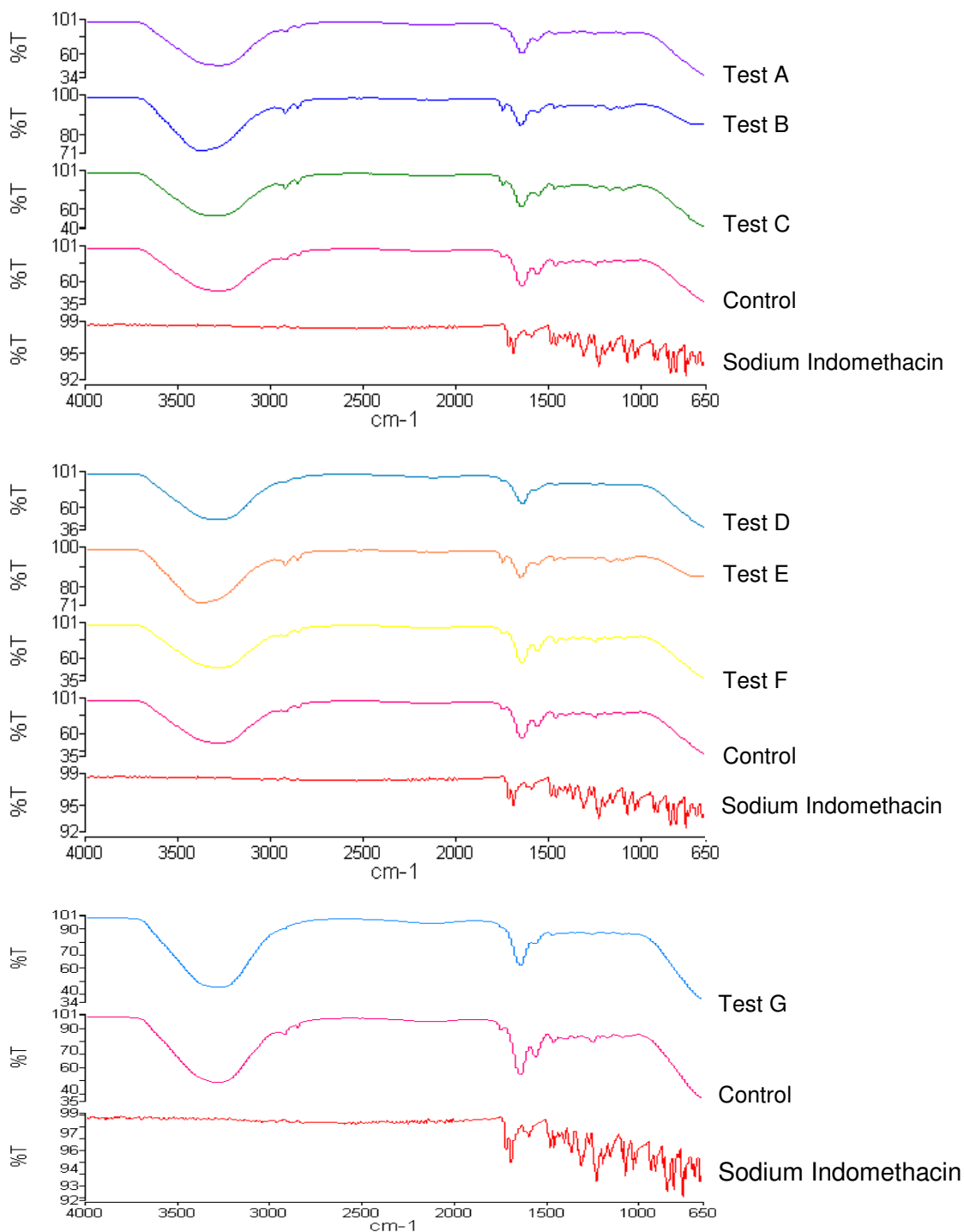
Figure 7.8: Infrared spectra of the porcine skin samples utilized in the *ex vivo* studies.

The 1460-1462cm^{-1} vibration could correspond to the CH$_3$ bending which originated mostly from the skin keratins (Rodriguez *et al.*, 2009), as well as the CH$_2$ scissoring mode (Ongpipattanakul *et al.*, 1994; He *et al.*, 2009).

179

The symmetric stretching band is particularly susceptible to changes and was therefore employed for classification of the lipid matrix as a means to determine changes correlated to permeation. The CH_2 symmetric and asymmetric absorbance peak positions shift by $2cm^{-1}$ indicating increased lipid fluidity which is in turn representative of a decrease in diffusional resistance to drug permeation. It should be noted that the FTIR spectra display an absence of peaks pertaining to sodium indomethacin, consequently it can be assumed that the drug did not stay entrapped in the skin and either may have diffused through or did not have sufficient penetration ability.

7.3.3. Quantification of microbial skin load as per *ex vivo* studies

The SC is vital in protecting against microbial entry. In the pharmaceutical industry, safety is as important as product efficacy, thus the study determining microbial penetration of a microneedle array in comparison to a hypodermic needle is well motivated for. The plates were inoculated with 100µL of the respective solutions as any volume greater than this may not penetrate and soak in the agar, thus skewing results and making accurate counting difficult.

The present study, utilizing the representative micro-organisms: Gram-positive (*S. epidermidis*), Gram-negative (*P. aeruginosa*) and yeast (*C. albicans*) have indicated that microneedles do allow for microbial permeation but to a lesser extent when compared with permeation across a skin surface treated with the gold standard hypodermic needle (Table 7.2). In the various test models employed in this study, the microbial agent permeation across the porcine tissue was far less significant when microneedles were used.

Table 7.2: Representative results of microbial studies.

Test	Micro-organism	Microbial load (CFU)	Control Cumulative microbial permeation after 24 hours (CFU)	Microbial load counts after permeation (CFU)	Microbial adherence to skin on removal (CFU)	
					Epidermis	Stratum corneum
Hypodermic needle	*S. epidermidis*	2.1×10^8	2×10^7	70	1.8×10^7	4×10^6
	P. aeruginosa	1.6×10^9	8.7×10^7	547	6×10^7	1×10^7
	C. albicans	1.8×10^8	1.92×10^7	432	2.2×10^8	1.4×10^8
Microneedle puncture & removal	*S. epidermidis*	2.1×10^8	2.56×10^6	-	-	1×10^7
	P. aeruginosa	1.6×10^9	2.2×10^7	-	-	6×10^6
	C. albicans	1.8×10^8	3.5×10^6	-	-	1.7×10^7
Microneedle puncture	*S. epidermidis*	2.1×10^8	1.03×10^6	50	4×10^3	6×10^6
	P. aeruginosa	1.6×10^9	5.1×10^6	210	1.1×10^3	9×10^6
	C. albicans	1.8×10^8	1.06×10^6	324	1.2×10^3	8×10^7

(-) no colonies detected

Assessment of adherence to the skin tissue in the hypodermic needle tests revealed that significantly more ≈107CFU of the microbial solution remained on the epidermis, while this amount decreased ≈101CFU at the level of the SC. More noticeably is the decline in adherence of *S. epidermidis* which could be as result of its nature as a facultative anaerobe (Figure 7.9). Microbial permeation continued over the 24hour period indicating no active means of permeation. After 24 hours, the microbial permeation from using the microneedle was lower in comparison to that of the hypodermic needle. The inherent elasticity of the porcine tissue could have allowed for the individual microneedle-induced holes to seal to a greater extent than the much larger single hole created by hypodermic needle puncture (Donnelly *et al.*, 2009).

(a)   (b)
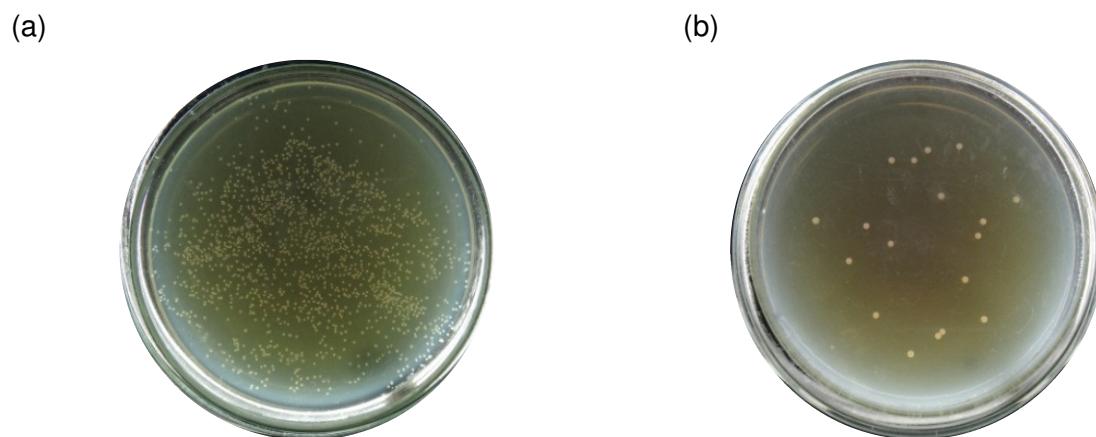
Figure 7.9: Agar plates of *S. epidermidis* after (a) hypodermic needle and (b) microneedle array adherence studies. All results for other test organisms presented in a similar fashion.

7.3.4. Quantification and comparative analysis of microbial adherence of the microneedle array and the hypodermic needle

Microbial permeation in each case was greater than 10^6CFU when hypodermic needles were employed. The permeation when utilizing microneedle, however, was significantly less, with microbial permeations of less than 10^2CFU observed (Figure 7.10). According to Seal and co-workers (2000), depending on the type of pathogen and dose response factors, an estimation of the number of invading micro-organisms required to cause an infection is 104CFU.

(a)
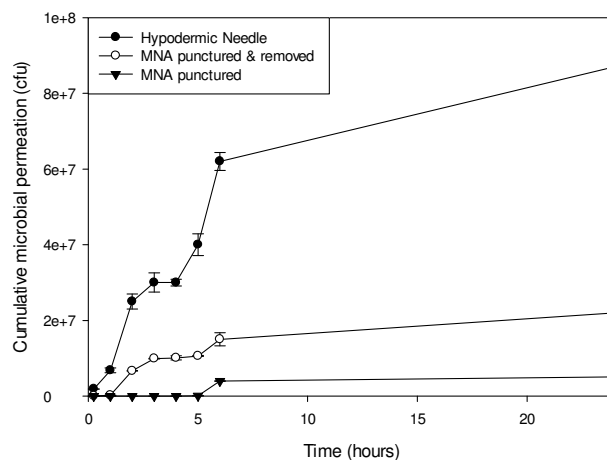
(b)
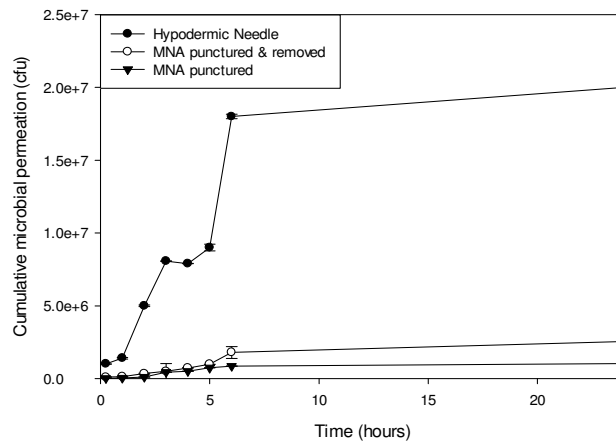
(c)
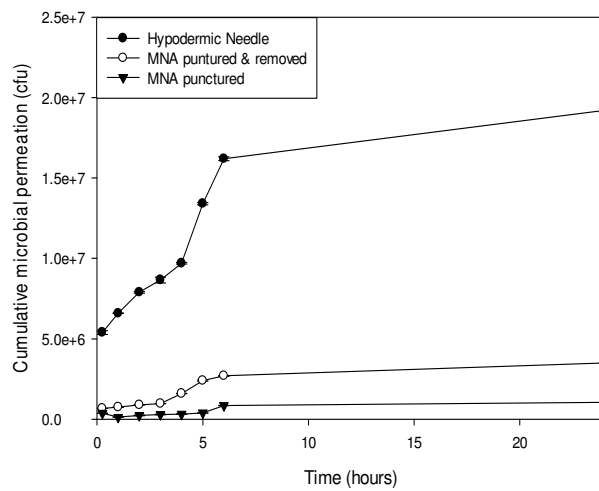
Figure 7.10: Microbial permeation results as per *ex vivo* studies using (a) *S. epidermidis* (b) *P. aeruginosa* (c) *C. albicans* (N=3; SD≤2.26×10^6 in all cases).

7.4. Concluding remarks

This investigation has proven the efficacy of the EMH capable of attaining electro-modulated drug release in the *ex vivo* porcine model. Furthermore, the results have concluded that, in addition to the responsive nature of the EMHM device, the use of microneedles resulted in significantly less microbial permeation than their hypodermic counterpart. Even though microbial permeation was present with the use of the MNAs, it must be noted that its significance was far to less to cause infection of any type. Due to the skin's antimicrobial properties it is thus unlikely that the MNA application would cause local or systemic infection in immune-competent patients under normal circumstances even though microbial adherence to the MNAs was clearly shown. This investigation has lead to the conclusion that safety in patients may be enhanced should the MNAs be aseptically manufactured and not be re-used without cleaning.

IN VIVO EVALUATION OF THE TRANSDERMAL ELECTRO-MODULATED HYDROGEL-MICRONEEDLE DEVICE IN THE SPRAGUE DAWLEY RAT MODEL

8.1. Introduction

*Ethics clearance for this in vivo investigation was obtained from the Animal Ethics Screening Committee (AESC) of the University of the Witwatersrand (No. 2013/13/04; Appendix 11.4).

The past century has seen many medical scientific and advances in the field of both science and medicine, in which *in vivo* release studies have played a vital role (Quimby, 2002; Festing and Wilkinson, 2007; Stokes and Marsman, 2014). Therapeutic efficacy studies were conducted using a Sprague Dawley rat model so as to evaluate the pharmacokinetic properties of the EMHM device *in vivo,* with the plasma release profile being compared to that of the *in vitro* release profile to foster and *in vitro-in vivo* correlation (IVIVC) for the provision of a more realistic clinical extrapolation.

The development of an IVIVC is essential in establishing the predictive mathematical relationship between the *in vitro* and the *in vivo* performance. In addition the IVIVC determines the efficacy of the formulation or delivery system (Van Buskirk *et al.*, 2012; Sjögren, 2014). Historically, IVIVC has been applied to extended release from oral solid dosage forms but it has also been used to correlate *in vitro* skin permeation data to the *in vivo* drug profiles in transdermal delivery research (Emami, 2006; Van Buskirk *et al.*, 2012). FDA guideline defines rules and reliability criteria of IVIVC for extended release forms, exemplifying the following levels of correlations (Ostrowski and Baczek, 2010):

Level A   Directly associated with linear, superimposable relationship between the rate of absorption *in vivo* and dissolution rate *in vitro* through all available time points. In some cases non-linear relationship may be also appropriate.

Level B   Based on statistical moment analysis, where mean residence time *in vivo* is compared to mean dissolution time *in vitro*. Because a number of *in vivo* curves could result in similar residence time values, the obtained relationship is not direct.

Level C (single point)   Represents a single point relationship between one pharmacokinetic parameter (e.g. AUC) and one dissolution parameter (e.g. amount of substance released at a certain time point).

Level C (multiple point)   A relationship exists between one or more pharmacokinetic parameters and dissolution at several *in vitro* time points should be represented by early, middle and late stage of dissolution profile.

Level D   Represents a semi-quantitative rank order correlation not useful for regulatory purposes.

Level A correlation is generally the most desirable form and represents the highest order as the *in vitro* method allows for predictability of the in *vivo* results, and a direct correspondence exists at each time point (Emami, 2006). The ability of the *in vitro* methods to completely mimic the *in vivo* methods confers confidence in the method's capability to act as a surrogate for *in vivo* studies. In addition, it is only level A correlations that are accepted by regulatory agencies as a basis for replacing *in vivo* bioequivalence studies with *in vitro* dissolution tests (Ostrowski and Baczek, 2010). Predicted error (%PE) criteria is used to evaluate a Level A IVIVC as per FDA guidelines. A reliable predicted level A correlation exists, when an average absolute PE for AUC and C_{max} is below 10 % and PE for individual formulation does not exceed 15 %. An average absolute %PE of 10-20 % requires additional *in vivo* and *in vitro* data sets as the predictability is inconclusive. In addition to the PE, the correlation co-efficient (R^2) may be used to evaluate a level A correlation with R^2>0.9 indicating and existing IVIVC (% *in vivo* absorbed vs. % *in vitro* dissolved; El-Yazigi and Sawchuk, 1985).

In Chapter 7, porcine skin tissue was used to conduct the *ex vivo* studies. Van Ravenzwaay and Leibold (2004) evaluated transport of compounds with various lipophilicities across rat and human skins *in vitro* and *in vivo* in rats. In all cases the *in vitro* dermal penetration through rat skin was higher than *in vivo* and rat skin was approximately 11-fold more permeable than human skin. To prevent false positive results and to more closely simulate human permeation, porcine tissue was thus used. Although porcine skin, when compared to rat skin, has a closer permeability character to that of a human, many studies have been

conducted on rats with transdermal devices (Durrheim *et al*., 1980; Bond and Barry 1988; Hinz *et al*., 1989; Roy *et al*., 1994; Godin and Touitou, 2007). The pig model would not be feasible for the *in vivo* studies due to the difficulty of extracting the minute drug amounts from the plasma. Due to their low blood volumes, mice were not used in this study as blood collection size and frequency of collections would be limited.

Rat skin and human skin are similar with respect to their permeation by narcotic drugs and skin characteristics (Roy *et al*., 1994; Table 8.1). Studies have found that hairless rat skin has provided a highly representative view of permeability (Durrheim *et al*., 1980; Bond and Barry 1988; Hinz *et al*., 1989). Regarding the rat skin, permeation kinetic parameters are frequently comparable with human skin (Godin and Touitou, 2007). In addition, the rat is particularly docile and its size allows for manipulation, easy handling and is relatively low cost (Suckow *et al*., 2006; Godin and Touitou, 2007). These findings have ultimately led to the selection of the Sprague Dawley rat as the test model.

Table 8.1: Comparative thickness and electrical resistance of skin strata in rat, mice and humans (Wester and Maibach, 1989; Davies *et al*., 2004).

	Stratum Corneum (µm)	Epidermis (µm)	Whole skin (mm)	Electrical Resistance (kΩ/cm^2)
Human	17	47	2.97	3.94
Rat	18	32	2.09	0.98
Mouse	9	29	0.70	6.33

Dosing of sodium indomethacin in humans requires multiple dosing throughout the day due to the rapid elimination of the drug (Chapter 3, Section 3.3.4). Multiple daily dosing is not possible in the rat due to its slow metabolism. Thus to avoid toxicity, dosing was done at weekly intervals as opposed to dosing at 30 minute intervals detailed in Chapter 3 and subsequently required an additional *in vitro* release study to determine the drug release over a period of 35 days. In addition, key parameters such as the *in vivo* release rate of sodium indomethacin into the blood plasma, as well as the biocompatibility of the device in terms of histopathological studies were evaluated and subsequently detailed herein.

8.2. Materials and Methods

8.2.1. Materials

The Sprague Dawley rats utilized in this study were obtained as per the Central Animal Services (CAS) protocols at the University of the Witwatersrand. Indomethacin was purchased from Sigma Aldrich (St. Louis, MO, USA). Double de-ionized water was obtained from a Milli-Q system, (Milli- Q, Millipore, Johannesburg). All solvents utilized for UPLC-UV detection were of UPLC grade and all other reagents were of analytical grade. The preparation of the optimized EMHM device has been discussed earlier in this thesis as per the requirements found in Chapter 5, Section 5.2.2.

8.2.2. *In vitro* drug release analysis

Due to the requirements of dosing on a weekly basis, drug release analysis was repeated using the method detailed in Chapter 3 Section 3.2.4.3, with electro-stimulation and sampling undertaken on days 0, 7,14,21,28.

8.2.3. Design and construction of a portable electro-stimulating device

In order to attain electro-responsive drug delivery, a portable electro-stimulating device capable of delivering an optimized voltage of 3.63V was constructed consisting of four 1.5V battery cells connected in series to a low-resistance light bulb and a resistor of variable resistance. Iron electrodes were used to deliver the required voltage to the EMHM device. A multi-meter was connected in series to the circuit to assess the amount of current passing through it at any given time (Figure 8.1).
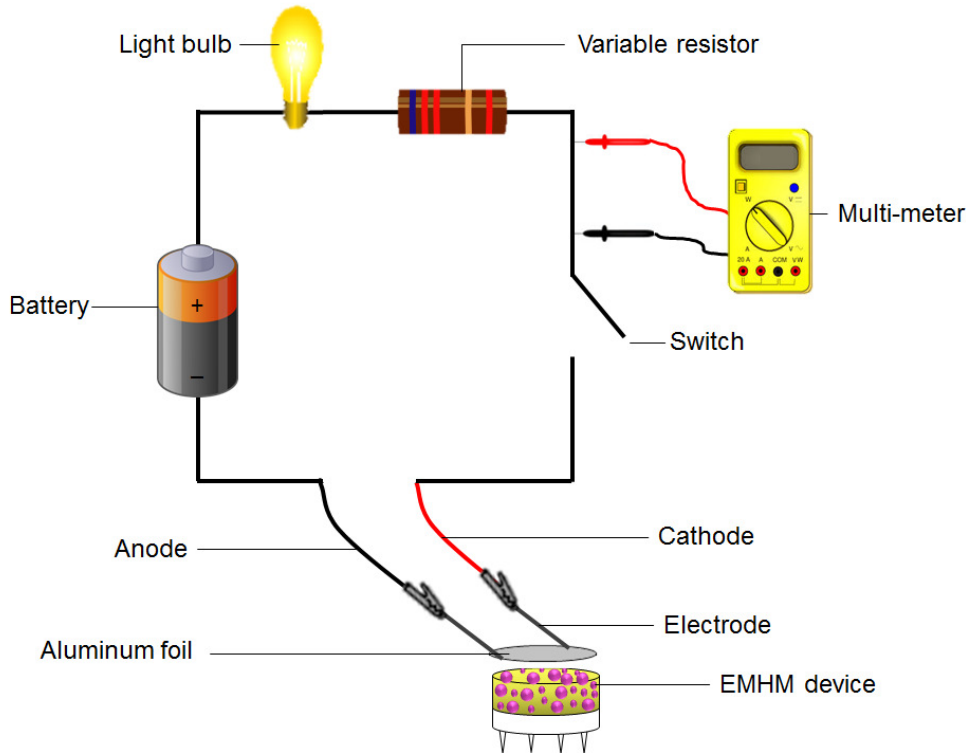
Figure 8.1: Schematic representation of the portable electro-stimulating device on the Electro-Modulated Hydrogel- Microneedle array device.

8.2.4. Sterilization of the Electro-Modulated Hydrogel Microneedle device

Prior to transdermal application, the EMHM device was subjected to gamma (γ) irradiation sterilization. γ-Radiation is mainly used for the sterilization of pharmaceuticals as the procedure leaves no residual radioactivity within the material or device and is a common means of microbial control as well as sterilization procedure for medical devices, implants and single-use devices (da Silva Aquino, 2012; Magda *et al.*, 2014). The application of electromagnetic radiation emitted from the isotopes of the radionuclide, Cobalt 60 (^{60}Co), damages the nucleic acids of micro-organisms at the molecular level, ultimately providing its bactericidal or bacteriostatic function (da Silva Aquino, 2012). A routine minimum dose of 25kGy is applied for many pharmaceutical products, biological tissues and medical devices and was thus chosen as the dose to provide effective antimicrobial sterilization of the EMHM device (da Silva Aquino, 2012; Appendix 11.5).

γ-Sterilization employing a ^{60}Co source at 25kGy of the batches of the EMHM device (~75mg) was undertaken at Synergy Sterilization SA (Pty) Ltd., Isando, Johannesburg, South Africa). The CAS of the University of the Witwatersrand, Johannesburg, South Africa supplied the anesthetic agent Isofor® (isoflurane), and euthanasia agents (sodium

phenobarbitone) for administration to the rats. Their respective dosages are provided in Table 8.2. All other reagents used were of standard analytical grade of the highest purity.

Table 8.2: Drugs and recommended dosages as administered to rats.

Drug	Route	Dose	Frequency
Isofor®	Inhalation	5% initial 2% maintenance	As required
Sodium Indomethacin	Intravenous injection	0.8mg/100g body weight	Once off
Sodium phenobarbitone	Intraperitoneal injection	200mg/kg	On euthanasia

8.2.5. Structural analysis of the Electro-Modulated Hydrogel post-sterilization

FTIR was performed as detailed in Chapter 4, Section 4.2.3 to assess the possibility of any deformation or degradation that may have occurred in the EMHM device due to the γ-irradiation process at the 25kGy dose.

8.2.6. Sterility analysis of the Electro-Modulated Hydrogel- Microneedle device using agar diffusion studies

Sterility of injectable formulations is vital to ensure protection of patients or animal models against the possibility of infection. To ensure sterility of the EMHM devices after γ-radiation sterilization, microbial analyses were conducted to determine the presence of any existing contamination.

For this, the EMHM devices were placed into sterile water (10mL) and vortex mixed. The resultant solution was inoculated (100µL) onto TSA plates using the spread plate technique and incubated at 37℃ for 24 hours. Samples of the EMHs and MNAs were transferred onto the solidified agar using sterile forceps to ensure accuracy of results. As a control, *Escherichia coli* (*E. coli*) and *Staphylococcus aureus* (*S. aureus*) were inoculated onto the TSA to ensure the ability of TSA to allow growth for these organisms. A further control of uninoculated agar was added to ensure sterility of the TSA prior to analysis. All control plates were incubated to the conditions outlined. The sterility analyses were repeated using Thioglycolate to account for the growth of anaerobes.

8.2.7. Animal husbandry

Non-fasted rats were housed in single cages with a 12hour light/dark cycle. The rats were individually housed and were provided with a standard rat diet and water *ad libitum* under a controlled temperature (±25℃). The rats were acclimatized to the laboratory for 7 days prior to *in vivo* experimentation. Their state of well-being was ascertained by weighing them weekly. Housing conditions were according to the SOPs of the CAS which follow the South African Standard for the care and use of animals for scientific purposes.

8.2.8. Design of the *in vivo* experimental study

A total of 18 Sprague-Dawley rats with an initial weight of ~225-350g were used in the study. The rats were randomly assigned to 3 groups (N=6 and N=3 per sub-group). The experimental procedures for each of the groups were as follows (Figure 8.2):
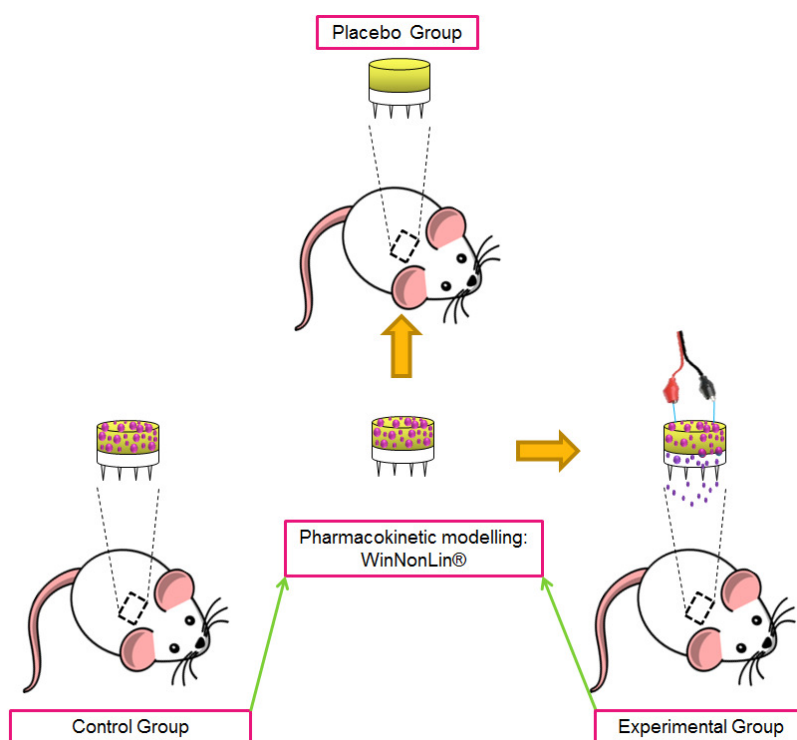
Figure 8.2: Schematic of the design of the *in vivo* study.

Group 1: Control study

The rats in this group received IV administration of sodium indomethacin (0.8mg/100g body weight) 15 minutes prior to blood sampling (Lacroix and Rivest, 1996).

Group 2: Experimental study

The rats in this group received the drug-loaded EMHM device placed on the thoracic region. The device was subjected to electro-stimulation of 3.63V at the required time intervals. According to Mohr and co-workers (1987), rats can withstand voltages of up to 20V before strong muscular contraction and high blood flow velocity occurs.

Group 3: Placebo study

The rats were assessed for any signs of discomfort or behavioral changes and received the EMHM device without electro-stimulation.

All 6 rats in a study group (3 rats in sub-group [a] and 3 rats in sub-group [b]) were administered with the respective delivery system at Day 4 for all study groups. In study group 1, the blood sampling time points for sub-group (1a) were prior to and 15 minutes after intravenous administration of sodium indomethacin with blood samples in the remaining 3 rats (sub-group 1b) taken 2 days later. In study group 2, all rats were administered with the EMHM device with electro-stimulation on Day 4. Blood sampling of sub-group 2a was undertaken prior to and 15 minutes after electro-stimulation. Blood sampling for sub-group 2b was undertaken 2 days after electro-stimulation. Sampling at these time points were taken to prove the presence of sodium indomethacin in the rat's cardio-vascular system after 2 days ($t_{1/2}$ ~7-10 hours), which would not be present at the next weekly electro-stimulation (Elahi *et al.*, 2009). Furthermore, the reason for staggering the sampling points as well as using the 3 rats in sub-group 2b is due to the inability of rats to provide more than 1mL of blood per week excluding use of the rats in sub-group 2a. The total number of blood samples, per rat was limited to 10 samples during the period of the study. The timeline detailing the *in vivo* study with respect to study group 2 can be found in Figure 8.3.The EMHM device was maintained on the skin surface throughout the study. The above electro-stimulation procedure was repeated on all rats on days 11, 18, 25 and 32 with blood sampling of sub-group 2a taken on days 11, 18, 25 and 32 prior to and 15 minutes after electro-stimulation. Blood sampling of the remaining 3 rats in sub-group 2b was undertaken 2 days after electro-stimulation on Days 6, 13, 20, 27 and 34. The blood sampling procedure undertaken for group 2 was repeated for study group 3 without electro-stimulation of the device which was administered on Day 4 and maintained on the skin surface throughout the period of the study.
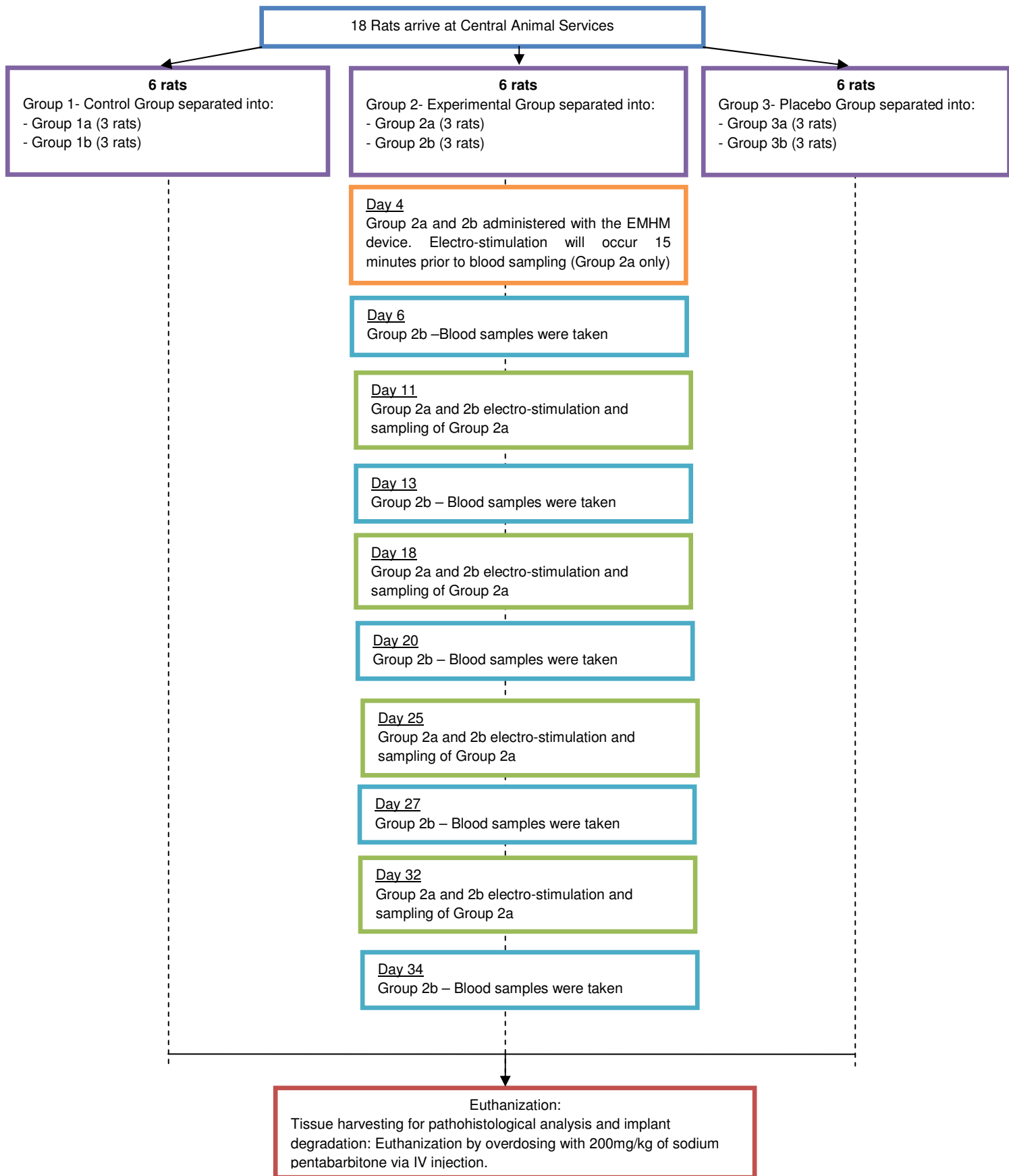
Figure 8.3: Schematic showing the design of the *in vivo* studies model.

8.2.8.1. Procedure for the application of the Electro-Modulated Hydrogel-Microneedle device

Prior to the application of the EMHM device, the dorsal surface of the rats were shaved whilst they were under anesthetic so as to prevent any undue distress. It should be noted that the absence of a hair coat mimics the human skin better than hairy skin as evident by the numerous studies using hairless species, such as nude mice and hairless rats (Simon and Maibach, 1998). The EMHM device was placed onto the thoracic region between the shoulder blades and was secured through the use of a plaster. The rat was bandaged around the torso in order to prevent removal of the device as a result of scratching. The EMH was hydrated using double de-ionized water (1µL). Aluminum foil, serving as the conducting interface, was placed onto the EMH prior to electro-stimulation (Figure 8.4a).The voltage was applied using the portable electro-stimulating device as per Section 8.2.3. The voltage of 3.63V was applied onto the aluminum foil for a period of 1 minute. Figure 8.4b outlines the gross clinical presentation of the rats following transdermal application.

(a)
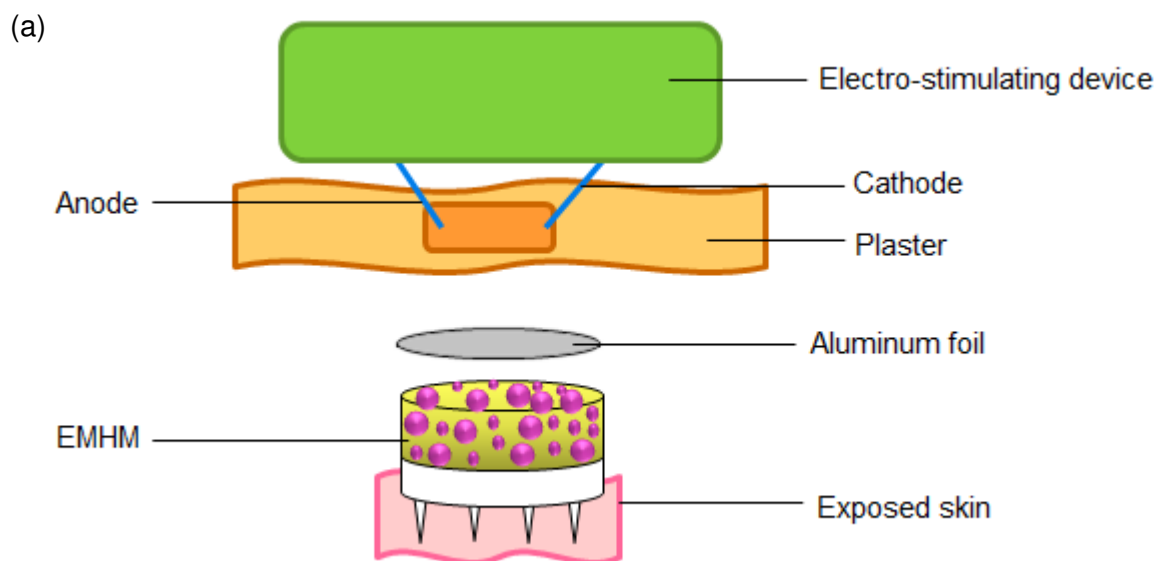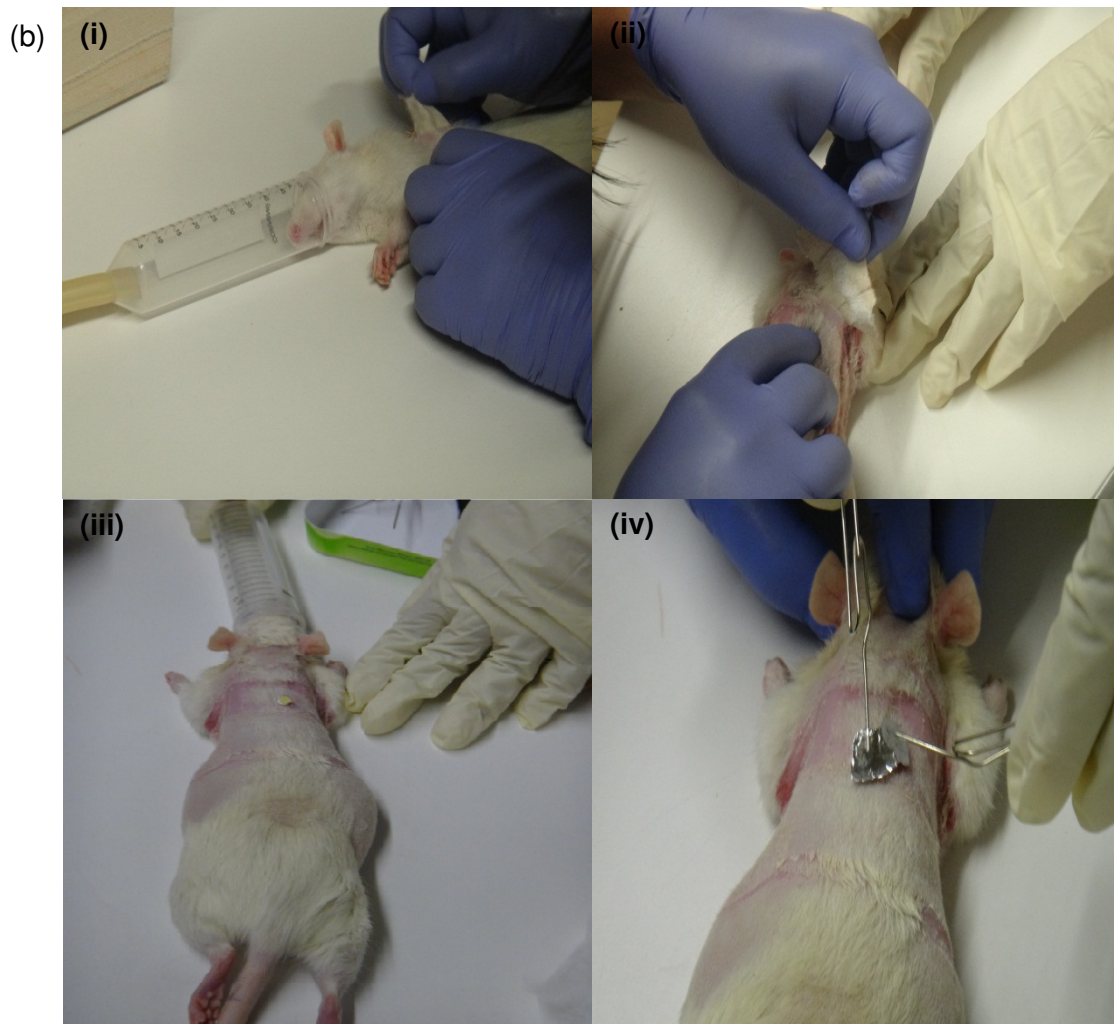
Figure 8.4: (a) Schematic of the Electro-Modulated Hydrogel-Microneedle device (b) Sampling procedure of the Electro-Modulated Hydrogel-Microneedle device (i) The rat placed into the anaesthetizing chamber (ii) Bandage and plaster removal (iii) The Electro-Modulated Hydrogel-Microneedle device in contact with the skin. (iv) The application of the electro-stimulus to the device.

8.2.8.2. Procedure for blood collection, sampling and treatment

A plastic restraint device was used to allow for easy blood collection, allowing minimal movement and thus preventing any undue pain through self-inflicted injury. Animal restraint time was reduced to an absolute minimum on welfare grounds. The blood collection technique employed use of the tail vein (Hoff, 2000). Prior to blood collection, the tail was warmed by dipping it into slightly heated water to induce vessel dilation and subsequently, easy blood collection. Blood samples (0.5mL) were collected using a 1mL syringe pre-flushed with heparin.

After withdrawal, blood samples were placed into 2mL polypropylene tubes that were also pre-flushed with heparin. Blank blood for base-line data was withdrawn 1 week prior to application of the device.

After collection, the blood samples were centrifuged at 12000 RCF (TG16-WS, Nison Instrument Limited, Shanghai, China) for 10 minutes. The supernatant, containing the plasma, was carefully aspirated and transferred into a clean collection tube and frozen at -80°C immediately until further analysis. The conventional group received 0.4mL sodium indomethacin through the tail vein. At 15 minutes and 48 hours, blood was withdrawn and treated as described.

8.2.8.3. Postoperative monitoring of the rats

Postoperative care included monitoring the rats for the duration of the study to ensure that the anesthesia had worn off and that the rats maintained good health. The rats that received the EMHM device were examined twice a day to insure that the bandages remained intact and so that the device was in continuous contact with the skin, and that no complications have occurred since application. Any signs of severe undue distress, such as hyperactivity or restlessness, hypersensitivity and sedation, would have constituted removal from the study. These points also constituted useful data in ascertaining the biosafety of the delivery system. The rats that received IV administration of sodium indomethacin were evaluated for signs of anorexia, dehydration and weakness (Taiwo and Conteh, 2008).

8.2.9. Quantification of the *in vivo* release of the anti-inflammatory agent using Ultra-Performance Liquid Chromatography analysis

An UltraPerformance Liquid Chromatographic (UPLC) method was developed employing a Waters® ACQUITY™LC system (Waters®, Milford, MA, USA) coupled with a photodiode array detector (PDA), and Empower® Pro Software (Waters®, Milford, MA, USA). The UPLC was fitted with an Aquity UPLC® High Strength Silica (HSS) RP18 column, with a particle size of 1.8µm and pore size of 100Å. An isocratic method with a run time of 7 minutes was developed using acetonitrile and 0.1%$^v/_v$ formic acid in double deionized water as the mobile phase in a 50:50 ratio. The flow rate was 0.25mL/minute with an injection volume of 10µL. The PDA detector was set at 254nm. Naproxen sodium was used as the internal standard (IS). The assay procedure was performed at room temperature (21±0.5ºC).

8.2.9.1. Preparation of calibration standards

The standard stock solutions of sodium indomethacin and the naproxen sodium, the internal standard, were prepared in ultra-pure double de-ionized water (Milli-Q, Millipore, Johannesburg). A working standard solution (5mg/100mL) was used to prepare the calibration standards of concentrations ranging from 0.2-1µg/mL by diluting suitable amounts of the solution with deionized water before injection.

8.2.9.2. Sample preparation of plasma samples utilizing liquid-liquid extraction

Indomethacin is highly protein bound (Raveendran *et al.*, 1992) thus a liquid-liquid plasma extraction procedure was applied to the rat plasma containing sodium indomethacin. The simple technique is both rapid and relatively cost effective per sample as compared to other techniques and near quantitative recoveries (90%) of most drugs can be obtained (Prabu and Suriyaprakash, 2012). Stored and frozen study samples were allowed to environmentally equilibrate at room temperature (25±0.5℃). Aliquots of plasma (500µL) were transferred into polypropylene tubes. Acetonitrile (500µL) was added to the tubes and the plasma solution vortexed for 2 minutes for precipitation of the plasma proteins. The mixture was then centrifuged at 12000RCF (Nison Instrument Limited, Shanghai, China) for 10 minutes. The supernatant was subsequently removed and filtered through 0.22µm Cameo Acetate membrane filters. To an aliquot of 100µL plasma, the internal standard solution (5mg/100mL) was added and vortexed for 2 minutes. The final solution was transferred into Waters® certified UPLC vials for analysis. Measurements were conducted on each three samples in triplicate.

8.2.9.3. Validation of liquid-liquid extraction procedure

The precision and accuracy of the extraction process was determined by repeating the extraction procedure mentioned in Chapter 8, Section 8.2.8.2 on 3 consecutive days to allow for the determination of inter-day precision and accuracy, (N=3 for each day) and intra-day variability consisting of multiple injections of samples during a 24 hour period (N=3). Accuracy was estimated using the mean percentage error, based upon differences between actual and predicted concentrations. The precision, expressed as a percentage, was evaluated by calculating the intra- and inter-day variability coefficients of variation (Boon *et al.*, 2006). The extraction process was further validated by the use of the IS, naproxen sodium as theoretically, the peak area of the naproxen sodium should always be similar in every sample as a constant quantity is always utilized. The extraction yield percentage was calculated by comparing the peak areas obtained from the extracted sodium indomethacin in the plasma (AUC_{plasma}) to the peak areas obtained from sodium indomethacin extraction from standard solutions ($AUC_{standard}$) of the same concentration using Equation 8.1:

$$\% \text{ yield } = \frac{AUC_{plasma}}{AUC_{standard}} \times 100 \qquad\qquad \textbf{Equation 8.1}$$

8.2.9.4. Construction of a calibration curve for the quantification of sodium indomethacin release from the Electro-Modulated Hydrogel Microneedle device

Blank plasma samples were thawed to room temperature. Aliquots (100µL) of the plasma samples were transferred to polypropylene tubes and were subsequently spiked with standard solutions of sodium indomethacin and the IS at differing concentrations (N=5), vortexed for 2 minutes, and subjected to the extraction procedure detailed in Chapter 8, Section 8.2.9.2 of this chapter. The sodium indomethacin/naproxen sodium peak area ratios were plotted against the corresponding sodium indomethacin concentrations (µg/mL) and a statistical representation of the degree at which the function fits the set of values (R^2 value) was computed for the curve.

8.2.10. Histomorphological determination of stratum corneum penetration

Histomorphological analysis, post-euthanasia, was performed to ascertain the biocompatibility and tolerance to the EMHM device through the localized inflammatory response of the rats. Excised skin samples of the EMHM device application site, hypodermic needle puncture site and a control skin sample (fixed in 10%$^v/_v$ neutral buffered formalin) were sent to IDEXX laboratories (Pretoria, South Africa). Following the routine histological processing, the inflammatory response was analyzed by preparation of histological slides for determining development of inflammatory cell infiltrates. Cells analyzed as indicators for inflammation included macrophages, dendritic cells, histiocytes, Kuppfer cells and mastocytes (Hemmati *et al.*, 2010).

8.2.11. Pharmacokinetic modeling employing noncompartmental and compartmental algorithms

Based on the *in vitro* and *in vivo* release dynamics of sodium indomethacin from the EMHM device, compartmental analysis was undertaken using pharmacokinetic data analysis and was achieved using PKSolver, a menu-driven add-in program for Microsoft Excel written in Visual Basic for Applications (VBA). Polynomial regression analysis was used for the correlation between the observed and predicted values. The developed mathematical framework (Figure 8.5) represents the phenomena of transdermal drug delivery across skin using the EMHM device.
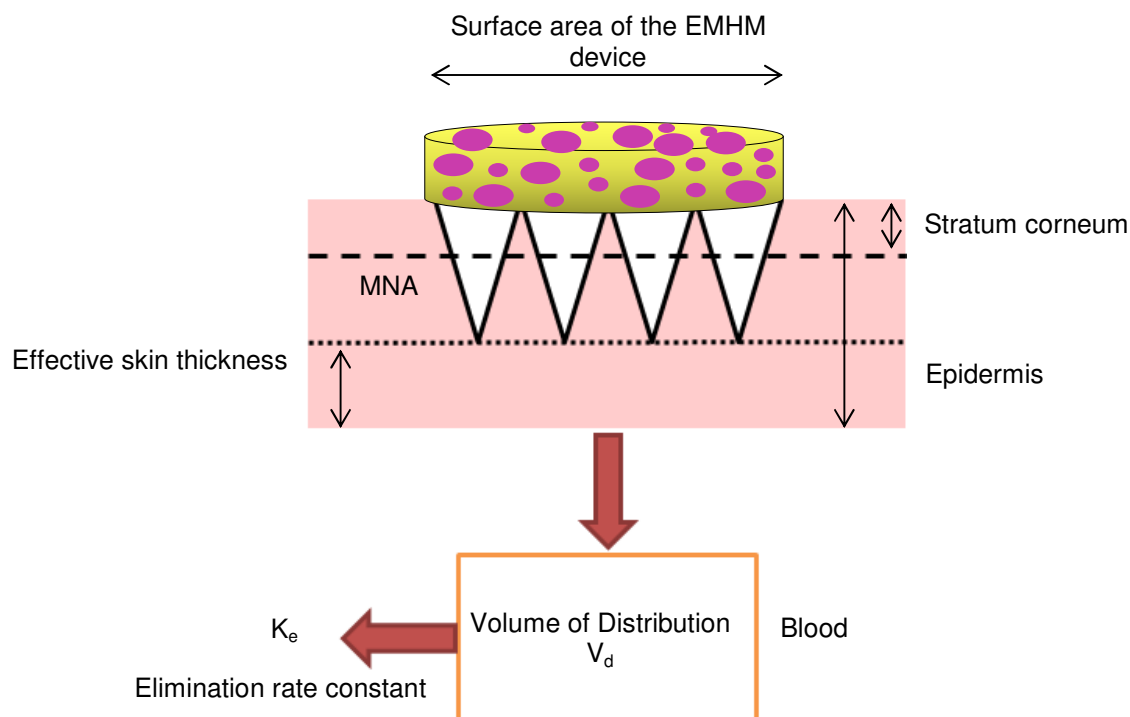
Figure 8.5: Schematic for microneedle array transdermal drug delivery.

The rate-limiting barrier of skin is the viable skin and the insertion of the MNA overcomes the resistance of the SC. The concentration of sodium indomethacin at the interface between the skin tissue and needle edge is defined to be the same as the concentration of sodium indomethacin in the EMH component of the delivery device. The back diffusion from the MNA edge towards the SC is ignored because their diffusion coefficient in the SC is estimated to be too small (i.e. 3.08×10^{-7} cm^2 h^{-1}; Ogiso *et al.*, 1993). Sodium indomethacin diffuses across the skin obeying Fick's second law until it reaches blood vessels. This transport behavior is controlled by different parameters such as the diffusion coefficient, thickness of viable epidermis and length of microneedle (Al-Qallaf *et al.*, 2007). The drug permeated through the skin is absorbed into the blood and the body pharmacokinetics follows a one-compartment model which depicts the body as a simple homogeneous compartment (Xu and Weisel, 2005). The one-compartment model was used because it is assumed that the drugs distribute rapidly between blood and tissue (Shiflet and Shiflet, 2006).

Compartmental analysis was instituted to quantitatively evaluate and predict the *in vivo* fate of indomethacin from the EMHM device by modeling the concentration-time data. Data analysis was carried out by segmenting the combined *in vivo* release profile into individualistic profiles prior to analysis. Pharmacokinetic considerations led to tentative

consideration of three pharmacokinetic models: one compartment model; one compartment model with T_{lag}; and two compartment model). The EMHM device was considered as a single extravascular dose with transdermal application as it is intended for systemic action and is thus administered extravascularly. It is important to note that when drugs are administered extravascularly, systemic delivery is not instantaneous. For this reason, absorption is a prerequisite for pharmacological effects. When the extravascular route is used, the following assumptions are made when determining the pharmacokinetic parameters (Jambhekar and Breen, 2009):

- the characteristics of one compartment model is exhibited
- absorption and elimination follow the first-order process and passive diffusion is operative at all the time
- the drug is eliminated in the unchanged form (i.e. no metabolism occurs)
- the drug is monitored in the blood

In Chapter 5, Section 5.3.13, although the kinetic models were generated for the electro-responsive capabilities of the device *in vitro*, the same models when applied to drug release *in vivo* resulted in similar R^2, AIC and SBC values, and thus were not employed for *in vivo* release kinetics as the models do not necessarily cater for the pulsatile-like behavior of the electro-responsive system.

8.2.11.1. Pharmacokinetic analysis for in vitro-in vivo correlation establishment

WinNonLin® software (V5.3 with IVIVC Toolkit Build 20091211139, Pharsight Software, Statistical Consultants Inc., Apex, NC, USA) was employed for establishing a Level A IVIVC where the input data comprised *in vitro* sodium indomethacin release data, as well as *in vivo* plasma data. Development and validation are essential components in evaluating an IVIVC model with the development of Level A IVIVC model following a two-stage process:

1. Deconvolution: Used to estimate the time course of drug input using a mathematical model based on the convolution integral i.e. the amount of overlap of one function (Levin, 2006). The observed fraction of the drug absorbed is estimated based on the Wagner-Nelson method (Wang and Nedelman, 2002). Following estimation of pharmacokinetic parameters, the IVIVC model is developed using the observed fraction of the drug absorbed and the amount of the drug dissolved. Based on the IVIVC model, the predicted fraction of the drug absorbed is calculated from the observed fraction of the drug dissolved.

2. Convolution: a model independent method based on the superposition principle where the predicted fraction of *in vivo* drug concentrations is convolved to the predicted plasma concentrations (or other relevant body fluid concentration in the case of this investigation). Thereafter, determination of the predictability of a level A correlation focuses on estimating the percent prediction error (%PE) between the observed and predicted plasma concentration profiles, such as the difference in pharmacokinetic parameters (C_{max}, and the area under the curve from time zero to infinity, $AUC_{0-\infty}$).

Advantages of the convolution approach relative to deconvolution-based IVIVC approaches include the following (Emami, 2006):

- The relationship between the plasma drug concentrations and the *in vitro* release is modeled directly in a single stage as opposed to an indirect two stage approach.
- The model directly predicts the plasma concentration time course. As a result the modeling focuses on the ability to predict measured quantities (not indirectly calculated quantities such as the cumulative amount absorbed).
- The results are more readily interpreted in terms of the effect of *in vitro* release on conventional bioequivalence metrics such as maximum drug concentration.

The proposed evaluation approach focuses on the determination of the predictability of a level A correlation focusing on estimating the %PE between the observed and predicted plasma concentration profiles, such as the difference in pharmacokinetic parameters (C_{max}), and the area under the curve from time zero to infinity ($AUC_{0-\infty}$). The %PE was calculated at each time point (Equation 8.2) and was used as a criterion for the assessment of the internal and external predictability of the IVIVC.

$$\%PE = \frac{observed - predicted}{observed} \times 100$$

Equation 8.2

8.3. Results and Discussion

8.3.1. Fourier Transform Infrared analysis of the Electro-Modulated Hydrogel-Microneedle device post-gamma irradiation

Chemical bonds are broken when materials are exposed to radiation (da Silva Aquino, 2012), thus FTIR analysis was used to detect chemical changes (if any) on the treated samples. The FTIR spectra of the untreated and γ-irradiated EMH were different in the intensity of representative signals (Figure 8.6). No other chemical modifications of significance were displayed on the FTIR spectra. A detailed discussion on the FTIR spectra of the EMH can be found in Chapter 4, Section 4.3.2.
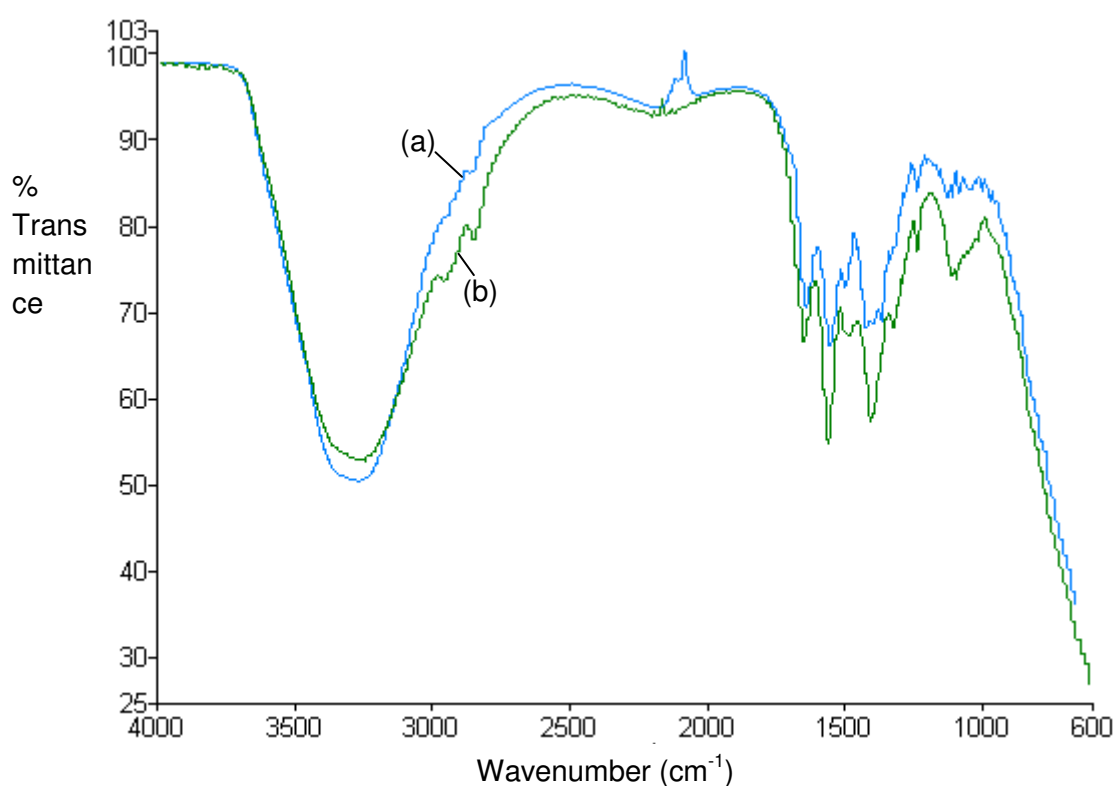
Figure 8.6: Fourier Transform Infrared spectra of the Electro-Modulated Hydrogel (a) prior to and (b) post γ-irradiation at 25kGy.

8.3.2. Validation of the sterilization procedure using microbiological assays

The incubated TSA plates inoculated with washes from the sterilized devices revealed no microbial growth, indicating that the devices were sterile prior to *in vivo* studies (Figure 8.7). The control plates displayed growth of *E. coli* and *S. aureus* assuring the ability of TSA to allow growth of these organisms. Similar results were obtained using Thioglycolate.
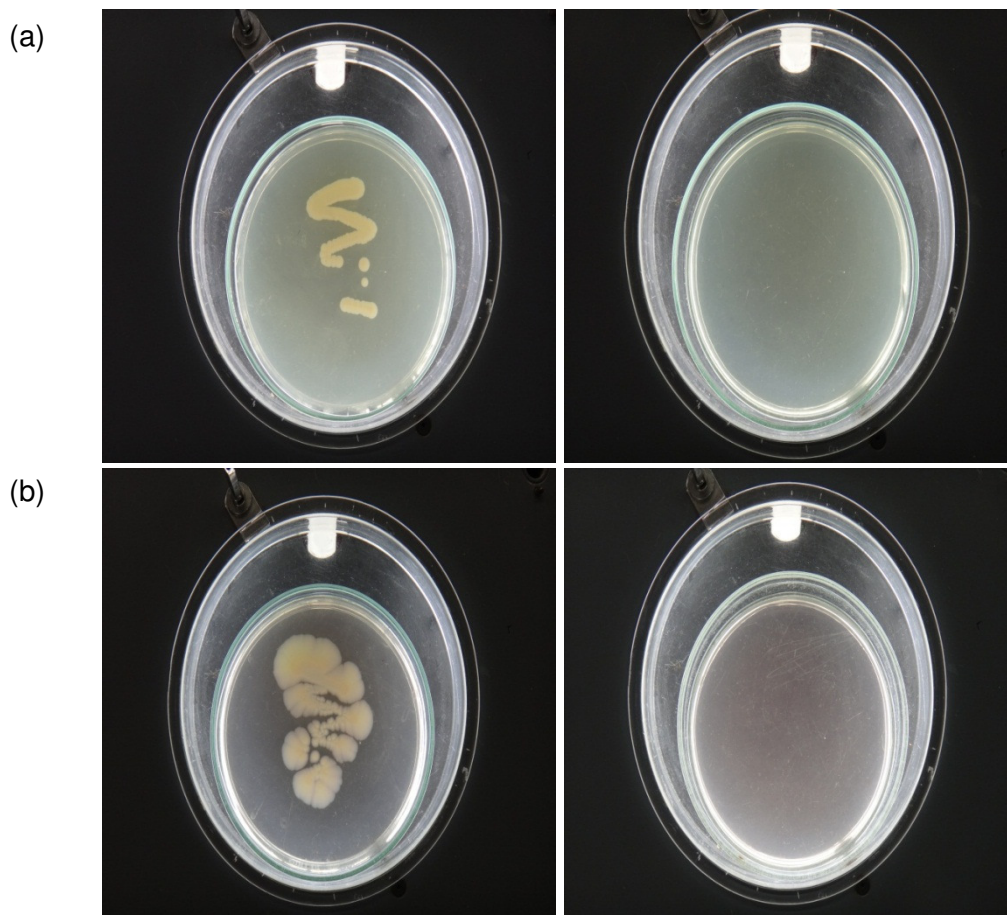
Figure 8.7: Digital images of (a) the *E.coli* control and sterility test and the (b) *S. aureus* control and sterility test.

8.3.3. Application procedure of the Electro-Modulated Hydrogel -Microneedle device

The EMHM device was well tolerated and its efficacy successfully demonstrated in the Sprague Dawley rat model. The fact that the application was well tolerated was affirmed via histopathology in Section 8.3.6.

8.3.4. Validation of the extraction procedure

The mean coefficient of variation in the intra-day and inter-day precision studies was determined to be 0.21% and 0.17%, respectively. Mean extraction of sodium indomethacin from the plasma was determined to be 91.12% (SD≤5.56).The liquid-liquid extraction method was determined to be the optimum condition that provided both high recovery and purity of sodium indomethacin from the plasma proteins.

8.3.5. *In vivo* release of sodium indomethacin in the rat model from the Electro-Modulated Hydrogel- Microneedle device

The UPLC calibration curve for plasma sodium indomethacin is depicted in Figure 8.8 (a). The typical chromatogram (Figure 8.9b) displays retention times of 3.49 and 5.65 minutes for sodium indomethacin and the IS, respectively, with a total run time of 7 minutes. The concentration of sodium indomethacin calculated from the integration area under the peaks was linearly related to the internal standard over the concentration range of 0.2-1µg/mL based on calibration curves, with a R^2 of 0.99. Particle retention observed at 1-2.5 minutes is negligible (Boon *et al.*, 2006).

(a)
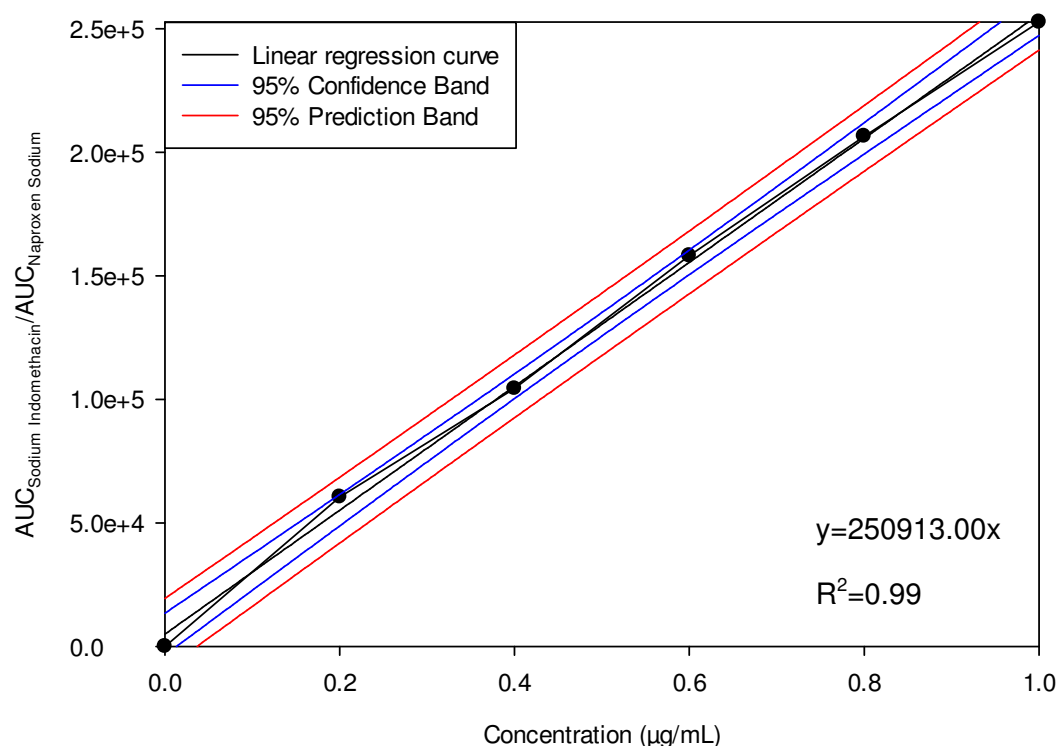
(b)
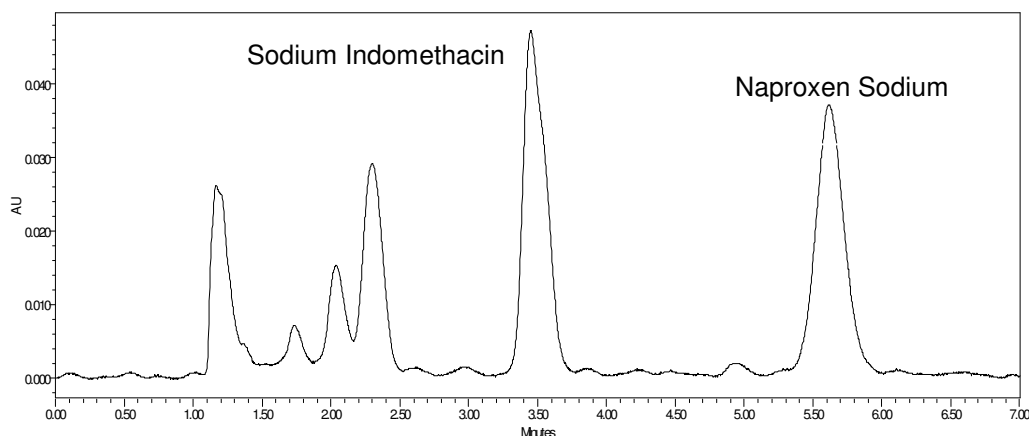
Figure 8.8: (a) Calibration curve of sodium indomethacin at 254nm (b) Typical chromatogram of sodium indomethacin in plasma.

The *in vivo* release profiles (Figure 8.9) of sodium indomethacin from the EMHM device as well as from the control group display results where the transdermal device displayed lower levels of release (due to transdermal vs. intravenous administration) in the plasma as compared to that of the control. Peak levels of 1.04×10^{-6} μg/mL of sodium indomethacin were reached after the initial electro-stimulation. Furthermore, drug was released in desired electro-responsive manner with the release profiles depicting no irregularities or fluctuations. No visible signs of discomfort or abnormal behavior were observed in the study suggesting that the doses entering the systemic circulation and thus reiterate the success of the drug delivery system.
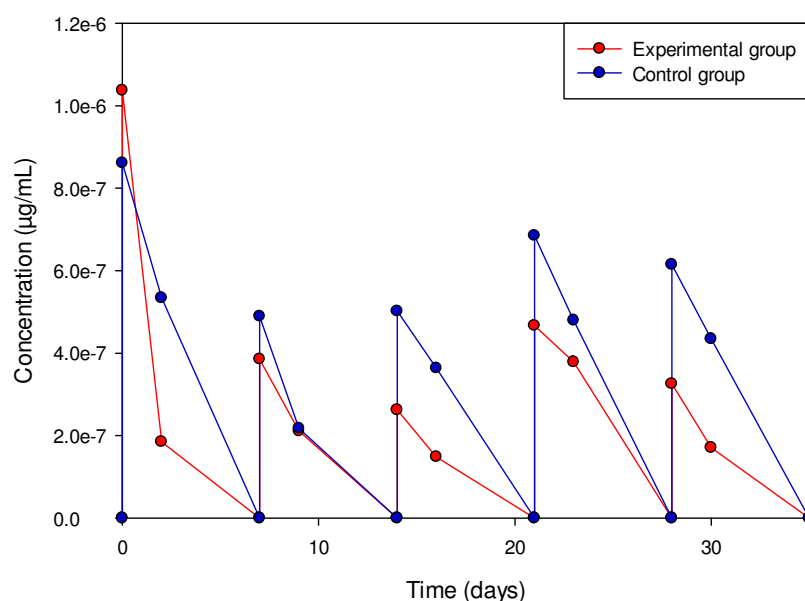
Figure 8.9: *In vivo* drug concentrations attained for the control and experimental groups (SD≤ 2.55×10^{-6}; n=6).

8.3.6. Histomorphological analysis of the excised skin tissue

Histomorphological evaluation was undertaken on all the samples from each study group and was stained with hematoxylin and eosin (H&E). Sections from the control skin tissue in which no microneedle or hypodermic needle punctured the skin are provided for comparison and showed normal morphology without the presence of inflammation or signs of any visible damage (Figure 8.10).
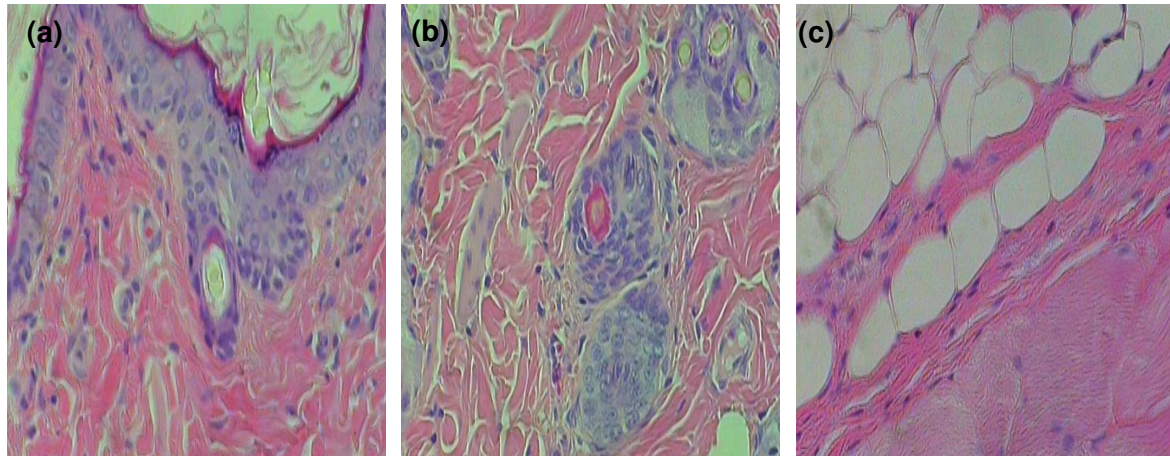
Figure 8.10: Light microscopy images of the H&E stained slides of the region of the control skin sample showing (a) normal skin from the thoracic shoulder region (b) dermis and hair follicles (c) Fat and muscle.

Histological evaluation of the control skin section indicates normal epidermis, dermis and hair follicles as well as glands with no specific lesions present in the skin and underlying dermal stroma. Microchannels were effectively created as indicated by methylene blue staining and histological sectioning (Figure 8.11a). Minor pathological changes were recorded in the epidermis of the samples that were exposed to application of the EMHM device proving shallow penetration of the MNAs. Histological evaluation of the adnexal glands, muscle layer as well as the hair follicles with sweat glands and sebaceous glands and surrounding dermal stroma do not reveal any histological changes, indicative of the MNA's non-invasive nature (Chen *et al.*, 2013; Figure 8.11b).
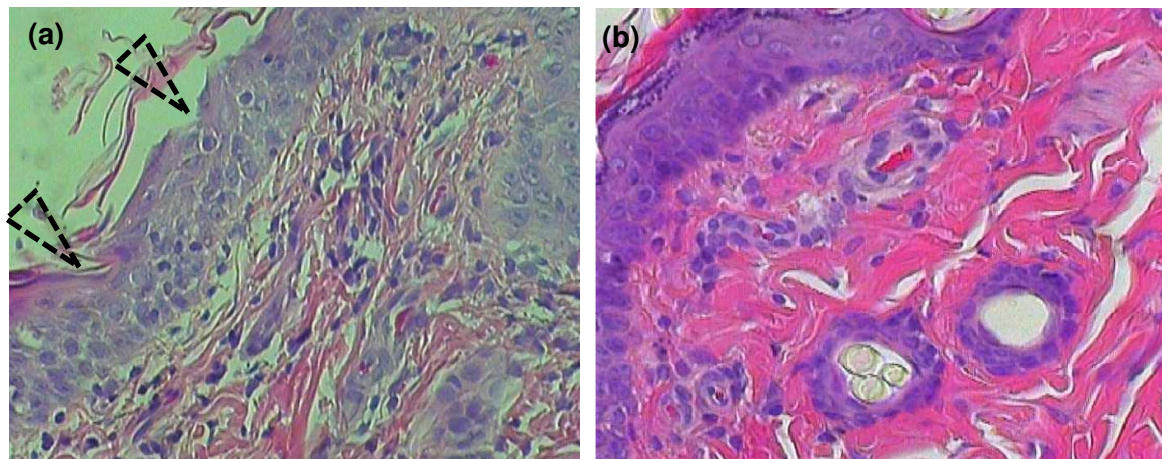
Figure 8.11: Light microscopy images of the H&E stained slides showing (a) the region of the Electro-Modulated Hydrogel-Microneedle Device puncture site and (b) the underlying subcutis and muscle.

Microscopical evaluation of the hypodermic needle puncture site depicts a greater disruption of the epidermal layer as opposed to the microneedle device (Figure 8.12a). Mild perivascular cuffing was confirmed by the presence few mononuclear cells around some of the deeper capillaries translating into epidermal injury. Minimal lymphocytic perivascular infiltrates were present with perivascular distribution in the deep dermis and necrosis (Figure 8.12b). Similar results were observed by Juul and co-workers (Juul *et al.*, 2012).
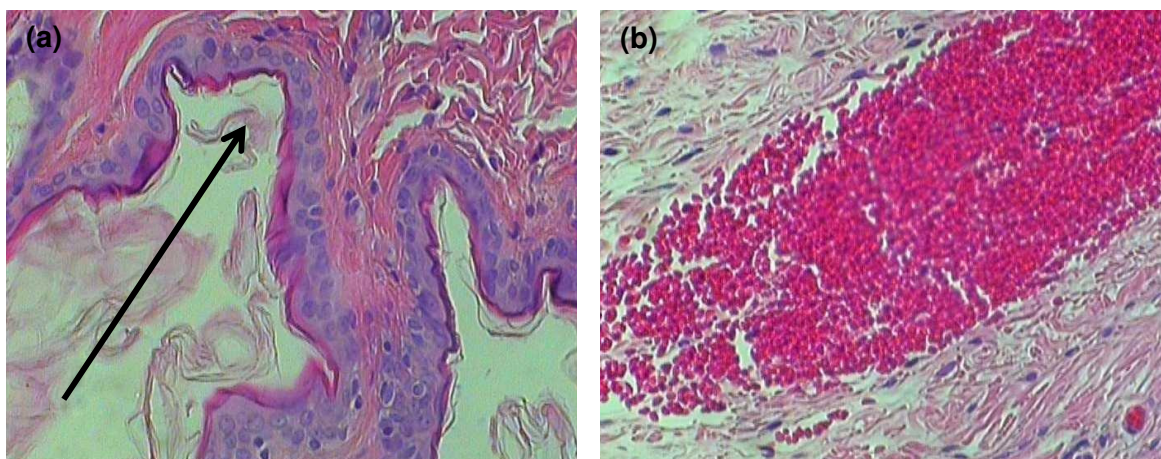
Figure 8.12: Light microscopy images of the H&E stained slides showing (a) the region of the hypodermic needle puncture site and (b) focal hemorrhage in the underlying dermis.

8.3.7. Interpretation of the extravascular noncompartmental and compartmental pharmacokinetic model analysis

The extravascular pharmacokinetic analysis results of the compartmental analysis for sodium indomethacin are presented in Figure 8.13 and Table 8.3. In this study it is assumed that tissue distribution is governed by dissolution and lipid partitioning. The most favorable AIC and SBC values were generated by a one compartment model without lag (AIC= -135.912 and SBC= -136.334) and thus best described the release of sodium indomethacin. R^2 allowed to further validate the differentiation between the models (0.999 without lag and 0.984 with lag). Furthermore, the standard error (SE) and the sum of squares of residuals (SS) determined an overall lower variability in the data pertaining to the model without lag (5.364×10^{-7}, 6.05×10^{-13}) than that with lag (7.599×10^{-7}, 6.07×10^{-13}). The regression residual (r obs-pre) of the observed versus predicted values was inconclusive in determining the most appropriate model, differing by 0.001.
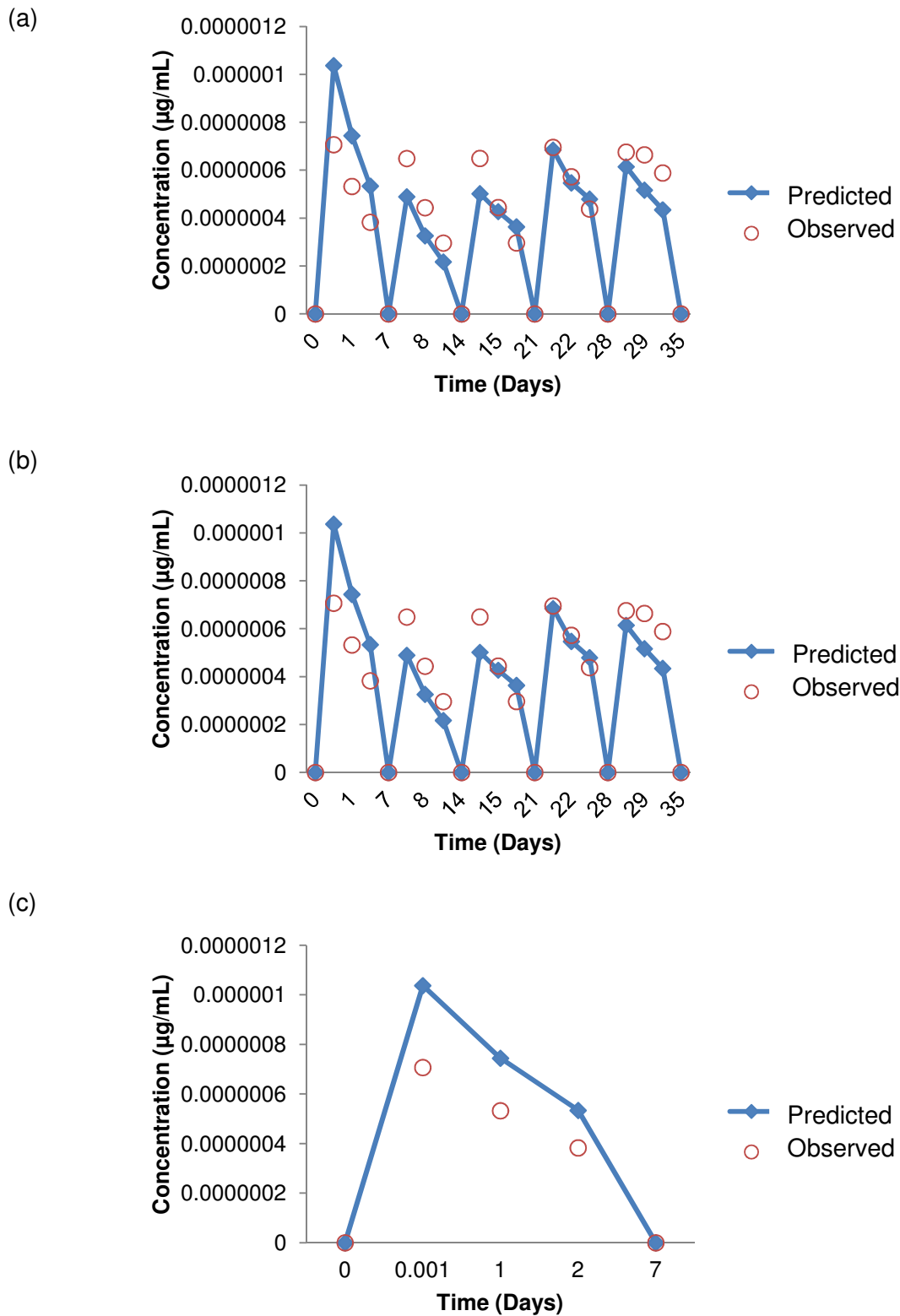
Figure 8.13: Results for extravascular pharmacokinetic analysis employing (a) no lag and (b) lag (c) extension of pharmacokinetic analysis employing lag over a 7 day period.

Table 8.3: Compartmental analysis of plasma data after extravascular input without and with lag.

Parameter	Unit	Average Value	Diagnostics	Value
Extravascular model without T_{lag}			
A	µg/mL	1.008×10^{-6}	r obs-pre	-0.18
k_a	1/d	3.184	SS	6.05×10^{-13}
k_{10}	1/d	0.318	R^2	0.999
$t_{1/2ka}$	D	0.240	SE	5.364×10^{-7}
$t_{1/2k10}$	D	2.4047	AIC	-135.9121
V/F	(mg)/(µg/mL)	2.758×10^{7}	SBC	-136.334
CL/F	(mg)/(µg/mL)/d	8.77×10^{6}		
T_{max}	D	0.887		
C_{max}	µg/mL	7.021×10^{-7}		
AUC_{0-t}	µg/mL*d	2.225×10^{-6}		
AUC_{0-inf}	µg/mL*d	3.142×10^{-6}		
AUMC	µg/mL*d^2	1.346×10^{-5}		
MRT	D	3.185		
Extravascular model with T_{lag}			
A	µg/mL	5.038×10^{-6}	r obs-pre	-0.181
k_a	1/d	15.919	SS	6.07×10^{-13}
k_{10}	1/d	1.592	R^2	0.984
T_{lag}	D	0.003	SE	7.599×10^{-7}
$t_{1/2ka}$	D	1.202	AIC	-132.144
$t_{1/2k10}$	D	12.019	SBC	-134.707
V/F	(mg)/(µg/mL)	1.379×10^{8}		
CL/F	(mg)/(µg/mL)/d	4.389×10^{7}		
T_{max}	D	4.437		
C_{max}	µg/mL	3.51×10^{-6}		
AUC_{0-t}	µg/mL*d	1.113×10^{-5}		
AUC_{0-inf}	µg/mL*d	1.571×10^{-5}		
AUMC	µg/mL*d^2	6.730×10^{-5}		
MRT	D	19.073		

A: the zero time intercept associated with the Alpha phase (*an initial phase of rapid decrease in plasma concentration due distribution)*

k_a: *1st order absorption rate constant*

k_{10}:   *Elimination rate constant*

T_{lag}:   *Finite time taken for a drug to appear in systemic circulation following extravascular administration*

$t_{1/2ka}$:   *Absorption half-life rate constant*

$t_{1/2k10}$:   *Elimination half-life rate constants*

V/F: *The volume of distribution of the absorbed fraction*

CL/F: *The observed total body clearance for extravascular administration*

T_{max}:   *Time at which the maximum concentration (Cmax) is observed*

C_{max}:   *Maximum observed concentration occurring at Tmax*

AUC_{0-t}:   *Area Under the Curve (AUC) from the dosing time to the last measurable concentration*

AUC_{0-inf}:   *AUC from dosing time extrapolated to infinity*

AUMC: *Area Under the Moment Curve*

MRT: *Mean Residence Time is the average amount of time the drug remains in a compartment or system*

The first order absorption rate constant (k_a) obtained was 3.184/day, accounted for by the ionized form of the basic drug electrostatically interacting with acidic phospholipids (Rodgers *et al.*, 2005 [a]). In addition to electrostatic interactions with acidic phospholipids, the basic drug is also soluble in tissue water, allowing for the partition into neutral lipids and neutral phospholipids (Rodgers *et al.*, 2005 [a]) resulting in a $t_{1/2k10}$ of 2.4047 days. The obtained elimination rate constant (k_{10}) was 0.318 days (approximately 7.2 hours), consistent with the $k_{10\,as}$ indicated by Gurnasinghani and co-workers (1989) of 2.6-11.2 hours.

In contrast to unionized molecules, ionized drug species do not partition into tissue lipids, and hence have a low $t_{1/2ka}$ (Rodgers *et al.*, 2005 [a]; Li *et al.*, 2007) of 0.240 days for transdermal administration and 2.976 days for intravenous administration. The EMHM drug delivery device resulted in a lower AUC_{0-t} of 2.225×10^{-6} µg/mL per day as compared to an AUC_{0-t} of 0.066µg/mL per day when sodium indomethacin was delivered intravenously (Table 8.4), this result lies in a difference in plasma protein binding rather than tissue binding as described earlier (Rodgers *et al.*, 2005[b]). The pharmacokinetic data obtained demonstrate that, compared with intravenous administration, the C_{max} (7.021×10^{-7}µg/mL for the EMHM device and 0.0172µg/mL for intravenous administration), AUC_{0-t} (2.225×10^{-6}µg/mL per day for the EMHM device and 0.066µg/mL per day for intravenous administration) and MRT values (3.185 days for the EMHM device and 4.584 days for intravenous administration) of sodium indomethacin after transdermal administration are significantly reduced. This may be caused by the longer period of absorption of sodium indomethacin when given as a transdermally, and most likely reflects the change in the drug over the entire disposition phase rather than the elimination during the terminal phase (Li *et al.*, 2008). The decreased AUC_{0-t} and MRT values suggest that the potential side effects from indomethacin may be diminished due to increased peak concentrations, allowing the pharmacological effects to be relatively low and delayed (Li *et al.*, 2008). It should be noted, however, that plasma concentrations are more likely to stay elevated for longer in patients than in rats under similar experimental conditions due to different pharmacokinetic parameters .i.e. human versus rat volume of distribution (V_d; 18 versus 1L volume), longer human versus rat distribution half-life ($t_{1/2ka}$ 29.208 versus 0.240 days; Ogiso *et al.*,1993), and longer human versus rat elimination half-life ($t_{1/2k10}$ 5.448 versus 2.405 days; Ogiso *et al.*,1993). In contrast to intravenous administration, the transdermal EMHM device enables sodium indomethacin levels to be maintained and also provides the possibility of administering the drug as and when required. The time to reach the maximum concentration (C_{max}) was 0.89 days or 21.29 hours for the transdermal route and was instantaneous for the intravenous route. This is a key factor in determining the usefulness of transdermal application as a therapeutic system. The low C_{max} and prolonged T_{max} after transdermal

administration were due to the barrier properties of the skin which lead to an early accumulation of the drug in the skin followed by a sustained release into the systemic circulation. The reservoir effect after removal of the electro-stimulus might be due to the slow elimination (2.4047 days) of the drug which had accumulated in skin tissues indicating that the therapeutic levels of sodium indomethacin for the Sprague Dawley rat (0.8mg/kg) were attained and maintained, ultimately proving the therapeutic ability of the electro-responsive drug delivery system.

Table 8.4: Results of noncompartmental analysis of plasma data after extravascular input.

Parameter	Unit	Value
λ_z	1/d	0.233
$t_{1/2}$	d	2.976
T_{max}	d	0.000
C_{max}	µg/mL	0.017
T_{lag}	d	0.000
$C_{last\,obs}/C_{max}$		0.333
AUC_{0-t}	µg/mL*d	0.066
$AUC_{0-inf\,obs}$	µg/mL*d	0.091
$AUC_{0-t/0-inf\,obs}$		0.729
$AUMC_{0-inf\,obs}$	µg/mL*d^2	0.416
$MRT_{0-inf\,obs}$	d	4.584

λ_z:	*1st order rate constant of the terminal (log-linear) portion of the curve terminal elimination rate constant*
$t_{1/2}$:	*Terminal phase half-life. The time it takes for the concentration levels to fall to 50% of their value.*
C_{last}:	*The last quantifiable concentration following dosing*
$AUC_{0-inf\,obs}$:	*AUC from dosing time extrapolated to infinity based on the last observed concentration*
$AUMC_{0-inf\,obs}$:	*AUMC extrapolated to infinity based on the last observed concentration*
$MRT_{0-inf\,obs}$:	*MRT extrapolated to infinity*

8.3.8. Establishment of an *in vitro-in vivo* correlation

The IVIVC regarding a transdermal drug delivery system of this nature has not been examined apparent by the lack of available literature. An extravascular single-dose, first-order absorption one compartment model without lag was selected for sodium indomethacin for development of the IVIVC model, being the best fit as predicted by initial pharmacokinetic analysis. As described in Chapter 5, Section 5.3.12, in terms of the R^2 and AIC, dissolution data was best described in terms of the Makoid-Banaker model (a multiple linear regression method).

A Level A correlation was developed by calculating the amount of sodium indomethacin absorbed employing the Wagner Nelson method using the linear trapezoidal rule. To

ascertain that a level A IVIVC was obtained, the percentage of drug absorbed up to time *t* was plotted versus the amount of drug released *in vitro* (Figure 8.14).

(a)
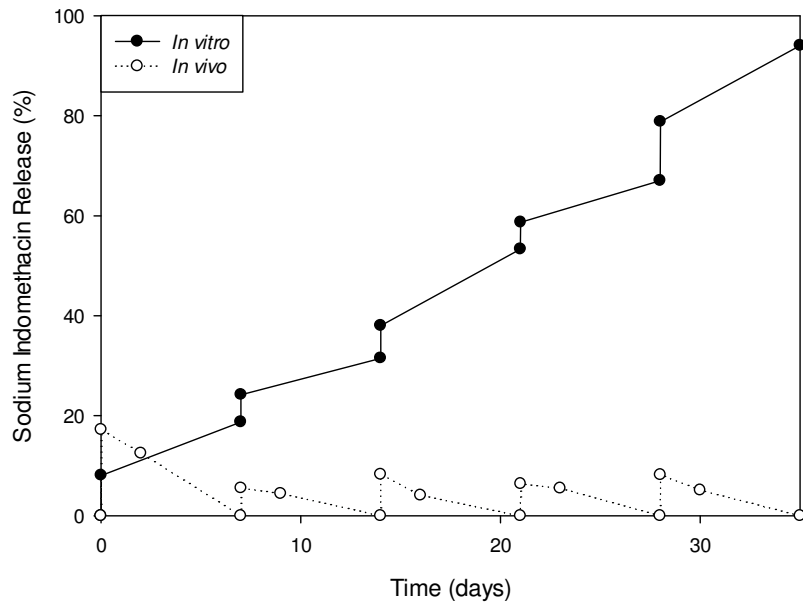
(b)
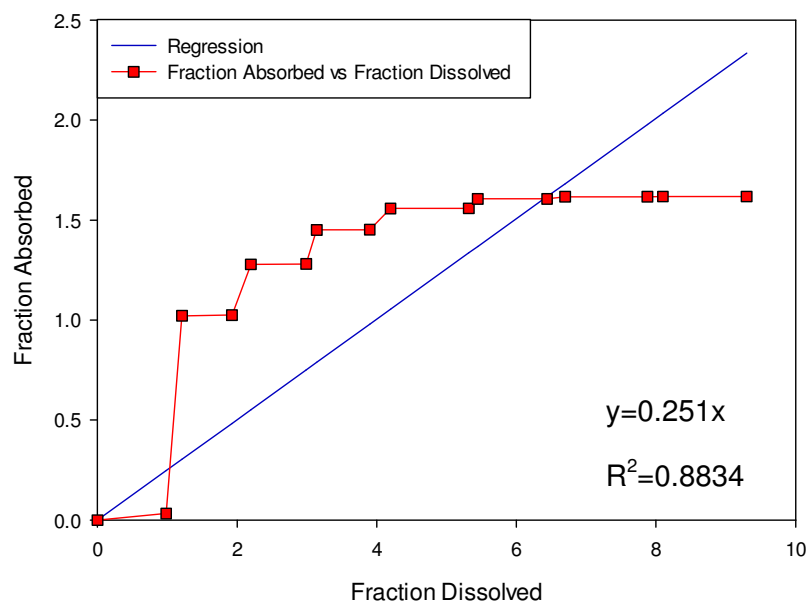
Figure 8.14: (a) Drug release profiles of the *in vitro* release and the observed mean *in vivo* release profile extracted using deconvolution analysis of sodium indomethacin from the device (b) Regression plot showing the relationship between the fraction of indomethacin absorbed *in vivo* and the fraction released *in vitro*.

The initial release of ±10% observed after electro-stimulation has allowed for the drug to be maintained within the rat's therapeutic levels. Level A analysis yielded an R^2 value of 0.8834 indicating that the *in vitro* data was predictive of *in vivo* data with 88.34% accuracy. However, the imperfect superimposability observed in the *in vitro/in vivo* plot may result from residual release from the hydrogel matrix, accounting for the increase in drug release after electro-stimulation on day 0 to day 7. In addition, the model dependent Wagner-Nelson method is used for a one-compartment model, and hence, does not take into account the multi-compartmental transdermal system nor does it account for the pulsatile (electro-responsive) release (Emami, 2006). However, misinterpretation on the terminal phase of the plasma profile may be possible in the occurrence of a flip-flop phenomenon in which the rate of absorption is slower than the rate of elimination The initial spike *in vivo* release of sodium indomethacin from the EMHM device can be accounted for by the size of the rats as they generally have a higher metabolism compared to humans (Sjögren *et al.*, 2014).

Evidence exists of altered topical absorption due to changing blood flow as a consequence of elevated temperature (Singh and Roberts, 1994). Consequently, the non-superimposable plots may result due to epidermal clearance, an important determinant of topical absorption influencing the therapeutic activity in transdermal therapy (Dancik *et al.*, 2008). Five scenarios of topical absorption have been identified by Reddy and co-workers (1998):

(i) Finite exposure time in which the vehicle containing the absorbing chemical is removed. Chemical in the SC reservoir continues diffusing into the systemic compartment (i.e. the body) after the exposure ends.

(ii) Decreasing the vehicle concentration where the vehicle volume is small enough that dermal penetration causes the vehicle concentration to decrease significantly enough to affect the rate of dermal absorption.

(iii) Limited blood flow rate where represented by the situation where chemical penetrates through the SC faster than the reduced blood flow rate can remove it.
(iv) Increasing the blood concentration where there is sufficient blood flow but the blood concentration builds enough to reduce the skin penetration rate.

(v) Absorption onto the skin from the blood in which the direction of dermal absorption is reversed. That is, chemical absorbs into the skin from the blood, to which chemical has been abruptly added (e.g., by IV bolus). The penetrating chemical is then released into a vehicle, such as water during a shower or bath.

Equation 8.3 relates the steady-state ratio of the concentrations of drug in the epidermis ($C_{epidermis}$) and in the applied vehicle (C_v) (Roberts, 1991) as:

$$\frac{C_{epidermis}}{C_v} = \frac{k_p}{k_p + CL_{dermis*}}$$

Equation 8.3

Where k_p is the permeability coefficient of the drug and $CL_{dermis*}$ is the clearance into the dermis per unit area of application. Equation 8.3 shows that the epidermal concentration $C_{epidermis}$ depends on the relative magnitude of dermal clearance, which is determined mainly by blood flow, and the permeability coefficient k_p. Situations in which k_p is of a similar order of magnitude to clearance, such as disruption of the barrier or vasoconstriction, enable blood flow to play a greater role in determining topical absorption. When blood flow is much higher than k_p, epidermal clearance will be the determinant of epidermal concentration (Walters and Brain, 2009). In this situation, Equation 8.3 can be reduced to Equation 8.4:

$$\frac{C_{epidermis}}{C_v} = \frac{k_p}{CL_{dermis*}}$$

Equation 8.4

Also of importance in establishing the release kinetics of sodium indomethacin from a transdermal system, is metabolism occurring in the skin. Even though the nature of skin enzymes differs qualitatively and quantitatively from those in the liver (Walters and Brain, 2009), there is still potential for molecular biotransformation within the skin (Wilkinson and Williams, 2008). While the activities of many metabolic processes are much lower in skin than in liver, certain enzymes, such as N-acetyltransferases and those involved in reductive processes have demonstrated fairly high activity (Table 8.5; Hotchkiss, 1998).

Table 8.5: Comparison between specific activities of cutaneous enzymes compared with hepatic enzymes (Hotchkiss, 1998).

Enzymatic System	Substrate	Cutaneous-specific Activity (% hepatic)
Sulfotransferases	1-Naphthol	10
Acetyltransferases	p-Aminobenzoic acid	18
	2-Aminofluorene	15
Glucuronosyl transferases	Bilirubin	3
	1-Naphthol	2-50
Glutathione transferases	cis-Stilbene oxide	49
	Styrene oxide	14
Epoxide hydrolases	*cis*-Stilbene oxide	9-11
	trans-Stilbene oxide	24-25
	Styrene oxide	6
Cytochrome P-450s	Aldrin	0.4-2.0
	Aminopyrine	1
	Diphenyloxazole	2-3
	Ethylmorphine	0.5
	7-Pentoxyresorufin	20-27

A challenge faced by transdermal drug delivery methods is irritation and permeation of hydrophilic agents due to the lipophilic nature of the skin. Determining the bioequivalence of topically applied dosage forms presents difficulties as very low blood levels of a specific drug following transdermal application has proven to be particularly difficult. To properly determine the dermatopharmacokinetics, the tape-stripping method can be employed as a future output (Chapter 9).

8.4. Concluding Remarks

In vivo studies revealed a good preliminary indication of the of the EMH system's electro-responsive capabilities, ultimately facilitating the immediate release of the entrapped drug into the tissues and could significantly desensitize the patient to chronic pain whilst prohibiting any adverse effects. Sodium indomethacin levels in the plasma were 6.29×10^{-9} to 6.76×10^{-7} µg/mL, less than that obtained by the conventional IV administration, but well within the therapeutic range. In addition, the drug delivery system was well tolerated, showing no signs of inflammation. A Level A correlation as determined by IVIVC correlation further provided evidence on the feasibility of the EMHM device. However, it should be noted that a direct comparison between devices of this nature were not possible as such similar devices do not exist. Ultimately, the study served as determining the feasibility of such a prototype device for expanding it to human trials. Future studies should focus on

ascertaining the comprehensive pharmacokinetics of the device as an ideal opportunity for investigating dose proportionality.

CHAPTER 9
CONCLUSION AND RECOMMENDATIONS

9.1. Conclusions

Numerous transdermal delivery systems currently exist on the market since its introduction in the 1970's (Paudel *et al.*, 2010), yet the market still remains restricted to a narrow range of drugs. Throughout this thesis, the EMHM device has proven its success as a prototype device pharma-engineered for the treatment of chronic pain. The ability to overcome permeation challenges through the use of microneedles serves as a stepping-stone in the development of transdermal delivery.

Thus in order to take this present study to final development and marketing, modifications to the device are necessary so that the it's made portable and convenient with the size and number of the microneedles relative to its function and placement. A modification that is apparent includes a housing whereby the electrical component may be housed (Figure 9.1).

(a)

Electrode/backing plate

Electro-modulated hydrogel

Battery and housing

Circuit

Microneedle Array

(b)

Device Monitor

Adhesive
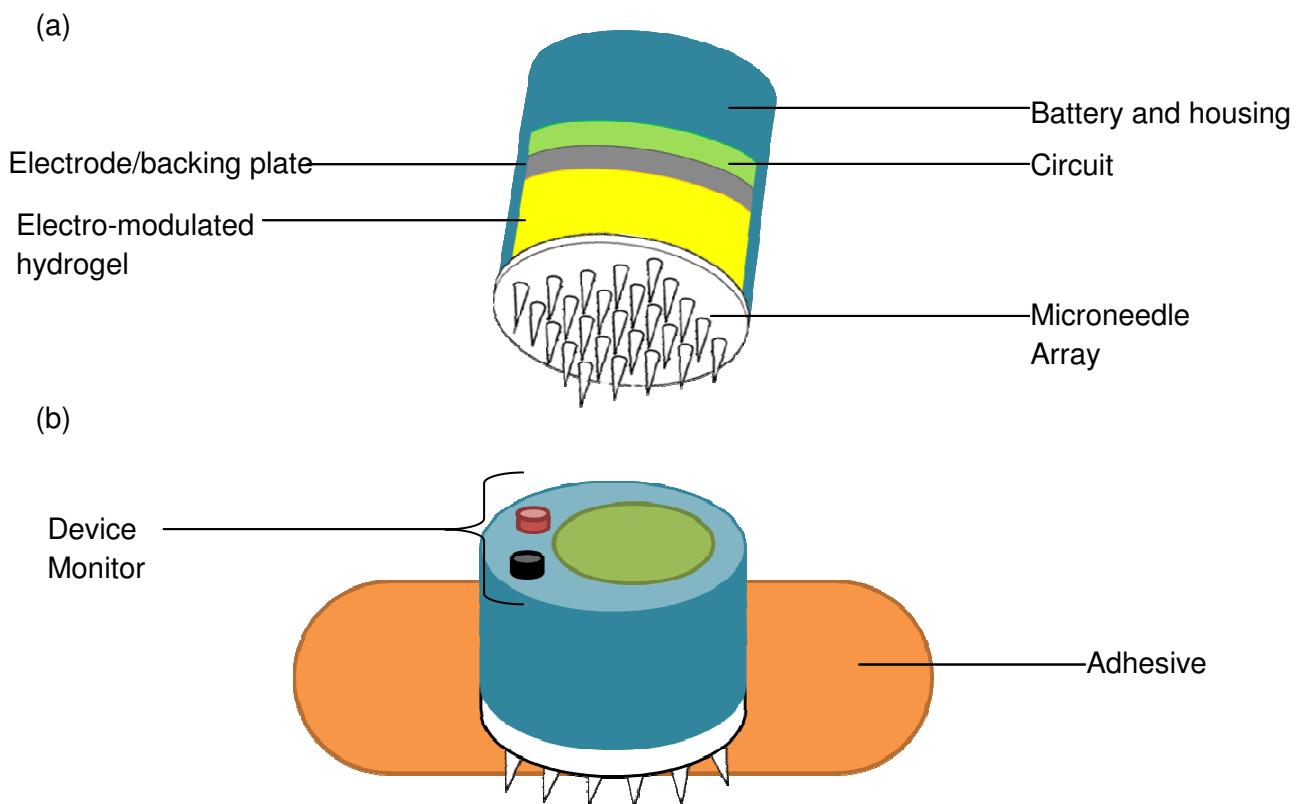
Figure 9.1: (a) Schematic of the components of the proposed prototype (b) Top view of the drug delivery device.

9.2. Future Recommendations

The need for tailored therapeutics has become more apparent and imperative with time. Combining pharmaceutical technology with that of mechanical has the potential to advance the field of advanced drug delivery and chronic care. Outlined are few of the many aspects that such a (modified) device developed in this research may therapeutically assist.

9.2.1. Diseases pertaining to the inner ear

Treatment relating to diseases of the inner ear has proven to be ineffective mainly due to the blood-cochlear barrier preventing the transfer of most compounds from the bloodstream to the inner ear. As a result, the inner ear poses on the most technologically challenging areas for targeted drug delivery. Treatment of auditory diseases, tinnitus, balance disorders and sensorineural hearing loss necessitates advanced systems capable of both targeted and sustained drug delivery, rapidly increasing its clinical significance (Pararas *et al.*, 2012). The delicate structures of the inner ear together with the relative inaccessibility of the cochlea necessitate the need of miniaturized delivery systems capable of a time sequenced fashion over an extended duration.

9.2.2. Treatment of autoimmune skin disorders

Cyclosporin is clinically used for the treatment of autoimmune diseases, including skin disorders like psoriasis, and inflammatory diseases (Lallemand *et al.*, 2003). Topical delivery of the immunosuppressant is a promising strategy to treat skin disorders, as systemic delivery side effects are avoided. However inadequate drug penetration in the skin is attributed to its ineffectiveness. Though chemical methods are more accepted and clinically viable, the vast majority of formulations tested to date were aimed at increasing the transdermal delivery, to which the uses of such a microneedle device may greatly assist.

9.2.3. Intravaginal drug delivery

Vaginal administration of drugs, specifically used for the treatment of female-related conditions such as hormone replacement therapy, contraception, osteoporosis, infections, breast or cervical cancer, infertility, is a feasible alternative to parenteral or oral delivery methods (Bernkop-Schnurch and Hornof, 2003). However, novel high performance intravaginal drug delivery systems for female health are still needed as it is challenging to provide prolonged high drug concentrations in the vagina. Although cohesive polymers exist to ensure a prolonged residence time in the vagina, non-toxic permeation enhancers are needed. Modifications to the developed system may be able to combat the afore-mentioned challenges by developing a possible MNA-based osmotic pump device containing an encapsulated medicament. The device can be applied through existing applicators to the

fornix region whereby swelling provide the osmotic pressure gradient to enable drug release. In such a delivery device, the MNAs will serve as a dual-functioning adherence and penetration enhancer without causing pronounced irritation

9.2.4. Ocular drug delivery

In ocular pharmacokinetics, bioavailability in the eye can be as low as 5% or perhaps less (Urtti and Salminen, 1993). The complicated anatomy and physiology of the eye makes it a highly protected organ with its unique structure restricting entry of drug molecules to the site of action, especially to the posterior segment of the eye (Figure 9.2). Ocular iontophoresis, in which a mild electric current is applied to enhance ionized drug penetration in to the ocular tissue, has recently gained interest due to its non-invasive ability delivery (Gaudana *et al*., 2008). Complications such as endophthalmitis, retinal detachment and intravitreal hemorrhages associated with intraocular injections can be overcome with the iontophoretic method. Drug delivery to the posterior segment of the eye has recently employed the use of microneedles showing excellent *in vitro* scleral penetration and rapid dissolution of coating solution after insertion when coated solid metal microneedles were used. Employing the current developed drug delivery device that is pre-loaded with ocular drugs may prove to enhance the already successful results.
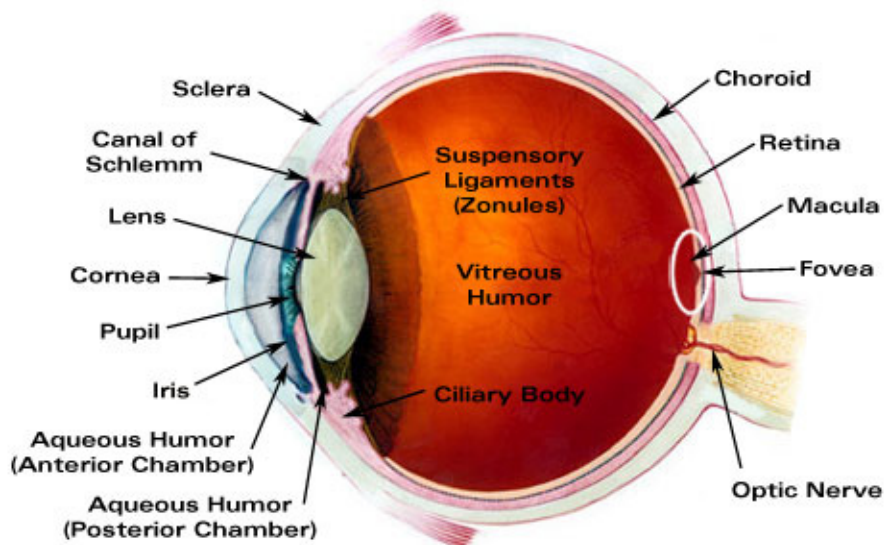
Figure 9.2: Vertical sagittal section of the adult human eye.

9.2.5. Dermatopharmacokinetic studies

To further build on *in vivo* studies conducted in Chapter 8 of this thesis, the dermatopharmacokinetics may be determined by the FDA-approved tape-stripping or dermatopharmacokinetic method. This method is based on the dermal reservoir principle; consisting of a standardized protocol whereby consecutive layers of SC cells are sampled

through repeated applications and removal of adhesive tape on the skin surface (Shah *et al.*, 1998). A hypothesis exists that if a compound is applied to the skin for a short duration of time such as 30 minutes, and is subsequently removed, the amount of drug in the upper layers of the SC will be predictive of the overall bioavailability of the compound.

Using analysis of each tape strip, it has been shown that the concentration of drug in the SC decreases in a log linear fashion, and that about 90% of the concentration is found in the first 10 strips, the following 10 strips contribute less than 5% to the concentration (Caron *et al.*, 1990). Quantification of the mass of SC cells removed by the tape-stripping method can be determined as an auxiliary test to further validate the sampling methodology by analyzing the protein content of the strips (Weigmann, *et al.*, 1999; Dreher *et al.*, 2005). Evaluating the SC thickness could be undertaken prior to or preferably during the dermatopharmacokinetic experiment (Kalia *et al.*, 2001).

9.3. Future Outlook

An optimized electro-responsive prototype device with potential for commercialization has been developed in this study. Results obtained from the *in vivo* study are promising and show excellent biocompatibility, however, there is a need for developing a novel pharmacokinetic model for such novel responsive systems.

Furthermore, the novel drug delivery device developed herein has the ability to broaden the transdermal market for conventional drugs for new therapeutic indications and could find application in the site-specific therapeutic management of various states throughout the body. The development of such a device has emerged as a significant alternative to other delivery platforms and has thus challenged the preconceived notions on what the transdermal market has to offer. In the addition, the research process governing the development of such drug delivery devices has the potential for the discovery and synthesis of novel polymer materials.

Attainment of the research objectives will, and has, permitted the presentation of the obtained results at conferences as well as and publication in peer-reviewed journals. With the potential for commercialization, the EMHM device can be patented. Innovative research into novel drug delivery systems forms a pivotal thrust of South Africa's research goals, through enhancement of the technological platform.

10. References

Abu-Saied, M.A., Abdel-Halim, E.S., Fouda, M.M.G., Al-Deyab, S.S., 2013. Preparation and Characterization of Iminated Polyacrylonitrile for the Removal of Methylene Blue from Aqueous Solutions. International Journal of Electrochemical Science 8, 5121-5135.

Alarcon, J.B., Hartley, A.W., Harvey, N.G., Mikszta, J.A., 2007. Preclinical evaluation of microneedle technology for intradermal delivery of influenza vaccines. Clinical and Vaccine Immunology 14 (4), 375-381.

Alexander, A., Dwivedi, S., Ajazuddin, Giri, T.K., Saraf, S., Saraf, S., Tripathi, D.K., 2012. Approaches for breaking the barriers of drug permeation through transdermal drug delivery. Journal of Controlled Release 164 (1), 26-40.

Allenby, A.C., Fletcher, J., Schock, C., Tees, T.F.S., 1969. The effect of heat, pH and organic solvents on the electrical impedance and permeability of excised human skin. British Journal of Dermatology 81, 31-39.

Almousa, A.A., Ikeda, R., Wada,M., Kuroda, N., Hanajirib,R., Nakashima, K., 2011. HPLC-UV method development for fentanyl determination in rat plasma and its application to elucidate pharmacokinetic behavior after i.p. administration to rats. Journal of Chromatography B 879, 2941- 2944.

Ameri, M., Maa, C.M., Daddona, P., 2006. *Microprojection array patch for transdermal delivery of vascular endothelial growth factors*. World International Property Organization, WO/2006/023684.

Annenkov, V.V., Danilovtseva, E.N., Tenhu, H., Aseyev, V., Hirvonen, S-P., Mikhaleva, A.I., 2004. Copolymers of 1-vinylimidazole and (meth)acrylic acid: Synthesis and polyelectrolyte properties. European Polymer Journal 40, 1027-1032.

Al-Qallaf, B., Das D.B., 2009. Optimizing microneedle arrays to increase skin permeability for transdermal drug. Annals of the New York Academy of Sciences 1161, 83-94.

Al-Qallaf, B., Das, D.B., Mori, D., Cui, Z., 2007. Modelling transdermal delivery of high molecular weight drugs from microneedle systems. Philosophical Transactions of the Royal Society A 365, 2951-2967.

Archer, D. F., Cullins, V., Creasy, D. W., Fisher, A. C., 2004. The impact of improved compliance with a weekly contraceptive transdermal system (Ortho Evra) on contraceptive efficacy. Contraception 69, 189-195.

Ariga, K., Yamauchi, Y., Rydzek, G., Ji, Q, Yonamine, Y., Wu, K. C.-W., Hill, J.P. 2014. Layer-by-layer nanoarchitectonics: invention, innovation, and evolution. Chemistry Letters 43, 36-68.

Arora A., Prausnitz M., Mitragotri S., 2008. Micro-scale Devices for Transdermal Drug Delivery. International Journal of Pharmaceutics 364(2), 227-236.

Arndt, K.-F., Richter, A., Ludwig, S., Zimmermann, J., Kressler, J., Kuckling, D., Adler, H.-J., 1999. Poly(vinyl alcohol)/poly(acrylic acid) hydrogels: FT-IR spectroscopic characterization of crosslinking reaction and work at transition point. Acta Polymerica 50, 383-390.

Aoyagi, S., Izumi, H., Isono, Y., Fukuda, M., Ogawa, H., 2007.Laser fabrication of high aspect ratio thin holes on biodegradable polymer and its application to a microneedle. Sensors and Actuators A: Physical 139, 293-302.

Autolab Application Note EC07, 2011. Comparison between Staircase Cyclic Voltammetry and Cyclic Voltammetry Linear Scan. Metrohm Autolab B.V.

Babita, K., Kumar, V., Rana, V., Jain, S., Tiwary, A.K., 2006. Thermotropic and spectroscopic behaviour of skin: relationship with percutaneous permeation enhancement. Current Drug Delivery 3, 95-113.

Baek, C., Han, M., Min, J., Prausnitz, M.R., Park, J-H., Park, J.H., 2011. Local transdermal delivery of phenylephrine to the anal sphincter muscle using microneedles. Journal of Controlled Release 154, 138-147.

Baird-Parker, A. C. (1962), The Occurrence and Enumeration, According To A New Classification, Of Micrococci And Staphylococci in Bacon and on Human and Pig Skin. Journal of Applied Bacteriology 25, 352-361.

Bajpai, A. K., Bajpai, J., Soni, S. N., 2009. Designing Polyaniline (PANI) and Polyvinyl Alcohol (PVA) Based Electrically Conductive Nanocomposites: Preparation, Characterization

and Blood Compatible Study. Journal of Macromolecular Science Part A-Pure and Applied Chemistry 46 (8), 774-782.

Bajpai, K., Bajpai, J., Soni, S. N., 2008. Preparation and characterization of electrically conductive composites of poly(vinyl alcohol)-g-poly(acrylic acid) hydrogels impregnated with polyaniline (PANI). eXPRESS Polymer Letters 2, 26-39.

Bal, S.M., Caussin, J., Pavel, S., Bouwstra, J.A., 2008. *In vivo* assessment of safety of microneedle arrays in human skin. European Journal of Pharmaceutical Sciences 35, 193-202.

Bal, S.M., Kruithof, A.C., Zwier, R., Dietz, E., Bouwstra, J.A., Lademann, J., Meinke, M.C., 2010. Influence of microneedle shape on the transport of a fluorescent dye into human skin *in vivo*. Journal of Controlled Release 147(2), 218-224.

Balci, N., Toppare, L., Bayramli, E., 1995. Conducting polymer composites of pyrrole with polyacrylic acid and epoxy matrices. Composites 26 (3), 229-231.

Banga, A.K., Chien, Y.W., 1993. Hydrogel-Based Iontotherapeutic Delivery Devices for transdermal Delivery of Peptide/Protein Drugs. Pharmaceutical Research 10 (5), 697-702.

Bariya, S.H., Gohel, M.C., Mehta, T.A., Sharma, O.P., 2012. Microneedles: an emerging transdermal drug delivery system. Journal of Pharmacy and Pharmacology 64, 11-29.

Barry, B., 2002. Transdermal drug delivery. In: E.M. Aulton, ed. 2002. *Pharmaceutics, The science of dosage forms design*. New York: Churchill Livingstone, pp. 499-33.

Barry, B., Williams, A., 2003. Penetration enhancers. Advanced Drug Delivery Reviews 56, 603-618.

Bawa, P., Pillay, V., Choonara, Y.E., du Toit, L.C., Ndesendo, V.M.K., Kumar, P., 2011. A Composite Polyelectrolytic Matrix for Controlled Oral Drug Delivery. AAPS PharmSciTech 12, 227-238.

Becker N., Thomsen, A.B., Olsen, A.K., Sjogren, P., Bech, P., Eriksen, J., 1997. Pain epidemiology and health related quality of life in chronic non-malignant pain patients referred to a Danish multidisciplinary pain center. Pain 73, 393-400.

Becker*,* H.*,* Gärtner*,* C.*,* 2008. Polymer Microfabrication Methods for Microfluidic Devices. Analytical and Bioanalytical Chemistry 390*,* 89-111.

Beresford, L. 2007 Pain at the Pump. Available from: http://www.the-hospitalist.org/details/article/233931/Pain_at_the_Pump.html [Last accessed 10 March 2012]

Bernkop-Schnurch, A., Hornof, B., 2003. Intravaginal Drug Delivery Systems. American Journal of Drug Delivery 1, 241-254.

Bhattarai, N, N., Gunn, J., Zhang, M., 2009. Chitosan-based hydrogels for controlled, localized drug delivery. Advanced Drug Delivery Reviews 62, 83-99.

BioRad Electrophoresis tech note 1156, Acrylamide Polymerization-A Practical Approach. Paul Menter. BioRad Laboratories.

Birchall, J.C., 2006. Microneedle array technology: the time is right but is the science ready? Expert Review of Medical Devices 3 (1), 1-4.

Birchall, J. C., Clemo, R., Anstey, A., John, D.N., 2011. Microneedles in Clinical Practice-An Exploratory Study into the Opinions of Healthcare Professionals and the Public. Pharmaceutical Research 28, 95-106.

Bond, J.R., Barry, B.W., 1988. Hairless Mouse Skin is Limited as a Model for Assessing the Effects of Penetration Enhancers in Human Skin. Journal of Investigative Dermatology 90, 810-813.

Boon, V., Glass, B., Nimmo, A., 2006. High-Performance Liquid Chromatographic Assay of Indomethacin in Porcine Plasma with Applicability to Human Levels. Journal of Chromatographic Science 44, 41-44.

Bos, J. D., Meinardi, M. M., 2000. The 500 Dalton rule for skin penetration of chemical compounds and drugs. Experimental Dermatology 9, 165-169.

Box G.E.P., Behnken D.W., 1960. Some new three level designs for the study of quantitative variables. Technometrics 2, 455-475.

Brodner, G., Mertes, N., Buerkle, H., Marcus, M.A., Van Aken, H., 2000. Acute pain management: analysis, implications and consequences after prospective experience with 6349 surgical patients. European Journal of Anaesthesiology 17,566- 575.

Brogden, N.K., Milewski, M., Ghosh, P., Hardi, L., Crofford, L.J., Stinchcomb, A.L., 2012. Diclofenac delays micropore closure following microneedle treatment in human subjects. Journal of Controlled Release 163(2), 220-229.

Bronaugh, R.L., Maibach, H.I., 1999. *Percutaneous Absorption: Drugs- Cosmetics-Mechanisms-Methodology*. New York, NY: Marcel Dekker.

Brown, M.B., Martin, G.P., Jones, S.A., Akomeah, F.K., 2006. Dermal and Transdermal Drug Delivery Systems: Current and Future Prospects. Drug Delivery 13, 175-187.

Burnette, R.R., Ongpipattanakul, B. (1988) Characterization of the pore transport properties and tissue alteration of excised human skin during iontophoresis. Journal of Pharmaceutical Sciences 77, 132-137.

Bystrova, S., Lüttge, R., 2011. Micromoulding for ceramic microneedle arrays, Microelectronic Engineering 88, 1681-1684.

Cai, W., Gupta, R. B. and Updated by Staff 2012. Hydrogels. Kirk-Othmer Encyclopedia of Chemical Technology. 1-20.

Caron, J.C., Queille-Roussel, C., Shah, V.P., Schaefer, H., 1990. The correlation between the drug penetration and vasoconstriction of hydrocortisone creams in human. Journal of the American Academy of Dermatology 23,458-462.

Chai, S.Y, Kim, Y.J., Jung, M.H., Chakraborty, A.K., Jung, D., Lee, W.I., 2009. Heterojunctioned $BiOCl/Bi_2O_3$, a new visible light photocatalyst. Journal of Catalysis 262,144-149.

Chaterji, S., Kwon, I.K., Park, K., 2007. Smart polymeric gels: Redefining the limits of biomedical devices. Progress in Polymer Science 32, 1083-1122.

Chen, C.H., LaRue, J.C., Nelson, R.D., Kulinsky, L., Madou, M.J., 2012. Electrical Conductivity of Polymer Blends of Poly (3, 4- ethylenedioxythiophene):

Poly(styrenesulfonate) : N-Methyl-2-pyrrolidinone and Polyvinyl Alcohol. Journal of Applied Polymer Science 125 (4), 3134-3141.

Chen, M-C., Huang, S-F., Lai, K-Y., Ling, M-H., 2013. Fully embeddable chitosan microneedles as a sustained release depot for intradermal vaccination. Biomaterials 34, 3077-3086.

Chen, X., Prow, T.W., Crichton, M.L., Jenkins, D.W.K., Roberts, M.S., Frazer, I.H., Fernando, G.J.P., Kendall, M.A.F., 2009. Dry-coated microprojection array patches for targeted delivery of immunotherapeutics to the skin. Journal of Controlled Release 139(3), 212-220.

Chiarello, K., 2004. Breaking the Barrier: Advances in Transdermal Technology. Pharmaceutical Technology, 46-56.

Chiranjib, B.D., Chandira, M., Jayakar, B., Sampath, K.P. 2010. Recent Advances in Transdermal Drug Delivery System. International Journal of PharmTech Research 2 (1), 68-77.

Choi, S.O., Rajaraman, S., Yoon, Y.K., Wu, X., Allen, M.G., 2006. 3-D Metal patterned microstructure using inclined UV exposure and metal transfer micromoulding technology, Solid-State Sensor, Actuator, and Microsystems Workshop, 2006.

Choonara, Y.E., Pillay, V., Ndesendo, V.M.K., du Toit, L.C., Kumar, P., Khan, R.A., Murphy, C.S., Jarvis, D-L., 2011. Design of Polymeric Nanoparticles by Synthetic Wet Chemical Processing Strategies for the Sustained Delivery of Anti-Tuberculosis Drugs. Colloids and Surfaces B: Biointerfaces 87, 243-254.

Choonara, Y.E., Pillay, V., Singh, N., Khan, R.A., Ndesendo, V.M.K., 2008. Chemometric, physicomechanical and rheological analysis of the sol–gel dynamics and degree of crosslinking of glycosidic polymers. Biomedical Materials 3, 1-15.

Choosakoonkriang, S., Lobo, B.A., Koe, G.S., Koe, J.G., 2003. Middaugh, C.R. Biophysical characterization of PEI/DNA complexes. Journal of Pharmaceutical Sciences 92, 1710-1722.

Chu, L.Y., Prausnitz, M.R., 2011. Separable arrowhead microneedles. Journal of Controlled Release 149,242-249.

Clar, E.J., Cambral, M., Sturelle, C., 1982. Study of skin horny layer hydration and restoration by impedance measurement. Cosmetics & Toiletries 97, 33-40.

Cogen, A.L., Nizet, V., Gallo, R.L., 2008. Skin microbiota: a source of disease or defence? British Journal of Dermatology 158(3), 442-455.

Cormier, M., Johnson, B., Ameri, M., Nyam, K., Libiran, L., Zhang, D.D., Daddona, P., 2004. Transdermal delivery of desmopressin using a coated microneedle array system. Journal of Controlled Release 97, 503-511.

Cosman, F., Lane, N.E., Bolognese, M.A., Zanchetta, J.R., Garcia-Hernandez, P.A., Sees, K., Matriano, J.A., Gaumer, K., Daddona, P.E., 2010. Effect of Transdermal Teriparatide Administration on Bone Mineral Density in Postmenopausal Women. The Journal of Clinical Endocrinology & Metabolism 95(1), 151-158.

da Silva Aquino, K.A., 2012. Sterilization by Gamma Irradiation, Gamma Radiation, Prof. Feriz Adrovic (ed.), ISBN: 978-953-51-0316-5, InTech, Available from: http://www.intechopen.com/books/gammaradiation/sterilization-by-gamma-irradiation

Dancik, Y., Jepps, O.G., Roberts, M.S., 2008. Beyond stratum corneum. In: M.S. Roberts, K.A. Walters, eds. 2008. *Dermal Absorption and Toxicity Assessment*. 2nd ed. New York: Informa Healthcare, pp. 209-250.

Davidson, A., Al-Qallaf, B., Das, D.B., 2008. Transdermal drug delivery by coated microneedles: Geometry effects on effective skin thickness and drug permeability. Chemical Engineering Research and Design 86 (11), 1196-1206.

Davies, D.H., Smith, J.D.B., Phillips, D.C., 1973. Copolymerization of acrylic acid with 1-substituted imidazoles. Macromolecules 6, 163-168.

Davies, D.J., Ward, R.J., Heylings, J.R., 2004. Multi-species assessment of electrical resistance as a skin integrity marker for *in vitro* percutaneous absorption studies. Toxicology *in Vitro* 18(3), 351-358.

Davis, S.P., Martanto, W., Allen, M.G., Prausnitz, M.R., 2005. Hollow metal microneedles for insulin delivery to diabetic rats. IEEE Transactions on Biomedical Engineering 52, 909-915.

Dawson, J.F., 2014. Moderation in Management Research: What, Why, When, and How. Journal of Business Psychology 29, 1-19.

Dejonckheere, M., Desjeux, L., Deneu, S., Ewalenko, P., 2001. Intravenous tramadol compared to propacetamol for postoperative analgesia following thyroidectomy. Acta anaesthesiologica Belgica 52, 29-33.

Delgado-Charro, M.B., Guy, R.H., 2001. Transdermal iontophoresis for controlled drug delivery and non-invasive monitoring, STP Pharma Sciences 11 (6), 403-414.

DeMuth, P. C., Min, Y., Huang, B., Kramer, A. J., Miller, A. D., Barouch, D. H., Hammond, P. T., Irvine, D. J., 2013. Polymer multilayer tattooing for enhanced DNA vaccination. Nature Materials 12, 367-376.

DeMuth, P.C., Moon, J.J., Suh, H., Hammond, P.T., Irvine, D. J., 2012. Releasable Layer-by-Layer Assembly of Stabilized Lipid Nanocapsules on Microneedles for Enhanced Transcutaneous Vaccine Delivery. ACS Nano 6, 8041-8051.

Dick, I.P., Scott, R.C., 1992. Pig ear skin as an in-vitro model for human skin permeability. Journal of Pharmacy and Pharmacology 44, 640-645.

Ding, Z., Verbaan, F.J., Bivas-Benita, M., Bungener, L., Huckriede, A., van den Berg, D.J., Kersten, G., Bouwstra. J.A., 2009. Microneedle arrays for the transcutaneous immunization of diphtheria and influenza in BALB/c mice. Journal of Controlled Release 136 (1), 71-78.

Doddaballapur, S., 2009. Microneedling with dermaroller. Journal of Cutaneous *and* Aesthetic Surgery 2, 110-111.

Donnelly, R.F., Singh, T.R.R., Alkilani, A.Z., McCrudden, M.T.C., O'Neill, S., O'Mahony, C., Armstrong, K., McLoone, N., Kole, P., Woolfson, A.D., 2013. Hydrogel-forming microneedle arrays exhibit antimicrobial properties: Potential for enhanced patient safety. International Journal of Pharmaceutics 451, 76- 91.

Donnelly, R.F., Singh, T.R.R., Tunney, M.M., Morrow, D.I.J., McCarron, P.A., O'Mahony, C., Woolfson, A.D., 2009. Microneedle Arrays Allow Lower Microbial Penetration Than Hypodermic Needles *In Vitro*. Pharmaceutical Research 26 (11), 2513-2522.

dos Reis, E.F., Campos, F.S., Lage, A.P., Leite, R.C., Heneine, L.G., Vasconcelos, W.L., Lobato,Z.I.P.,Mansur, H.S., 2006. Synthesis and Characterization of Poly (Vinyl Alcohol) Hydrogels and Hybrids for rMPB70 Protein Adsorption. Materials Research 9 (2), 185-191.

Doukas, A., 2004. Transdermal delivery with a pressure wave. Advanced Drug Delivery Reviews 56, 559-579.

Dreher, F., Modjtahedi, B.S., Modjtahedi, S.P., Maibach, H.I., 2005. Quantification of stratum corneum removal by adhesive tape stripping by total protein assay in 96-well microplates. Skin Research and Technology 11, 97-101.

Du Toit, L.C. A Bioresponsive Polymeric Implant for Site-Specific Prolonged Drug Delivery. A thesis submitted to the Faculty of Health Sciences, University of the Witwatersrand, in fulfilment of the requirements for the degree of Doctor of Philosophy, 2013.

Duncan, J.I., Payne, S.N., Winfield, A.J., Ormerod, A.D., Thomson, A.W., 1990. Enhanced percutaneous absorption of a novel topical cyclosporin A formulation and assessment of its immunosuppressive activity, British Journal of Dermatology 123,631-640.

Durrheim, H., Flvnn. G. L., Himchi. W. I., Behl. C. R., 1980. Permeation of hairless mouse skin I: Experimental methods and comparison with human epidermal permeation by alkanols. Journal of Pharmaceutical Sciences 69 (7), 781-786.

Edelberg, R., 1972. Electrical activity of the skin. Its measurement and uses in psychophysiology. In: N.S. Greenheld, R.A. Sternbach, eds. *Handbook of Psychophysiology*. New York: Holt, Rinehart, and Winston, pp. 367-418.

Elahi, M., Inayat, Q., Wazir, F., Huma, Z., 2009. Adaptation of Rat Gastric Mucosa Exposed to Indomethacin: A Histological Study. Gomal Journal of Medical Sciences July-December 7(2), 143-148.

El-Yazigi, A., Sawchuk, R.J., 1985. *In vitro-in vivo* correlation and dissolution studies with oral theophylline dosage forms. Journal of Pharmaceutical Sciences 74, 161-164.

Elliott, J.E., Macdonald, M., Nie, J., Bowman, C.N., 2004. Structure and swelling of poly(acrylic acid) hydrogels: effect of pH, ionic strength, and dilution on the crosslinked polymer structure. Polymer 45, 1503-1510.

Emami, J., 2006. *In vitro - In vivo* Correlation: From Theory to Applications. Journal of Pharmaceutical Sciences 9, 31-51.

Escobar-Chávez, J.J., Bonilla-Martínez, D., Villegas-González, M.A., Molina-Trinidad, E., Casas-Alancaster, N., Revilla-Vázquez, A.L., 2011. Microneedles: A Valuable Physical Enhancer to Increase Transdermal Drug Delivery. The Journal of Clinical Pharmacology 51, 964-977.

Fang, J. Y., Sung, K.C., Wang, J.J., Chu, C.C., Chen, K.T., 2002. The effects of iontophoresis and electroporation on transdermal delivery of buprenorphine from solutions and hydrogels. Journal of Pharmacy and Pharmacology 54(10), 1329-37.

Festing, S., Wilkinson, R. 2007. The ethics of animal research. Talking Point on the use of animals in scientific research. EMBO Reports 8(6), 526-530.

Fischer, G.A., 2005. Iontophoretic drug delivery using the IOMED Phoresor® system. Expert Opinion on Drug Delivery 2(2), 391-403.

Fisher, F.B., 2004. The Role of Controlled-Release Opioids in the Treatment of Chronic Pain. Journal of American Physicians and Surgeons 9, 52-54.

Flynn, G., Yalkowsky, S. H., Roseman, T. J., 1974. Mass transport phenomena and models. Journal of Pharmaceutical Sciences 63, 479-510.

Flynn, G.L., 1979. Topical drug absorption and topical pharmaceutical systems. In: G.S. Banker, C.T. Rhodes, eds. 1979. *Modern Pharmaceutics.* New York: Marcel Dekker, pp. 263.

Frank, D.H., Roe, D.J., Sherry Chow, H-H., Guillen, J.M., Choquette, K., Gracie D., Francis, J., Fish , A., Alberts, D.S., 2004. Effects of a High-Selenium Yeast Supplement on Celecoxib Plasma Levels A Randomized Phase II Trial. Cancer Epidemiology, Biomarkers & Prevention 13, 299-303.

Fukushima, K., Ise, A., Morita, H., Hasegawa, R., Ito, Y., Sugioka, N., Takada, K., 2011. Two-layered dissolving microneedles for percutaneous delivery of peptide/protein drugs in rats. Pharmaceutical Research 28, 7-21.

Galambos, A. F., Stockton, W. B., Koberstein, J. T., Sen, A., Weiss, R. A., 1987. Observation of cluster formation in an ionomer. Macromolecules 20, 3091-3094.

Gardeniers, H.J.G.E., Lüttge, R., Berenschot, E.J.W., de Boer, M.J., Yeshurun, S.Y., Hefetz, M.,van't Oever, R., van den Berg, A., 2003. Silicon micromachined hollow microneedles for transdermal liquid transport. Journal of Microelectromechanical Systems 12(6), 855-862.

Gaudana, R., Jwala, J., Boddu, S.H.S., Mitra, A.K., 2008. Recent Perspectives in Ocular Drug Delivery. Pharmaceutical Research 26, 1197-1216.

Geetha, S., Rao, C.R.K., Vijayan, M., Trivedi, D.C., 2006. Biosensing and drug delivery by polypyrrole. Analytica Chimica Acta 568, 119-125.

Gerstel, M. S., Place, V. A. 1976. Drug delivery device. Patent (serial number *U.S. 3,964, 482*).

Gill, H.S., Prausnitz, M.R., 2007. Coated microneedles for transdermal delivery. Journal of Controlled Release 117, 227-237.

Giménez-Martín, E., Ontiveros-Ortega, A., Espinosa-Jiménez, M., Perea-Carpio, R., 2007. Electrokinetic effect and surface free energy behavior in the adsorption process of a reactive dye onto Leacril pretreated with polyethyleneimine ion. Journal of Colloid and Interface Science 311, 394-399.

Giri, A., Bhowmick, M., Pal, S., Bandyopadhyay, A., 2011. Polymer hydrogel from carboxymethyl guar gum and carbon nanotube for sustained trans-dermal release of diclofenac sodium. International Journal of Biological Macromolecules 49, 885-893.

Giudice, E.L., Campbell, J.D., 2006. Needle-free vaccine delivery. Advanced Drug Delivery Reviews 58, 68-89.

Golden, G.M., Guzek, D.B., Harris, R.R., McKie, J.E., Potts, R.O., 1986. Lipid thermotropic transitions in human stratum corneum. Journal of Investigative Dermatology 86, 255-259.

Grass, J., 2005. Patient-Controlled Analgesia. Anesthesia & Analgesia 101, S44 -S61.

Gratieri, T., Alberti, I., Lapteva, M., Kalia, Y.N., 2013. Next generation intra-and transdermal therapeutic systems: Using non- and minimally-invasive technologies to increase drug delivery into and across the skin. European Journal of Pharmaceutical Sciences 50(5), 609-622.

Gray, G.M., Yardley, H.J., 1975. Lipid compositions of cells isolated from pig, human, and rat epidermis. Journal of Lipid Research 16, 434-440.

Gudeman, L.F., Peppas, N.A., 1995. pH-Sensitive membrane from poly(vinyl alcohol)/poly(acrylic acid) interpenetrating networks. Journal of Membrane Science 107, 239-248.

Guiseppi-Elie, A., 2010. Electroconductive hydrogels: Synthesis, characterization and biomedical applications. Biomaterials 31, 2701-2716.

Gurnasinghani, M.L., Bhatt, H.R., Lalla, J.K., 1989. Indomethacin delivery from matrix controlled release indomethacin tablets. Journal of Controlled Release 8, 211-222.

Hamidi, M., Azadi, A., Rafiei, P., 2008. Hydrogel nanoparticles in drug delivery. Advanced Drug Delivery Reviews 60, 1638-1649.

Hamilton, G., Baskett, T., 2000. In the arms of Morpheus: the development of morphine for postoperative pain relief. Canadian Journal of Anesthesia 47, 367-374.

Harada, K., Murakami, T., Kawasaki, E., Hagashi, Y., Yamamoto, S., Yata, N., 1993. *In vitro* skin permeability to salicylic acid of human, rodent and shed snake skin. Journal of Pharmacy and Pharmacology 45, 414-418.

Hassan, C.M., Peppas, N.A., 2000. Structure and Applications of Poly(vinyl) alcohol hydrogels produced by conventional crosslinking or by freeze/thawing methods. Advances in Polymer Science 153, 37-65.

Haq, M.I., Smith, E., John, D.N., Kalavala, M., Edwards, C., Anstey, A., Morrissey, A., Birchall, J.C., 2009. Clinical administration of microneedles: skin puncture, pain and sensation. Biomed Microdevices 11, 35-47.

He, W., Guo, X., Xiao, L., Feng, M., 2009. Study on the mechanisms of chitosan and its derivatives used as transdermal penetration enhancers. International Journal of Pharmaceutics 382, 234-243.

Hedge, N.R., Kaveri, S.V., Bayry J., 2011. Recent advances in the administration of vaccines for infectious diseases: microneedles as painless delivery devices for mass vaccination. Drug Discovery Today 16 (23/24), 1061-1068.

Hemmati, A.A., Arzi, A., Sistani, N.S., Mikaili, P., 2010. The Hydro-Alcoholic Extract of Pomegranate Seed Has Anti-Inflammatory Effects on Formalin-Induced Inflammation in Rat Hind Paw. Research Journal of Biological Sciences 5 (8), 561-564.

Hennink, W.E., van Nostrum, C.F., 2002. Novel crosslinking methods to design Hydrogels. Advanced Drug Delivery Reviews 54, 13-36.

Henry, S., McAllister, D.V., Allen, M.G., Prausnitz, M.R., 1998. Microfabricated microneedles: a novel approach to transdermal drug delivery. Journal of Pharmaceutical Sciences 87 (8), 922-925.

Heylings, J. R., Clowes, H.M., Hughes, L., 2001. Comparison of tissue sources for the skin integrity function test (SIFT). Toxicology *in Vitro* 15, 597-600.

Hinz, R.S., Hodson, C.D., Lorence, C.R., Guy., R.H., 1989. *In Vitro* Percutaneous Penetration: Evaluation of the Utility of Hairless Mouse Skin. Journal of Investigative Dermatology 93, 87-91.

Hoare, T.R., Kohane, D.S., 2008. Hydrogels in drug delivery: Progress and challenges. Polymer 49, 1993-2007.

Hoff J., 2000. Methods of blood collection in the mouse. Lab Animal 29(10), 47- 53.

Hotchkiss, S.A.M., 1998. Dermal metabolism. In: M.S. Roberts, K.A. Walters, eds. *Dermal Absorption and Toxicity Assessment*, 2nd ed. 1998. New York: Informa Healthcare, pp.43-101.

Hube, B., 2004. From commensal to pathogen: stage- and tissue-specific gene expression of *Candida albicans*. Current Opinion in Microbiology 7, 336-341.

Hui, X., Anigbogu, A., Singh, P., Xiong, G., Poblet, N., Liu, P., Maibach, H.I, 2001. Journal of Pharmaceutical Sciences 90(9), 1269-1276.

Iler, R.K., 1966. Multilayers of colloidal particles, Advances in Colloid and Interface Science 21, 569-594.

Im, J.S., Bai, B., Lee, Y.S., 2010. The effect of carbon nanotubes on drug delivery in an electro-sensitive transdermal drug delivery system. Biomaterials 31, 1414-1419.

Institute of Medicine Report from the Committee on Advancing Pain Research, Care, and Education. Relieving Pain in America, A Blueprint for Transforming Prevention, Care, Education and Research. Accessed 16 January 2013, at: http://books.nap.edu/openbook.php? record id=13172&page=1.

Ito, Y., Hasegawa, R., Fukushima, K., Sugioka, N., Takada, K., 2010. Self-dissolving micropile array chip as percutaneous delivery system of protein drug, Biological and Pharmaceutical Bulletin 33, 683-690.

Izuka, A., Winter, H.H., Hashimoto, T., 1992. Molecular weight dependence of viscoelasticity of polycaprolactone critical gels. Macromolecules 25, 2422-2428.

Jacobi, U., Kaiser, M., Toll, R., Mangelsdorf, S., Audring, H., Otberg, N., Sterry, W., 2007. Lademann Porcine ear skin: an *in vitro* model for human skin. Skin Research and Technology 13, 19-24.

Jacobsen, J., 2001. Buccal iontophoretic delivery of atenolol.HCl employing a new *in vitro* three-chamber permeation cell. Journal of Controlled Release 70(1-2), 83-95.

Jagur-Grodzinski, J., 2010. Polymeric gels and hydrogels for biomedical and pharmaceutical applications. Polymers for Advanced Technologies 21, 27-47.

Jambhekar, S.S., Breen, P.J., 2009. Basic Pharmaceutics. London: Pharmaceutical Press.

Jeffs, S.A., Hall, J.E., Morris S., 2002. Comparison of morphine alone with morphine plus clonidine for postoperative patient-controlled analgesia. British Journal of Anaesthesia 89, 424-427.

Jianqi, F., Lixia, G., 2002. PVA/PAA thermo-crosslinking hydrogel fiber: preparation and pH-sensitive properties in electrolyte solution. European Polymer Journal 38, 1653-1658.

Joshi, K., 2008. Dissertation: Transdermal Drug Delivery Systems and Their Use of Polymers. [pdf]. Available at: < http://www.engr.sjsu.edu/bmes/assets/papers/Joshi_Kasturi.pdf > [Accessed 6 March 2012].

Jung, P.G., Lee, T.W., Oh, D.J., Hwang, S.J., Jung, I.D., Lee, S.M., Ko, J.S., 2008. Nickel microneedles fabricated by sequential copper and nickel electroless plating and copper chemical wet etching. Sens Mater 20, 45-53.

Juul, K.A., Bengtsson, H., Eyving, B., Kildegaard, J., Lav, S., Poulsen, M., Serup, J., Stallknecht, B., 2012. Influence of hypodermic needle dimensions on subcutaneous injection delivery-a pig study of injection deposition evaluated by CT scanning, histology, and backflow. Skin Research and Technology 18(4), 447-455.

Kalia, Y.N., Alberti, I., Naik, A., Guy, R.H., 2001. Assessment of topical bioavailability *in vivo*: the importance of stratum corneum thickness. Skin Pharmacology and Applied Skin Physiology 14, 82-86.

Kalia, Y.N., Naik, A., Garrison, J., Guy, R.H., 2004. Iontophoretic drug delivery. Advanced Drug Delivery Reviews 56, 619-658.

Karande, P., Mitragotri, S., 2003. Dependence of skin permeability on contact area. Pharmaceutical Research 20,257-263.

Katzung, B.G., 2007. Basic and Clinical Pharmacology 10th Ed. McGraw-Hill Medical, New York, USA.

Kim, J.D., Kim, M., Yang, H., Lee, K., Jung, H., 2013. Droplet-born air blowing: Novel dissolving microneedle fabrication. Journal of Controlled Release 170(3), 430-436.

Kim, K.S., Simon, L., 2011. Modeling and design of transdermal drug delivery patches containing an external heating device. Computers & Chemical Engineering 35, 1152-1163.

Kim, Y.C., Quan, F.S., Yoo, D.G., Compans, R.W., Kang, S.M., Prausnitz, M.R., 2009. Improved influenza vaccination in the skin using vaccine coated microneedles. Vaccine 27, 6932-6038.

Kim, Y-C., Park, J-H, Prausnitz, M.R., 2012. Microneedles for drug and vaccine delivery. Advanced Drug Delivery Reviews 64 (14), 1547- 1568.

Kirkland, J.J., 1956. Porous Thin-Layer Modified Glass Bead Supports for Gas Liquid Chromatography. Analytical Chemistry 37, 1458-1461.

Knutson, K., Potts, R.O., Guzek, D.B., Golden, G.M., McKie, J.E. Lambert, W.J., Higuchi, W.I., 1985. Macro and molecular physical chemical considerations in understanding drug transport in the stratum corneum. Journal of Controlled Release 2, 67-87.

Kolawole O.A., Pillay V. and Choonara Y.E., 2007. Novel Polyamide 6,10 Variants Synthesized by Modified Interfacial Polymerization for Application as a Rate-Modulated Monolithic Drug Delivery System.Journal of bioactive and compatible polymers 22, 281-313.

Kumar, P., Pillay, V., Choonara, Y.E., Modi, G., Naidoo, D., du Toit, L.C., 2011. In silico theoretical molecular modeling for Alzheimer's disease: The nicotine-curcumin paradigm in neuroprotection and neurotherapy. International Journal of Molecular Sciences 12, 694-724.

Kumar, P., Choonara, Y.E., du Toit, L.C., Modi, G., Naidoo, D., Pillay, V., 2012. Novel High-Viscosity Polyacrylamidated Chitosan for Neural Tissue Engineering: Fabrication of Anisotropic Neurodurable Scaffold via Molecular Disposition of Persulfate-Mediated Polymer Slicing and Complexation. International Journal of Molecular Sciences 13, 13966-13984.

Kumar, R., Philip, A., 2007. Modified Transdermal Technologies: Breaking the Barriers of Drug Permeation via the Skin. Tropical Journal of Pharmaceutical Research 6 (1), 633-644.

Kumamoto, C.A., 2011. Inflammation and gastrointestinal Candida colonization. Current Opinion in Microbiology 14, 386-339.

Lacroix S., Rivest S., 1996. Role of cyclo-oxygenase pathways in the stimulatory influence of immune challenge on the transcription of a specific CRF receptor subtype in the rat brain. Journal of Chemical Neuroanatomy 10(1), 53-71.

Langer, R., 2004. Transdermal drug delivery: past progress, current status, and future prospects. Advanced Drug Delivery Reviews 56, 557-558.

Lallemand, F., Felt-Baeyens, O., Besseghir, K., Behar-Cohen, F., Gurny, R., 2003. Cyclosporine A delivery to the eye: a pharmaceutical challenge. European Journal of Pharmaceutics and Biopharmaceutics 56, 307-318.

Larsen, W. A., McCleary, S. J., 1972. The Use of Partial Residual Plots in Regression Analysis. Technometrics 14, 781-790.

Lavon, I., Grossman, N., Kost, J., 2005. The nature of ultrasound-SLS synergism during enhanced transdermal transport. Journal of Controlled Release 107,484-494.

Lawler, J.C., Davis, M.J., Griffith, E.C., 1960. Electrical characteristics of the skin. The impedance of the surface sheath and deep tissues. Journal of Investigative Dermatology 34, 301-308.

Lawson, P. T., 2000. Laboratory Animal Technician Training Manual, American Association for Laboratory Animal Science.

Lee, H., Jeon, H.Y., Park, S., Lee, H., Bae, S., 2011. Micro Needle Array Fabrication for Drug Delivery and Drug Delivery Evaluation Test Using Optical Inspection Module. IPCBEE 2, 101-104.

Lee, J.N., Park, C., Whitesides, G.M., 2003. Solvent Compatibility of Poly(dimethylsiloxane)-Based Microfluidic Devices. Analytical Chemistry 75, 6544-6554.

Lee, K. Y., Mooney, D. J., 2001. Hydrogels for Tissue Engineering. Chemical Reviews 101, 1869-1879.

Lee, K., Jung, H., 2012. Drawing lithography for microneedles: A review of fundamentals and biomedical Applications. Biomaterials 33, 7309-7326.

Lee, K., Lee, C.Y., Jung, H., 2011. Dissolving microneedles for transdermal drug administration prepared by stepwise controlled drawing of maltose. Biomaterials 32, 3134-3140.

Lee, P. J., Ahmad, N., Langer, R., Mitragotri, S., Prasad Shastri, V., 2006. Evaluation of chemical enhancers in the transdermal delivery of lidocaine. International Journal of Pharmaceutics 308, 33-39.

Lehmann, K.A., 2005. Recent Developments in patient controlled analgesia. Journal of Pain and Symptom Management 29 (5), 72-89.

Levin, M., 2006. Pharmaceutical process scale-up. In: M. Levin, ed. 2006. *Drugs and the Pharmaceutical Sciences*. Taylor & Francis, pp. 464.

Lewandowski, W., Jacobson, A., 2011. Bridging the Gap between Mind and Body: A Biobehavioral Model of the Effects of Guided Imagery on Pain, Pain Disability, and Depression. ACNS-BC Pain Management Nursing, 1-11.

Li, Q., Weina, P., Milhous, W.K., 2007. Pharmacokinetic and pharmacodynamics profiles of rapid-acting artemisinins in the antimalarial therapy. Current Drug Therapy 2, 210-223.

Li, T., Fang, L., Ren, C., Wang, M., Zhao, L., 2008. Determination of transdermally and orally applied indomethacin in rat plasma and excised skin and muscle samples. Asian Journal of Pharmaceutical Sciences 3(6), 269-275.

Li, W. Z.,Huo,M.R.,Zhou,J.P.,Zhou,Y.Q.,Hao,B.H.,Liu,T.,Zhang,Y.,2010.Super-short solid silicon microneedles for transdermal drug delivery applications. International Journal of Pharmaceutics, 389, 122-129.

Lin, C., Metters, A.T., 2006. Hydrogels in controlled release formulations: Network design and mathematical modeling. Advanced Drug Delivery Reviews 58, 1379-1408.

Lin, S.Y., Hou, S.J., Hsu, T.H.S., Yeh, F.L., 1992. Comparisons of different animal skins with human skin in drug percutaneous absorption studies. Methods and Findings in Experimental and Clinical Pharmacology 14, 645-654.

Liu, S., Jin, M-N., Quan, Y-S., Kamiyama, F., Kusamori, K., Katsumi, H., Sakane, T., Yamamoto, A., 2012. The development and characteristics of novel microneedle arrays fabricated from hyaluronic acid, and their application in the transdermal delivery of insulin. Journal of Controlled Release 161(3), 933-941.

Liu, S., Jin, M-N., Quan, Y-S., Kamiyama, F., Kusamori, K., Katsumi, H., Sakane, T., Yamamoto, A., 2013. Transdermal delivery of relatively high molecular weight drugs using novel self-dissolving microneedle arrays fabricated from hyaluronic acid and their characteristics and safety after application to the skin. European Journal of Pharmaceutics and Biopharmaceutics 86 (2), 267-276.

Liu, T.X., Liu, Z.H., Ma, K.X., Shen, L., Zeng, K.Y., He, C.B., 2003. Morphology, thermal and mechanical behavior of polyamide 6/layered-silicate nanocomposites. Composites Science and Technology 63, 4331-4337.

Liu, Y., Servant, A., Guy, O.J., Al-Jamal, K.T., Williams, P.R., Hawkins, K.M., Kostarelos, K., 2011. An Electric-field Responsive Microsystem for Controllable Miniaturised Drug Delivery Applications. Procedia Engineering 29, 984-987.

Lojou, E., Bianco, P., 2007. Key role of the anchoring PEI layer on the electrochemistry of redox proteins at carbon electrodes Consequences on assemblies involving proteins and clay. Electrochimica Acta 52, 7307-7314.

Luiz, L.M.; de Torresi, S.I.C., 2005. Conducting polymer-hydrogel composites for electrochemical release devices: Synthesis and characterization of semi-interpenetrating polyaniline-polyacrylamide networks. Electrochemistry Communications *7*, 717-723.

Lüttge, R., Berenschot, E.J.W., de Boer, M.J., Altpeter, D.M., Vrouwe, E.X. van den Berg, A., Elwenspoek, M., 2007. Integrated Lithographic Molding for Microneedle-Based Devices. Journal of Microelectromechanical Systems 16 (4), 872-884.

McAllister, D.V., Wang, P.M., Davis, S.P., Park, J.H., Canatella, P.J., Allen, M.G., Prausnitz., M.R., 2003. Microfabricated needles for transdermal delivery of macromolecules and nanoparticles: fabrication methods and transport studies. PNAS 100 (24), 13755-13760.

McCann, M.T., Gilmore, B.F., Gorman, S.P., 2008. Staphylococcus epidermidis device-related infections: pathogenesis and clinical management. Journal of Pharmacy and Pharmacology 60, 1551-1571.

Magda, J., Cho, C-H., Streitmatter, S., Jevremovic, T., 2014. Effects of gamma rays and neutron irradiation on the glucose response of boronic acid-containing "smart" hydrogels. Polymer Degradation and Stability 99, 219-222.

Matriano, J.A., Cormier, M., Johnson, J., Young, W.A., Buttery, M., Nyam, K., Daddona, P.A., 2002. Macroflux microprojection array patch technology: a new and efficient approach for intracutaneous immunization. Pharmaceutical Research 19, 63-70.

Martanto, W., Moore, J.S., Couse, T., Prausnitz, M.R., 2006. Mechanism of fluid infusion during microneedle insertion and retraction. Journal of Controlled Release 112(3), 357-361.

Martin, C.J., Allender, C.J., Brain, K.R., Morrissey, A., Birchall, J.C., 2012. Low temperature fabrication of biodegradable sugar glass microneedles for transdermal drug delivery applications. Journal of Controlled Release 158, 93-101.

Matsuo, K., Hirobe, S., Yokota, Y., Ayabe, Y., Seto, M., Quan, Y-S., Kamiyama, F., Tougan, T., Horii, T., Mukai, Y., Okada, N., Nakagawa, S., 2012. Transcutaneous immunization using a dissolving microneedle array protects against tetanus, diphtheria, malaria, and influenza. Journal of Controlled Release 160(3), 495-501.

Merino, V., López, A., Kalia, Y.N., Guy, R.H., 1999. Electrorepulsion versus electroosmosis: effect of pH on the iontophoretic flux of 5-fluorouracil. Pharmaceutical Research 16, 758-761.

Merkel, T.C., Bondar, V.I., Nagai, K., Freeman, B.D., Pinnau, I.J., 2000. Gas sorption, diffusion, and permeation in poly(dimethylsiloxane). Journal of Polymer Science, Part B: Polymer Physics Part B 38, 415-434.

Merskey H. &Bogduk N., eds., 1994. *Classification of chronic pain: descriptions of chronic pain syndromes and definitions of pain terms,* 2nd ed. Seattle, WA: International Association for the Study of Pain Press.

Milligan, K., Lanteri-Minet, M., Borchert, K., Helmers, H., Donald, R., Kress, H.G., Adriaensen, H., Moulin, D., Järvimäki, V., Haazen, L., 2001. Evaluation of long term efficacy and safety of transdermal fentanyl in the treatment of chronic noncancer pain. Journal of Pain 2, 197-204.

Mitragotri, S., Ray, D., Farrell, J., Tang, H., Yu, B., Kost, J., Blankschtein, D., Langer, R., 2000. Synergistic effect of low-frequency ultrasound and sodium lauryl sulfate on transdermal transport. Journal of Pharmaceutical Sciences 89,892-900.

Mohamadnia, Z., Zohuriaan-Mehr, A.J., Kabiri, K., Jamshidi, A., Mobedi, H., 2007. pH-sensitive IPN hydrogel beads of carrageenan-alginate for controlled drug delivery. Journal of Bioactive and Compatible Polymers 22(3), 342-356.

Mohr, T., Akers, T.K., Wessman, H.C., 1987. Effect of High Voltage Stimulation on Blood Flow in the Rat Hind Limb. Physical Theapy 67(4), 526-533.

Morales, M.E., Gallardo Lara V., Calpena, A.C., Domenech J, Ruiz, M.A., 2004. Comparative study of morphine diffusion from sustained release polymeric suspensions. Journal of Controlled Release 95, 75-81.

Morales, M.E., Lopez G., Gallardo V., Ruiz, M. A., 2011. Oral Suspensions of Morphine Hydrochloride for Controlled Release: Rheological Properties and Drug Release. Molecular Pharmaceutics 8, 629-634.

Moreira, H.R., Munarib, F., Gentilini, R., Visai, L., Granja, P.L., Tanzi, Petrini, P., 2014. Injectable pectin hydrogels produced by internal gelation: pH dependence of gelling and rheological properties. Carbohydrate Polymers 103, 339-347.

Mudry, B., Carrupt, P., Guy, R.H., Delgado-Charro, M.B., 2007. Quantitative structure-permeation relationship for iontophoretic transport across the skin. Journal of Controlled Release 122(2), 165-172.

Murdan, S., 2003. Electro-responsive drug delivery from hydrogels. Journal of Controlled Release 92, 1-17.

Murdoc, C.J., Crooks, B.A., Miller, C.D., 2002. Effect of the addition of ketamine to morphine in patient controlled analgesia. Anaesthesia 57, 484-488.

Nagasaki, G., Tanaka, M., Saito, A., Sato, M., Nishikawa, T., 2002. Postoperative analgesia with morphine with or without diclofenac after shoulder surgery. Masui 51, 846-850.

Naficy, S., Brown, H.R., Razal, J.M., Spinks, G.M., Whitten, P.G., 2011. Progress Toward Robust Polymer Hydrogels. Australian Journal of Chemistry 64, 1007-1025.

Naik, A., Kalia, Y.N., Guy, R.H., 2000. Transdermal drug delivery: overcoming the skin's barrier function. Pharmaceutical Science & Technology Today 3(9), 318-326.

Namdeo, T.B, Vidaya, R.I., Sushi, S.I.S.P., 2010. The Effects of Lactose, Microcrystalline Cellulose and Dicalcium Phosphate on Swelling and Erosion of Compressed HPMC Matrix Tablets: Texture Analyzer. Iranian Journal of Pharmaceutical Research 9(4),349-358.

Nanjundswamy, N.G., Dasankoppa, F.S., Sholapur, H.N., 2009. A Review on Hydrogels and Its Use in In Situ Ocular Drug Delivery. Indian Journal of Novel Drug Delivery 1(1), 11-17.

O'Brien, T., Breivik, H., 2012. The impact of chronic pain-European patients' perspective over 12 months. Scandinavian Journal of Pain 3, 23-29.

O'Connell, E.M., Peiffer, D.G., Root, T.W., Cooper, S.L., 1996. Morphological Studies of Lightly Sulfonated Polystyrene Using ^{23}Na NMR: Effects of Polydispersity in Molecular Weight. Macromolecules 29, 2124-2130.

O´Neil G., Paech, M., Wood, F., 1997. Preliminary clinical use of a patient controlled intranasal analgesia (PCINA) device. Anaesth Intensive Care 25, 408-412.

Ochoa, M., Mousoulis, C., Ziaie B., 2012. Polymeric microdevices for transdermal and subcutaneous drug delivery. Advanced Drug Delivery Reviews 64, 1603-1616.

Ogiso, T., Aki, M., Ku, T., 1993. Effect of Various Enhancers on Transdermal Penetration of Indomethacin and Urea, and Relationship between Penetration Parameters and Enhancement Factors. Journal of Pharmaceutical Sciences 84 (4), 482-488.

Oh, S.Y., Leung, L., Bommannan, D., Guy. R.H., Potts, R.O., 1993. Effect of current, ionic strength and temperature on the electrical properties of skin. Journal of Controlled Release 27, 115-125.

Okay, O., Sariisik, S.B., Zor, S.D., 1998. Swelling Behavior of Anionic Acrylamide-Based Hydrogels in Aqueous Salt Solutions: Comparison of Experiment with Theory. Journal of Applied Polymer Science 70, 567-575.

Ongpipattanakul, B., Francoeur, M. L., Potts, R. O., 1994. Polymorphism in stratum corneum lipids. Biochimica et Biophysica Acta 1190, 115-122.

Pain Research Center, University of Utah, 2012. Advantages and disadvantages of pain therapies. [online] Available at: < http://www.painresearch.utah.edu/cancerpain/table8.html > [Accessed 23 March 2012]

Painter, J., 2005. Pain Management and Patient-Controlled Analgesia. In: Center for Safety and Clinical Excellence, *Pain Management and Patient-Controlled Analgesia: Improving Safety and Quality of Care.* San Diego, California 17-18 November 2005.carefusion.com: CareFusion.

Pakravan, M., Heuzey, M.C., Ajjia, A., 2011. A fundamental study of chitosan/PEO electrospinning. Polymer 52, 4813-4824.

Pararas, E.E.L., Borkholder, D.A., Borenstein, J.T., 2012. Microsystems technologies for drug delivery to the inner ear. Advanced Drug Delivery Reviews 64, 1650-1660.

Park, J.H, Allen, M.G., Prausnitz, M.R., 2005. Biodegradable polymer microneedles: Fabrication, mechanics and transdermal drug delivery. Journal of Controlled Release, 104, 51-66.

Park, J.H., Choi, S.O., Kamath, R., Yoon, Y.K., Allen, M.G., Prausnitz, M.R., 2007. Polymer particle-based micromoulding to fabricate novel microstructures. Biomedical Microdevices, 9, 223-234.

Pattani, A., McKay, P.F., Garland, M.J., Curran, R.M., Migalska, K., Cassidy, C.M., Malcolm, R.K., Shattock, R.J., McCarthy, H.O., Donnelly, R.F., 2012. Microneedle mediated intradermal delivery of adjuvanted recombinant HIV-1 CN54gp140 effectively primes mucosal boost inoculations. Journal of Controlled Release 162(3), 529-537.

Paudel, K.S., Milewski, M., Swadley, C.L., Brogden, N.K., Ghosh, P., Stinchcomb, A.L., 2010. Challenges and opportunities in dermal/transdermal delivery. Therapeutic Delivery 1, 109-131.

Pekel, N., Guner, A., Guven, O., 2002. Conductometric and viscometric investigation of poly(*N*-vinylimidazole)-metal ion complex formation. Journal of Applied Polymer Science 85, 376-384.

Percec, V., Bera, T.K., 2002. A New Strategy for the Preparation of Supramolecular Neutral Hydrogels. Biomacromolecules 3, 272-279.

Perennes ,F. , Marmiroli ,B. , Matteucci , M. , Tormen , M., Vaccari , L. , DiFabrizio , E., 2006. Sharp bevelled tip hollow microneedle arrays fabricated by LIGA and 3D soft lithography with polyvinylalcohol. Journal of Micromechanics and Microengineering 16, 473-479.

Posadas, D., Florit, M.I., 2004. The redox switching of electroactive polymers. Journal of Physical Chemistry B 108, 15470-15476.

Prabu, S.L., Suriyaprakash T. N. K., 2012. Extraction of Drug from the Biological Matrix: A Review, Applied Biological Engineering - Principles and Practice, Dr. Ganesh R. Naik (Ed.), ISBN: 978-953-51-0412-4, InTech, DOI: 10.5772/32455. Available from: http://www.intechopen.com/books/applied-biological-engineering-principles-and-practice/extraction-of-the-drug-from-the-biological-matrix

Prausnitz, M.R., 2004. Microneedles for transdermal drug delivery. Advanced Drug Delivery Reviews 56, 581- 587.

Prausnitz, M.R., Mikszta, J.A., Cormier, M., Andrianov, A.K., 2009. Microneedle-based vaccines. Current Topics in Microbiology and Immunology 333, 369-393.

Prausnitz, M.R., Mitragotri, S., Langer, R., 2004. Current status and future potential of transdermal drug delivery. Nature Reviews Drug Discovery 3, 115-124.

Patenaude, M., Campbell, S., Kinio, D., Hoare, T., 2014. Tuning Gelation Time and Morphology of Injectable Hydrogels Using Ketone–Hydrazide Cross-Linking. Biomacromolecules 15, 781-790.

Qiu, Y., Park, K., 2001. Environment-sensitive hydrogels for drug delivery. Advanced Drug Delivery Reviews 53, 321-339.

Quimby, F.W., 2002. Animal Models in Biomedical Research. In: J.G. Fox, L.C. Anderson, F.M. Loew, F.W.Quimby, eds. 2002. *Laboratory Animal Medicine (Second Edition).* New York, Academic Press. Ch 30.

Quintero, S.M.M., Ponce, F.R.V., Cremona, M., Triques, A.L.C., d'Almeida, A.R., Braga, A.M.B., 2010. Swelling and morphological properties of poly(vinyl alcohol) (PVA) and poly(acrylic acid) (PAA) hydrogels in solution with high salt concentration. Polymer 51, 953-958.

Rachakonda, V.K., Yerramsetty, K.M., Madihally, S.V., Robinson Jr., R.L., Gasem, K. A. M., 2008. Screening of Chemical Penetration Enhancers for Transdermal Drug Delivery Using Electrical Resistance of Skin. Pharmaceutical Research 25, 2697-2704.

Raoof, J., Ojani, R., Nematollahi, D., Kiani, A., 2009. Digital simulation of the cyclic voltammetry study of the catechols electrooxidation in the presence of some nitrogen and carbon nucleophiles. International Journal of Electrochemical Science 4, 810-819.

Raphael, A.P., Meliga, S.C., Chen, X., Fernando, G.J., Flaim, C., Kendall, M.A., 2013. Depth-resolved characterization of diffusion properties within and across minimally-perturbed skin layers. Journal of Controlled Release 166(2), 87-94.

Raphael, A.P., Prow, T.W., Crichton, M.L., Chen, X.F., Fernando, G.I.P., Kendall, M.A.F., 2010. Targeted, needle-free vaccinations in skin using multi layered, densely-packed dissolving microprojection arrays. Small 6, 1785-1793.

Rasheed, H., HariBabu, R., KhajaMohiddin, M.D., Vineela, J., Raviteja, A., RaviKishore, P., Gajavalli, S., Naidu, L.V., 2011. Transdermal Drug Delivery System - Simplified Medication Regimen - A Review. Research Journal of Pharmaceutical, Biological and Chemical Sciences 2(4), 223-238.

Raveendran, R., Heybroek, W.M., Caulfield, M., Abrams, S.M., Wrigley, P.F., Slevin, M., Turner, P., 1992. Protein binding of indomethacin, methotrexate and morphine in patients with cancer. International Journal of Clinical Pharmacology Research 12, 117-122.

van Ravenzwaay, B., Leibold, E., 2004. A comparison between *in vitro* rat and human and *in vivo* rat skin absorption studies. Human & Experimental Toxicology 23, 421-430.

Ritger, P.L., Peppas, N.A., 1987. A simple equation for description of solute release II. Fickian and anomalous release from swellable devices. Journal of Controlled Release 5, 37-42.

Reddy, M.B., mccarley, K.D., bunge, A.L., 1998. Physiologically Relevant One-Compartment Pharmacokinetic Models for Skin. 2. Comparison of Models when Combined with a Systemic Pharmacokinetic Model. Journal of Pharmaceutical Sciences 87, 482-490.

Reuben, S.S., Connelly, N.R., Lurie, S., Klatt, M., Gibson, C.S., 1998. Dose response of ketorolac as an adjunct to patient-controlled analgesia morphine in patients after spinal fusion surgery. Anesthesia & Analgesia 87, 98-102.

Roberts, M.E., Mueller, K.R., 1990. Comparisons of *in vitro* nitroglycerin (TNG) flux across Yucatan pig, hairless mouse and human skins. Pharmaceutical Research 7, 673-676.

Roberts, M.S., 1991. Structure-permeability considerations in percutaneous absorption. In: R.C. Scott, R.H. Guy, J. Hadgraft *et al.*, eds. 1991. London: IBC Technical Services, pp. 210-228.

[a] Rodgers, T., Leahy, D., Rowland, M. 2005. Physiologically- based pharmacokinetic modeling 1: predicting the tissue distribution of moderate-to-strong bases. Journal of Pharmaceutical Sciences 94,1259-1276.

[b] Rodgers, T., Leahy, D., Rowland, M. 2005. Tissue distribution of basic drugs: Accounting for enantiomeric, compound and regional differences amongst b-blocking drugs in rats. Journal of Pharmaceutical Sciences 94, 1237-1248.

Rodriguez, G., Barbosa-Barros L., Rubio, L., Cócera, M., Díez, A., Estelrich, J., Pons, R., Caelles, J., De la Maza, A., Lopez, O., 2009. Conformational changes in stratum corneum lipids by effect of bicellar systems. Langmuir 25, 10595-10603.

Rodriguez, R., Alvarez-Lorenzo, C., Concheiro, A., 2003. Cationic cellulose hydrogels: kinetics of the crosslinking process and characterization as pH-/ ion-sensitive drug delivery systems. Journal of Controlled Release. 86, 253-265.

Rogovina, L.Z., Vasil'ev, V.G., Braudo, E.E., 2008. Definitions of the concept of polymeric-gel. Journal of Polymer Science 50, 85-92.

Roy, S.D., Hou, S-Y. E., Witham, S. L., Flynn, G. L., 1994. Transdermal Delivery of Narcotic Analgesics: Comparative Metabolism and Permeability of Human Cadaver Skin and Hairless Mouse Skin. Journal of Pharmaceutical Sciences 83 (12), 1723-1728.

Ru, M.T, Dordick, J.S., Reimer, J.A., Clark, D.S., 1998. Optimizing the Salt-Induced Activation of Enzymes in Organic Solvents: Effects of Lyophilization Time and Water Biotechnology and Bioengineering 63, 232-241.

Sachdeva, V., Banga, A.K., 2011. Microneedles and their applications. Recent Patents on Drug Delivery & Formulation 5, 95-132.

Santell, J.P., 2005. Preventing errors that occur with PCA pumps. US Pharmacist 30(1), 58-60.

Sato, K., Sugibayashi, K., Morimoto, Y., 1991. Species differences in percutaneous absorption of nicorandil. Journal of Pharmaceutical Science 80, 104-107.

Savage, S.R., Kirsh, K.L., Passik, S.D., 2008. Challenges in Using Opioids to Treat Pain in Persons with Substance Use Disorders. Addiction Science & Clinical Practice 4(2), 4-25.

Scheindlin, S., 2004. Transdermal Drug Delivery: Past, Present, Future. Molecular Interventions 4 (6), 308-312.

Schwarz, J.C., Klang, V., Hoppel, M., Mahrhauser, D., Valenta, C., 2012. Natural microemulsions: Formulation design and skin interaction. European Journal of Pharmaceutics and Biopharmaceutics 81, 557-562.

Seal, D.V., Hay, R.J., Middleton, K.R. Skin and wound infection: investigation and treatment in practice. London: Informa Healthcare; 2000. pp. 5-8.

Sechzer, P.H., 1971. Studies in pain with the analgesic-demand system. Anesthesia & Analgesia 50, 1-10.

Seethapathy, S., Górecki, T., 2011. Applications of polydimethylsiloxane in analytical chemistry: A review. Analytica Chimica Acta 750, 48-62.

Shah, U.U., Roberts, M., Gul, M., Tuleu, C., Beresford, M.W., 2011. Needle-free and microneedle drug delivery in children: a case for disease-modifying antirheumatic drugs (DMARDs). International Journal of Pharmaceutics 416(1), 1-11.

Shah, V.P., Flynn, G.L., Yacobi, A, Maibach, H.I., Bon, C., Fleischer, N.M., Franz, T.J., Kaplan, S.A., Kawamoto, J., Lesko, L.J., Marty, J-P., Pershing, L.K., Schaefer, H., Sequeira, J.A., Shrivastava, S.P., Wilkin, J., Williams, R.L., 1998. Bioequivalence of topical dermatological dosage Forms-methods of evaluation of bioequivalence. Pharmaceutical Research 15,167-171.

Sharma, G., Rao, G., Bansal, A., Dang, S., Gupta, S., Gabrani, R., 2014. Pseudomonas aeruginosa biofilm: Potential therapeutic targets. Biologicals 42, 1-7.

Sharma, R.N., Pancholi, S.S., 2011. Optimization techniques in pharmaceutical industry: A Review. Journal of Current Pharmaceutical Research 7, 21-28.

Shen, Y., Zhang, X., Lu, J., Zhang, A., Chen, K., Li, X., 2009. Effect of chemical composition on properties of pH-responsive poly(acrylamide-co-acrylic acid) microgels prepared by inverse microemulsion polymerization. Colloids and Surfaces A: Physicochemical and Engineering Aspects 350, 87-90.

Shi, Q., Jackowski, G., 1998. One-dimensional polyacrylamide gel electrophoresis, in: B.D. Hames, ed. 1998. *Gel Electrophoresis of Proteins: A Practical Approach,* 3rd ed. Oxford: Oxford University Press, pp.1-52.

Shiflet, A. B., Shiflet, G. W., 2006. Introduction to computational science: modeling and simulation for the sciences. Wofford College, SC: Princeton University Press.

Shimamura, T., Tairabune, T., Kogo, T., Ueda, H., Numajiri, S., Kobayashi, D., Morimot, Y., 2004. Investigation of the Release Test Method for the Topical Application of Pharmaceutical Preparations: Release Test of Cataplasm Including Nonsteroidal Anti-inflammatory Drugs Using Artificial Sweat. Chemical & Pharmaceutical Bulletin 52,167-171.

Sieg, A., Wascotte, V., 2009. Diagnostic and therapeutic applications of iontophoresis. Journal of Drug Targeting 17(9), 690-700.

Silvanto, M., Lappi, M., Rosenberg, P.H., 2002. Comparison of the opioid-sparing efficacy of diclofenac and ketoprofen for 3 days after knee arthroplasty. Acta Anaesthesiologica Scandinavica 46, 322-328.

Silverstein, R.M., Webster, F.X., Kiemle, D., 2005. *Spectrometric Identification of Organic Compounds.* 7th ed. John Wiley & Sons, Inc.

Simon, G.A., Maibach, H.I., 1998. Relevance of hairless mouse as an experimental model of percutaneous penetration in man. Skin Pharmacology and Applied Skin Physiology 11, 80-86.

Simon, G.A., Maibach, H.I., 2000. The pig as an experimental animal model of percutaneous permeation in man: qualitative and quantitative observations-an overview. Skin Pharmacology and Applied Skin Physiology 13, 229-234.

Singh, P., Maibach, H.I., 1996. Iontophoresis: an alternative to the use of carriers in cutaneous drug delivery. Advanced Drug Delivery Reviews 18,379-394.

Singh, P., Roberts, M.S., 1994. Effects of vasoconstriction on dermal pharmacokinetics and local tissue distribution of compounds. Journal of Pharmaceutical Sciences 83, 783-791.

Sinko, P.J., Singh, Y., Troy, D.B. eds., 2010. *Martin's Physical Pharmacy and Pharmaceutical Sciences.* 6th ed. Philadelphia: Wolter Kluwer Health/Lippincott Williams & Wilkins.

Sivamani, R.K., Liepmann, D., Maibach, H.I., 2007. Microneedles and transdermal applications. Expert Opinion on Drug Delivery 4(1), 19-25.

Sjögren, E., Abrahamsson, B., Augustijns, P., Becker, D., Bolger, M.B., Brewster, M., Brouwers, J., Flanagan, T., Harwood, M., Heinen, C., Holm, R., Juretschke, H-P., Kubbinga, M., Lindahl, A., Lukacova, V., Münster, U., Neuhoff, S., Nguyen, M.A., Peer, A.v., Reppas, C., Hodjegan, A.R., Tannergren, C., Weitschies, W., Wilson, C., Zane, P., Lennernäs, H., Langguth, P., 2014. *In vivo* methods for drug absorption – Comparative physiologies, model selection, correlations with *in vitro* methods (IVIVC), and applications for formulation/API/excipient characterization including food effects, European Journal of Pharmaceutical Sciences 57, 95-151.

Small, C.J., Too, C.O., Wallace, G.G., 1997. Responsive conducting polymer-hydrogel composite. Polymer Gels and Networks 5, 251-265.

Smart, W.H., Subramanian, K., 2000. The Use of Silicon Microfabrication Technology in Sullivan, S.P., Murthy, N., Prausnitz, M.R., 2008. Minimally invasive protein delivery with rapidly dissolving polymer microneedles. Advanced Materials 20, 933-938.

Spizzirri, U.G., Hampel, S., Cirillo, G., Nicolettac, F.P., Hassan, A., Vittorio, O., Picci, N., Iemma, F., 2013. Spherical gelatin/CNTs hybrid microgels as electro-responsive drug delivery systems. International Journal of Pharmaceutics 448,115- 122.

Stamer, U.M., Höthker, F., Lehnen, K., Stüber, F., 2003. Postoperative analgesie mit tramadol und metamizol. Kontinuierliche infusion versus patientenkontrollierte analgesie. Anaesthesist 52, 33-41.

Stapleton, J.V., Austin, K.L., Mather L.E., 1978. Postoperative pain (letter). BMJ 1, 1499.

Stokes. W.S., Marsman, D.S., 2014. Animal Welfare Considerations in Biomedical Research and Testing. In: K.Bayne, P.V. Turner, eds., 2014. *Laboratory Animal Welfare*. New York: Academic Press. Ch 9.

Suckow M.A., Weisbroth S.H., Franklin C.L., 2006. The laboratory rat. American College of Laboratory, Animal Medicine Series 2, 767.

Tadicherla, S., Berman, B., 2006. Percutaneous dermal drug delivery for local pain control. Therapeutics and Clinical Risk Management 2(1), 99-114.

Taiwo, V.O., Conteh, O.L., 2008. The rodenticidal effect of indomethacin: pathogenesis and pathology. Veterinarski Arhiv 78, 167-178.

Tanaka, N., Imai, K., Okimoto, K., Ueda, S., Tokonaga, Y., Ibuki, R., Higaki, K., Kimura, T., 2006. Development of novel sustained-release system, disintegration-controlled matrix tablet (DCMT) with solid dispersion granules of nilvadipine (II): *In vivo* evaluation. Journal of Controlled Release 112, 51-56.

Tang, C., Saquing, C.D., Harding, J.R., Khan, S.A., 2010. *In Situ* Cross-Linking of Electrospun Poly(vinyl alcohol) Nanofibers. Macromolecules 43, 630-637.

Tao, S.L., Desai, T.A., 2003. Microfabricated drug delivery systems: from particles to pores. Advanced Drug Delivery Reviews 55 (3), 315-328.

Teo, M.A., Shearwood, C., Ng, K.C., Lu, J., Moochhala, S., 2005. *In vitro* and *in vivo* characterization of MEMS microneedles. Biomedical Microdevices 7 (1), 47-52.

Thommes, M., 2010. Physical Adsorption Characterization of Nanoporous Materials. Chemie Ingenieur Technik 82, 1059-1073.

Tiwari, S.B., Rajabi-Siahoomi, A.R., 2008. Extended-release oral drug delivery technologies: monolithic matrix systems. Methods in Molecular Biology 437, 217-243.

Toole, J., Silagy, S., Maric, A., Fath, B., Quebe-Fehling, E., Ibarra de Palacios, P., Laurin, L., Giguere, M., 2002. Evaluation of irritation and sensitisation of two 50 microg/day oestrogen patches. Maturitas 43, 257-263.

Tong, P., Zografi, G., 1999. Solid-state characteristics of amorphous sodium indomethacin relative to its free acid. Pharmaceutical Research 16(8),1186-1192.

Tori, H., Tasumi, M., 1996. Theoretical analyses of the amide-I infrared bands of globular proteins. In: H.H. Mantsch, D. Chapman, eds. 1996. *Infrared Spectroscopy of Biomolecules.* New York: Wiley-Liss, pp. 1-18.

Touitou, E., 2002. Drug delivery across the skin. Expert Opinion on Biological Therapy 2, 723-733.

Tsai, T-S. A Stimulus Actuated Polymeric Device for the Prolonged Therapeutic Management of Moderate to Severe Chronic Pain. A dissertation submitted to the Faculty of Health Sciences, University of the Witwatersrand, in fulfillment of the requirements for the degree of Master of Pharmacy, 2011.

Tumarkin, E., Kumacheva, E., 2009. Microfluidic generation of microgels from synthetic and natural polymers. Chemical Society Reviews 38 (8), 2149-2496.

Ünlügenc, H., Gündüz, M., Özalevli, M., Akman H., 2002. A comparative study on the analgesic effect of tramadol, tramadol plus magnesium, and tramadol plus ketamine for postoperative pain management after major abdominal surgery. Acta Anaesthesiologica Scandinavica 46, 1025-1030.

Urtti, A., Salminen, L., 1993. Minimizing systemic absorption of topically administered ophthalmic drugs. Survey of Ophthalmology 37, 435-457.

Van Buskirk, G.A., Arsulowicz, D., Basu, P., Block,L., Cai, B.,. Cleary, G.W., Ghosh, T., González, M.A., Kanios, D., Marques, M., Noonan, P.K., Ocheltree, T., Schwarz, P., Shah, V., Spencer, T.S, Tavares, L., Ulman,K., Uppoor, R., Yeoh, T., 2012. Passive Transdermal Systems Whitepaper Incorporating Current Chemistry, Manufacturing and Controls (CMC) Development Principles. AAPS PharmSciTech 13, 218-230.

Van der Maaden, K., Jiskoot, W., Bouwstra, J., 2012. Microneedle technologies for (trans)dermal drug and vaccine delivery. Journal of Controlled Release 161 (2), 645-655.

Vanbever, R., Preat, V., 1999. *In vivo* efficacy and safety of skin electroporation. Advanced Drug Delivery Reviews 35, 77-88.

Vandervoort, J., Ludwig, A., 2008. Microneedles for transdermal drug delivery: a mini review. Frontiers in Bioscience 13, 1711-1715.

Vassal, N., Salmon, E., Fauvarque, J.F., 2000. Electrochemical properties of an alkaline solid polymer electrolyte based on P(ECH-co-EO). Electrochimica Acta 45, 1527-1532.

Verbaan, F.J., Bal, S.M., van den Berg, D.J., Groenink, W.H., Verpoorten, H., Lüttge, R., Bouwstra, J.A., 2007. Assembled microneedle arrays enhance the transport of compounds varying over a large range of molecular weight across human dermatomed skin. Journal of Controlled Release 117,238-245.

Verhoeven, M., Bystrova, S., Winnubst, L., Qureshi, H., de Gruijl, T., Scheper, R.J., Lüttge, R., 2012. Applying ceramic nanoporous microneedle arrays as a transport interface in egg plants and an ex-vivo human skin model. Microelectronic Engineering 98, 659-662.

Verma, R.K., Garg, S., 2001. Current Status of Drug Delivery Technologies and Future Directions. Pharmaceutical Technology On-Line 25 (2), 1-14.

Vrdoljak, A., McGrath, M.G., Carey, J.B., Draper, S.J., Hill, A.V.S., O'Mahony, C., Crean, A.M., Moore, A.C., 2012. Coated microneedle arrays for transcutaneous delivery of live virus vaccines. Journal of Controlled Release 159(1), 34-42.

Walters, K.A., Brain, K.R., 2009. Topical and Transdermal Delivery. In: M. Gibson, ed. 2009. *Preformulation and Formulation.* 2nd ed. New York: Informa Healthcare, pp.475- 517.

Wang, Y., Fan, Q., Song, Y., Michniak, B., 2003. Effects of fatty acids and iontophoresis on the delivery of midodrine hydrochloride and the structure of human skin. Pharmaceutical Research 20(10), 1612-1618.

Wang Y., Nedelman J., 2002. Bias in the Wagner-Nelson estimate of the fraction of drug absorbed. Pharmaceutical Research 19(4), 470-476.

Weigmann, H., Lademann, J., Pelchrzim, R., Sterry, W., Hagemeister, T., Molzahn, R., Schaefer, M., Lindscheid, M., Schaefer, H., Shah, V.P., 1999. Bioavailability of clobetasol propionatequantification of drug concentrations in the stratum corneum by dermatopharmacokinetics using tape stripping. Skin Pharmacology and Applied Skin Physiology 12, 46-53.

Weinbroum, A.A., Gorodetzky, A., Nirkin, A., Kollender, Y., Bickels, J., Marouani, N., Rudick, V., Meller, I., 2002. Dextromethor phan for the reduction of immediate and late postoperative pain and morphine consumption in orthopedic oncology patients: a randomized, placebo-controlled, doubleblind study. Cancer 95, 1164-1170.

Weiss, R. A., Lundberg, R. D., Turner, S. R., 1985. Comparisons of Styrene Ionomers Prepared by Sulfonating Polystyrene and Copolymerizing Styrene with Styrene Sulfonate, Journal of Polymer Science Part A: Polymer Chemistry 23, 549-568.

Wendorf, J.R., Ghartey-Tagoe, E.B., Williams, S.C., Enioutina, E., Singh, P., Cleary, G.W., 2011. Transdermal delivery of macromolecules using solid-state biodegradable microstructures. Pharmaceutical Research 28, 22-30.

Wester, R.C., Maibach, H.I., 1989. *In vivo* methods for percutaneous absorption measurements. In: R.L. Brounaugh, H.I. Maibach, eds. 1989. *Percutaneous absorption: mechanisms-methodology-drug delivery*, 2nd ed. New York: Marcel Dekker Inc., pp. 215-237.

Wilkinson, S.C., Williams, F.M., 2008. Cutaneous metabolism. In: M.S. Roberts, K.A. Walters, eds. 2008. *Dermal Absorption and Toxicity Assessment.*, 2nd ed. New York: Informa Healthcare, pp. 89-115.

Williams, A.C., Barry, B.W., 2004. Penetration enhancers. Advanced Drug Delivery Reviews 56 (5), 603-618.

Wilson, E.J., 2011. *Three Generations: The Past, Present, and Future of Transdermal Drug Delivery Systems.* [pdf]. Available at: < www.freece.com/Files/.../3%20Gen%20Homestudy%20(TV).pdf > [Accessed 23 January 2012].

Woodall, K.L., Martin, T.L., McLellan, B.A., 2008. Oral abuse of fentanyl patches (Duragesic): seven case reports.Journal of Forensic Sciences 53(1), 222-225.

Xie, Y., Xu, B., Gao, Y., 2005. Controlled transdermal delivery of model drug compounds by MEMS microneedle array. Nanomedicine: Nanotechnology, Biology and Medicine 1, 184-190.

Xu, F., Kang, E., Neoh, K., 2006. pH- and temperature-responsive hydrogels from crosslinked triblock copolymers prepared via consecutive atom transfer radical polymerizations. Biomaterials 27, 2787-2797.

Xu, X., Weisel, C. P., 2005. Human respiratory uptake of chloroform and haloketones during showering. Journal of Exposure Analysis and Environmental Epidemiology 15, 6–16.

Yadav, V., 2012. Transdermal Drug Delivery System: Review. International Journal of Pharmaceutical Sciences and Research 3(2), 376-382.

Yamamoto, Y., Yamamoto, T., 1987. Measurement of electrical bio-impedance and its applications. Medical Progress Through Technology 12, 171-183.

Yang, T., Hussain, A., Bai, S., Khalil, I.A., Harashima, H., Ahsan, F., 2006. Positively charged polyethylenimines enhance nasal absorption of the negatively charged drug, low molecular weight heparin. Journal of Controlled Release 115, 289-297.

You, X., Chang, J-H., Ju, B-K., Pak, J.J., 2011. Rapidly dissolving fibroin microneedles for transdermal drug delivery. Materials Science and Engineering: C, 31, 1632-1636.

Yue, Y.M., Xu, K., Liu, X-G., Chen, Q., Sheng, X., Wang, P-X., 2008. Preparation and Characterization of Interpenetration Polymer Network Films Based on Poly(vinyl alcohol) and Poly(acrylic acid) for Drug Delivery. Journal of Applied Polymer Science 108, 3836-3842.

Yun, J., Im, J.S., Lee, Y-S., Kim, H-I., 2011. Electro-responsive transdermal drug delivery behavior of PVA/PAA/MWCNT nanofibers. European Polymer Journal 47, 1893-1902.

Zhang, J., Michniak-Kohn, B., 2011. Investigation of microemulsion microstructures and their relationship to transdermal permeation of model drugs: Ketoprofen, lidocaine, and caffeine. International Journal of Pharmaceutics 421, 34-44.

Zhang, Y., Brown, K., Siebenaler, K. Determan, A., Dohmeier, D., Hansen, K., 2012. Development of Lidocaine-Coated Microneedle Product for Rapid Safe, and Prolonged Local Analgesic Action. Pharmaceutical Research, 29, 170-177.

Zhang, Y., Huo, M., Zhoua, J., Xie, S., 2010. PKSolver: An add-in program for pharmacokinetic and pharmacodynamic data analysis in Microsoft Excel. Computer methods and programs in biomedicine 99, 306-314.

Zhang, X.Z., Wu, D.Q., Chu, C.C., 2004. Synthesis, characterization and controlled drug release of thermosensitive IPN-PNIPAAm hydrogels. Biomaterials 25, 3793-3805.

11. Appendices

11.1. Doctoral Publications

11.1.1. Review Paper 1

REVIEW

Patient-Controlled Analgesia: Therapeutic Interventions Using Transdermal Electro-Activated and Electro-Modulated Drug Delivery

SUNAINA INDERMUN,[1] YAHYA E. CHOONARA,[1] PRADEEP KUMAR,[1] LISA C. DU TOIT,[1] GIRISH MODI,[2] REGINA LUTTGE,[3,4,5] VINESS PILLAY[1]

[1]Department of Pharmacy and Pharmacology, Faculty of Health Sciences, University of the Witwatersrand, Parktown, Johannesburg 2193, South Africa

[2]Department of Neurology, Division of Neurosciences, Faculty of Health Sciences, University of the Witwatersrand, Parktown, Johannesburg 2193, South Africa

[3]MESA+ Institute for Nanotechnology, University of Twente, Enschede 7500AE, The Netherlands

[4]MyLife Technologies BV, Enschede 7500AE, The Netherlands

[5]Department of Mechanical Engineering, Microsystems Group and Institute for Complex Molecular Systems (ICMS), Eindhoven University of Technology, Eindhoven 5600MB, The Netherlands

ABSTRACT: Chronic pain poses a major concern to modern medicine and is frequently undertreated, causing suffering and disability. Patient-controlled analgesia, although successful, does have limitations. Transdermal delivery is the pivot to which analgesic research in drug delivery has centralized, especially with the confines of needle phobias and associated pain related to traditional injections, and the existing limitations associated with oral drug delivery. Highlighted within is the possibility of further developing transdermal drug delivery for chronic pain treatment using iontophoresis-based microneedle array patches. A concerted effort was made to review critically all available therapies designed for the treatment of chronic pain. The drug delivery systems developed for this purpose and nondrug routes are elaborated on, in a systematic manner. Recent developments and future goals in transdermal delivery as a means to overcome the individual limitations of the aforementioned delivery routes are represented as well. The approval of patch-like devices that contain both the microelectronic-processing mechanism and the active medicament in a small portable device is still awaited by the pharmaceutical industry. This anticipated platform may provide transdermal electro-activated and electro-modulated drug delivery systems a feasible attempt in chronic pain treatment. Iontophoresis has been proven an effective mode used to administer ionized drugs in physiotherapeutic, diagnostic, and dermatological applications and may be an encouraging probability for the development of devices and aids in the treatment of chronic pain. © 2013 Wiley Periodicals, Inc. and the American Pharmacists Association J Pharm Sci 103:353–366, 2014

Keywords: chronic pain; drug transport; electro-conductive hydrogel; iontophoresis; microneedle arrays; patient-controlled analgesia; permeation enhancers; polymeric drug delivery systems; transdermal drug delivery

INTRODUCTION

Although hailed as a medical breakthrough for pain treatment, the risks and limitations of patient-controlled analgesia (PCA) outweigh the benefits associated with its use, the main risk being overdose and subsequent death and the main limitation being high costs. Many clinicians believe that analgesic doses need to be increased to provide adequate pain relief, yet they fail to see the underlying problem related to drug delivery. Although numerous pain treatment therapies are available on the market, a point regarding drug delivery made by Stapleton et al.[1] still holds true:

"The plethora of new parenteral agents which the pharmaceutical companies have introduced over the past 20 years is not a reminder that we have not found the right drug but a reminder that we have not found the optimal mode of administration of perfectly adequate analgesic drugs."

Pain according to the International Association for the Study of Pain can be defined as "an unpleasant sensory and emotional experience associated with actual or potential tissue damage, or described in terms of such damage."[2] Three classifications of chronic noncancer pain (CNCP) are identified: nociceptive, neuropathic, and functional.[2] The management of CNCP has proven to be challenging to both the clinician and patient, resulting in time-consuming, complex, and sometimes unsuccessful or inadequate treatment.[3,4] Chronic pain may result from numerous medical conditions and although there are corresponding large numbers of specific injections, rehabilitation programs, and pharmacological treatments available, many patients are still left with continued pain even after repeated treatment attempts, necessitating controlled delivery of analgesic drugs.

As CNCP causes sleeplessness and depression, and interferes with normal physical and social functioning,[5] the impact and prevalence of chronic pain warrants serious attention as the condition may influence the overall quality of life.[3,4]

11.1.2. Review Paper 2

Review

Current advances in the fabrication of microneedles for transdermal delivery

Sunaina Indermun [a], Regina Luttge [b,c,d], Yahya E. Choonara [a], Pradeep Kumar [a], Lisa C. du Toit [a], Girish Modi [a,e], Viness Pillay [a,*]

[a] Department of Pharmacy and Pharmacology, Faculty of Health Sciences, University of the Witwatersrand, 7 York Road, Parktown, Johannesburg 2193, South Africa
[b] MESA + Institute for Nanotechnology, University of Twente, Enschede 7500AE, The Netherlands
[c] MyLife Technologies BV, Enschede 7500AE, The Netherlands
[d] Department of Mechanical Engineering, Microsystems Group and Institute for Complex Molecular Systems (ICMS), Eindhoven University of Technology, Eindhoven 5600MB, The Netherlands
[e] Department of Neurology, Division of Neurosciences, Faculty of Health Sciences, University of the Witwatersrand, 7 York Road, Parktown, 2193, Johannesburg, South Africa

ARTICLE INFO

ABSTRACT

The transdermal route is an excellent site for drug delivery due to the avoidance of gastric degradation and hepatic metabolism, in addition to easy accessibility. Although offering numerous attractive advantages, many available transdermal systems are not able to deliver drugs and other compounds as desired. The use of hypodermic needles, associated with phobia, pain and accidental needle-sticks has been used to overcome the delivery limitation of macromolecular compounds. The means to overcome the disadvantages of hypodermic needles has led to the development of microneedles for transdermal delivery. However, since the initial stages of microneedle fabrication, recent research has been conducted integrating various fabrication techniques for generating sophisticated microneedle devices for transdermal delivery including progress on their commercialization. A concerted effort has been made within this review to highlight the current advances of microneedles, and to provide an update of pharmaceutical research in the field of microneedle-assisted transdermal drug delivery systems.

© 2014 Elsevier B.V. All rights reserved.

Contents

* Corresponding author. Tel.: +27 11 717 2274; fax: +27 11 642 4355.
  E-mail address: viness.pillay@wits.ac.za (V. Pillay).

11.1.3. Research Paper 1

An interfacially plasticized electro-responsive hydrogel for transdermal electro-activated and modulated (TEAM) drug delivery

CrossMark

Sunaina Indermun[a], Yahya E. Choonara[a], Pradeep Kumar[a], Lisa C. du Toit[a], Girish Modi[b], Regina Luttge[c], Viness Pillay[a,*]

[a] University of the Witwatersrand, Faculty of Health Sciences, Department of Pharmacy and Pharmacology, 7 York Road, Parktown, Johannesburg 2193, South Africa
[b] University of the Witwatersrand, Faculty of Health Sciences, Division of Neurosciences, Department of Neurology, 7 York Road, Parktown, Johannesburg 2193, South Africa
[c] MESA+Institute for Nanotechnology, University of Twente, 7500AE Enschede, The Netherlands

ARTICLE INFO

ABSTRACT

This paper highlights the use of hydrogels in controlled drug delivery, and their application in stimuli responsive, especially electro-responsive, drug release. electro-conductive hydrogels (ECHs) displaying electro-responsive drug release were synthesized from semi-interpenetrating networks (semi-IPNs) containing a poly(ethyleneimine) (PEI) and 1-vinylimidazole (VI) polymer blend as the novel electro-active species. The semi-IPNs are systems comprised of polyacrylic acid (PAA) and poly(vinyl alcohol) (PVA). This paper attempts to investigate the various attributes of the electro-responsive ECHs, through institution of a statistical experimental design. The construction of a Box–Behnken design model was employed for the systematic optimization of the ECH composition. The design model comprised of three variables, *viz.* poly(ethyleneimine) volume; 1-vinylimidazole volume; and applied voltage, critical to the success of the formulation. Electro-responsive drug release was determined on formulations exposed to varying environments to ascertain the optimal environment for the said desired release. A comparison method of formulation water content and swelling through gravimetric analysis was also conducted. Matrix resilience profiles were obtained as an insight to the ability of the ECH to revert to its original structure following applied stress. Response surface and contour plots were constructed for various response variables, namely electro-responsive drug release, matrix resilience and degree of swelling. The outcomes of the study demonstrated the success of electro-responsive drug release. The findings of the study can be utilized for the development of electro-responsive delivery systems of other drugs for the safer and effective drug delivery. Volumes of poly(ethyleneimine) (>2.6 mL) and 1-vinylimidazole (>0.7 mL), resulted in ideal therapeutic electro-responsive drug release (0.8 mg) for indomethacin. Lower amounts of poly(ethyleneimine) and amounts of 1-vinylimidazole ranging from 0.2 to 0.74 mL are consistent with greater than 1.6 mg release per stimulation. Swelling of <25–45% was seen.

© 2013 Elsevier B.V. All rights reserved.

1. Introduction

Controlled-release formulations of opioid analgesics are widely assumed to be less subject to abuse than their immediate-release counter-parts in their ability to provide better quality of pain relief (Fisher, 2004). Drug delivery has been defined by Flynn (1979) as 'the use of whatever means possible, be it chemical, physico-chemical or mechanical, to regulate a drug's access rate to the body's central compartment, or in some cases, directly to the involved tissues". Drug delivery accounts for the carrier, the target and the route. It has advanced into a plethora of devices or processes that are designed to make therapeutic agents more efficacious through modified release, augmented therapeutic index and bioavailability, and enhanced patient acceptance and patient compliance. Advancements in drug delivery technology have thus proven to bring commercial and therapeutic value to drug delivery products.

The unique capabilities of hydrogels allows for an electric current to be used as an environmental signal in the induction of a required hydrogel response (Qiu and Park, 2001). The use of an electric-stimulus offers advantages such as the duration of electric pulses, intervals between pulses, the availability of equipment which allows precise control with regards to the magnitude of current, *etc.* (Murdan, 2003). Currently a large volume of literature exists on the *in vivo* use of electric currents, in the form of electroporation and iontophoresis, in the field of transdermal and

11.2. Research Presentations

Sunaina Indermun, Yahya E. Choonara, Pradeep Kumar, Lisa C. Du Toit, Girish Modi, Regina Lüttge and Viness Pillay.

Design, Development and Optimization of a Bipolymeric Interfacially Plasticized Electroresponsive Hydrogel (BiPErG) for Transdermal Electro-Activated and Modulated (TEAM) Drug Delivery

Chronic pain affects more than 50 million people causing significant physical and emotional disability ultimately leading to substantial declines in many other areas of living. Transdermal Delivery Systems (TDSs) is the pivot to which research in drug delivery has centralized especially with the confines of needle phobias and associated pain related to traditional injections, and the existing limitations such as hepatic/ gastrointestinal metabolism, palatability issues and hepatotoxicity associated with oral drug delivery. Highlighted in this study is the development of a Transdermal Electro-Activated and Modulated (TEAM) drug delivery device for chronic pain treatment using transdermal Bipolymeric Interfacially Plasticized Electroresponsive Hydrogel (BiPErG) that involves the combination of an Electro-Conductive Hydrogel (ECH) and a microneedle array (MNA) patch. MNA technology has been proposed as a hybrid to overcome the individual limitations of both injections and patches through an ultra-minimally invasive, virtually pain-free delivery mechanism. The system has been designed and proved to maintain therapeutic drug plasma levels. Design of experiments (DOE) was implemented for the prediction of an optimized formulation by constrained optimization. Evaluation of the design formulations by *in vitro* studies has indicated that the formulations meet the desired pharmaceutical requirements in terms of matrix resilience, swellability and electro-modulated drug release both with the candidate drug, indomethacin, and other potent drugs such as morphine hydrochloride, fentanyl citrate and celecoxib. Results from the *ex vivo* evaluation across porcine skin of the optimized formulation had also demonstrated that the device has achieved the aim of electro-activated and modulated drug delivery.

Sunaina Indermun, Yahya E. Choonara, Pradeep Kumar, Lisa C. Du Toit, Girish Modi, Regina Lüttge and Viness Pillay.

An Electro- Modulated Transdermal Drug Delivery System for the Treatment of Chronic Pain

The development of a Transdermal Electro-Activated and Modulated (TEAM) drug delivery device for the treatment of chronic pain using a Bipolymeric Interfacially Plasticized Electro-responsive Hydrogel (BiPErG) which is a combination of an Electro-Modulated Hydrogel (EMH) and a microneedle array (MNA). MNA technology has been opted to construct an ultra-minimally invasive, virtually pain-free delivery mechanism to overcome the individual limitations of both injections and patches. Design of experiments using a Box-Behnken design model was implemented for the optimization of predetermined therapeutic and pharmaceutical parameters. *In vitro* evaluation indicated that the formulations meet the desired pharmaceutical requirements in terms of matrix resilience, swellability and electro-responsive drug release both with the candidate drug, indomethacin, and other potent drugs such as morphine hydrochloride, fentanyl citrate and celecoxib. *Ex vivo* evaluation of the optimal formulation across porcine skin demonstrated that without electro-stimulation, significantly less drug release was obtained (±0.4540mg) as compared to electro-stimulation (±2.93mg). *In vivo* release studies were conducted to foster an *in vitro/in vivo* correlation, providing a more realistic clinical extrapolation of the therapeutic ability of the delivery system. In this study, therapeutic efficacy of the EMH-MNA device was evaluated following transdermal application to the Sprague Dawley rat model. *In vivo* profiles displayed contrasting results where the transdermal device displayed significantly higher levels of drug release in the plasma (5.71×10^{-7} µg/mL) as compared to conventional intravenous delivery (2.894×10^{-7} µg/mL) proving the developed system as an efficient electro-modulated delivery device for bioactives through the skin.

11.3. Calibration Curves
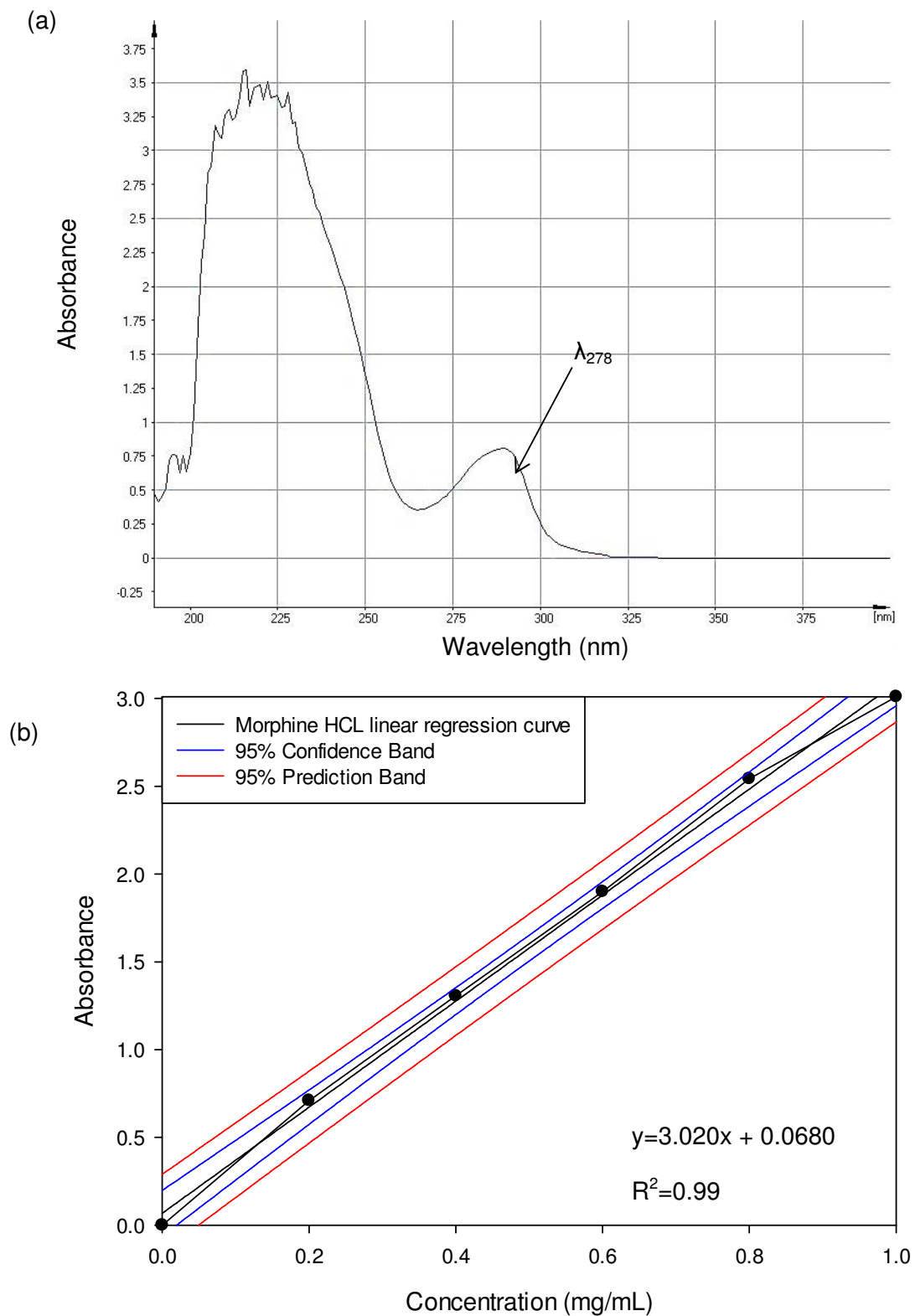
11.3.1. Morphine HCL

(a)

(b)

Figure 11.3.1: (a) UV Spectra of morphine HCL in PBS (WinASPECT, Version 1.6.13.0, 2002, Analytik Jena AG, Germany) and (b) Calibration curve of morphine HCL in PBS at 278nm.

11.3.2. Celecoxib

(a)

(b)

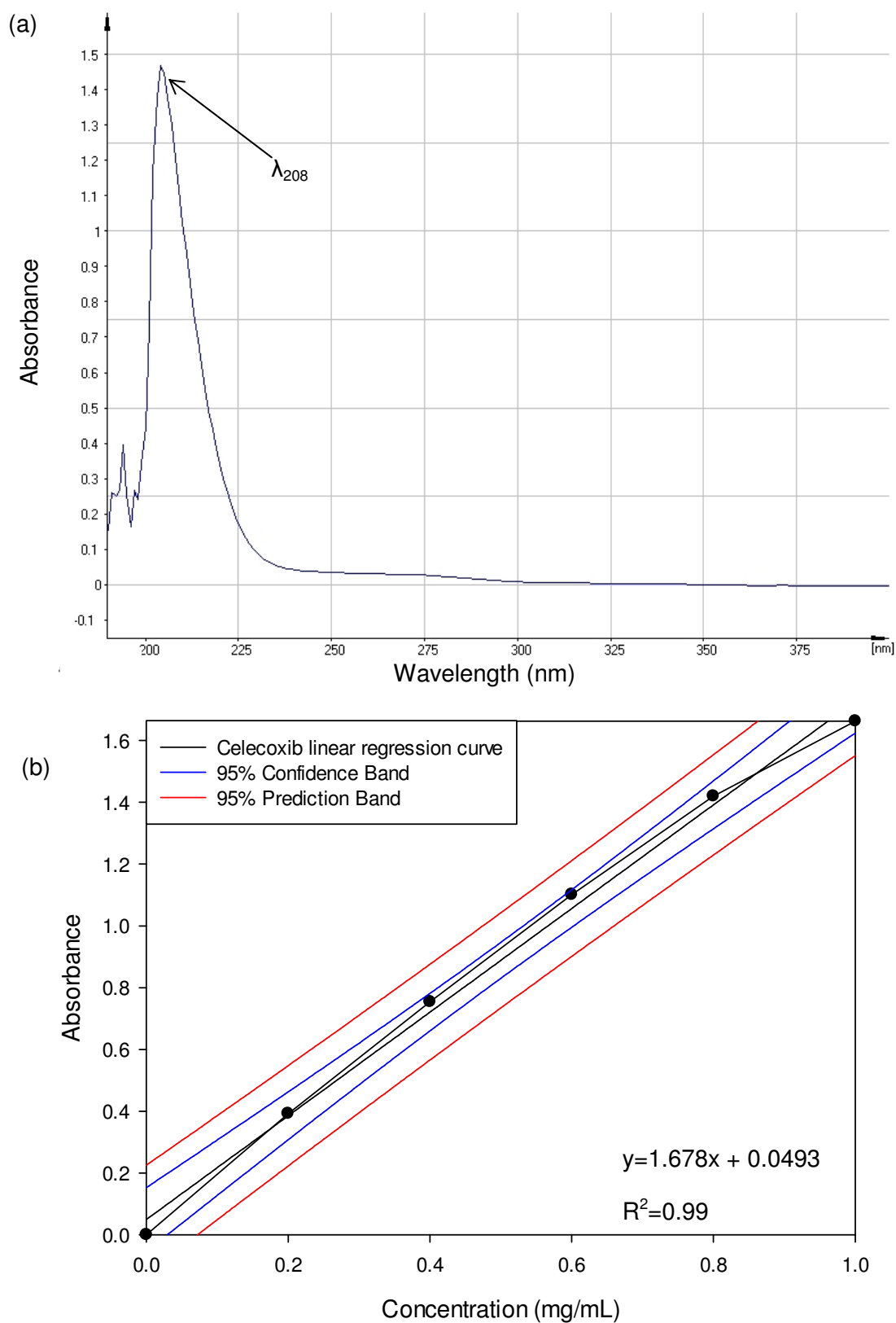$$y = 1.678x + 0.0493$$

$$R^2 = 0.99$$

Figure 11.3.2: (a) UV Spectra of celecoxib in PBS (WinASPECT, Version 1.6.13.0, 2002, Analytik Jena AG, Germany) and (b) Calibration curve of celecoxib in PBS at 208nm.
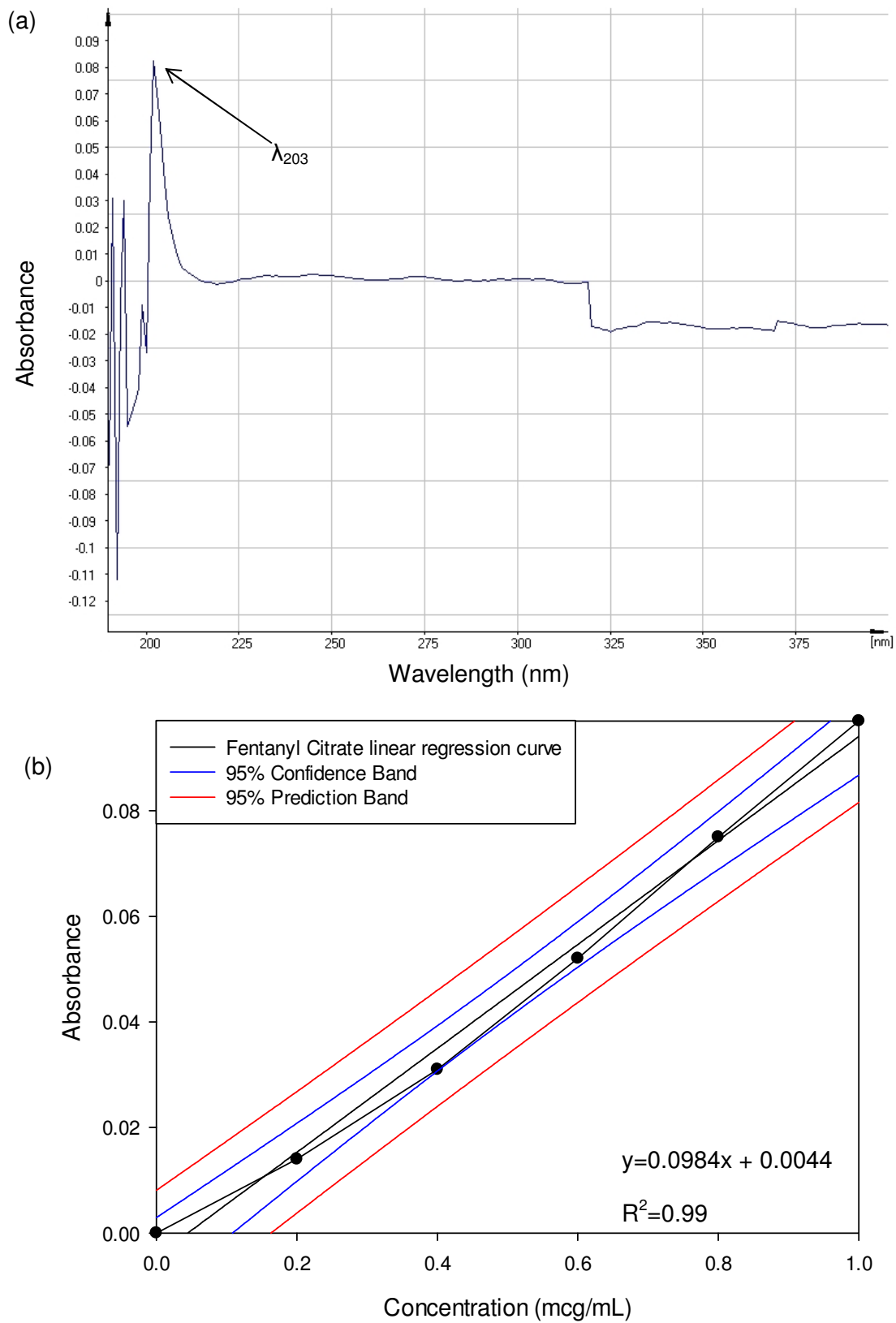
11.3.3. Fentanyl citrate

Figure 11.3.3: (a) UV Spectra of fentanyl citrate in PBS (WinASPECT, Version 1.6.13.0, 2002, Analytik Jena AG, Germany) and (b) Calibration curve of fentanyl citrate in PBS at 203nm.

11.4. Animal Ethics Clearance Certificate

AESC3

STRICTLY CONFIDENTIAL

ANIMAL ETHICS SCREENING COMMITTEE (AESC)

CLEARANCE CERTIFICATE NO.   2013/13/04

APPLICANT: Ms S Indermun

SCHOOL: Therapeutic Sciences
DEPARTMENT: Pharmacy
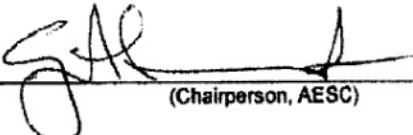**LOCATION:**

PROJECT TITLE: An in-vivo evalution of the use of a microneedle array patch for
                        the electrically-stimulated painless administration of bioactivities
                        through the skin of a rat model

Number and Species
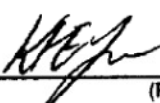
36 Sprague-Dawley rats, approx body mass 225 grams

Approval was given for to the use of animals for the project described above at an AESC meeting held on 20130319. This approval remains valid until 20150318.

The use of these animals is subject to AESC guidelines for the use and care of animals, is limited to the procedures described in the application form and to the following additional conditions:

Signed: _____   Date: _26/3/2013._
              (Chairperson, AESC)

I am satisfied that the persons listed in this application are competent to perform the procedures therein, in terms of Section 23 (1) (c) of the Veterinary and Para-Veterinary Professions Act (19 of 1982)

Signed: _____   Date: _27/3/2013_
              (Registered Veterinarian)

cc: Supervisor: Professor V Pillay
    Director: CAS

Works 2000/Iain0015/AESCCert.wps

263

11.5. Sterilization Certificate

synergyhealth

our work protects your world

http://www.synergyhealthplc.com

Certificate of Irradiation

Date Issued: 30-Apr-2014   ZA01S11149293-1-1

This is to certify that Synergy Sterilisation South Africa (Pty) Ltd has where appropriate delivered an irradiation process in accordance with:

EN ISO 11137-1:2006 Sterilisation of Health Care Products
EN ISO 9001:2008 Quality Management System
EN ISO 13485:2012 Quality System - Medical Devices

FACTORY USAGE (INTERNAL PROCESS)
PO BOX 3219
ISANDO
GAUTENG 1620
SOUTH AFRICA

Order Information

Account Number:	107141
Synergy Health Sales Part Reference:	1072195
Customer Reference Number:	13/03/2014
Product Description:	SUNAINA SAMPLE 1KG BOX 25KGY
Validation Reference:	MAP2014
Quantity Received:	1
Customer Minimum Specification kGy:	25.0
Customer Maximum Specification kGy:	35.0

Irradiation Data

Reference Dose Range kGy:	27.6 - 27.6
Calculated Minimum Dose kGy:	27.5
Calculated Maximum Dose kGy:	32.8

Irradiation Release Authorised By Synergy Health plc

Registered Office: P O Box 3219, Kempton Park, Gauteng, 1620, SOUTH AFRICA
Company Registration No: 1998/024219/07 VAT Number: 4790187357
Page 1 of 1